

**Analysis of the modifying influence
of Plastin 3 (PLS3) on
Spinal Muscular Atrophy (SMA) by
generation of transgenic mouse models**

Inaugural-Dissertation
zur
Erlangung des Doktorgrades
der Mathematisch-Naturwissenschaftlichen Fakultät
der Universität zu Köln

Vorgelegt von
Bastian Ackermann
aus Geldern

Köln 2011

The Doctoral Thesis “Analysis of the modifying influence of Plastin 3 (PLS3) on Spinal Muscular Atrophy (SMA) by generation of transgenic mouse models” was performed at the Institute of Human Genetics, Institute of Genetics and Centre for Molecular Medicine Cologne (CMMC) of the University of Cologne from July 2007 to 2011.

Berichterstatter: Prof. Dr. rer. nat. Brunhilde Wirth
Prof. Dr. rer. nat. Sigrun Korsching

Tag der letzten Prüfung: 20.10.2011

Meinen Eltern

Table of contents

List of abbreviations	v
1 Preamble	1
2 Introduction	3
2.1 Autosomal recessive proximal spinal muscular atrophy (SMA) – Symptoms and classification.....	3
2.1.1 <i>SMN1</i> and <i>SMN2</i> as SMA determining	5
2.1.2 SMN protein.....	6
2.1.3 SMN function	6
2.1.4 SMA mouse models	12
2.1.5 Therapeutic strategies in SMA treatment	13
2.2 PLS3 - a fully protective modifier of SMA.....	14
2.2.1 <i>PLS3</i> gene.....	17
2.2.2 PLS3 protein.....	17
2.2.3 PLS3 function	19
2.2.4 Other potential SMA modifiers – knowledge from invertebrates.....	21
2.3 Development of the neuromuscular system.....	22
2.3.1 The process of axonal pruning in NMJ refinement.....	22
2.3.2 Actin dynamics in axon growth	23
2.3.3 Acetylcholine receptor (AChR) prepatterning	26
2.3.4 The role of presynaptic signaling in AChR clustering and refinement	26
2.3.5 MuSK downstream signaling and the importance of cytoskeletal dynamics in AChR clustering	28
2.3.6 Mutations in NMJ genes cause myasthenic syndromes	30
3 Study Aims	34
4 Materials and methods.....	35
4.1 Equipment.....	35
4.2 Chemicals.....	37
4.3 Reagents for molecular biology.....	37
4.3.1 Reagents for DNA work	37
4.3.2 Reagents for radioactive DNA work.....	38
4.3.3 Reagents for protein work	38
4.3.4 Reagents for work with bacteria.....	38
4.3.5 Reagents for cell culture	38
4.3.6 Reagents for histo- and immunohistochemical methods	39
4.3.7 Kits	40

4.4	Enzymes.....	41
4.4.1	Restriction enzymes	41
4.4.2	Other enzymes.....	41
4.5	Material for the work with mice.....	41
4.5.1	Mouse dissection equipment.....	41
4.5.2	Reagents for Embryo transfers / Cryoconservation	42
4.6	Antibodies.....	42
4.6.1	Primary antibodies and staining reagents.....	42
4.6.2	Secondary antibodies	42
4.7	Solutions and media.....	43
4.7.1	Frequently used solutions.....	43
4.7.2	Cell culture media	44
4.7.3	Solutions for bacterial work	45
4.7.4	Solutions for the work with DNA.....	45
4.7.5	Solutions for Southern blotting	46
4.7.6	Solutions for Western blotting.....	47
4.7.7	Solutions for histo- and immunohistochemical work.....	49
4.8	Primer.....	51
4.9	Generated plasmids / GVOs.....	54
4.10	Software, internet programs and databases.....	54
4.11	Molecular biology methods.....	55
4.11.1	Working with DNA.....	55
4.11.2	Working with RNA.....	61
4.11.3	Working with bacteria	62
4.12	Protein biochemical and immunological methods.....	64
4.12.1	Working with proteins	64
4.12.2	Immuno- and histochemical staining procedures.....	67
4.13	Eukaryotic cell culture procedures.....	70
4.13.1	Common cell-culture techniques	70
4.13.2	Murine embryonic fibroblasts.....	71
4.13.3	Murine embryonic stem cells	72
4.14	Working with mice.....	77
4.14.1	Mouse inbred strains	77
4.14.2	Preparation of mouse tissues and organs.....	80
4.14.3	The <i>Cre/loxP</i> system for conditional gene-deletion or activation	82
4.15	Statistical methods.....	83
5	Results.....	84
5.1	Generation of the <i>Rosa26</i> targeting construct.....	84
5.1.1	<i>Rosa26</i> targeting and structure of the targeting construct.....	84

5.1.2	3 Step (A-C) strategy for cloning <i>PLS3V5</i> into the <i>Rosa26</i> targeting vector – Overview.....	85
5.2	Transgenesis of ES cells.....	89
5.2.1	Stable integration of the targeting construct into the genome of ES cells	89
5.3	Generation of <i>PLS3V5</i> transgenic mice.....	94
5.3.1	Nomenclature of the <i>PLS3V5</i> transgenic mouse lines generated in this thesis - Overview	94
5.3.2	Generation of chimeras and identification of transgenic <i>PLS3</i> -floxed mice.....	95
5.3.3	Generation of the <i>PLS3V5</i> -ubi line by permanent deletion of the stop cassette in <i>PLS3V5</i> -floxed mice	97
5.4	Ubiquitous expression of <i>PLS3V5</i> in an SMA mouse model.....	101
5.4.1	Quantitative and qualitative assessment of <i>PLS3V5</i> ubiquitous expression on wt background	101
5.4.2	Generation of an SMA mouse model for the overexpression analysis of <i>PLS3V5</i>	112
5.4.3	Functional analysis of <i>PLS3V5</i> expression on the SMA phenotype	120
5.5	Motor neuron specific expression of <i>PLS3V5</i> on a wt background.....	134
5.5.1	Effects of motor neuron specific expression of <i>PLS3V5</i>	134
6	Discussion.....	140
6.1	Generation of a <i>PLS3V5</i> expressing mouse.....	140
6.2	The genetic background influences the phenotypic severity in Hung SMA mice.....	142
6.3	The effects of <i>PLS3V5</i> overexpression on the morphology of murine embryonic fibroblasts.....	144
6.4	Effects of <i>PLS3V5</i> overexpression at NMJ level.....	145
6.4.1	Increased AChR clusters – effect of pre- or postsynaptic <i>PLS3V5</i> action?	145
6.4.2	Delayed axonal pruning in <i>PLS3V5</i> overexpressing mice	148
6.4.3	Innervation defects in Hung SMA mice and hyperinnervation of endplates in <i>PLS3V5</i> expressing animals	150
6.5	Why does <i>PLS3V5</i> overexpression not ameliorate the survival of SMA mice? SMN and <i>PLS3V5</i> protein amounts as limiting factors.....	152
6.6	Does <i>PLS3V5</i> act together with or independent of <i>Smn</i> ?.....	156
6.7	Future prospects and next steps.....	157
7	Summary.....	160
8	Zusammenfassung.....	162
9	Publications, presentations, posters and awards.....	165
10	References.....	168
11	Appendix.....	viii

12 Acknowledgements	xiii
13 Erklärung.....	xiv
14 Curriculum Vitae.....	xv

List of abbreviations

%	percent
A	adenine
approx.	approximately
bp	base pair
BSA	bovine serum albumin
C	cytosine
cDNA	coding DNA
cds	coding sequence
cen	centromeric
cm	centimeter
cM	centimorgan
CNS	central nervous system
d	day/days
DEPC	diethylpyrocarbonate
D-MEM	Dulbecco's modified Eagle medium
DMSO	dimethylsulfoxide
DNA	deoxyribonucleic acid
dNTP	deoxynucleotriphosphate
e.g.	Exempli gratia
EBV	Epstein-Barr virus
EDTA	ethylenediaminetetraacetic acid
EGTA	ethylene glycol tetraacetic acid
ESE	exonic splicing enhancer
ESS	exonic splicing silencer
et al.	et alii
FCS	fetal calf serum
FDA	Food & Drug Administration
FL	full length
G	guanine
h	hours
HAT	histone acetyltransferase
HDAC	histone deacetylase
HMT	histone methyltransferase
kb	kilobases
kDa	kilodalton
l	liter

m	milli-/month/months
M	molar
Mb	megabases
MDa	megadalton
min	minutes
ml	milliliter
mm	millimeter
mM	millimolar
mRNA	messenger RNA
n.d.	not determined
n.s.	not significant
ng	nanogram
nm	nanometer
nM	nanomolar
nmol	nanomol
OMIM	Online Mendelian Inheritance in Man
P	postnatal day
p	probability (statistical significance)
PAA	polyacrylamide
PAGE	polyacrylamide gel electrophoresis
PBS	phosphate-buffered saline
PCR	polymerase chain reaction
pH	power of hydrogen
pmol	picomol
RNA	ribonucleic acid
RNAi	RNA interference
rpm	revolutions per minute
RT	reverse transcription
s.c.	subcutaneous
SAHA	suberoylanilide hydroxamide acid
SD	standard deviation
SDS	sodium dodecyl sulfate
SEM	standard error of the mean
siRNA	small interfering RNA
SMA	autosomal recessive spinal muscular atrophy
SMN	survival motor neuron
T	thymidine

TEMED	N,N,N',N'-tetramethylethylenediamine
ter	telomeric
UV	ultraviolet
VPA	valproic acid
wt	Wild-type
μ	micro-
μg	microgram
μl	microliter
μm	micrometer
μM	micromolar

1 Preamble

Spinal muscular atrophy (SMA) is a neurodegenerative disease caused by the homozygous loss of the *survival motor neuron gene 1* (*SMN1*) (Lefebvre et al., 1995). Motor neurons, their axons and distal neuromuscular junctions (NMJs) have been demonstrated to be severely affected in SMA, resulting in muscle weakness and atrophy. Next to *SMN1*, a nearly identical copy gene is present in all SMA patients, termed *SMN2*. Importantly, however, a silent c.C280T transition is present in exon 7 of *SMN2*, causing the disruption of an exonic splicing enhancer (ESE) (Lorson et al., 1999, Cartegni and Krainer, 2002). Finally, this leads to exon 7 skipping in ~90 % of the transcripts and the production of truncated $\Delta 7$ SMN protein with reduced oligomerization capacity and stability (Lorson et al., 1998). Due to genetic drift, the *SMN2* copy number is highly variable among the population, ranging from zero to a maximum of four copies per allele. Since ~10 % of *SMN2* transcripts still code for full length (FL) SMN, SMA severity is inversely correlated with *SMN2* copy number (Burghes, 1997, Brahe, 2000, Feldkotter et al., 2002).

In the past, so called discordant families have been described in which homozygously *SMN1*-deleted individuals are fully asymptomatic despite carrying an identical number of *SMN2* copies as their affected siblings. From such observations, it has been concluded that other SMA-modifying factors must be present in these patients. In 2008, high levels of the actin filament bundling protein PLS3 have been shown to act fully protective in *SMN1*-deleted unaffected individuals of six discordant SMA families in our group (Oprea et al., 2008). Further functional analyzes revealed that *PLS3* overexpression is able to rescue axon outgrowth defects in *Smn*-depleted PC12 cells as well as motor neurons derived from SMA mice. Most strikingly, however, *PLS3* overexpression was able to rescue axon outgrowth defects in a zebrafish model of SMA *in vivo*.

The main goal of the present work was to study the effects of *PLS3* overexpression on a mouse model of SMA. For this purpose and using the Cre/*loxP* system, a V5-tagged version of human *PLS3* was targeted into the murine *Rosa26* locus in order to ubiquitously or tissue specific overexpress *PLS3*. *PLS3V5* transgenic mice were next crossed on an SMA background. As careful morphological analysis revealed, *PLS3V5* overexpression led to clear improvements of neuromuscular connectivity at the NMJ level (delayed axonal pruning, highly arborized axon terminals, highly occupied Acetylcholine receptor (AChR) clusters, increase in the size of AChR clusters). Moreover, motor neuron specific expression of *PLS3* in a wt background was sufficient to increase muscle fiber size in P21 mice, indicating that the observed changes at NMJ level are indeed functional.

The following introduction is subdivided into three parts (2.1, 2.2 and 2.3). The first part (2.1) starts with a detailed explanation of the clinical picture of SMA and is then leading to the underlying molecular causes of the disease. Based on the knowledge from different animal

models, the section continues with a description of SMN protein function with particular focus on the role of SMN in axons. Although no cure is available yet, the first section will close with a brief overview of potential therapeutic strategies for SMA treatment.

In the second part of the introduction (2.2), the discovery of PLS3 as a fully protective modifier of SMA in homozygously *SMN1*-deleted individuals of discordant families will be described. After a short overview on *PLS3* gene and protein structure, PLS3 function will be explained, again, with particular focus on PLS3 function in the axon. Finally, recent data on other potential modifiers of SMA from invertebrate screens will be discussed.

As *PLS3V5* overexpression led to significant improvements of neuromuscular connectivity at NMJ level of SMA mice, the third part of the introduction (2.3) deals with the development of the neuromuscular system in general. As *PLS3V5* overexpression led to delayed axonal pruning, an overview about this fundamental developmental process will be given first. Moreover, *PLS3V5* overexpression resulted in highly arborized nerve terminals as well as increased postsynaptic AChR cluster. Therefore, further information will be presented on the mechanisms underlying axon growth as well as AChR cluster patterning, with particular focus on the role of actin dynamics in both processes.

2 Introduction

2.1 Autosomal recessive proximal spinal muscular atrophy (SMA) – Symptoms and classification

First described in the late 19th century by Werdnig and Hoffmann (University of Vienna and Heidelberg, respectively), SMA is the leading genetic cause of infant death today (Montes et al., 2009). In the western European population, SMA has an incidence of 1 in 6.000 to 10.000 births with a carrier frequency of 1:35 (Pearn, 1978, Czeizel and Hamula, 1989, Emery, 1991, Feldkotter et al., 2002). SMA is caused by the homozygous deletion or mutation of the *survival motor neuron 1 gene (SMN1)* located on chromosome 5q13 (Brzustowicz et al., 1990, Melki et al., 1990) and results in the degeneration of α -motor neurons in the anterior ventral horns of the spinal cord as well as their respective efferent axons. As a consequence, affected individuals suffer from progressive weakening of muscles. In the severe Type I SMA (see below), first signs of muscle weakening are often noticed already during the 3rd trimester of pregnancy as fetal movements decrease abnormally (MacLeod et al., 1999). Importantly, the decrease of fetal movements has been shown to be accompanied by progressive loss of motor neurons (Markowitz et al., 2004). Together, these findings suggest that in severely affected SMA patients the onset of disease occurs *in utero*. The first postnatal symptom common to all severity types is weakening of the proximal voluntary muscles, e.g. limb or intercostal muscle of the chest. With ongoing progression and depending on the severity type of disease, further symptoms include a weak cough, dyspnea and even bulbar involvement (Rudnik-Schöneborn et al., 1994). Although diaphragmatic strength is usually intact, weakening of intercostal chest muscles can lead to a severely restrictive lung deficit and finally to the need of ventilatory support (Markowitz et al., 2004). Later symptoms, especially in the less affected Type II, III or IV patients (see below), typically include progressive weakening of also the distal muscle. Since muscles of the legs are affected first, patients will usually be wheelchair bound or suffer major problems in climbing stairs or getting up from the floor. Even though a recent study in mouse indicated that cellular proliferation, migration and development in hippocampal regions of the brain might be affected patient's sensation and cognitive abilities usually remain intact (D'Angelo and Bresolin, 2006, Wishart et al., 2010).

The denervation of muscle finally results in atrophy, whereby often a few residual motor neurons stay connected. The uncontrolled and sporadic firing of such remaining motor neurons leads to twitching (fasciculation), particular of the tongue and fingers, a finding often used in diagnosis (Markowitz et al., 2004). When there are additional clinical grounds for suspecting a diagnosis of SMA in a newborn, e.g. hypotonia or headlag, DNA based tests offer quick and reliable sureness. The two most common methods used for the detection of

SMN1 deletions are (i) a PCR based approach with subsequent test restriction (Scheffer et al., 2001) or (ii) Multiplex Ligation-dependent Probe Amplification (MLPA) (Scarciolla et al., 2006, Zapletalova et al., 2007). Since in 5 % of all patients the loss of *SMN1* function is caused by a deletion of one allele and a small intragenic (subtle) deleterious mutation on the second allele or, very infrequently, from subtle mutations on both alleles (Alias et al., 2009, Vezain et al., 2011), sometimes sequencing must be recruited to determine the exact cause.

In the following, the classification of SMA into the four Types I, II, III and IV and their characteristics will be briefly outlined.

Type I SMA (Werdnig-Hoffmann disease, MIM #253300):

Type I SMA, also called the infantile acute form, is the most severe type of SMA and accounts for ~50 % of all SMA cases (Werdnig, 1891, Pearn, 1978, Markowitz et al., 2004). The onset of disease is usually before the age of 6 months, but often around the time of birth. Prognosis for type I SMA patients is poor. In different studies, the survival of patients with disease onset in the first three months was determined to ~7 months (Rudnik-Schoneborn et al., 2009). The proportion of patients surviving more than 2 years is ~6 % (Cobben et al., 2008, Rudnik-Schoneborn et al., 2009). SMA type I patients will never be able to sit or even walk independently. Proximal intercostal muscles (muscle of the chest) are strongly affected, resulting in severe breathing problems and increased infection rate.

Type II SMA (Intermediate form, MIM #253550):

The onset of type II SMA is between 6 months to 18 years, with most patients being diagnosed within the first year to 18 months. Affected children are usually able to sit without support, but walking is almost impossible. The prognosis is extremely variable in SMA type II patients and depends to a large extent on the degree of respiratory muscle involvement and the problems associated with the development of kyphoscoliosis (abnormal curvature of the spine) (Talbot, 1999). In a comprehensive study with 240 SMA type II patients the survival rate was 98.5 % at 5 years and 68.5 % at 25 years (Zerres et al., 1997).

Type III SMA (Kugelberg-Welander, MIM #253400):

Type III SMA is a very heterogenous form of SMA with first mild symptoms occurring after the first 18 months of life (Kugelberg and Welander, 1956). Most patients are diagnosed between 2 and 12 years of age. Typically, walking and running as well as climbing stairs are possible, but become increasingly difficult with age. The prognosis for SMA type III patients is good since life expectancy is almost normal. Type III SMA is further subclassified into type IIIa, with onset before the age of 3 years, and type IIIb SMA, with onset after the 3rd year.

SMA Type IV (Adult form, MIM #271150):

SMA type IV is a very mild form of SMA with late median onset beyond 30 years of age (Pearn, 1978, Zerres et al., 1995). As in all SMA forms, weakness is progressive, but affects mostly proximal muscle while distal muscle function is preserved. Type IV patients have a normal life expectancy.

2.1.1 *SMN1* and *SMN2* as SMA determining genes

In the year 1995 and after a long search, the *survival of motor neuron 1 gene (SMN1)* has been identified as the SMA causing gene (Lefebvre et al., 1995). *SMN1* lies within the telomeric part of a 500 kb duplicated region on chromosome 5q13 (Brzustowicz et al., 1990) (Figure 1). The *SMN1* gene spans a 28 kb genomic region and comprises 9 exons (1, 2a, 2b, 3, 4, 5, 6, 7, 8). The coding sequence of *SMN1* is 882 bp and produces a ~1.7 kb transcript (together with 5' and 3' UTR) which is ubiquitously expressed, but particularly high in spinal cord. The mRNA codes for a protein of 294 amino acids having a molecular weight of 38 kDa. Furthermore, *SMN1* was found to be highly conserved between all organisms, underlining its essential function (Miguel-Aliaga et al., 1999, Paushkin et al., 2000).

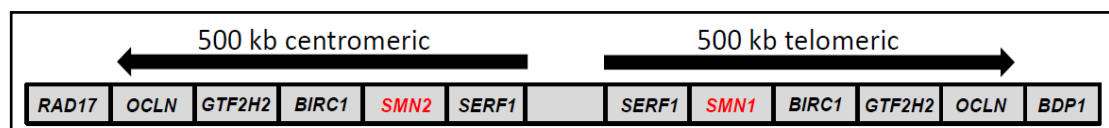


Figure 1: 500 kb telomeric and centromeric region containing *SMN1* and its duplicated version *SMN2*, respectively.

In the centromeric region, a nearly identical copy of *SMN1* is located, termed *SMN2*, which has been found to be present in all SMA patients. *SMN2* differs from *SMN1* by only 5 silent discrepancies: A synonymous mutation in exon 7 (c.C280T in *SMN2*), exon 8 (nt 27869 G>A), intron 6 (nt 27092 G>A) and another two in Intron 7 (nt 27289 A>G and 27404 A>G) (Lefebvre et al., 1995, Burglen et al., 1996).

Already at their discovery, it was found that *SMN1* and *SMN2* have distinct splicing patterns. In humans only carrying *SMN1*, solely the full length transcript (FL-SMN) containing exon 7 was present. However, controls carrying both *SMN1* and *SMN2* additionally showed a transcript lacking exon 7 ($\Delta 7$ SMN2) (Lefebvre et al., 1995). Based on these observations, it was found that the c.C280T transition in exon 7 of *SMN2* causes the disruption of an exonic splicing enhancer (ESE) (Lorson et al., 1999, Cartegni and Krainer, 2002). This in turn results in exon 7 skipping in about 90 % of the total transcripts while 10 % of *SMN2* transcripts are still full length. The skipping of exon 7 leads to a frameshift and an alternative stop codon in exon 8. Finally, this produces a truncated protein ($\Delta 7$ SMN2) of reduced oligomerization capacity and stability (Lorson et al., 1998). *SMN2* lies within a highly repetitive genomic region prone to rearrangements. Therefore, the *SMN2* copy number is variable among the population. Since still about 10 % of the total *SMN2* transcript code for

fully functional SMN protein, the *SMN2* copy number is inversely correlated with the disease phenotype and prognosis (Burghes, 1997, Brahe, 2000, Feldkotter et al., 2002).

Although not absolute, *SMN1* deficient SMA type I patients usually carry 1 or 2 *SMN2* copies, SMA type II patients 2 or 3 and SMA type III patients 3 or 4 copies of *SMN2*. Infrequently, patients are observed that develop the relatively mild SMA type III despite having only 2 *SMN2* copies. The other way around, type I SMA patients were described carrying 3 *SMN2* copies. This may be because of true variation caused by modifying genes or other external factors, intragenic mutations within *SMN2*, or *SMN2* genes partially deleted or duplicated as a result of deletions or gene conversions involving either the 5' or 3' end of the *SMN* genes (Feldkotter et al., 2002). Moreover, up to now three unrelated patients have been described who possessed *SMN2* copy numbers that did not correlate with the observed mild clinical phenotypes and who all carried a c.G859C substitution in the *SMN2* gene (Prior et al., 2009, Vezain et al., 2010). In their study, the authors were able to demonstrate that this mutation creates a new exonic splicing enhancer favoring exon 7 inclusion and consequentially increasing SMN levels in the patients. Therefore, not only the number of *SMN2* copies can affect the disease severity but also sequence variations within *SMN2*.

2.1.2 SMN protein

SMN is a 294 aa protein of about 38 kDa in size and is encoded by 8 exons (Lefebvre et al., 1995). SMN has been shown to be ubiquitously expressed with especially high levels in the central nervous system (CNS) and the liver (Liu and Dreyfuss, 1996, Carvalho et al., 1999, Young et al., 2000, Young et al., 2001). While SMN shows diffuse distribution in the cytoplasm, it is present in punctate structures in the nucleus termed gemini of Cajal bodies (CBs), or gems (Liu and Dreyfuss, 1996). Gems are often located proximal to or overlapping with Cajal bodies (CB), structures that are implicated to play an important role in the nuclear biogenesis of spliceosomal small nuclear ribonucleoproteins snRNPs (Darzacq et al., 2002, Jady et al., 2003). The SMN protein has several functional domains, including an N-terminal RNA-binding-domain (RBD, exon 2b and 3), a Tudor domain involved in Sm protein interaction (exon 3), a proline-rich stretch (exon 4 and 5), which can interact with profilin as well as a C-terminal YG-box (exon 6 and 2) that is important for self-oligomerization (Lorson et al., 1998, Bertrand et al., 1999, Selenko et al., 2001, Bowerman et al., 2007, Bowerman et al., 2009).

2.1.3 SMN function

After the current model, SMN has multiple roles in a plethora of cellular processes and pathways, however, its most recognized and studied function is in the assembly of small nuclear ribonucleoproteins (snRNP), important factors within the spliceosome. As will be demonstrated in the results part of this thesis, the modifying factor PLS3V5 positively

influences axonal integrity and nerve connectivity in SMA mice at the level of the neuromuscular junction (NMJ). Therefore, a particular focus of this chapter is on the function of SMN in axonal transport and growth as well as NMJ maturation. Last but not least, recent findings about an involvement of muscle and other non-neuronal tissues in SMA disease will be outlined.

I. The SMN complex and its function in snRNP assembly:

SMN has been shown to play an important role in the assembly of small nuclear ribonucleoproteins (snRNPs), important factors within the spliceosome (Fischer et al., 1997, Meister et al., 2001, Pellizzoni et al., 2002, Gubitz et al., 2004, Eggert et al., 2006, Burghes and Beattie, 2009). snRNPs are important in splice site (ss) recognition and catalytic removal of introns from pre-mRNA and consist of a U small nuclear RNA (snRNA) (U1, U2, U4, U5, U11 or U12) and a heptameric ring of Sm proteins (D1, D2, E, F, G and D3, B) (Raker et al., 1999). It was demonstrated in the past that Sm proteins can self-assemble on snRNAs *in vitro*, however, *in vivo* this process requires the SMN complex (Meister et al., 2001, Meister et al., 2002, Pellizzoni et al., 2002, Pellizzoni, 2007). In this conformation the SMN complex, containing the assembled snRNPs, is then transferred into the nucleus. There, snRNPs are further processed and matured in the gems while the SMN complex translocates out of the nucleus again (Chari et al., 2009). The SMN complex (approx. 1 mDa) itself is comprised of many factors, which are called gemins due to their subcellular localization similar to that of SMN (including gems (Carissimi et al., 2006)). SMN is believed to act as the core backbone of the complex, however the exact stoichiometry of SMN and its binding partners is still unknown.

Based on these findings, it is assumed that *SMN1*-deletion impacts on correct splicing. Therefore, attempts have been undertaken to investigate the impact of SMN depletion on splicing in an SMA mouse model. Indeed, analysis revealed differences in pathways associated with neuronal development as well as cellular injury. Nevertheless, it is hard to distinguish between splice or expression changes due to secondary stress reactions, and changes that are truly caused by SMN depletion (Zhang et al., 2008b, Baumer et al., 2009).

II. SMN function in translational regulation and axonal transport:

A function of SMN in translational regulation was suggested based on the observation that SMN localizes in granules that are transported along the axons of neurons and that show colocalization with ribosomal RNAs (Zhang et al., 2003). Local protein synthesis is important for axonal integrity, this fact being in line with the observation that SMN deficient neurons show defects in axonal outgrowth and pathfinding (McWhorter et al., 2003, Carrel et al., 2006, van Bergeijk et al., 2007, Oprea et al., 2008, Holt and Bullock, 2009).

The effects of Smn deficiency were also studied in primary motor neuron cultures from SMA mice (Rossoll et al., 2003). Even though motor neurons derived from SMA mice showed the same survival as wt motor neurons, the axon length was significantly reduced. Previous electron microscopic (EM) analyses showed that Smn protein is associated with axonal microtubules (Bechade et al., 1999, Pagliardini et al., 2000, Rossoll et al., 2003). Furthermore, in murine motor neurons Smn protein colocalized with hnRNP R (Rossoll et al., 2002), which in turn was shown to associate with β -Actin mRNA. Therefore, it was speculated that a complex of Smn and hnRNP R might be involved in axonal β -actin mRNA transport or processing (Rossoll et al., 2003). Indeed, hnRNP protein was only present in a punctuate pattern along motor axons of SMA mice and, presumably due to defects in transport, β -actin protein was severely reduced in the growth cones of such. These results suggest that the localization of β -actin mRNA and hnRNP R to growth cones depends on the presence of Smn and that cytoskeletal defects in the growth cones and axons might contribute to SMA pathology (Rossoll et al., 2003).

Besides hnRNP R, many other interaction partners of SMN were identified in the past that have important function in RNA binding or translational regulation, e.g.: hnRNP Q, KH-type splicing regulatory protein (KSRP), Hu antigen D (HuD) and fragile X mental retardation protein (FMRP) (Rossoll and Bassell, 2009, Fallini et al., 2011). Since FMRP associates with polyribosomes and has been proven to be a negative regulator of translation by associating with mRNAs, SMN might impact on the regulative ability of FMRP through physical interaction (Piazzon et al., 2008).

III. The role of SMN in axonal growth and neuromuscular junction (NMJ) maturation:

SMN has been observed to be expressed at highest levels during embryonic and fetal stages compared to the postnatal period (Burllet et al., 1998), indicating essential function of SMN during development. Additional expression analyses revealed the presence of SMN *in vivo* in neurites and growth cones of motor neurons in mouse and rat spinal cord, embryonic chick forebrain and *in vitro* in primary rat cortical neurons transfected with recombinant SMN as well as in differentiating, neuron-like mouse P 19 cells (Bechade et al., 1999, Pagliardini et al., 2000, Dodds et al., 2001, Jablonka et al., 2001, Fan and Simard, 2002, Zhang et al., 2003, Briese et al., 2005). Using PC12 cells it was found that SMN protein levels increase during neuronal differentiation under continuous neuronal growth factor (NGF) treatment (van Bergeijk et al., 2007). Furthermore, it was shown in the same study that shRNA-mediated knockdown of SMN significantly reduced neurite length in PC12 cells while overexpression of SMN led to extensive sprouting. By testing different deletion constructs and transfecting into SMN depleted PC12 cells, the growth promoting region could be narrowed to a C-terminal fragment comprising amino acid (aa) residues 235-294 of the human SMN. In this construct

the tudor domain which is necessary for Sm protein-binding and thus, in turn, essential for SMN function in snRNP was completely missing. Therefore, these results could argue for distinct functions of SMN in snRNP-assembly / splicing and axons or dendrites (van Bergeijk et al., 2007).

It is well known, that axonal growth and branching strongly depend on actin dynamics (Pak et al., 2008, Schmidt and Rathjen, 2010). In this process, a set of actin binding proteins such as the main neuronal form of Profilin, Profilin IIa, play an important role. Profilin IIa can sequester actin monomers or promote polymerization by de-sequestering of actin from the thymosin/ β -actin pool and by adding these monomers to the free barbed ends of microfilaments (Pantaloni and Carrier, 1993, Sharma et al., 2005) (see also chapter 2.3.2). It has previously been shown that SMN can interact with Profilin IIa and influences the sequestering ability of Profilin IIa negatively, thereby triggering polymerization (Rossoll et al., 2002, Sharma et al., 2005). However, the effect of profilin polymerizing function on the actin cytoskeleton and thus on axonal growth is controversially discussed: While in one study the knockdown of individual profilin isoforms (I and II) had seemingly no effect and the double knockdown clearly inhibited axonal growth (Sharma et al., 2005), it was demonstrated elsewhere that the single knockdown of Profilin IIa was sufficient to stimulate neurite outgrowth (Da Silva et al., 2003). In combination with the finding of an SMN / hnRNP interaction, these observations indicate an involvement of SMN in axonal growth via the regulation of actin dynamics.

Besides observations from cell culture, the findings of axonal growth defects upon SMN depletion have been confirmed in a variety of different SMA animal models. In *Caenorhabditis elegans*, a less complete knockdown of *smn-1* leads to developmental arrest, reduced lifespan and axonal outgrowth defects, which finally results in locomotion deficits (Briese et al., 2009). Also in the fly *Drosophila melanogaster*, developmental and motor behavior deficits were observed (Chan et al., 2003). Further electrophysiological combined with morphological analysis revealed reduced endplate (Acetyl Choline Receptor (AChR) cluster) currents and endplate disorganization (Chan et al., 2003). These findings for the first time led to the suggestion of primary defects at the SMA NMJ. Also in the vertebrate *Xenopus laevis*, motor neuron abnormalities with reduced axonal outgrowth and abnormal formation of branching extensions have been described (Ymlahi-Ouazzani et al., 2010). Similarly, zebrafish deficient for *Smn* display motor axons with abnormal growth and branching, that often do not reach their most distant targets (McWhorter et al., 2003, Carrel et al., 2006, Oprea et al., 2008, Hao le et al., 2011).

While axonal defects have been frequently observed in these models and also *in vitro* in murine motor neurons, *in vivo* in SMA mouse models no defects in axonal outgrowth were detected (McGovern et al., 2008, Torres-Benito et al., 2011). In line with this fact, no changes

have been observed in SMA animals with regards to the number of axonal branches innervating single muscle fibers. Nevertheless, severe SMA mice have been shown to exhibit a significant reduction of axonal inputs per endplate during synapse elimination process, also termed axonal pruning (chapter 2.3.1), in proximal TVA muscle (Murray et al., 2008). Furthermore, electrophysiological recordings of synaptic activity at the NMJ have shown a number of abnormalities in *Smn* depleted mice (Torres-Benito et al., 2011). In the proximal slow twitch *Transversus abdominis* muscle (TVA), the quantal content (QC, amount of neurotransmitter released per action potential) was reduced up to ~50 % in the *SMNΔ7* mouse model (chapter 2.1.4), followed by ~40 % reduction in the distal and fast twitch muscles *Tibialis anterior* (TA), and ~25 % reduction in *Extensor digitorum longus* (EDL) (Ruiz et al., 2010). Since the amount of neurotransmitter per fused vesicle (quantal size) was not altered between control and SMA mice, it has been speculated that the reduction in QC was due to a decrease in release probability and/or in the number of docked vesicles (Kong et al., 2009, Ling et al., 2010, Ruiz et al., 2010, Torres-Benito et al., 2011). Indeed, measurements in SMA and control mice have confirmed significant changes in vesicle release probability as well as in the number of docked vesicles (Kong et al., 2009). Furthermore, also the distribution of vesicles in the presynapse appeared abnormal in SMA animals (Kariya et al., 2008).

The functional defects observed in NMJs of SMA mice manifest also in altered morphological appearance of both pre- and postsynaptic structures. SMA presynapses are often characterized by accumulations of Neurofilament (NF) and it is believed that NF accumulations participate in motor neuron dysfunction, e.g. by slowing down the transport of components required for axonal and synaptic maturation and maintenance (Cifuentes-Diaz et al., 2002, Kariya et al., 2008, Kong et al., 2009, Ruiz et al., 2010, Dachs et al., 2011, Torres-Benito et al., 2011). Further hallmarks of presynaptic defects include tiny nerve terminals that are often detached from the postsynaptic membrane, reduced sprouting and concomitantly large areas of postsynaptic membrane unoccupied by synaptic terminals. The defects observed at SMA postsynapses affect mainly the maturation process of Acetyl Choline receptor (AChR) clustering. While in wt ovoid AChR plaques are transformed into complex, pretzel-like shapes (characteristic of adult synapses), SMA animals display small and still oval shaped endplates with almost no gutters or perforations and postsynaptic membrane folds fail to form (Sanes and Lichtman, 1999, Torres-Benito et al., 2011). Postsynaptic responses remain slow compared to wildtype, which might in part be attributed to predominantly embryonic γ -subunit containing forms of AChR in SMA mice (Kong et al., 2009). However, the exact mechanisms underlying the maturation defects of NMJs in SMA remain elusive.

Together, these data suggest that NMJ pathology rather than axonal defects are the characteristic disease feature in SMA mice. Since NMJ defects are an early characteristic timely preceding motor neuron death, a dying back mechanism was suggested.

IV. SMN function in muscle and other non-neuronal tissues:

It has previously been shown in different studies that muscle specific overexpression of SMN is not sufficient to ameliorate the SMA phenotype in flies and mice in the absence of neuronal SMN. In turn, neuron specific expression alone significantly improved survival but did not fully rescue the SMA phenotype (Chan et al., 2003, Gavrulina et al., 2008). Therefore, it has been speculated that the observed motor defects might be caused by primary abnormalities in both muscles and motor neurons, or perhaps due to a failure of communication between these two tissues (Walker et al., 2008). There are several further hints that SMA is not only caused by defects in motor neurons, axons or at NMJ level. E.g., SMN depletion experiments revealed defects in fusion and proliferation of human and mouse myoblasts and also the maintenance of stable innervation seems to depend on muscle specific expression of SMN (Braun et al., 1995, Guettier-Sigrist et al., 2002, Arnold et al., 2004, Shafey et al., 2005). In accordance with a muscular involvement of SMN, *Smn* and its complex partners were found to localize to the Z-disc (Divides two Sarcomeres, anchor for actin filaments) of skeletal and cardiac muscle in mouse. Furthermore, *Smn* was proven to be a direct target of calpain, a protease with important function in Z-disc turnover (Walker et al., 2008, Fuentes et al., 2010, Anderton et al., 2011). In this context, myofibers from SMA mice display morphological defects that are consistent with a Z-disc deficiency (Walker et al., 2008). Besides the neuronal functions of *Smn*, these findings point at an additional role of *Smn* in the muscle.

Apart from muscle, SMN depletion has often been reported to affect also other non neuronal tissues, such as heart, bone, blood vessels and liver (Finsterer and Stollberger, 1999, Kelly et al., 1999, Hsieh-Li et al., 2000, Felderhoff-Mueser et al., 2002, Arai et al., 2005, Hachiya et al., 2005, Bach, 2007, Shanmugarajan et al., 2007, Khatri et al., 2008, Rudnik-Schoneborn et al., 2008, Araujo Ade et al., 2009, Meyer et al., 2009, Shanmugarajan et al., 2009, Bevan et al., 2010, Gogliotti et al., 2010, Heier et al., 2010, Hua et al., 2010, Michaud et al., 2010, Riessland et al., 2010, Shababi et al., 2010). These observations have led to the development of the so called threshold theory, which proposes different susceptibility of certain cells to SMN depletion: While motor neurons are affected at weakly reduced SMN levels, other tissues such as heart, bone and finally all tissue types get affected as SMN levels further decrease or are even completely absent (Sleigh et al., 2011).

2.1.4 SMA mouse models

In contrast to humans, where a second copy of *SMN1* is present, the *SMN1* orthologue in mouse, *Smn*, has been shown to exist as a single copy gene (DiDonato et al., 1997). The homozygous knockout of *Smn* is embryonically lethal, providing evidence that *Smn* is indispensable for cell survival (Schrank et al., 1997, Hsieh-Li et al., 2000, Park et al., 2010). Due to its early embryonic lethality, however, this SMA model was not useful to adequately study disease mechanisms. For this reason and to more accurately mimic the human situation, the aberrantly spliced human *SMN2* (*hSMN2*) gene was introduced into the *Smn*^{-/-} background as a genomic fragment (Hsieh-Li et al., 2000, Monani et al., 2000, Park et al., 2010).

In the SMA mice generated by Monani, the *hSMN2* transgene is present as one copy per transgenic allele. Homozygous *Smn*^{-/-};*hSMN2*^{tg/tg} mice (2 *hSMN2* copies) are viable but develop severe symptoms including motor neuron loss and motoric disability by P2 and die by P4 (Monani et al., 2000). Heterozygous *Smn*^{-/-};*hSMN2*^{tg/wt} with a total of 1 *hSMN2* copy, however, are embryonically lethal. Importantly, 8 copies of *hSMN2* have been shown to be sufficient to fully rescue the lethal SMA phenotype of the Monani mice, providing the first proof-of-concept study of the feasibility of modulating the *SMN2* gene for therapeutic purposes (Monani et al., 2000, Park et al., 2010).

The most commonly used SMA model today is the so called *SMN*Δ7-mouse (Le et al., 2005). This line carries the Monani-*hSMN2* transgene (1 *hSMN2* copy per allele) and additionally Δ7*hSMN2* (an *SMN* cDNA lacking exon 7), each homozygously, on the *Smn* null background. In *Smn*^{-/-};*hSMN2*^{tg/tg};*Δ7hSMN2*^{tg/tg} mice a modest attenuation of the SMA phenotype was observed with a mean survival of 13.3±0.3 d., demonstrating that also Δ7*SMN2* is at least partially functional and does not, as was previously alleged, act deleterious through dominant-negative effects (Kerr et al., 2000, Le et al., 2005).

Further SMA mouse models include the *Smn*^{2B/-} mouse line with a 3 bp substitution in the exon 7 exonic splicing enhancer (ESE) (mean survival ~P30) (Bowerman et al., 2009) or the *Smn*^{-/-};*hSMN2*^{tg/tg};*A2G*^{tg/wt} with an A2G missense mutation in the first exon of the *SMN1* transgene (mean survival ~8 mo) (Monani et al., 2003).

Recently, a stably integrated *Cre*-inducible SMA mouse was generated in which expression of full length *hSMN2* occurs after tamoxifen administration (Bebbee et al., 2011). Many approaches today aim at the successful restoration of SMN levels in motor neurons. Using self-complementary adeno-associated virus 9 (scAAV9) mediated *SMN1* gene transfer, researchers were able to fully rescue the SMA phenotype when treating early P1, but not P10 SMA animals (Foust et al., 2010). Such findings indicate a certain timing requirement for SMN inductive or delivery therapy. Therefore, inducible SMA models will be of great help in defining the optimum therapeutic window in SMA therapy.

In the year 2000, Hsieh-Li et al. generated another SMA mouse model, also termed Hung mice, by crossing an integrate carrying 2 *hSMN2* copies onto the *Smn*^{-/-} background. Heterozygous *Smn*^{-/-};*hSMN2*^{tg/wt} animals (2 *hSMN2* copies) show a background-dependent survival of ~10 (FVB) (Riessland et al., 2010) to ~14 d (C57BL/6N, this thesis) while homozygous mice of the genotype *Smn*^{-/-};*hSMN2*^{tg/tg} (4 *hSMN2* copies) are fully viable and fertile but show necrosis of the ears and tail. The Hung mouse model offers the big advantage of producing 50 % of SMA and 50 % of control mice in one litter. Since the Hung mouse model was in this study used to analyze the effect of *PLS3* overexpression on the SMA phenotype, this model including the breeding scheme for the production of SMA mice is described in chapter 5.4.2.1.

2.1.5 Therapeutic strategies in SMA treatment

Currently, a number of therapeutic strategies are investigated for their potential in SMA therapy, however, to date no cure is available.

Several approaches aim at the stimulation of *SMN2* transcription, since still around ~10% of *FL-SMN* transcript are produced by this locus. Drugs of the so called Histone deacetylase inhibitor (HDACi) class of substances have turned out promising candidates for the development of an SMA therapy. As the name suggests, HDACi block the activity of histone deacetylases (HDAC). Therefore, these drugs activate gene transcription by shifting the modification of histones towards an increased acetylation state. In several studies using different substances (e.g. Sodium butyrate, valproic acid (VPA), phenylbutyrate, Trichostatin A, suberoylanilide hydroxamic acid (SAHA), M344 and LBH589), HDAC inhibition was proven to activate *SMN2* expression when tested in cell culture or murine SMA models (Chang et al., 2001, Brichta et al., 2003, Sumner et al., 2003, Andreassi et al., 2004, Brahe et al., 2005, Brichta et al., 2006, Riessland et al., 2006, Avila et al., 2007, Mercuri et al., 2007, Tsai et al., 2008, Garbes et al., 2009, Hauke et al., 2009).

Another strategy aims at the correction of the *SMN2* splicing pattern towards increased levels of *FL-SMN* transcripts. Although attempts using antisense oligonucleotides (ASOs) such as morpholinos or RNAs (Lim and Hertel, 2001, Cartegni and Krainer, 2003, Dickson et al., 2008) have been proven successful in elevating *SMN* levels in cell culture and even when injected into the brain of SMA mice (Passini et al., 2011), delivery into the human CNS remains challenging.

An additional way to increase *SMN* levels in SMA patients might be to stabilize remaining *FL-SMN* protein. In 2004, it was discovered that *SMN* is degraded via the ubiquitin/proteasome pathway (Chang et al., 2004, Garbes et al., 2009). In line with this, treatment of SMA patient's cell lines with the proteasome inhibitor MG132 led to an increase in *SMN* protein. These results raise the possibility that proteasome inhibitors may be useful for the treatment of SMA.

Also stem cell therapy has been suggested as a potential treatment form of SMA. Indeed, when transplanted into the spinal cord of the *SMNΔ7* mouse model, neural stem cells differentiated into motor neuron like cells, protected host motor neurons from degeneration and significantly improved motoric ability as well as survival (Corti et al., 2010). However, it is unlikely that transplanted motor neurons form axons that reach their targets in the respective muscle tissue. Therefore, any positive effect is likely to be mediated through neuroprotection of host motor neurons by numerous factors released from the donor cells, such as brain-derived neurotrophic factor (BDNF), neurotrophin-3 (NT3), neurotrophin-4/5 (NT4/5) and nerve growth factor (NGF) (Ebert et al., 2009, Corti et al., 2010, Wyatt and Keirstead, 2010).

Last but not least, outstanding progress has been achieved in the development of a gene therapeutic approach to treat SMA in the last two years. In three independent studies, researchers used the self-complementary adeno-associated virus 9 (scAAV9) for gene delivery into motor neurons of SMA mice by intravenous injection (Foust et al., 2010, Valori et al., 2010, Dominguez et al., 2011). Most strikingly, scAAV9-SMN was able to cross the blood brain barrier (BBB), highly efficiently transduced motor neurons in the lumbar region of the spinal cord as well as muscle tissue and rescued the survival phenotype.

2.2 PLS3 - a fully protective modifier of SMA

Typically, genetically caused diseases display a broad phenotypic variability among patients. The reasons for such variability include environmental as well as intrinsic genetic factors that might influence the severity. Genetic factors with impact on a certain disease phenotype are referred to as genetic modifying genes, or short modifiers. In multifactorial genetic diseases, modifications may comprise complex genetic networks which are often hard to dissect. Therefore, “monogenic” diseases provide unique opportunities to dissect components as they each have a single etiology, relatively uniform treatments, and the contribution of the disease-causing gene is usually known to some degree (Antonarakis and Beckmann, 2006, Cutting, 2010). Often, different mutations in one single gene account for a broad spectrum of disease variability. E.g., in one of the most prevalent genes causing deafness, *connexin 26* (CNX26), different mutations can result in either a recessive or a dominant inheritance mode (Rabionet et al., 2000). The finding, however, that patients with one and the same mutations often strongly vary in their phenotypic appearance suggests the existence of other modifying genes or variants.

For a long time, *SMN2* was the only known SMA-modifying gene with a strongly inverse correlation of *SMN2* copy number and SMA severity (Feldkotter et al., 2002). Interestingly, however, homozygously *SMN1*-deleted patients and parents have been reported who are completely healthy, whereas members of the same family carrying the identical genotype show SMA symptoms according to the *SMN2* copy number (Brahe et al., 1995, Cobben et al., 1995, Hahnen et al., 1995, Wang et al., 1996). The observation that siblings with identical

SMN2 copy number and homozygous absence of *SMN1* can show variable phenotypes has suggested that SMA is also modified by other unknown factors (Helmken and Wirth, 2000).

In 2008, the actin filament bundling protein PLS3 was identified as the first SMA modifying protein besides *SMN2* in a total of six discordant families (Oprea et al., 2008). In these discordant families, a small proportion of individuals homozygous for the absence of *SMN1* are fully asymptomatic despite carrying an identical number of *SMN2* copies as their affected siblings (mostly 3 – 4, reflecting SMA type III). Via differential gene expression (micro-array) analysis and as confirmed by qRT-PCR as well as protein analysis, *PLS3/PLS3* was then found to be highly upregulated in Epstein-Barr-virus (EBV)-transformed lymphoblastoid (LB) cell lines of unaffected individuals compared with their affected siblings. Expression of PLS3 in blood is very rare, as it could be shown only in ~5 % of healthy controls. Furthermore, by detecting high PLS3 levels in native blood of an unaffected individual, it was ruled out that PLS3 expression in LBs was induced by Epstein-Barr virus transformation. Further expression analysis showed, that PLS3 is highly expressed in fetal and adult human spinal cord, as well as brain and muscle.

To functionally dissect the working mechanism underlying PLS3 protection, PLS3 overexpression analysis was performed in *Smn*-depleted neuronal PC12 cells and primary mouse motor neuron cultures derived from SMA mice. In both cases, PLS3 was able to rescue axon outgrowth defects typically observed in the absence of *Smn*. Most strikingly, however, PLS3 overexpression led to a full rescue of axon defects in *smn* depleted zebrafish (*Danio rerio*) embryos. Since PLS3 mainly functions in actin bundling, G- to F-actin ratios were determined in LB cells of affected and unaffected siblings. Here, it has been found that unaffected *SMN1*-deleted siblings who highly expressed *PLS3* had significantly increased F-actin levels in LBs, as compared with their affected siblings who lack *PLS3* expression. Also when overexpressed in HEK cells, PLS3 activity resulted in a highly significant increase in F-actin levels. These findings, together with the observed rescue of axonal outgrowth defects *in vitro* and *in vivo*, suggest a model by which PLS3 might exert its rescuing effect through a stabilization of the actin cytoskeleton in motor neurons.

As revealed by 2 dimensional blue-native–polyacrylamide gel electrophoresis (2D-BN-PAGE), PLS3 has been observed to be present in one ~500 and another ~200 kDa complex together with *Smn* in murine spinal cord. These observations have further been supported by the finding of indirect PLS3/*SMN* interaction as demonstrated in co-immunoprecipitation (Co-IP) experiments. Based on their findings, the authors have speculated that PLS3, apart from the actin filament stabilizing effect, might exert additional functions in cooperation with *Smn* within the complex. Interestingly, only females seem to be protected by high *PLS3* expression, since Oprea et al. (2008) observed that males highly expressing *PLS3* displayed a phenotype as expected based on *SMN2* copy number.

Most strikingly, the *Drosophila melanogaster* and *Caenorhabditis elegans* orthologues of PLS3, *Fim* and *plst-1*, have been demonstrated to ameliorate disease severity also in these organisms, suggesting that PLS3 is a cross species SMA modifier (Dimitriadi et al., 2010) (see also chapter 2.2.4).

After PLS3 had been shown to act as a gender specific modifier of SMA by Oprea et al. in 2008, three more studies focusing on the aspect of PLS3 protection were published in the following years. In 2009, Bowerman et al. presented a study investigating the role of profilin IIa, an actin binding protein, in SMA pathology (Bowerman et al., 2009). As it has been demonstrated before also by others, the knockdown of profilin IIa alone results in stimulation of neurite outgrowth, while overexpression of profilin IIa reduces neurite number and size (Da Silva et al., 2003). Furthermore, SMN and profilin IIa directly interact, whereby SMN has been shown to moderate and restrict profilin IIa negative function on actin polymerization (Sharma et al., 2005). Interestingly, Bowerman et al. have detected increased profilin IIa levels in motor neurons of SMA mice and therefore speculated that negatively acting profilin IIa might be causative for axonal defects in SMA. Moreover, the researchers detected lower PLS3 protein levels in brain and spinal cord of the *Smn*^{2B/-} SMA mouse model, this finding being in line with the idea of a Pls3/Smn complex formation in mouse. To investigate a possible negative effect of profilin IIa on axon development *in vivo*, Bowerman et al. crossed the profilin IIa knockout (*pfn2*^{-/-}) into the *Smn*^{2B/-} SMA background, hoping to see an amelioration of the SMA phenotype. Interestingly, the authors have been able to show that Pls3 levels were restored in *Smn*^{2B/-};*pfn2*^{-/-} animals compared to *Smn*^{2B/-};*pfn2*^{+/+} mice, suggesting a modulation of plastin 3 levels by profilin IIa. Unfortunately, however, despite the restoration of Pls3 levels in *pfn2*^{-/-};*Smn*^{2B/-} animals, this did not result in an amelioration of the SMA phenotype. Therefore, Bowerman et al. speculate that in addition to profilin IIa and plastin 3, other components of actin dynamics are also affected in SMA, which would explain why the simple downregulation of profilin IIa or upregulation of Pls3 is not sufficient on its own to ameliorate the SMA phenotype (Bowerman et al., 2009).

In another study, it has been investigated whether PLS3 might serve more broadly as a biomarker for SMA severity (Stratigopoulos et al., 2010). To investigate this question, *PLS3* expression was measured in whole blood from 88 types I, II, and III SMA patients. A clear correlation between *PLS3* expression and SMA phenotype was detected in postpubertal females, whereas in prepubertal females as well as age matched male patients no such coincidence was observable. Therefore, the authors conclude that it is unlikely that *PLS3* expression alone will be a generalizable biomarker for SMA in most clinical trials.

A third study assessed *PLS* expression in EBV-transformed lymphoblastoid and fibroblast cell lines from four SMA discordant families (Bernal et al., 2011). Based on expression analysis using LB cell lines, PLS3 has been excluded as the protective factor for two of the

four families investigated. In contrast, in the other two families, *PLS3* levels were 8-9 fold increased in unaffected siblings when compared to affected siblings. When investigating *PLS3* levels in fibroblasts of discordant siblings, Bernal et al. found that the *PLS3* expression levels exceeded those of blood ~12-200-fold. Based on this observation, they pointed out that the subtle positive changes obtained in LBs of the asymptomatic individuals may reflect a similar situation in their motor neurons and nerves and should therefore be considered cautiously. To exclude that higher *PLS3* levels in LB cells of unaffected siblings resulted from immortalization, Oprea et al. in their study investigated native blood of an unaffected sibling and found a similar increase as in the respective LB sample. Likewise, Bernal et al. used native blood as a control for all of their discordant families. Interestingly, *PLS3* expression levels were different when comparing LB cell lines with native blood of the same patient's cell lines. Therefore, the authors speculated that at least in their study immortalization or another unknown factor may influence the regulation of *PLS3* expression (Bernal et al., 2011). In summary, the results of this study only partially confirm the data presented in Oprea et al., 2008.

2.2.1 *PLS3* gene

Human *PLS3* (NP_001129497), also called *T-plastin*, *fimbrin* or *plastin 3*, was first cloned in 1988 and is located on Xq23 spanning a region of ~90 kb (Lin et al., 1988). *PLS3* comprises 16 exons and produces three mRNA transcript variants (1,2 and 3). Despite differences in the 5'UTR, Splice variants 1 and 2 encode exactly the same 1893 bp transcript. Splice variant 3, however, uses an alternate in-frame splice site in the coding region, producing an 81 bp shorter mRNA of 1812 bp in size. Plastins are highly conserved from lower eukaryotes to humans, reflecting their important role in the cell (Klein et al., 2004, Delanote et al., 2005). Next to *PLS3*, two homologous genes exist in humans, I-plastin and L-plastin, which are encoded by distinct genes on chromosomes 3 and 13, respectively (Lin et al., 1993a, Lin et al., 1993b, Lin et al., 1994). Additionally, analyses of intron/exon borders revealed that all three human Plastins have emerged from one ancestral gene (Lin et al., 1993b).

2.2.2 *PLS3* protein

PLS3 consists of 630 aminoacids (aa) and has a predicted size of ~70 kDa. The original name for *PLS3*, *fimbrin*, derives from its first described association with surface structures such as membrane ruffles, microvilli, microspikes and focal adhesions in chicken embryo fibroblasts and cultured rat mammary cells (Bretscher and Weber, 1980, Delanote et al., 2005). *PLS3*, L- and I-Plastin show 70 % similarity on aa level. While *PLS3* is expressed in almost all solid tissue (including human brain, spinal cord and muscle (Oprea et al., 2008)) and usually not in the hematopoietic system, L-plastin is mainly found in cells of the

hematopoietic lineage. The expression of L-plastin, in contrast, is restricted to intestinal tissues only, as was demonstrated by expression analysis including humans and rat (Lin et al., 1994). PLS3 has a modular structure consisting of two N-terminal EF-hand domains (helix-loop-helix structural domains) and two actin binding domains (ABD1 and ABD2), each comprising two calponin-homology (CH) domains (Figure 2).

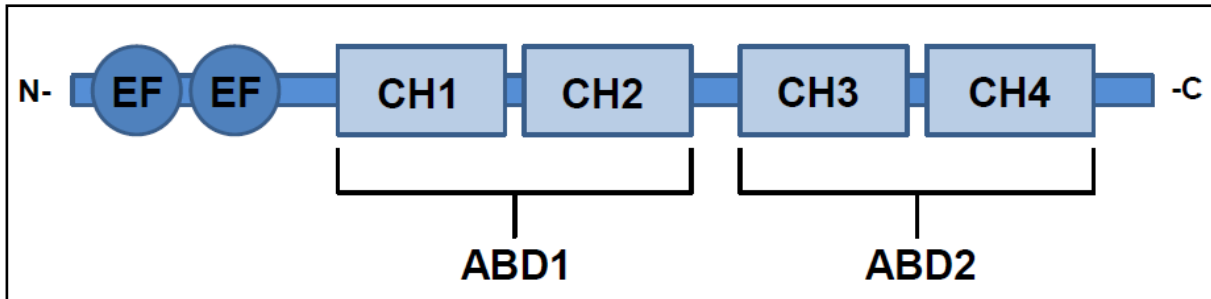


Figure 2: PLS3 protein structure: The 630 aa long protein has two N-terminal EF-hand domains followed by two actin binding domains (ABD1 and ABD2), each consisting of two calponin homology domains.

The EF-hand motif has a structure much like the spread thumb and forefinger of a hand, in which Ca^{2+} ions are coordinated by ligands within the loop. The CH domains are each composed of four α -helical segments. Three of the four helices form a loose bundle, while the fourth is oriented perpendicular to the major bundle.

The crystal structure of the complete PLS3 protein has not been determined yet, however, the fragmented parts including the N-terminal human ABD1 domain as well as the crosslinking core of *Schizosaccharomyces pombe* (*S.pombe*) and *Arabidopsis thaliana* (*A.thaliana*) have been resolved (Goldsmith et al., 1997, Klein et al., 2004). Recently, another study has been published in which the authors used cryo electron-microscopy (EM) and a single-particle approach to generate a 12-Å-resolution map of F-actin alone and F-actin decorated with the ABD2 domain of human L-plastin containing tandem CH-domains (Galkin et al., 2008). In their study the authors propose a working mechanism of PLS3 actin-bundling activity: Based on their findings, they propose that first ABD2 binds to one actin filament, which in turn “activates” ABD1 so that it may bind in a more ordered manner than that observed for free ABD1 to another actin filament with high affinity.

Based on crystallization experiments, it has been proposed that calcium binding to the N-terminal EF-hand domains of PLS3 might regulate its activity in actin bundling (Hanein et al., 1998). Based on calculations, the authors supposed that the EF-hand domains are needed for PLS/actin binding, however, calcium acts as a negative regulator in this interaction. Furthermore, by a digestion approach it was shown that a hot spot for proteolysis, between the putative EF-hands and the ABD1, becomes protease-resistant in the presence of calcium. Therefore, the authors followed that the observed calcium induced conformational change might be the mechanism behind the inhibition of PLS3/actin interaction (Hanein et al., 1998). In several studies the role of calcium in the regulation of plastin isoforms was

examined by studying the actin bundling activity of plastins at variable calcium concentrations. All three plastin isoforms show a rather weak homology regarding their calcium binding domains and this may suggest that their actin binding activities are differentially regulated by calcium (de Arruda et al., 1990, Delanote et al., 2005). L-plastin possesses all conserved and essential aa required for calcium binding and is indeed negatively regulated by calcium (Namba et al., 1992). Also I-plastin has been demonstrated to be negatively regulated by calcium. Despite above mentioned findings, however, a calcium dependent regulation of PLS3 is controversially discussed. Even though Hanein et al. showed conformational changes occurring in the ABD1-containing fragment of PLS3 in the presence of calcium, a regulatory influence of the calcium concentration on PLS3 activity was neither proven *in vitro*, nor *in vivo*. Moreover, another group showed that co-sedimentation of actin with T-plastin was not affected by free calcium concentrations of up to 2,2 $\mu\text{mol/l}$ (Giganti et al., 2005). Furthermore, in a depolymerization assay of the same study, calcium concentrations in the range of 4.6 nmol/L –1.6 $\mu\text{mol/L}$ had no impact on PLS3 activity. Also phosphorylation by protein kinase A (PKA) has been shown to influence L-plastin activity (Janji et al., 2006). However, although conserved, Ser7, has never been demonstrated to become phosphorylated in PLS3. Additionally, L-plastin binding activity to actin seems to be negatively regulated by increasing amounts of phospholipids, e.g. Phosphatidylinositol 4,5-bisphosphate (PIP_2) (Lebart et al., 2004). For I-plastin and PLS3, however, no such studies have been performed so far.

2.2.3 PLS3 function

PLS3 is an actin binding protein with its main function in actin filament cross-linking. Generally, plastins are located in focal adhesions, ruffling membranes, lamellipodia, filopodia, or in specialized surface structures with highly ordered microfilament bundles such as microvilli and stereocilia. Sometimes they co-localize with stress fibers (Bretscher and Weber, 1980, Delanote et al., 2005). PLS3 function in actin bundling and the consequences of overexpression have nicely been demonstrated *in vitro* in fibroblast-like CV-1 and epithelial LLC-PK1 cells (Arpin et al., 1994). In CV-1 cells, *PLS3* overexpression resulted in a rounding-up of cells, concomitantly with a significant reorganization of the actin cytoskeleton. In this regard, actin filaments became organized into polygonal networks in the cortical region of the cells. In LLC-PK1 epithelial cells, *PLS3* overexpression led to a high increase in length and density of brush border microvilli, particularly at the periphery of the cells. Furthermore, *PLS3* overexpression resulted in a significant diminution of focal contacts, presumably due to extensive remodeling of the actin cytoskeleton, implying a possible involvement of PLS3 in cell movement processes. Another study focused on the mechanism underlying PLS3 induced cytoskeletal rearrangements (Giganti et al., 2005). Here, beads were coated with the VCA domain of Wiskott/Aldrich-syndrome protein (WASP) to recruit the

actin-branching and polymerizing complex Arp2/3. This alone resulted in actin polymerization at the surface of the beads and movements of such when placed in cell-free extracts. Importantly, it was shown that PLS3 increased the velocity of VCA beads movement, stabilized actin comets and concomitantly displaced cofilin, an actin-depolymerizing protein. Since a mutated form of the ABD1 domain unable in cross-linking was sufficient to induce the above described effects, Giganti et al. propose a novel mechanism of action for PLS3 in which this protein might contribute to Arp2/3 mediated actin assembly independently of cross-link formation. In other words: PLS3 on the one hand stabilizes actin filaments through cross-linking and additionally triggers Arp2/3-mediated actin polymerization. Since the Arp2/3 complex nucleates a branched actin network found, e.g., in the lamellipodium at the leading edge of migrating cells, this fact highlights the significance of PLS3 function for protrusive membrane-outgrowth and more generally, cell motility. A role of PLS3 in cell motility was further confirmed in studies by Serio et al., who found that T-plastin is important for actin tail formation in the pathogenic bacteria *Rickettsia parkeri* (*R. parkeri*) and for its actin-based motility in mammalian cells (Serio et al., 2010). In line with this, PLS3 was shown to play an important role in invasion of the bacteria *Shigella flexneri* and *Salmonella typhimurium* (Prevost et al., 1992, Adam et al., 1995, Zhou et al., 1999a). In both cases, PLS3 causes actin cytoskeleton rearrangements in the host cells that lead to the formation of actin protrusions engulfing the bacteria and finally resulting in phagocytosis and uptake of the pathogen.

PLS3 was furthermore implicated to play a role in DNA repair and cell cycle control and consequentially also in cancer. By differential mRNA display, it has been demonstrated that PLS3 is 12-fold more abundant in cisplatin-resistant cell lines from bladder, prostatic, head and neck cancer (Hisano et al., 1996). In this regard, cisplatin is an anti-cancer drug intercalating with DNA and interfering with DNA-repair. Accordingly, the downregulation of PLS3 was found to be associated with higher cisplatin sensitivity. Additionally, the increased sensitivity of cancer cells to DNA interfering drugs as caused by *plastin3* downregulation, has also been shown for the Topoisomerase II-blocking agent VP-16 (Ikeda et al., 2005). In line with these findings, higher PLS3 levels were also detected in UV-radiation resistant cell lines (Higuchi et al., 1998). Also in Sézary syndrom, the most common form of cutaneous T-cell lymphoma, the presence of sézary cells was correlated with high levels of PLS3 in peripheral blood mononuclear cells (PBMCs) (Capriotti et al., 2008, Tang et al., 2010). Vice versa, PLS3 levels dropped upon chemotherapeutic treatment and completely disappeared after bone marrow transplantation in a patient. In another study, higher levels of PLS3 were correlated with G2-phase arrest upon X-radiation in Chinese hamster ovary (CHO) cells (Sasaki et al., 2002). However, when PLS3 was downregulated via antisense knockdown, radiation-induced G2 arrest was short and decreased in transfected cells. The authors have

therefore speculated that downregulation of PLS3 may be involved in cancer development through G2/M cell-cycle control in mammalian cells. These results highlight low levels of PLS3 as possibly causative for cancer development, different from the before mentioned findings, where high PLS3 levels were associated with cancerous state. Possibly, species- or cell type specific differences might explain these opposite observations. In this line, it is also unclear whether up- or downregulation of PLS3 in the various cancer forms is causative for, or is a result from cancer development. Next to PLS3, the L-plastin isoform is an even more prevalent cancer marker, since it is expressed in a high percentage of tumor-derived cells, but never in normal diploid cells of solid tissues (Leavitt and Kakunaga, 1980, Leavitt, 1994).

Apart from cancer, PLS3 is also involved in the human autoimmune disease systemic lupus erythematosus (SLE). In an animal model for this disease as well as in human patients, antibodies against L- and T-plastin were found in serum (De Mendonca Neto et al., 1992, Mine et al., 1998, Shinomiya et al., 2003, Delanote et al., 2005). However, it has to be determined in how far these antibodies contribute to the loss of cell function or other aspects of SLE.

Due to interaction with ataxin-2 (ATX2) in yeast and also murine brain, PLS3 has additionally been implicated in the regulation of RNA metabolism and translational pathway. In this context, ATX2 is known to interact with cytoplasmic poly(A)-binding protein (PABP) that functions in translation initiation and mRNA decay regulation and forms part of stress granules (Ralser et al., 2005a). The finding of an interaction of PLS3 and ATX2 has been further underlined by the observation of a stabilizing effect of ATX2 on PLS3 when overexpressed (Ralser et al., 2005b).

2.2.4 Other potential SMA modifiers – knowledge from invertebrates

There are several examples, where invertebrate modifier screens have identified conserved human disease-related genes and/or functional pathways (Kim, 2007, Schlegel and Stainier, 2007, Silverman et al., 2009). In this context, SMN orthologs are also present in *Drosophila melanogaster* (*D.m.*, *DmSmn*) and *Caenorhabditis elegans* (*C.e.*, *Cesmn-1*) and loss of function studies have revealed growth and neuromuscular defects as well as larval lethality in both organisms (Miguel-Aliaga et al., 1999, Chan et al., 2003, Rajendra et al., 2007, Chang et al., 2008, Briese et al., 2009).

In 2008, a study was set out to find modifying factors of SMA in the invertebrate model *D.m.* (Chang et al., 2008). In this screen, a total of 27 modifiers were identified able to rescue the lethal SMA phenotype. Surprisingly, despite the essential role of SMN in snRNP assembly, none of the modifying factors identified function in RNA processing. Moreover, three of the identified genes were orthologous to human BMP type II receptor (*BMPRII*), Fragile X relative protein 2 (*FXR2*) and dynein light chain LC8-type 2 (*DYNLL2*), all of which have been associated with functions at the NMJ (Aberle et al., 2002, Marques et al., 2002,

Pan et al., 2004). Interestingly, also high levels of the actin bundling protein α -actinin were associated with an enhancement of the SMA phenotype in this screen. In another study, RNAi knockdown of α -actinin was able to rescue the growth defects observed in *Cesmn-1* depleted *C.e.* (Dimitriadi et al., 2010). Therefore, the identification of α -actinin as another actin bundling protein with impact on SMA severity highlights the importance of cytoskeletal organization in SMA pathology.

In a second screen using *C.e.* as SMA model, 4 more modifiers were identified (Dimitriadi et al., 2010): nuclear cap binding protein 2 (*ncbp-2*), the predicted protein T02G5.3, G-protein coupled receptor kinase 2 (*grk-2*), and FMRF-like peptide family member (*flp-4*). Apart from T02G5.3, the other 3 genes are present as orthologs also in human. Since these candidates represent potential new targets for SMA therapy, their function should be further analyzed in the disease context in vertebrates. Furthermore, the *D.m.* and *C.e.* orthologs of PLS3, Fim and *plst-1*, were in the same study tested for their potential to modify the SMA phenotype. Most strikingly, Fim and *plst-1* were confirmed as SMA modifiers in both organisms, verifying the previous findings by Oprea et al. and suggesting that PLS3 is a cross species modifier of SMA.

2.3 Development of the neuromuscular system

NMJ pathology is one of the striking disease features in SMA mice and chronologically precedes motor neuron loss in the ventral horns of the spinal cord (Kariya et al., 2008, Murray et al., 2008, Kong et al., 2009). In the context of SMA, NMJ abnormalities include both pre- and postsynaptic defects, among these abnormal neurofilament (NF) accumulation in the nerve terminals, poor terminal arborization, immature plaque-like AChRs and embryonic γ -subunit containing forms of the receptor (Wyatt and Keirstead, 2010). In the present work, *PLS3* was overexpressed in SMA mice to test whether high levels of PLS3 are able to rescue the SMA phenotype, similar to the situation in humans (chapter 2.2). *PLS3* overexpression was shown to result in significant pre as well as postsynaptic changes at the NMJ of SMA mice. Therefore, an overview about fundamental processes driving axon growth and specification (axonal pruning) as well as NMJ development and refinement will be given in the following chapters.

2.3.1 The process of axonal pruning in NMJ refinement

In the present thesis, overexpression of PLS3 has been shown to delay axon withdrawal from the NMJ during the process of axonal pruning. How is axonal pruning defined and what is the mechanism underlying this developmental process?

Per definition, axonal pruning is a strategy to selectively remove exuberant neuronal branches and connections in the immature nervous system to ensure the proper formation of functional circuitry (Low and Cheng, 2006). Perinatally, individual AChR cluster are

innervated by numerous nerve terminals. During the axonal pruning process, all but one presynaptic connections are removed, so that finally one endplate gets innervated by one single motor nerve ending (Lichtman and Colman, 2000, Luo and O'Leary, 2005). It is assumed that 50 % of the postmitotic neurons of the vertebrate nervous system do not survive until adulthood. However, it is important to note that controlled apoptotic events in the context of neuronal plasticity are a phenomenon highly distinct from axonal pruning. Namely, axon pruning enables removal of exuberant or misguided axon branches in the absence of cell death, whereas other appropriate connections of the same neuron are maintained (Vanderhaeghen and Cheng, 2010).

Historically, the two most popular mechanisms to explain how these axons disappear were axon retraction and Wallerian-type degeneration. During axon retraction, axonal contents are believed to be shuttled to other axon branches, however, axon retraction has never been directly documented at the neuromuscular junction (NMJ) (Riley, 1981, Bishop et al., 2004). Alternatively, it was believed that axons might undergo a classical Wallerian-type degeneration, as has been suggested by ultrastructural data (Rosenthal and Taraskevich, 1977, Bishop et al., 2004). However, what speaks against this last mentioned possibility is that Wallerian-type degeneration usually removes entire axon arbors rather than a subset of axon's branches. As new tools with better spatial and temporal resolution have become available, these opportunities revealed a new and unexpected mechanism termed axosome shedding (Bishop et al., 2004). In the process of axon shedding, retreating axons leave behind dismantled bulbs at their tips. These bulbs are removed over time as they get subdivided into smaller remnants, termed axosomes. Most importantly, by fluorescent confocal microscopy it could be proven that engulfing Schwann cells incorporated axosome material, therefore actively driving axonal recycling (Bishop et al., 2004).

The molecular factors driving axonal pruning at the NMJ (small scale pruning) are largely unknown (Vanderhaeghen and Cheng, 2010). However, some molecules driving large scale axonal pruning (E.g. of neurons in the corticospinal tract (CST) or in the central nervous system (CNS)) have been identified. These molecules are subdivided into intrinsic and extrinsic proteins. As for intrinsic factors, e.g. the homeodomain transcription factor *Otx1* has been identified (Weimann et al., 1999). As major extrinsic factors hormones and trophic factors have been suggested, however, their effects are often broad and nonspecific (Vanderhaeghen and Cheng, 2010).

2.3.2 Actin dynamics in axon growth

It was demonstrated in the present work, that *PLS3* overexpression results in an increase of presynaptic nerve arborization and occupancy of AChR clusters at the NMJ. Furthermore, *PLS3* led to a delay in the axonal pruning process (chapter 2.3.1), indicating that *PLS3* might exert a positive effect on axonal integrity. To understand how *PLS3* accomplishes

“stabilizing” function on axons, a basic knowledge about fundamental mechanisms driving axonal growth and the involvement of the actin cytoskeleton in this process is required.

Axons grow out from the tip region of neurites, the so called growth cones. Growth cones are highly complex structures subdivided into three distinct zones (Figure 3): (i) The central zone (C domain), (ii) the intermediary transition zone (T domain) and (iii) the peripheral zone (P domain). In the central zone, microtubules enter from the axon shaft and polymerize. These filaments act mainly as transport system for organelles and vesicles into the growth cone.

The P domain represents the cortex of the growth cone and consists of actin filaments. Such filaments are crucial for the formation of filopodia (finger like protrusions containing bundled actin filaments) and lamellipodia (flattened, veil-like membrane extensions containing an unbundled actin network) (Stiess and Bradke, 2011). The T domain contains both, microtubules and actin filaments and the interplay between both systems leads to neurite extension (Schaefer et

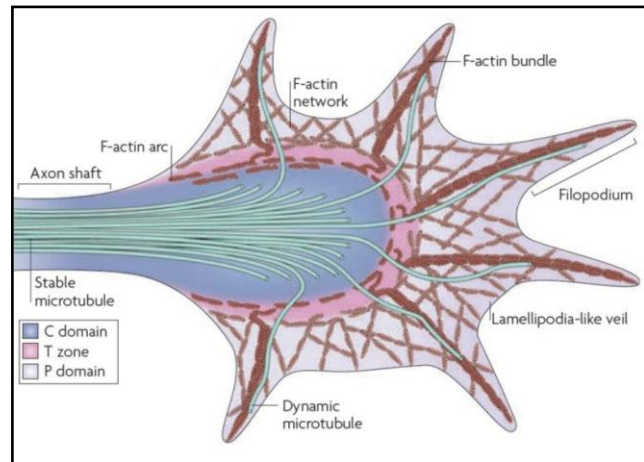


Figure 3 Structure of a growth cone at the distal tip of a neurite (Taken from (Lowery and Van Vactor, 2009)).

al., 2008, Stiess and Bradke, 2011). The process of axonal extension can be seen as a continuous repetition of the three phases protrusion, engorgement, and consolidation (Goldberg and Burmeister, 1986). During the protrusion phase, actin polymerizes in the P domain and filopodial/lamellipodial structures are formed and progress in the direction of outgrowth. The following engorgement phase is characterized by a disassembly of actin filaments in the T domain, which previously inhibited microtubules from entering the P domain. Finally, in the consolidation phase an actin free corridor is formed in the T domain so that microtubules can invade the P domain. Thereupon, vesicles and organelles can be transported into the newly formed area (Stiess and Bradke, 2011).

Today, a whole plethora of factors is known that act on actin dynamics and modulate axon growth. One important actin destabilizing factor (ADF) is Cofilin. Cofilin is present in the T zone of the growth cone and localizes to the pointed (-) end of actin filaments, where it severs and depolymerizes actin (Pak et al., 2008). This way, Cofilin regenerates the available globular actin (G-actin) pool, a necessary prerequisite for axon outgrowth. In line with this, it could be shown that overexpression of the active form of Cofilin triggered axon growth while depletion impaired axon formation (Garvalov et al., 2007). As it was mentioned earlier in this thesis (chapter 2.1.3), profilin IIa is another key component regulating axon dynamics and has even been proven to interact with SMN (Rossoll et al., 2002, Sharma et

al., 2005). Profilin IIa accelerates the ADP/ATP exchange in G-actin monomers. This way, profilin IIa is able to trigger the polymerization of Actin filaments. Against intuition, the polymerization of Actin per se does not account for enhanced axonal growth. Moreover, overexpression of profilin IIa resulted in reduced neurite outgrowth while the knockdown had the opposite effect (Da Silva et al., 2003). In this context, it has been demonstrated, indeed, that a more dynamic and less condensed actin cytoskeleton in the growth cone defines the future axon, whereas growth cones of designated neurites remain rather static and retain a rigid actin cytoskeleton (Bradke and Dotti, 1999, Kunda et al., 2001). Profilin IIa is activated by the Rho/Rock cascade. This pathway, in turn, is negatively controlled by plasma ganglioside sialidase (PMGS). The fact that profilin IIa is a negative regulator of axonal growth was further supported by the finding of high levels of PMGS in the designated axon during axon specification (Da Silva et al., 2005). While the described consequences of profilin IIa function suggest that actin polymerization acts negatively on axon growth, other examples exist where controlled actin polymerization is supportive for axon formation and elongation. The Wiskott-Aldrich syndrom protein (WASP) family is known to transduce signals from membrane receptors to the actin cytoskeleton. Through complex formation together with verprolin-homologous protein (VE), WASP and VE (WAVE) mediate actin polymerization via recruitment of the actin-related protein 2/3 (Arp2/3) complex (Takenawa and Suetsugu, 2007). In this context, the Arp2/3 complex closely resembles the structure of G-actin and serves as nucleation site for new actin filaments. In fact, the knockdown of Arp2/3 complex results in axonal growth defects (Takenawa and Suetsugu, 2007). Together, these results highlight the importance of actin dynamics (actin severing and polymerization) for correct axonal growth.

Next to actin polymerization or depolymerization, also the connections between actin filaments, as mediated by actin-crosslinking as well as branching proteins, are important for cytoskeleton dynamics and thus for axonal growth. Bundling proteins typically found in filopodia of growth cones e.g. include α -actinin, fascin, CamKII, Myosin, AblIM, Filamin as well as PLS3 (Letourneau and Shattuck, 1989, Lundquist et al., 1998, Cohan et al., 2001, Dent and Gertler, 2003, Okamoto et al., 2007, Oprea et al., 2008). The formation of filopodial structures requires the presence of parallel actin bundles, however, in lamellipodia actin is predominantly organized into a branched dendritic network. Therefore, actin branching proteins such as Arp2/3 complex are dominating in lamellipodia while actin bundling proteins are predominantly present in filopodia.

As it was indicated above, also the microtubule network has important function in axonal growth. Microtubules consist of alternating α/β -tubulin heterodimers and have a dynamic plus-end (+) and a less dynamic minus-end (-). At the (+)-end, microtubules polymerize (rescue) or shrink (catastrophe). Disturbance of proper microtubule function has in the past

been associated with defects in axonal growth and the other way around, the stabilization of microtubules in dendrites can initiate axon specification (Baas, 2002, Hoogenraad and Bradke, 2009).

Taken together, the Actin and microtubule network and their respective regulators are the key cellular systems in defining axon specification, growth and maintenance.

2.3.3 Acetylcholine receptor (AChR) pre patterning

Neuromuscular junctions (NMJ) are the contacts formed by a motor neuron's axon and a muscle target cell. The communication between nerve and muscle is established through neurotransmitter release from the presynaptic nerve terminal and receptor mediated signal perception and transduction at the postsynapse. The excitatory signals secreted by the presynapse vary between organisms. E.g., in *Drosophila* glutamate acts as the excitatory neurotransmitter, while in the vertebrate system Acetyl Choline (ACh) is presynaptically released and bound by ACh receptors (AChR) at the postsynaptic site. In vivo studies have shown that prior axon arrival AChRs cluster along the central region of muscle fibers in a process termed AChR-pre patterning (Lin et al., 2001, Yang et al., 2001). Supporting the idea of pre patterning, aneural AChR clustering was also observed in mice that lack phrenic or motor nerves (Yang et al., 2000, Wu et al., 2010). The muscle-specific receptor tyrosine kinase MuSK is required for both, aneural and neural clustering (Zhang et al., 2004, Wu et al., 2010). Interestingly, in *MuSK*^{-/-} mice the absence of aneural clusters is associated with nerve terminals straying from the central regions of muscle fibers (DeChiara et al., 1996, Lin et al., 2001, Yang et al., 2001, Zhang et al., 2004, Jing et al., 2009). These findings indicate an important role of AChR clustering in guiding axons to their distinct muscle targets. Regarding AChR pre patterning, it is important to mention that fundamental differences exist between species. While AChR pre patterning in mice and zebrafish seems to confine axonal guidance along the central muscle fiber region, there is no evidence for aneural clustering in *Drosophila melanogaster* *Caenorhabditis elegans* so far. In *Drosophila melanogaster*, motor neurons seek out target regions independently of the target cell while in *Caenorhabditis elegans*, motor neurons form so called "en passant" interactions with muscle arms actively searching for presynaptic terminals (Keshishian et al., 1996, Wu et al., 2010).

With ongoing development, axons innervate some but not all clusters, whereby the size of innervated clusters increases and primitive clusters will finally disappear.

2.3.4 The role of presynaptic signaling in AChR clustering and refinement

During the process of axonal pruning, all but one remaining nerve connection will disappear with ongoing development so that endplates become innervated by one single motor axon only. Also at postsynaptic level, clear morphological changes can be observed as axons are specified. As the NMJ matures, the size of innervated AChR cluster slowly

increases. Furthermore, the postsynaptic membrane invaginates to form junctional folds, and AChRs are concentrated only at the crests of the junctional folds, giving the synapse a characteristic pretzel-like appearance (Sanes and Lichtman, 2001, Wu et al., 2010). The process of NMJ assembly is orchestrated by positively and negatively acting factors, most important to mention here Agrin and Acetylcholine (ACh), respectively (Figure 4).

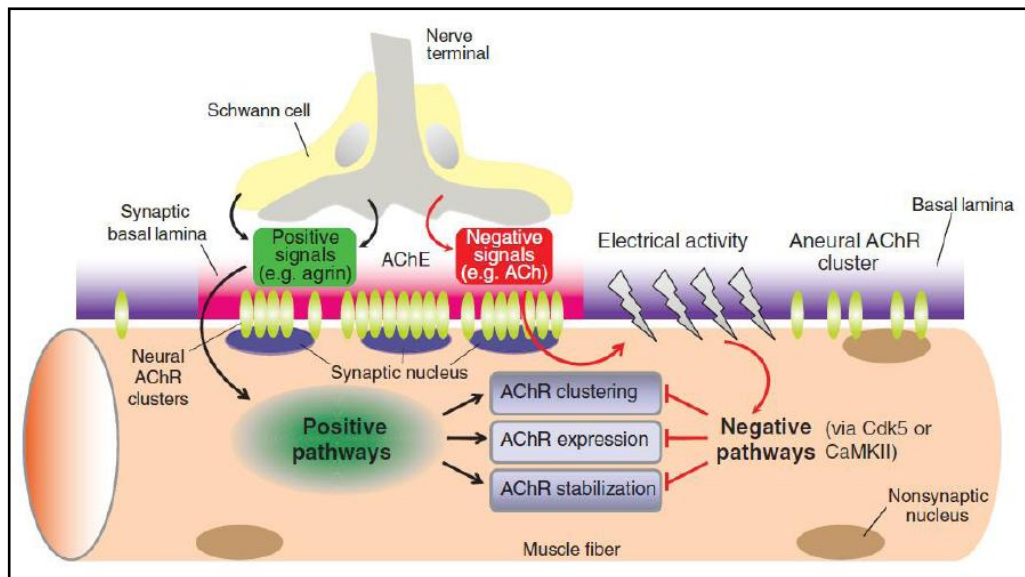


Figure 4: Circuitry in AChR clustering at the NMJ. Positive signals, such as Agrin-MuSK signaling, postsynaptically activate certain pathways that trigger AChR clustering, expression and stabilization. Counteracting negative signals, such as ACh stimulate the serine/threonine kinases cyclin-dependent kinase 5 (Cdk5) and Ca^{2+} /calmodulin-dependent kinase II (CaMKII) to inhibit AChR clustering, to suppress AChR expression and to destabilize AChR clusters in entire muscle fibers. Positive and negative signals together refine AChR clustering to sites of axonal innervation. (Taken from (Wu et al., 2010).

The most central pathway in NMJ assembly is the Agrin/Lrp4/MuSK pathway. Agrin is a glycoprotein synthesized in motor neurons and is transported along the axons to the nerve terminals where it is synaptically released. Agrin is the essential key player in the induction of AChR clustering and postsynaptic differentiation, a fact that has been proven by several different observations. In mice deficient for Agrin (*Agrin*^{-/-}), NMJs do not form with several postsynaptic marker proteins being absent and AChR dispersed throughout the mutant muscle fiber (Gautam et al., 1996). Interestingly, however, pre patterning of AChR still occurs indicating that this process is Agrin independent (Lin et al., 2001, Yang et al., 2001). Furthermore, Agrin is able to induce ectopic AChR clustering in adult muscle and elicits the formation of the postsynaptic apparatus in denervated muscle (Gesemann et al., 1995, Jones et al., 1997, Bezakova et al., 2001, Wu et al., 2010).

MuSK is a receptor tyrosine kinase and has been identified as a protein stringently colocalizing with AChR at NMJs (Valenzuela et al., 1995). In *MuSK*^{-/-} mice, NMJs do not form, no pre patterning of AChR is observable and also upon innervation AChR are evenly distributed throughout the muscle fiber (DeChiara et al., 1996, Lin et al., 2001, Yang et al.,

2001). Moreover, Agrin is not able to induce AChR clustering in *MuSK*^{-/-} mice, however, MuSK can restore Agrin sensitivity (Glass et al., 1996, Zhou et al., 1999b, Herbst and Burden, 2000). Together, these findings underline the necessity of interplay of both Agrin and MuSK in the formation of nerve-induced AChR clustering (Wu et al., 2010). Most interestingly, MuSK seems to represent an important factor for retrograde signaling from the post- to the presynapse. This assumption is based on the observation that *MuSK*^{-/-} mice exhibit highly branched and arborized motor neuron terminals, which is indicative for a role of MuSK in presynaptic differentiation (Wu et al., 2010).

As has been described, both Agrin and MuSK mediate AChR clustering in vertebrate NMJ formation. Nevertheless, a direct interaction between Agrin and MuSK has never been observed. Recently, Lrp4 was identified as a coreceptor of MuSK that can directly interact with Agrin (Kim et al., 2008). *Lrp4*^{-/-} exhibit NMJ defects closely similar to that observed in *MuSK*^{-/-} mice (Weatherbee et al., 2006). That Lrp4 is the long searched linker in Agrin mediated MuSK signaling was confirmed by studies demonstrating that Lrp4 is necessary for Agrin-induced MuSK activation and AChR clustering in cultured muscle cells (Kim et al., 2008, Zhang et al., 2008a, Wu et al., 2010). The downstream functions of MuSK signaling will be outlined in chapter 2.3.5.

Presynaptically released ACh is the main excitatory signal inducing muscle contraction in vertebrates and at the same time the most important negatively acting factor in NMJ assembly. The first evidence for ACh being a negative regulator of AChR clustering came from the observation that AChR grow faster and larger in mice deficient for choline acetyltransferase (ChAT), an enzyme essential for ACh biosynthesis (Misgeld et al., 2002, Brandon et al., 2003). Further functional analyses revealed that ACh activates the serine/threonine kinase cyclin dependent kinase 5 (Cdk5) or Ca²⁺/calmodulin-dependent protein kinase II (CaMKII) (Tang et al., 2001, Fu et al., 2005, Lin et al., 2005). These pathways have been connected with negative regulatory roles in AChR assembly, expression and stabilization. Importantly, the negative effect of ACh is global affecting the entire muscle fiber. Therefore, positive and negative outcome of Agrin-MuSK and ACh signaling, respectively, together accounts for the correct refinement of AChR clusters to positions of axonal innervation.

2.3.5 MuSK downstream signaling and the importance of cytoskeletal dynamics in AChR clustering

As it will be outlined in chapter 5.4.3.3, *PLS3* overexpression resulted in an increase in AChR cluster size when ubiquitously overexpressed in SMA mice. Importantly, motor neuron specific overexpression of *PLS3* was sufficient to increase endplate size, suggesting that increased presynaptic arborization and occupancy contribute to the endplate size increase. Nevertheless, based on the experiments performed in this work a muscle specific effect of

PLS3V5 cannot be entirely excluded. Indeed, cytoskeletal rearrangements in the muscle are a prerequisite for proper AChR clustering, suggesting that also muscle specific PLS3V5 might account for the observed increase in AChR size.

As it was explained in chapter 2.3.4, MuSK is indirectly activated by Agrin binding to its coreceptor Lrp4. Upon interaction and as a prerequisite for AChR clustering, MuSK is rapidly internalized via endocytosis (Zhu et al., 2008). One consequence of MuSK activation is the rearrangement of cytoskeletal structures. Such rearrangements are assumed to be pre-conditional for AChR anchorage and redistribution, as well as shaping postsynaptic membrane into folds opposed to presynaptic active zones (Dobbins et al., 2006). Upon Lrp4 mediated Agrin-MuSK interaction, tyrosine kinase Abl and the metalloenzyme geranylgeranyl transferase I (GGT) get activated. Both proteins in turn activate small GTPases of the Rho family (Weston et al., 2000, Weston et al., 2003). One target of Rho GTPases is p21 activated kinase (Pak1), a serine/threonine kinase that has been shown to phosphorylate and hence activate the actin binding protein Cortactin. Cortactin is located in the cytoplasm and promotes actin polymerization and rearrangements through interaction with the (Arp2/3) complex (see also chapter 2.2.3). The finding that Cortactin might act in Agrin-MuSK mediated cytoskeletal rearrangements is in line with previous reports showing an involvement of Cortactin in promoting lamellipodia formation, invadopodia formation, cell migration, and endocytosis (Kelley et al., 2010, Astro et al., 2011, Zhu et al., 2011). Moreover, it has been demonstrated that AChR clustering is directly regulated via Cofilin-directed vesicular trafficking (Lee et al., 2009). Next to Pak1, other targets of Rho GTPases have been identified that are actively involved in cytoskeletal rearrangements, among these Wiskott-Aldrich syndrome protein (WASP) family proteins, which activate the Arp2/3 complex and Rho-associated protein kinase (ROCK). ROCK is a key regulator of actin organization since it can phosphorylate a variety of effectors assumed in the regulation of the actin cytoskeleton, including LIM kinase, myosin light chain (MLC) and MLC phosphatase (Riento and Ridley, 2003).

Another important factor for neural and aneural AChR clustering is Rapsyn. Rapsyn has been shown to interact with AChR as well as the actin bundling protein α -Actinin in an Agrin-MuSK signaling dependent manner (Moransard et al., 2003, Dobbins et al., 2008). Therefore, it is assumed that Rapsyn anchors AChR to the Actin cytoskeleton and hence stabilizes AChR clusters. Furthermore, Agrin-MuSK signaling intensifies the interaction between Rapsyn and the chaperone heat shock protein 90 β (HSP90 β). Rapsyn is a very unstable protein, however, bound to HSP90 β the AChR/Actin linking function of Rapsyn might be preserved. Furthermore, also HSP90 β itself has been demonstrated to exert actin filament cross-linking activity. Additionally, Agrin binding strengthens the interaction of Rapsyn with the protease Calpain, resulting in a suppression of Calpain activity. Calpain, in turn, is

involved in the activation of Cdk5, a negative regulator of AChR clustering acting on cytoskeletal dynamics. Therefore, Rapsyn/Calpain interaction establishes another link between AChR clustering and cytoskeletal dynamics. Interestingly in this context is the finding, that Smn is a direct target of Calpain in muscle cells (Walker et al., 2008). Defects in synaptic release are a hallmark of SMA. Therefore, reduced Agrin amounts might indirectly account for an increased Smn turnover in muscle cells and contribute to the known muscular SMA phenotype. In other studies, Agrin was shown to induce the association of AChR with the tumor suppressor adenomatous polyposis coli (Apc) (Wang et al., 2003). Furthermore, this interaction turned out to be a necessary pre-requisite for AChR clustering. Apc itself is able to directly interact with Actin filaments and microtubules or to recruit further cytoskeleton-associated proteins (E.g. Asef, Iqgap1) to AChR, contributing to cytoskeletal rearrangement (Kawasaki et al., 2000, Watanabe et al., 2004, Wu et al., 2010).

The above mentioned downstream cascades following Agrin-mediated MuSK activation highlight the importance of cytoskeletal dynamics in the process of AChR clustering.

2.3.6 Mutations in NMJ genes cause myasthenic syndromes

In many of the above mentioned genes, mutations have been identified which are causative for the development of the neuromuscular disorder congenic myasthenic syndrome (CMS). Depending on the mutated gene, CMS are subdivided into three categories: Presynaptic (e.g. Choline acetyltransferase (*CHAT*), synaptic (Acetylcholinesterase collagenic tail peptide (*COLQ*)) and postsynaptic (e.g. Acetylcholine receptor (*ACHR*)). For all categories, different subtypes of CMS exist displaying highly variable phenotypic severity (Table 1). General clinical features of variable phenotypic strength and time of onset common to many CMS forms comprise muscle weakness accompanied by reduced mobility as well as swallowing and often respiratory problems (Barisic et al., 2011). The symptoms are often similar to Myasthenia Gravis (MG), with the difference that MG is an autoimmune disease with circulating antibodies mostly against the ACHR (~85 – 90 % of patients, (Guptill and Sanders, 2010)) and sometimes against the MUSK receptor (~8 %, (Sanders et al., 2003)).

MG therapy includes treatment with Acetylcholinesterase (ACHE) inhibitors or immunosuppressants (Angelini, 2011). In CMS, immunotherapy is not useful. Instead, AChE inhibitors and/or the potassium channel blocker 3,4-diaminopyridine (3,4-DAP), quinidine, fluoxetine or ephedrine have been shown to improve disease symptoms (Abicht and Lochmuller, 1993, Argov, 2009).

Table 1: Congenital myasthenic syndromes (CMS) with associated NMJ genes and clinical picture of the different types. White background: Presynaptic genes, light gray: synaptic genes, dark gray: postsynaptic genes (Abbreviations: **mNE** = mainly Northern European, **n.d.** = not determined)

Gene / OMIM Name	Type of CMS	Detection frequency	Population	Literature (exemplary)
Choline Acetyltransferase / <i>CHAT</i>	CMS-EA	< 3 % ¹	Diverse origin (mNE)	(Ohno et al., 2001)
Acetylcholinesterase collagenic tail peptide / <i>COLQ</i>	EAD	< 7,5 % ¹	Diverse origin (mNE)	(Donger et al., 1998, Ohno et al., 1998, Shapira et al., 2002, Yeung et al., 2010)
Acetylcholine receptor (AChR) subunits (α , β , δ , γ , ϵ) / <i>CHRNA1</i> , <i>CHRNB1</i> , <i>CHRND</i> , <i>CHRNG</i> , <i>CHRNE</i>	<i>CHRNA1</i> : FC/SCCMS, MPS (lethal type) <i>CHRNB1</i> : SCCMS, CMS ass. with ACHR deficiency <i>CHRND</i> : FC/SCCMS; MPS (lethal type) <i>CHRNG</i> : MPS, MPS (lethal type) <i>CHRNE</i> : MG, FC/SCCMS, CMS ass. with ACHR deficiency	<i>CHRNA1</i> ¹ : < 0,5 % <i>CHRNB1</i> ¹ : < 0,5 % <i>CHRND</i> ¹ : < 0,5 % <i>CHRNG</i> : < very rare, (<2X10 ⁵ in the US) <i>CHRNE</i> ¹ : 10 – 30 %	<i>CHRNA1</i> : Diverse origin (mNE) <i>CHRNB1</i> : Diverse origin (mNE) <i>CHRND</i> : Diverse origin (mNE) <i>CHRNG</i> : US citizens <i>CHRNE</i> : Roma/southeastern European individuals, The Maghreb (especially Algeria and Tunisia), Diverse origin (mNE)	<i>CHRNA1</i> : (Garchon et al., 1994, Engel et al., 1996, Wang et al., 1999, Michalk et al., 2008) <i>CHRNB1</i> : (Engel et al., 1996, Quiram et al., 1999) <i>CHRND</i> : (Gomez et al., 2002, Shen et al., 2002, Michalk et al., 2008) <i>CHRNG</i> : (Hoffmann et al., 2006, Morgan et al., 2006, Amalnath et al., 2011) <i>CHRNE</i> : (Uchitel et al., 1993, Ohno et al., 1995, Engel et al., 1996, Croxen et al., 2002)
Muscle-specific tyrosine kinase / <i>MUSK</i>	CMS ass. with ACHR deficiency	< 1 % ¹	Diverse origin (mNE)	(Chevessier et al., 2004, Mihaylova et al., 2009, Maselli et al., 2010)

Gene / OMIM Name	Type of CMS	Detection frequency ¹	Population	Literature (exemplary)
43 kDa receptor-associated protein of the synapse (Rapsyn) / <i>RAPSN</i>	CMS ass. with ACHR deficiency	< 10 % ¹	Diverse origin (mNE)	(Ohno et al., 2002, Muller et al., 2006, Gaudon et al., 2010)
Downstream of tyrosine kinase 7 / <i>DOK-7</i>	LGM	~ 1 % ¹	n.d.	(Rodolico et al., 2002, Beeson et al., 2006, Srouf et al., 2010)
Sodium channel, voltage gated, type IV, alpha polypeptide / <i>SCN4A</i>	HYPP, PMC, HOKPP2	< 0,5 % ¹	Diverse origin (mNE)	(Ptacek et al., 1991, Bulman et al., 1999)
Type of CMS	Clinical picture ²			
CMS-EA (Congenital myasthenic syndrome with episodic apnoea)	Sudden and recurrent episodes of apnoea, bulbar weakness precipitated by infection, fever, either neonatal onset respiratory distress with progressive improvement over time but then further respiratory relapses in adulthood, or late onset (during infancy or childhood) respiratory crises with a more unpredictable course of disease			
EAD (COLQ) (Endplate Acetylcholinesterase (AChE) deficiency)	Broad clinical heterogeneity (often severe) with early onset with progressive disability or later onset with much milder progression over the years, onset of symptoms in the neonatal period, evidence of delayed motor milestones, frequent early respiratory complications, sometimes needing ventilator support, ocular involvement, ptosis, ophthalmoparesis, pupillary reactions			
FCCMS (Fast channel congenital myasthenia gravis)	Caused by mutations in various ACHR subunits and reduced ACh responsiveness, sometimes decreased neonatal movements, contractures of both hands, neonatal hypotonia, weak cry, respiratory difficulties, poor feeding, fatigue, ptosis, ophthalmoplegia, facial weakness, weakness of the neck flexor muscles, high-arched palate, micrognathia, large ears			
HOKPP2 (Hypokalemic periodic paralysis type 2)	Onset in childhood to adolescence, hypokalemia, paralytic episodes of all limbs, infrequent but severe attacks, myotonia (sometimes temperature depending), muscle weakness			

Type of CMS	Clinical picture ²
HYPP (Hyperkalemic periodic paralysis)	Hyperkalemia, muscle weakness (periodic), myotonia (sometimes ocular), bidirectional cardiac dysrhythmia, facial dysmorphism, muscle hypertrophy, severe constipation, psychomotor delay, progressive myopathy
LGM (Limb-girdle myasthenia)	Often early onset, weakness within first 5 years of life, difficulty in walking, in adulthood proximal weakness in upper and lower limbs as well as neck and trunk, fatigue, ptosis, facial weakness, bulbar symptoms, respiratory difficulties
SCCM (Slow channel congenital myasthenia symptom)	Caused by mutations in various AChR subunits and, selective severe neck, wrist, finger extensor weakness Onset varies from childhood to adult, varies from mild to severe progressive, ventilatory insufficiency may require assisted ventilation
MPS (Multiple pterygium syndrome (prenatally lethal and Escobar))	Pterygia of the neck, elbows, and/or knees and joint contractures (arthrogryposis), small stature, scoliosis, flexion contraction of fingers, facial dysmorphism
PMC (Paramyotonia congenita)	Early childhood to adolescence onset, myotonia (increased by exposure to cold), intermittent flaccid paresis, not necessarily dependent on cold or myotonia, lability of serum potassium, nonprogressive nature, lack of atrophy or hypertrophy of muscles

1: Detection frequency based on individuals with CMS investigated in (Abicht and Lochmuller, 1993, Beeson et al., 2005, Engel and Sine, 2005, Amalnath et al., 2011)

2: Clinical manifestations of the different CMS types are very heterogenously and thus not exhaustively listed in this table. Taken from OMIM and (Lajoie, 1961, Gamstorp, 1963, Bradley et al., 1990, Abicht and Lochmuller, 1993, Bulman et al., 1999, Sugiura et al., 2000, Ohno et al., 2001, Miller et al., 2004, Barisic et al., 2005, Beeson et al., 2006, Hoffmann et al., 2006, Morgan et al., 2006, Gay et al., 2008, Mihaylova et al., 2008, Schara and Lochmuller, 2008, Selcen et al., 2008, Huze et al., 2009, Schara et al., 2010, Barisic et al., 2011)

3 Study Aims

Spinal muscular atrophy (SMA) is the leading genetic cause of infant death and caused by the homozygous loss of the *survival of motor neuron 1 (SMN1)* gene. A nearly identical copy gene, *SMN2*, possesses a C to T transition in exon 7, resulting in the disruption of an exonic splicing enhancer (ESE) and consequentially skipping of exon 7 in 90 % of the total transcript. However, *SMN2* still produces around 10 % full length (FL) transcript. Although *SMN2* does not fully compensate the *SMN1* loss, residual FL-*SMN2* is able to ameliorate SMA symptoms. Since *SMN2* copy number is variable in the population ranging from zero to a maximum of four per allele, SMA severity is inversely correlated with *SMN2* copy number. For a long time *SMN2* was the only known modifying gene of SMA. However, in 2008, the actin bundling protein *PLS3* was identified as another SMA modifying gene showing high upregulation in *SMN1*-deleted unaffected siblings of discordant SMA families. In a detailed functional study, *PLS3* has been found to rescue axonal outgrowth defects in neuronal cell cultures as well as in a zebrafish SMA model.

The main aim of the present study was to investigate whether *PLS3* overexpression is able to rescue the disease phenotype in an SMA mouse model. Using the Cre/*loxP* system, a V5-tagged version of human *PLS3 (PLS3V5)* should be targeted into the *Rosa26* locus in order to motor neuron (MN) specifically or ubiquitously express the transgene. Prior to further analysis, expression of *PLS3V5* on mRNA and protein level as well as the subcellular localization of the transgene should be analyzed in detail.

Since *PLS3* has been demonstrated to be unexpectedly overexpressed in the hematopoietic system of discordant SMA siblings, it was next planned to ubiquitously overexpress *PLS3V5* in the Hung SMA mouse model. In unaffected *SMN1*-deleted siblings of discordant families, *PLS3* overexpression fully compensates SMA symptomatic. To study the effects of *PLS3V5* overexpression on the clinical picture of SMA mice, motoric tests (tube test, righting reflex test) as well as weight and survival measurements should be performed.

It has been shown in the past that MN death and defects at the neuromuscular junction (NMJ) are a hallmark of SMA, finally resulting in atrophy of the muscles. To study the effects of *PLS3* overexpression on MN, NMJ and muscle development, detailed immuno-/histological analysis should be performed on these tissues (MN size, presynaptic connectivity, Acetylcholine receptor (AChR) cluster size, muscle fiber size). Furthermore, possible cell autonomous effects of *PLS3V5* overexpression should be studied by motor neuron specific activation of the transgene using the *Hb9-Cre* line.

The findings presented in this thesis provide new insights into the mechanisms underlying *PLS3*-mediated protection in unaffected SMA patients of discordant families. Furthermore, understanding *PLS3V5* function in the disease context might ultimately reveal new cellular pathways and potential candidate genes for the development of therapeutic strategies.

4 Materials and methods

4.1 Equipment

▪ Analytical balance	ARJ 120-4M	<i>Sartorius</i>
▪ Autoradiography cassette	Developer Cassettes	<i>Siemens</i>
	Avanti J-20XPI	<i>Beckman Coulter</i>
▪ Bacterial incubators		
▪ Standard	Kelvitron T	<i>Heraeus</i>
▪ Shaking	Innova 44	<i>New B.scientific</i>
▪ FACS	FACS Vantage SE	<i>BD</i>
▪ Cell counting chamber	Neubauer chamber	<i>Optik Labor</i>
▪ Cell incubator	Hera Cell 150	<i>Hereaus</i>
▪ Centrifuges	Allegra X22-R	<i>Beckman Coulter</i>
	5415 D	<i>Eppendorf</i>
	5415 R	<i>Eppendorf</i>
	Avanti J-20XPI	<i>Beckman Coulter</i>
	Concentrator 5301	<i>Eppendorf</i>
▪ Developer machines	Curix 60	<i>Agfa</i>
	DNA engine Tetrad 2	<i>MJ research</i>
▪ Electrophoresis chambers		
▪ Agarose gels	SGE-020-02	<i>CBS-scientific</i>
▪ SDS-PAA gels	Mini-Protean 3 cell	<i>Biorad</i>
	Protean II xi	<i>Biorad</i>
▪ Electroporation cuvettes	GP cuvettes, 0.4 cm	<i>Biorad</i>
▪ Electroporation system	Gene pulser Xcell	<i>Biorad</i>
▪ Embedding apparatus	EG 1150c	<i>Leica</i>
▪ Flattening table	HI 1220	<i>Leica</i>
▪ Floating water bath	FBC 620	<i>FischerBrand</i>
▪ Geiger counter	LB 1210B	<i>Berthold</i>
▪ Glass staining chamber		
▪ Glaskasten		<i>Roth</i>
▪ Färbegestell		<i>Roth</i>
▪ Drahtbügel		<i>Roth</i>
▪ Heating block	HTMR-133	<i>HLC</i>
▪ Hot plate magn. stirrer	MR 3000	<i>Heidolph</i>
▪ Imaging system	ChemiDoc XRS	<i>Biorad</i>
▪ Microplate reader	Safire ²	<i>Tecan</i>
▪ Microscopes		

▪	Fluorescent microscope Axioplan 2	<i>Zeiss</i>
▪	Inverted microscope DMIL	<i>Leica</i>
▪	Confocal microscope TCS-SP	<i>Leica</i>
▪	Confocal microscope META 510	<i>Zeiss</i>
▪	Stereo microscope S8 APO	<i>Leica</i>
▪	Microwave Micro combi	<i>Bosch</i>
▪	Multi channel pipettes	
•	12 channel pipette	<i>Finpipette</i>
•	8 channel pipette 4780	<i>Eppendorf</i>
▪	pH-meter pH Level 1	<i>Inolab</i>
▪	Photometer cuvettes UV-Vette	<i>Eppendorf</i>
▪	Pipettes 0.5-10 μ l	<i>Eppendorf</i>
	2-20 μ l	<i>Eppendorf</i>
	10-100 μ l	<i>Eppendorf</i>
	20-200 μ l	<i>Eppendorf</i>
	100-1000 μ l	<i>Eppendorf</i>
▪	Power supplies PowerPac 1000	<i>Biorad</i>
	PowerPac HC	<i>Biorad</i>
	Protean II xi	<i>Biorad</i>
▪	Real time thermocycler Light cycler 1.5	<i>Roche</i>
▪	Rotary Microtome RM2255	<i>Leica</i>
▪	Shaker 3015	<i>GFL</i>
	VS.R23	<i>Grant BOEHEL</i>
▪	Spectrophotometer BioPhotometer	<i>Eppendorf</i>
	Nanodrop ND-1000	<i>Peqlab</i>
▪	Staining chamber Rotilabo [®]	<i>Roth</i>
▪	Thermocycler GeneAmp 9700	<i>Applied Biosystems</i>
	DNA engine Tetrad 2	<i>MJ research</i>
▪	Tissue culture hood Hera Safe	<i>Hereaus</i>
▪	Tissue processor TP 1020	<i>Leica</i>
▪	Vacuum pump BVC 21	<i>Vacuubrand</i>
▪	Vibratomes Vibratome Series [®] 1000	<i>Pelco</i>
	VT 1200 S	<i>Leica</i>
▪	Water bath par. sections HI 1210	<i>Leica</i>
▪	Western blot chambers Mini-Protean 3 cell	<i>Biorad</i>
	Protean II xi	<i>Biorad</i>

4.2 Chemicals

If available, chemicals used in this work were purchased as purity grade “pro analysis”. For RNA isolation and analysis only RNase-free chemicals were used. Most chemicals and reagents were purchased from the following companies:

▪ Applichem	Darmstadt	<i>Germany</i>
▪ GE Healthcare	Freiburg	<i>Germany</i>
▪ Life science (formerly Invitrogen)	Leek	<i>Netherlands</i>
▪ Merck	Darmstadt	<i>Germany</i>
▪ Perkin Elmer	Rodgau-Jügesheim	<i>Germany</i>
▪ Promega	Mannheim	<i>Germany</i>
▪ Qiagen	Hilden	<i>Germany</i>
▪ Roche Molecular Biochem.	Mannheim	<i>Germany</i>
▪ Roth	Karlsruhe	<i>Germany</i>
▪ Sigma Aldrich	Taufkirchen	<i>Germany</i>

Frequently used chemicals include:

▪ 2-Propanol	<i>Applichem</i>
▪ Acetic acid	<i>Applichem</i>
▪ Chloroform : Isoamyl alcohol 24:1	<i>Applichem</i>
▪ Ethanol (EtOH)	<i>Applichem</i>
▪ Glycerol	<i>Applichem</i>
▪ Hydrochloric acid (37 %, HCL)	<i>Applichem</i>
▪ Methanol (MeOH)	<i>Applichem</i>
▪ Phenol	<i>Applichem</i>
▪ Potassium acetate (KAc)	<i>Applichem</i>
▪ Sodium acetate, anhydrous (NaAc)	<i>Sigma</i>
▪ Sodium Chloride (NaCl)	<i>Applichem</i>
▪ Sodium hydroxide (NaOH)	<i>Applichem</i>
▪ Tris (hydroxymethyl)-aminomethane (TRIS)	<i>Applichem</i>
▪ TRIZMA-base	<i>Sigma</i>
▪ Xylol	<i>Applichem</i>

4.3 Reagents for molecular biology

4.3.1 Reagents for DNA work

▪ 100 bp & 1 kb DNA ladder	<i>Applichem</i>
▪ Agarose	<i>Sigma</i>
▪ dNTPs	<i>Peqlab</i>

- Ethidiumbromide *Applichem*
- Oligo d(T) primers 0.5 µg/µl *Fermentas*
- Proteinase K *Sigma*
- 10 x PCR buffer (from Taq kit) *Invitrogen*
- 50 mM MgCl₂
- TBE-10x-buffer *Applichem*

4.3.2 Reagents for radioactive DNA work

- Hybond XL membrane *GE-Healthcare*
- Probe Quant G50 micro columns *GE-Healthcare*
- Salm sperm DNA *Merck*
- α-[³²P]-dCTP radioisotope *Perkin Elmer*

4.3.3 Reagents for protein work

- Ammoniumpersulfate (APS) *Applichem*
- Aqua plus (29:1) Acrylamide *Applichem*
- Bromphenolblue *Applichem*
- Complete Mini Protease Inhibitor *Roche*
- Glycin *Applichem*
- Nitrocellulose membrane *Protran*
- Non fat dried milk powder *Applichem*
- Page Ruler Plus *Fermentas*
- Ponceau S *Sigma*
- Restore Western Blot Stripping Buffer *Pierce*
- RIPA-buffer *Sigma*
- SuperSignal West Pico ECL Substrate *Pierce*
- Tetramethylethylenediamine (TEMED) *Applichem*
- Whatman paper *Hartenstein*

4.3.4 Reagents for work with bacteria

- Ampicilin
- Bacto tryptone
- Bacto yeast extract

4.3.5 Reagents for cell culture

- 1x PBS Dulbecco w/o Ca²⁺, Mg²⁺, low endotoxin *Biochrom*
- Amphotericin B *Gibco*
- BacilloI® *Bode*
- Dimethylsulfoxide (DMSO) *Sigma*

▪ Disposable Filter Unit 0.2 µm FP30/0.2 CA-S	<i>Whatman</i>
▪ DMEM (+D-Glucose, +L-Glutamine, #41966)	<i>Gibco</i>
▪ DMEM (+D-Glucose, +Sodiumpyruvate, #10829-018)	<i>Gibco</i>
▪ DMEM high Glucose (4.5 g/l) – Glutamine (E15-009)	<i>PAA</i>
▪ DMEM high Glucose (4.5 g/l) + stable Glutamine (E15-883)	<i>PAA</i>
▪ Fetal Calf Serum (FCS, S0115)	<i>Biochrom AG</i>
▪ Gelatine (2 %)	<i>Sigma</i>
▪ Geneticin (G418-Sulfate)	<i>Gibco</i>
▪ Leukemia inhibitory factor 1000x (LIF)	<i>Embl</i>
▪ L-Glutamin (100 x), 200 mM	<i>Invitrogen</i>
▪ Mitomycin C (MMC)	<i>Sigma</i>
▪ Non essential amino acids 100x (NEA)	<i>Invitrogen</i>
▪ PenStrep (Penicillin Streptomycin)	<i>Invitrogen</i>
▪ RPMI transfection-buffer (w/o Phenol red)	<i>Gibco</i>
▪ Sodiumpyruvate 100mM (1000x)	<i>Invitrogen</i>
▪ Trypsin-EDTA-Solution	<i>Sigma</i>
▪ β-Mercaptoethanol 1000x (ME)	<i>Merck</i>

4.3.6 Reagents for histo- and immunohistochemical methods

▪ Acidic Eosin Y	<i>Sigma</i>
▪ Bovine serum albumine (BSA)	<i>Invitrogen</i>
▪ Cresyl violet acetate (Nissl)	<i>Sigma</i>
▪ Hard set mounting media (w/o DAPI)	<i>Vectashield</i>
▪ Hematoxylin	<i>Sigma</i>
▪ Horse serum (HS)	<i>Invitrogen</i>
▪ Mowiol® mounting media	<i>Polysciences, Inc.</i>
▪ Normal goat serum (NGS)	<i>Invitrogen</i>
▪ Paraformaldehyde (PFA)	<i>Riedel de Haen</i>
▪ Triton X-100	<i>Applichem</i>
▪ Tween-20	<i>Applichem</i>

4.3.7 Kits

- BCA Protein Assay Reagent *Pierce*
- EndoFree Plasmid Maxi Kit *Qiagen*
- LightCycler FastStar DNA Master SYBR green I *Roche*
- Qiagen MiniPrep Kit *Qiagen*
- QIAquick Gel Extraction Kit *Qiagen*
- QiaQuick PCR Purification Kit *Qiagen*
- QIAshredder *Qiagen*
- Quant-iT RiboGreen RNA assay Kit *Invitrogen*
- QuantiTect Reverse Transcription Kit *Qiagen*
- Rediprime™_{ML} Random Prime Labeling System *Ge Healthcare*
- RNase-free DNase I Set *Qiagen*
- RNeasy Mini Kit *Qiagen*
- SuperSignal West Pico ECL Substrate *Pierce*
- QIAEX II gel extraction system *Qiagen*
- BigDye Terminator V1.1 Sequencing Kit *Applied Biosystems*
- pcDNA3.1/V5-His Topo TA Expression kit *Invitrogen*

4.4 Enzymes

All enzymes were used with buffers recommended by the respective company

4.4.1 Restriction enzymes

▪ Asc I	<i>NEB</i>
▪ Bam HI	<i>NEB</i>
▪ Eco RI	<i>NEB</i>
▪ Eco RV	<i>NEB</i>
▪ Hind III	<i>NEB</i>
▪ Kpn I	<i>NEB</i>
▪ Nco I	<i>NEB</i>
▪ Not I	<i>NEB</i>
▪ Not I	<i>NEB</i>
▪ Pst I	<i>NEB</i>
▪ Xho I	<i>NEB</i>

4.4.2 Other enzymes

▪ Platinum [®] Taq DNA Polymerase High Fidelity	<i>Invitrogen</i>
▪ RNase A	<i>Qiagen (19101)</i>
▪ RNase-free DNase I	<i>Qiagen (79254)</i>
▪ Shrimp alkaline phosphatase I (SAP I)	<i>NEB (R0569)</i>
▪ T4 DNA-ligase	<i>Roche (481220)</i>
▪ Taq DNA Polymerase Recombinant	<i>Invitrogen</i>

4.5 Material for the work with mice

4.5.1 Mouse dissection equipment

▪ Cutfix Sterile Scalpel (5518040)	<i>Aesculap</i>
▪ Dissecting forceps (BD047R)	<i>Aesculap</i>
▪ Ear tags (1005-1)	<i>National Band & Tag Co.</i>
▪ Iris and ligature scissors (BC 100R)	<i>Aesculap</i>
▪ Micro forceps (FM002R)	<i>Aesculap</i>
▪ Micro scissors, Spring type (FD012R)	<i>Aesculap</i>
▪ Operating scissors (BC 321R)	<i>Aesculap</i>
▪ Splinter forceps (BD302)	<i>Aesculap</i>
▪ Splinter forceps curved (BD312)	<i>Aesculap</i>
▪ Surgical scissors (BC 341R)	<i>Aesculap</i>
▪ Tag applicator (1005-s1)	<i>National Band & Tag Co.</i>

4.5.2 Reagents for Embryo transfers / Cryoconservation

- | | |
|--|--------------|
| ▪ 100 Sterican | <i>Braun</i> |
| ▪ Gonadotropin from pregnant mare serum (PMSG) | <i>Sigma</i> |
| ▪ Human Chorionic Gonadotropin (hCG) | <i>Sigma</i> |
| ▪ Omnifix [®] -F 1 ml | <i>Braun</i> |

4.6 Antibodies

4.6.1 Primary antibodies and staining reagents

- | | |
|--|-----------------------------|
| ▪ α -bungarotoxin labeled with rhodamine (B35451) | <i>Invitrogen</i> |
| ▪ α -Choline Acetyltransferase (ChAt), goat (Ab144, Ab144P) | <i>Millipore</i> |
| ▪ α -GAPDH, monoclonal IgG1 (50A19A-1) | <i>Imgenex</i> |
| ▪ α -Neurofilament M (160kDa, MAB5254), rabbit | <i>Millipore</i> |
| ▪ α -Neurofilament, monoclonal (2H3-c) | <i>Hybridoma Bank</i> |
| ▪ α -RPL13a1, goat (sc-160039) | <i>Santa Cruz</i> |
| ▪ α -SMN, monoclonal IgG1 (S55920) | <i>BD Transduction Lab.</i> |
| ▪ α -Synaptic vesicle 2, monoclonal (SV2-c) | <i>Hybridoma Bank</i> |
| ▪ α -V5, monoclonal (R960CUS) | <i>Invitrogen</i> |
| ▪ α -V5, rabbit (ab9116) | <i>Abcam</i> |
| ▪ α -V5-HRP, monoclonal (R96125) | <i>Invitrogen</i> |
| ▪ α - β -actin, monoclonal IgG2a (A2228) | <i>Sigma</i> |
| ▪ α - β -tubulin, monoclonal IgG1 (T4026) | <i>Sigma</i> |

4.6.2 Secondary antibodies

- | | |
|--|-------------------|
| ▪ HRP-conjugated goat α -mouse IgG (115035000) | <i>Dianova</i> |
| ▪ HRP-conjugated goat α -rabbit IgG (31460) | <i>Pierce</i> |
| ▪ Donkey α -goat Alexa 568 IgG (H+L) (A11057) | <i>Invitrogen</i> |
| ▪ Donkey α -rabbit Alexa 568 IgG (H+L) (A10042) | <i>Invitrogen</i> |
| ▪ Donkey α -goat Alexa 488 IgG (H+L) (A11055) | <i>Invitrogen</i> |
| ▪ Goat α -mouse Alexa 488 IgG (H+L) (A10667) | <i>Invitrogen</i> |
| ▪ Donkey α -rabbit Alexa 350 IgG (H+L) (A10039) | <i>Invitrogen</i> |
| ▪ Goat α -rabbit Alexa 488 IgG (H+L) (11034) | <i>Invitrogen</i> |
| ▪ Goat α -mouse Alexa 568 IgG (H+L) (A11004) | <i>Invitrogen</i> |

4.7 Solutions and media

4.7.1 Frequently used solutions

Diethylpyrocarbonate (DEPC) treated H₂O (for 1 l):

DEPC	1 ml
Deionized H ₂ O	to a final volume of 1 l
→ Mix overnight and autoclave	

Phosphate buffered saline (PBS, 10 x, for 1 l):

NaCl	80.0 g
KCl	2.0 g
Na ₂ HPO ₄	14.4 g
KH ₂ PO ₄ (pH 7.3)	2.4 g
deionized H ₂ O	to a volume of 800 ml
→ adjust pH to 7.4	
deionized H ₂ O	to a final volume of 1 l
→ autoclave	

Sodium Dodecyl Sulfate (SDS) solution 10 % (for 100 ml):

SDS	10.0 g
deionized H ₂ O	to a final volume of 100 ml
→ dilute at 65°C, store at room temperature	

Tris-HCl (1 M, pH 6.8, for 400 ml):

Tris-HCl	60.0 g
deionized H ₂ O	to a final volume of 400 ml
adjust pH to 8.5 with concentrated HCl	

4.7.2 Cell culture media

All cell culture media were stored at 4°C. Freezing-media was used immediately. MMC-solution was aliquoted and frozen at -20°C. MEF- and ES cell culture was performed using media without addition of antimicrobial substances.

Murine embryonic fibroblast (MEF) media (Feeder for ES cell culture):

DMEM (E15-883, PAA)	500 ml
FCS (S0115, Biochrom)	70ml
Sodium pyruvate (100 x)	6 ml

Embryonic stem cell (ES) media (free of antibiotics and fungicides):

DMEM (E15-009, PAA)	500 ml
FCS (S0115, Biochrom)	90 ml
L Glutamine (100 x)	6 ml
LIF (1000 x)	1.2 ml
NEA (100 x)	6 ml
Sodium pyruvate (100 mM)	6 ml
β-mercaptoethanol	1.2 ml

Common Murine embryonic fibroblast (MEF) media:

DMEM (41966, Invitrogen)	500 ml
Amphotericin B (250 µg/ml)	1.4 ml
FCS (S0115)	50 ml
PenStrep (10 U/ml)	7 ml

Freezing media for MEF cells (for 1 ml):

DMSO	0.1 ml
FCS (S0115)	0.9 ml

Freezing media for ES cells (for 1 ml):

DMSO	0.2 ml
FCS (S0115)	0.8 ml

Mitomycin C (MMC) solution:

MEF media (w/o antimicrobials)	100 ml
MMC	1.0 g

4.7.3 Solutions for bacterial work

LB-Media (pH 7.5, for 2 l):

Bacto Trypton	20 g
Bacto yeast extract	10 g
NaCl	10 g

→ adjust pH to 7.5, autoclave and store at 4°C

LB-Agar (for 500 ml):

LB Media	500 ml
Agar	7.5 g

→ autoclave and store at 4°C

4.7.4 Solutions for the work with DNA

DNA loading buffer (10 x, for 50 ml):

0.1 % Brom phenol Blue	0.05 g
1% SDS	2.5 ml 20 % SDS
100 mM EDTA (pH 7.2-8.5)	10 ml 0.5 M EDTA (pH 7.2-8.5)
50 % Glycerol	28.7 ml 87 % Glycerol
Deionized H ₂ O	to a final volume of 50 ml

dNTP mix (for 1 ml):

dNTP (100 mM)	12.5 µl of each dNTP
Deionized H ₂ O	to a final volume of 1000 µl

Tail-tip lysis buffer (pH 7.4) (for 500 ml):

EDTA (0,5 M)	5ml
NaCl (5 M)	20 ml
SDS (20 %)	5 ml
Tris/HCl (1 M, pH 8.5)	50 ml
Deionized H ₂ O	to a final volume of 500 ml
Proteinase K (200µg/ml)	separately added to each approach

TBE buffer (5 x): for 1 l:

Tris base (445 mM)	54 g Tris base
Borate (445 mM)	27.5 g Boric acid
EDTA (10 mM)	20 ml 0.5 M EDTA (pH 8.0)
deionized H ₂ O	to a final volume of 1000 ml

TE⁻⁴ buffer (for 100 ml):

Tris (1 M, pH 8.0)	1 ml
EDTA (0.5 M, pH 8.0)	20 µl
deionized H ₂ O	to a final volume of 100 ml
RNAse A (50 µg/ml)	separately added to each approach

4.7.5 Solutions for Southern blottingPrehybridization mix (for 20 ml):

deionized H ₂ O	2 ml
EDTA (0.5 M, pH8)	40 µl
NaH ₂ PO ₄ (1 M)	10 ml
Sonicated and denatured Salm sperm DNA	1 ml add freshly (10 mg/ml)
SDS (20 %)	7 ml

Salm sperm DNA (10 mg/ml, for 100 ml):

Salm sperm (sonicated)	1 g
TE buffer (pH 8.0)	99 ml

→ Solve over night, store at 4°C

TE buffer (for 100 ml):

Tris/HCl (1 M, pH 8)	1 ml
EDTA (pH 8, 0.5 M)	0.2 ml
deionized H ₂ O	to a final volume of 100 ml

→ autoclave

Wash buffer:

Wash I:

SSC (20 x)	100 ml
SDS (10 %)	10 ml
deionized H ₂ O	to a final volume of 1 l

Wash II:

SSC (20 x)	10 ml
SDS (10 %)	10 ml
deionized H ₂ O	to a final volume of 1 l

→ Heat buffers to 68°C prior use

4.7.6 Solutions for Western blottingAmmonium Persulfate (APS) solution (10 %, for 10 ml):

APS	1.0 g
deionized H ₂ O	to a final volume of 10 ml

Blocking solution (6 %, for 100 ml):

Nonfat dry milk	6 g
TBS Tween buffer	to a final volume of 100 ml

Bradford solution (for 1l):

Coomassie Brilliant Blue G250	100 mg
H ₃ PO ₄ (85 %)	100 ml
Ethanol (95 %)	50 ml
deionized H ₂ O	to a final volume of

Electrophoresis buffer (10 x, for 1 l):

Tris-Base	30.29 g
Glycine	144.13 g
SDS	10.0 g
deionized H ₂ O	to a final volume of 1 l

Laemmli buffer for SDS PAGE (2x, for 100 ml):

Tris-Base	0.757 g
Glycerol	20 ml

Brom phenol Blue	10 mg
SDS	6 g
deionized H ₂ O	to a final volume of 90
β-Mercaptoethanol (prior to use)	10 ml

Ponceau solution (for 100 ml):

0.5 % Ponceau S	0.5 g
1 % Acetic acid glacial	1 ml
deionized H ₂ O	to a final volume of 100 ml

RIPA buffer (for 50 ml):

NaCl (150 mM)	1.5 ml 5 M NaCl
IGEPAL (1 %)	5 ml 10 % IGEPAL
Deoxycholic acid (DOC) (0.5 %)	2.5 ml 10 % DOC
SDS (0.1 %)	0.5 ml 10 % SDS
50 mM Tris (pH 8.6)	2.5 ml 1 M Tris (pH 8.6)
deionized H ₂ O	to a final volume of 50 ml

Separation gel for SDS PAGE (12 %, for 1 gel):

deionized H ₂ O	1.7 ml
acrylamide-bisacrylamide mix (29:1, 30 %)	2.0 ml
Tris (1.5M, pH 8.8)	1.3 ml
SDS	0.05 ml of 10 % SDS
APS	0.05 ml of 10 % APS
TEMED	0.002 ml

Stacking gel for SDS PAGE (for 1 gel):

deionized H ₂ O	0.68 ml
acrylamide-bisacrylamide mix (29:1, 30 %)	0.17 ml
Tris (1 M, pH 6.8)	0.13 ml
SDS (10 %)	0.01 ml
APS (10 %)	0.01 ml
TEMED	0.001 ml

TBS Tween buffer (for 5 l):

Tris (20 mM)	12.1 g
NaCl (137 mM)	40.0 g
Tween 20 (0.5 %)	25 ml
deionized H ₂ O	to a final volume of 5 l
→ adjust to pH 7.56	

Transfer buffer (for 5 l):

Tris-Base	12.1 g
Glycine	56.3 g
Methanol	1000 ml
deionized H ₂ O	to a final volume of 5 l

Tris-HCl (1 M, pH 6.8, for 400 ml):

Tris-HCl	60.0 g
deionized H ₂ O	to a final volume of 400 ml
→ adjust pH to 6.8 with concentrated HCl	

Tris-HCl (1.5 M, pH 8.8, for 400 ml):

Tris-HCl	90.5 g
deionized H ₂ O	to a final volume of 400 ml
→ adjust pH to 8.8 with concentrated HCl	

4.7.7 Solutions for histo- and immunohistochemical workBlocking (cell-stainings, for 20 ml):

NGS	1 ml
BSA	1 g
PBS	to a final volume of 20 ml

Blocking (paraffin sections, for 20 ml):

NGS (5 %)	1 ml
BSA (5 %)	1 ml
TBS	to a final volume of 20 ml

Blocking (Vibratome sections, for 200 ml):

Triton X 100 (20 %)	7 ml
DMSO (1 %)	2 ml
BSA (2 %)	4 g
PBS	to a final volume of 200 ml

Citrate buffer (0.01 M, pH 6.0, for 1 l):

Citrate monohydrate	2.1 g
deionized H ₂ O	to a final volume of 900 ml
→ adjust pH to 6.0	
deionized H ₂ O	to a final volume of 1 l
→ store at 4°C	

Cresyl violet acetate (Nissl) solution (for 1 l):

Cresyl violet acetate	5 g
deionized H ₂ O	to a final volume of 1 l

4 % Paraformaldehyde (PFA) in PBS (pH 7.3, for 1 l):

PFA	40 g
deionized H ₂ O	to a volume of 900 ml
→ adjust pH to 7.3	
deionized H ₂ O	to a final volume of 1 l
→ Aliquot and store at -20°C	

TBS (pH 7.5, 10 x, for 1 l):

NaCl	87.66 g
Tris	12.11 g
deionized H ₂ O	to a volume of 900 ml
→ adjust pH to 7.5	
deionized H ₂ O	to a final volume of 1 l

4.8 Primer

Primers were individually designed and purchased by Metabion in lyophilized form. Upon arrival, lyophilized primers were diluted to 100 pmol/μl stock solutions using deionized autoclaved water. Working solutions were obtained by diluting stock solutions to a final concentration of 10 pmol/μl.

Table 2: Primers for cloning a V5-tagged version of *PLS3* into the *Rosa26* targeting vector

Transcript / Description		Sequence (5' - 3')	ID#	Name	Annealing / Amplicon length
<i>PLS3</i> / Amplification of <i>PLS3</i> -coding sequence (cds)	for	GAGGTGCAGAAGTTGTCTGA	2454	Plst.3T_ex.1-2_fw	55°C / 1968 bp
	rev	CACTCTCTTCATTCCCCTGC	2586	PI_NO_stop_rev	
<i>PLS3V5</i> / Colony PCR	for	TAATACGACTCACTATAGGG	1840	T7	55°C / 721 bp
	rev	GTTGATTGCTCTTTCATCAATG	2457	Plst.3T_ex.3-4_rev	
<i>PLS3V5</i> / Amplification of <i>PLS3V5</i> with Asc I - overhang primers	for	GGCGCGCCACCATGGATGAGA TGGCTACCACTC	3289	AscI-PLS3 For	55°C / 2047 bp
	rev	GGCGCGCCTCAATGGTGATGG TGATGATGACCGGTA	3290	AscI-PLS3 REV	
<i>PLS3V5</i> with Asc I restriction overhangs / colony PCR	for	TGGTGACAGGAATAAAGATG	2456	Plst.3T_ex.3-4_fw	55°C / 1112 bp
	rev	ACTGTAAGATTACCAGGGCATC	2463	Plst.3T_ex.9-10_rev	

Table 3: *PLS3V5*-sequencing primer

Transcript	Sequence (5' - 3')		ID#	Name	Annealing
<i>PLS3V5</i>	for	GAGGTGCAGAAGTTGTCTGA	2454	Plst.3T_ex.1-2_fw	55°C
	for	TGGTGACAGGAATAAGATG	2456	Plst.3T_ex.3-4_fw	
	for	TGACCTGTTCAAAGCTGTTG	2458	Plst.3T_ex.5-6_fw	
	for	ATCATTAAGATCGGTTTGTTCG	2460	Plst.3T_ex.7-8_fw	
	for	GGACAAAAGGAAGGTGAACC	2462	Plst.3T_ex.9-10_fw	55°C
	for	TGAAGAAAGAACCTTCCGTAAC	2464	Plst.3T_ex.11-12_fw	
	for	ACTTTAGCTTTAGTCTGGCAGC	2466	Plst.3T_ex.13-14_fw	
	rev	CCTTCTTTCCTGTTGATTGC	2455	Plst.3T_ex.1-2_rev	
	rev	GTTGATTGCTCTTTCATCAATG	2457	Plst.3T_ex.3-4_rev	
	rev	TAAGTTCCTCCAAAGTCTCACC	2459	Plst.3T_ex.5-6_rev	
	rev	TGCAACCTAATTTATCTGCTTG	2461	Plst.3T_ex.7-8_rev	
	rev	ACTGTAAGATTACCAGGGCATC	2463	Plst.3T_ex.9-10_rev	
	rev	GTCGTCATTGGCTTTCTGAC	2465	Plst.3T_ex.11-12_rev	
	rev	AGAGCATACACTCTGGCTCC	2467	Plst.3T_ex.13-14_rev	

Table 4: Primers used in qRT-PCR

Transcript / Description	Sequence (5' - 3')		ID#	Name	Annealing / Amplicon length
<i>Hprt1</i>	for	TCAGTCAACGGGGGACATAAA	4118	musHprt1F1	63°C / 142 bp
	rev	GGGGCTGTACTGCTTAACCAG	4119	musHprt1R1	
Murine / human <i>PLS3</i>	for	ATGAGCTTGATGAACTCAA	4092	PLS3olFor1	66°C / 107 bp
	rev	TGGCATATTAGCTTCCTTGA	4093	PLS3olRev1	
murine <i>Pls3</i>	for	AGCTGATCTGTTTCAGCACACC	3301	Pls3_Mus_3_cDN A_for	63°C / 95 bp
	rev	ATACAAAGCAAGCCGGAATG	3302	Pls3_Mus_3_cDN A_rev	
<i>PLS3V5</i>	for	GCCAAGTATGCAGTGTCATG	3913	PLS3 RT For1.2	66°C / 230 bp
	rev	CCGAGGAGAGGGTTAGGGATAGG	3911	PLS3 RT Rev1	
<i>Rpl13a1</i>	for	TTCGGCTGAAGCCTACCAGA	4116	musRpl13aF3	63°C / 146 bp
	rev	CAAGATCTGCTTCTTCTTCC	4117	musRpl13aR3	

Table 5: Genotyping-primers

Inbred strain	Gene/ Transcript		Sequence (5' - 3')	ID#	Name	Annealing/ Amplicon length
SMA-Hung	WT <i>Smn</i>	for	ATAACACCACCACTC TTA CTC	3370	HungSMA_mouse _wt/Mut_fw_S1	59°C / 1050 bp
		rev	GTAGCCGTGATGCCATT GTCA	3372	HungSMA_mouse _wt_rev_H1	
	Hung KO	for	AGCCTGAAGAACGAGAT CAGC	3371	HungSMA_mouse _wt_rev_S2	59°C / 950 bp
		rev	ATAACACCACCACTCTTA CTC	3370	HungSMA_mouse _wt/Mut_fw_S1	
	<i>hSMN2</i> tg	for	CGAATCACTTGAGGGCA GGAGTTTG	3375	HungSMA_mouse _tghSMN2_fw_2F	59°C / 479 bp
		rev	AACTGGTGGACATGGCT GTTCATTG	3376	HungSMA_mouse _tghSMN2_rev_2 B	
PLS3V5	PLS3V5 rec	for	AAAGTCGCTCTGAGTTG TTATC	3650	Typ_forw	56°C / 380 bp
		rev	GATATGAAGTACTGGGC TCTT	3649	TYP_rev_wt	
	PLS3V5 wt	for	AAAGTCGCTCTGAGTTG TTATC	3650	Typ_forw	56°C / 576 bp
		rev	TGTCGCAAATTAAGTGTG AATC	3648	TYP_rev_CAGS	
Stop- cassette	Stop-in	for	AGGGTTTCCTTGATGAT GTCA	3988	<i>Rosa1</i> Stop for1	59°C / 505 bp
		rev	CATCAGGGGCTCGCGCC	3989	NeoStatRev	
	Stop-out	for	AGGGTTTCCTTGATGAT GTCA	3988	<i>Rosa1</i> Stop for1	59°C / 412 bp
		rev	CCTTCTTTCCTGTTGATT GC	2455	Plst.3T_ex.1- 2_rev	
CMV-Cre	<i>Cre</i>	for	CGCATAACCAGTGAAAC AGCAT	3104	Credel_fw	60°C / 600 bp
	<i>Cre</i>	rev	GAAAGTCGAGTAGGCGT GTACG	3105	Credel_rev	
<i>Hb9-Cre</i>	<i>Cre</i>	for	GTCCAATTTACTGACCGT ACACC	3140	Hb9Cre_fw	60°C / 704 bp
	<i>Cre</i>	rev	GTTATTCGGATCATCAGC TACACC	3141	Hb9Cre_rev	60°C / 704 bp

4.9 Generated plasmids / GVOs

The following Plasmids have been generated and were used in the context of this work. All insert sequences have been verified by sequencing.

Table 6: Plasmids generated and used in this study

Name	Vector backbone	GVO # / Description	Antibiotic	Colony PCR primer #	Product size (bp)
<i>PLS3</i> in Topo3.1V5/His, correct orientation	pcDNA3.1V5 / His Topo	500 / <i>PLS3</i> in pcDNA3.1V5/His in frame with tags	Amp Neo	1840 and 2457	721
<i>PLS3V5</i> Asc I in Topo zero blunt K2 180807	Zero blunt Topo	502 / <i>PLS3V5</i> with Asc I restriction overhangs in Zero blunt Topo	Kan Zeocin	2456 and 2463	1106
<i>PLS3V5</i> Asc I in <i>Rosa26</i> K1 20.09.07	<i>Rosa26</i> CAGS targeting vector	503 / <i>PLS3V5</i> cloned into <i>Rosa26</i> CAGS targeting vector	Amp Neo	2533 and 2459	864
<i>Rosa26</i> Sonde cut EcoRI BamHI KII	pCR Topo	501 / <i>Neo</i> probe cloned into pCR Topo	Amp Kan	no primers	-

4.10 Software, internet programs and databases

- | | |
|--|----------------------------|
| ▪ AxioVision Rel.4.7 (fluorescence imaging) | <i>Zeiss</i> |
| ▪ CellQuest | <i>BD</i> |
| ▪ Chromas 2.22 | <i>Technelysium Ltd</i> |
| ▪ EndNote9/X2 (reference organization) | <i>Thomson Research</i> |
| ▪ Lasergene Package (Sequence analysis) | <i>DNASTar Inc.</i> |
| ▪ Leica LCS confocal software | <i>Leica</i> |
| ▪ LightCycler Software (qRT-PCR analysis) | <i>Roche</i> |
| ▪ LSM 510 confocal working software | <i>Zeiss</i> |
| ▪ Office 2003/2007 (word processing etc.) | <i>Microsoft</i> |
| ▪ Photoshop CS (image editing) | <i>Adobe</i> |
| ▪ Quantity One 4.5.1 (densitometric analysis) | <i>Biorad</i> |
| ▪ Sequence Detection Software (qRT-PCR analysis) | <i>ABI</i> |
| ▪ SigmaPlot 9/10 (creation of graphs) | <i>Systat Software Inc</i> |
| ▪ Vector NTI | <i>Invitrogen</i> |
| ▪ XFluor4Safire ² software (platerreader) | <i>Tecan</i> |

- Ensembl <http://www.ensembl.org/>
- Gene Expression Atlas database <http://www.ebi.ac.uk/gxa/>
- Genecards <http://www.genecards.org/>
- Medline <https://www.ncbi.nlm.nih.gov/pubmed>
- NCBI <http://www.ncbi.nlm.nih.gov/>
- OMIM <http://www.ncbi.nlm.nih.gov/omim>
- UCSC <http://genome.ucsc.edu/>

4.11 Molecular biology methods

4.11.1 Working with DNA

4.11.1.1 Isolation of genomic DNA from tissue

To isolate DNA from tissue, the respective tissue (mostly tail tips) was incubated in 493 μ l lysis buffer + 7 μ l Proteinase K (200 μ g/ml) at 55°C o.n. until the tissue was completely resolved. Next, the samples were centrifuged for 5 min at 13.200 rpm. to sediment residual hair. The supernatant was transferred into a fresh 1.5 ml tube and 500 μ l of RT isopropanole were added to precipitate DNA. Tubes were then centrifuged for 10 min at 13.200 rpm to pellet the DNA. The supernatant was again discarded and the pellet was rinsed with 700 μ l 70 % EtOH to remove residual salts. After another centrifugation step for 10 min at 13.200 rpm, the EtOH was removed and the pellet was air-dried in a sterile incubator for 30 min. Finally, the pellet was resuspended in an adequate volume of TE⁻⁴/RNase (e.g. 70 μ l). 1 μ l of the DNA solution was used for subsequent genotyping PCR reactions. To obtain highly purified DNA, as it was needed for Southern blotting, phenol/chloroform extraction was performed (chapter 4.11.1.4).

4.11.1.2 Isolation of genomic DNA from cells

Attaching cells were first washed with PBS and then trypsinized using 1 x Trypsin solution for 5 min at 37°C in a sterile incubator. After trypsinization, the cells were transferred into an adequate collection tube and centrifuged for 5 min at 1200 rpm. Another washing step with 1 x PBS was added and the resulting pellet resolved in 493 μ l lysis buffer + 7 μ l Proteinase K. All subsequent steps were performed as in chapter 4.11.1.1.

4.11.1.3 Determination of DNA concentration

To determine DNA concentrations, the respective DNA solution was measured using the NanoDrop ND-1000 spectrophotometer (*Peqlab*). After blank with solvent, 1.5 μ l of DNA solution were applied. Absorptions at wavelengths of 260 and 280 nm were measured utilizing a path length of 0.2 mm. Next to the concentration, purity grade was automatically determined as the ratio of measured absorption at the wavelength of 260 nm and 280 nm.

The optimum range was between 1.8 and 2.0 whereby higher ratios indicate RNA contamination and lower ratios indicate protein- or EtOH contamination.

4.11.1.4 Phenol/chloroform extraction

Genomic DNA isolated from tissues is highly enriched with proteins. Since protein content can interfere with subsequent reactions, e.g. restriction digestions or sequencing, phenol/chloroform extraction was applied after DNA isolation. By building hydrogen bonds and via hydrophobic interactions, phenol is able to bind to denatured proteins. This property makes it possible to separate the organic from the aqueous solution. In brief, the protocol included the following steps: First, the supernatant of the cell lysate was mixed with an equal volume of phenol/chloroform (1:1) in a Phase Lock Gel™ Heavy tube. The tube was incubated for 5 min on a rotator, centrifuged for 5 min at 13.200 rpm and the aqueous supernatant transferred into a fresh Phase Lock Gel™ Heavy tube. An equal amount of chloroform was added to the solution to extract remaining phenol and another centrifugation step for 5 min at 13.200 rpm was performed. The purified DNA solution was transferred into a fresh 1.5 ml tube. Next, 3 Vol. of ice-cold 100 % EtOH together with 1/10 Vol. of 3 M NaAc (pH 5.2) were added to precipitate the solution o.n. at -20°C. The next day, tubes were centrifuged for 20 min at 13.200 rpm and the resulting pellet was washed once in 70 % EtOH. After another centrifugation step the pellet was air-dried and resuspended in an appropriate Vol. of TE⁻/RNase. Phenol/chloroform extraction was also applied to linearized plasmid prior to ligation and transfection of ES cells.

4.11.1.5 Agarose gel electrophoresis

The principle of gel electrophoresis is the size dependent separation of DNA fragments in a gel matrix applying an electric field. Since the ribose-phosphate backbone of DNA is negatively charged the DNA migrates towards the cathode (+ pole) in the electric field.

1 % standard gels were prepared by solving 2.0 g of agarose in 200 ml of 1 x TBE buffer under constant heating in a microwave. After cooling of the clear solution to about 50-60°C, ethidiumbromide was added to a final concentration of 1 µg/ml.

The solution was then poured into an appropriate gel tray with a well comb fixed properly and placed in the 4°C room. After solidifying, the gel tray was transferred into an electrophoresis chamber and covered with 1 x TBE. The comb was removed and PCR samples were supplemented with 5 µl of loading dye. The DNA solution was carefully pipetted into the slots and the gel was run at 120 V. When the respective bands were nicely separated, as controlled by using a UV hand lamp, the gel was documented using the ChemiDoc XRS Imaging system (*Biorad*).

4.11.1.6 Purification of DNA fragments out of agarose gels

To purify DNA fragments out of an agarose gel, the respective DNA band was cut out using a scalpel and transferred into a 1.5 ml tube. Normally, the QIAEX II gel extraction- and the QIAquick Gel Extraction Kit were used following the manufacturer's instructions. This method was used for the purification of PCR amplified fragments, probes for Southern blotting or vectors prior to cloning.

4.11.1.7 Polymerase chain reaction (PCR)

The polymerase chain reaction is an enzymatic method to specifically amplify certain regions of single-stranded DNA using sequence specific oligonucleotides (primers) (Mullis KB, 1986). For DNA amplification the thermostable and so called *Thermophilus aquaticus* (Taq) DNA polymerase was used. Starting from the 3'- end, Taq polymerase is able to synthesize complementary DNA sequences from single stranded template DNA. The PCR reaction consists of a series of the three steps denaturation, primer-annealing and elongation, termed cycles. An example of a typical cycling sequence is given in Table 7. Annealing temperatures of primers depend on the CG/AT content of the individual primer and the elongation time on the amplicon size, whereby Taq has an amplification speed of ~1 kb /1 min.

Table 7: Example of a typical thermocycler program

Step	Temperature [°C]	Duration
1.) Initial denaturation	95	10 min
2.) Denaturation	94	30 sec
3.) Annealing	XX (depending on primers)	
4.) Elongation	72	XX (depending on amplicon size)
Cycle to step 2 for 35 repetitions		
5.) Final extension	72	10 min

Typically, amplification volumes had a size of 25 µl for genotyping reactions and up to 80 µl for amplification of fragments to be cloned. An example for a standard 25 µl genotyping PCR reaction is given in Table 8.

Table 8: Example of a typical 25 µl genotyping PCR reaction

Component	Amount
dNTPs (200 µM of each, dATP, dCTP, dGTP, dTTP)	4 µl
MgCl ₂	0.75 µl
Forward primer (10 pmol)	1 µl
Reversed primer (10 pmol)	1 µl
10 x reaction buffer	2.5 µl
Taq polymerase (1 U)	0.2 µl
DNA	1 µl (or minimum 100 – 200 ng)
H ₂ O to a final volume of 25 µl	

4.11.1.8 Sanger sequencing

Underlying the Sanger method of DNA sequencing (Sanger F, 1977) is the use of dideoxynucleotide triphosphates (ddNTPs). When incorporated into an elongating DNA strand, ddNTPs terminate the PCR amplification reaction. In principle, a PCR reaction is performed with a mixture of DNA primer, a Taq DNA polymerase, normal deoxynucleotidephosphates (dNTPs), and modified ddNTPs. Each of the four ddNTPs is labeled with a different fluorescent dye allowing the identification of the final nucleotide by capillary electrophoresis. In this work, the BigDye Terminator V1.1 Sequencing Kit (*Applied Biosystems*) was used strictly following the manufacturer's instructions.

4.11.1.9 Enzymatic restriction digestion

Enzymatic restriction digestion was frequently used in site specific cloning reactions, for test restrictions of cloned plasmids or for restriction of genomic DNA prior to Southern blotting. Restriction endonucleases cut double- or single stranded DNA by hydrolyzing phosphodiester bonds between two nucleotides. The recognition nucleotide sequences specific for each of the different enzymes are termed restriction sites. For digestion of plasmids 2-5 µg and for genomic DNA 5-20 µg of DNA were restricted o.n. in a water bath at 37°C. To increase efficiency, a three-fold enzymatic excess was used for plasmid restriction. For genomic DNA restriction, an even 5-fold enzymatic excess was used in the reaction. Additionally, spermidin and DTT were added to the reaction when genomic DNA was digested. A typical example of a restriction reaction for plasmid and genomic DNA is given in Table 9.

Table 9: Exemplary restriction digestion reactions for 1.) plasmid and 2.) genomic DNA

Component	Amount
1.) Plasmid restriction (total Volume = 30 µl)	
Plasmid	2-5 µg
10 x buffer	3 µl
100 x BSA (if necessary)	0.3 µl
Enzyme	3 U / 1 µg of plasmid DNA
H ₂ O to a final volume of 30 µl	
2.) Genomic DNA restriction (total Volume = 50 µl)	
DNA	5-20 µg
10 x buffer	5 µl
100 x BSA	0.5 µl
DTT (1 M)	0.05 µl
Spermidine (1 M)	0.05 µl
Enzyme	5 U / 1 µg of genomic DNA
H ₂ O to a final volume of 50 µl	

4.11.1.10 Ligation of DNA fragments

Ligation reactions were carried out using T4-DNA ligase (*Roche*). This enzyme catalyzes the joining of two DNA strands between the 5'-phosphate and the 3'-hydroxyl groups of adjacent nucleotides in either a cohesive-ended or blunt-ended configuration. For ligation reactions, 5 U of T4-DNA ligase were mixed together with the respective vector and insert (molar ratio of 1:3, 200 ng of vector standard amount) as well as 1.5 µl of 10 x ligase buffer provided by the company and added to a total volume of 15 µl. The approach was incubated in a thermocycler o.n. at 16°C. Typically, 5 µl of the ligation reaction was used for the transformation of 1 vial TOP 10 cells.

4.11.1.11 Southern blotting

Via Southern blot technique, enzymatically restricted DNA is transferred to a nylon membrane and target fragments are detected via radioactively labeled DNA probes (Southern, 1975). In this work, Southern blotting was employed for the verification of correct insertion of the *Rosa26* targeting vector into its destined genomic region in ES cell clones and transgenic animals. Following preceding digestion of genomic DNA using *EcoR* I, two different probes were used to prove correct insertion of the *Rosa26* targeting construct: 1.) An external probe, termed *Rosa* probe, which binds 5' of the targeting construct in the intrinsic genomic region. This probe allows the detection of correct insertion into the *Rosa26* locus. 2.) An internal probe, called *Neo* probe, which binds in the *Neomycin* cassette of the targeting construct. Using this probe, random integration of the targeting construct into the genome could be detected. The phenomenon of random integration is strictly to avoid since insertion into other genes or their promoter regions can disrupt correct gene function.

4.11.1.12 Restriction and transfer of genomic DNA on a nylon membrane

Before genomic DNA of ES cells or tail tips was transferred to the nylon membrane it was digested with *EcoR* I o.n. (chapter 4.11.1.9) and separated on a 0.7 % agarose gel o.n. at 20-30 V. Prior to the transfer, a picture of the gel was taken using the ChemiDoc XRS Imaging system. The DNA standard was delineated by stitching through the gel using a 200 µl pipette tip. Before the transfer, the gel was carefully placed in 0.125 M HCl on a swinging incubator for 10 min to depurinate and break DNA into smaller pieces. In the next step, the gel was transferred to 0.4 M NaOH and incubated on a swinging incubator for another 20 min. This step is important for the denaturation of double stranded DNA. The Southern blot was assembled avoiding bubbles between the different layers. Before the membrane was placed on the Whatman papers, both were briefly preincubated in 0.4 M NaOH. Transfer was conducted for 16 h o.n.. The next day, the blot was disassembled and attaching gel rests were removed by a short wash in 2 x SSC. For fixing of the DNA, the membrane was

incubated for 2 h at 80°C in an incubator. The membrane was either directly used for subsequent steps or could be stored at RT for a longer time.

4.11.1.13 Radioactive labeling of probes and hybridization of the blot

Prior to hybridization of the nylon membrane with the radioactively labeled DNA probe, prehybridization was carried out by incubating the membrane in prehybridization mix (chapter 4.7.5) for 2-4 h at 65°C on a rolling incubator.

The sequence of the external *Rosa26* probe was subcloned into pCR Topo and was generated by enzymatic digestion of the vector with EcoR I and BamH I. The *Neo* probe was PCR-amplified directly from the *Rosa26* targeting vector (primer #3849 and 3850). Both probes were purified as described in 4.11.1.6. Radioactive labeling of the probes was performed using Rediprime™II Random Prime Labeling kit following the manufacturer's instructions and α -[³²P]-dCTP as radioisotope (25 μ Ci). To remove excess nucleotides, the probe was purified by centrifugation of the solution in a Probe Quant G50 micro column for 5 min. After a denaturation step at 95°C and cooling on ice, the labeled DNA probe was given to the membrane directly into the prehybridization mix. The membrane was incubated for 16 h o.n. on a rolling incubator at 65°C. The following day, hybridization mix containing the labeled probe was removed and unbound probe was washed off the membrane by stepwise 20 min incubation in prewarmed washing buffer I and II. Between the washing steps, radioactivity was monitored with a Geiger counter to avoid complete removal of the probe. When the value of measured radioactivity reached approx. 30-80 Becquerel, the membrane was shrink-wrapped in plastic foil and fixed in an autoradiography cassette. An X-ray film was placed upon the membrane and incubated, depending on the intensity of the signal, o.n. or longer at -80°C. For incubation of the same membrane with a different probe, the membrane was stripped by boiling in Southern stripping solution for 20 min. The membrane was then incubated with a different radioactively labeled probe. An overview about probes and expected fragment sizes is given in Table 10.

Table 10: DNA probes for Southern blotting and expected sizes

Name	Detection	Enzyme	Fragment sizes
<i>Rosa</i> probe	Correct insertion of the construct into the <i>Rosa26</i> locus of ES cells and transgenic mice	EcoR I	wt = 16 kb rec = 6.8 kb
<i>Neo</i> probe	Random insertion of the construct into the genome of ES cells and transgenic mice	EcoR I	rec = 6.8 kb in case of random integration: additional bands of undefined size

4.11.2 Working with RNA

All RNA work was performed using RNase free substances and material. Since RNA is less stable compared to DNA, samples were always thawed and kept on ice or otherwise stored at -80°C.

4.11.2.1 Isolation of total RNA from mouse tissues

Isolation of total RNA from mouse tissues was performed using the RNeasy Kit (*Qiagen*) and the QIAshredder (*Qiagen*) kit according to the manufacturer's instructions. Since the isolation of RNA from fatty tissues like brain and spinal cord can be problematic, an additional Qiazol[®] step was included prior use of the RNeasy Kit. The optional DNase I digestion in the RNeasy kit protocol was always conducted.

4.11.2.2 Determination of RNA concentration

Total RNA isolated from mouse tissues was used for quantitative real time PCR analysis (qRT-PCR). Since the photometric measurement of total RNA is rather imprecise, the Quant-iT[™] RiboGreen[®] RNA Assay Kit (*Invitrogen*) was conducted following the manufacturer's instructions. The kit is based on RiboGreen, a dye that is only fluorescent when bound to RNA. Therefore, the fluorescence intensity is directly correlated to the RNA concentration present in a sample. The assays were performed as triplicates in 96 well plates (Black, flat bottom, medium binding, #655076, *Greiner bio-one*) and analyzed with the TECAN Safire2 monochromator-based microplate reader (*Tecan*).

4.11.2.3 Reverse transcription of RNA into cDNA

Since RNA cannot be used as template in quantitative real time PCR (qRT-PCR) analyses, RNA was first reversely transcribed into cDNA. For this purpose, the QuantiTect Reverse Transcription Kit (*Qiagen*) was used following the manufacturer's protocol. To avoid contamination with genomic DNA, a DNase digestion step was included in the kit. Furthermore, oligo-dT primers (*Fermentas*) binding to the mRNA-specific poly-A tail were used to specifically transcribe mRNA only. For the individual samples 300 ng of total RNA were transcribed in a volume of 20 µl. Of the defined standard 600 ng of total RNA were transcribed in a volume of 20 µl.

4.11.2.4 Quantitative real time PCR (qRT-PCR)

Total RNA was isolated from tissues and reversely transcribed as explained in chapters 4.11.2.1 and 4.11.2.3. When used for qRT-PCR, cDNAs of the samples were diluted in a ratio of 1:5 in TE⁻⁴. For the standard, 16 µl were mixed with 24 µl of TE⁻⁴, properly mixed and diluted 8 times in a ratio of 1:2 to obtain all in all 9 dilutions. 3 µl of the diluted sample as well as the standard were used in a standard qRT-PCR reaction. An example of a standard reaction is given in Table 11. qRT-PCR was performed on a LightCycler 1.5 instrument using

Fast Start DNA Master SYBR Green I (*Roche*). To analyze measurements, the second derivative maximum method of the LightCycler software was recruited. Experiments were always conducted in triplicates. All primer combinations used in qRT-PCR including annealing temperature and amplicon size are given in Table 4.

Table 11: Example of a standard qRT-PCR reaction

Component	Amount [ul]
V[sample]	3
H ₂ O	2.7
MgCl ₂	1.2
Forward primer	1
Reversed primer	1
Fast start DNA Master mix	0.83
Polymerase	0.27

4.11.3 Working with bacteria

All cloning steps in this thesis were performed using TOP10 chemocompetent cells (*Invitrogen*). Only for the cloning of *PLS3V5* into the targeting vector, XL1-Blue chemocompetent cells (*Agilent Biotechnology*) were used.

4.11.3.1 Topo TA cloning

Transformation of Plasmids into TOP 10 cells was performed using the Topo TA cloning technology (*Invitrogen*). This technique makes use of the vaccinia virus derived enzyme topoisomerase I that can function as both, a restriction enzyme and as a ligase. The Topo-vectors are provided linearized and carry topoisomerase I covalently bound to each 3' phosphate of the extending thymine of the pentameric sequence 5'-(C/T)CCTT-3'. If a Taq-amplified PCR product is added to the buffered reaction solution, topoisomerase I ligates the overhanging adenosine rests of the PCR-fragment to the complementary 3' thymine of the vector. The Topo vectors used in this work were pcDNA3.1/V5-His Topo and Zero blunt Topo.

To clone a certain DNA fragment into a Topo cloning vector, the DNA fragment was first amplified using the *Taq* High Fidelity system (*Invitrogen*). The PCR product was purified using the QIAquick PCR purification system and eluted in TE⁻⁴-buffer. To ensure the specificity of the PCR reaction, a small aliquot of 5 µl of the PCR product was always tested on an agarose gel. If the expected size was detected on the gel, ligation into the respective Topo vector was performed as follows: 4 µl of PCR product was mixed with 1 µl of salt solution provided by the manufacturer. 1 µl of Topo vector was added and the solution was incubated for 10 min at RT. 2 µl of the cloning reaction were given to a vial of freshly thawed TOP10 chemocompetent cells. The vial was finger-flipped and incubated for 30 min on ice. Following incubation on ice, the heat shock was performed for 30 sec at 42°C. The tube was

transferred on ice and 250 μ l of RT S.O.C. medium was added. Next, the tube was shaken horizontally (200 rpm) for 1 h at 37°C. Different volumes of bacteria (e.g. 30 μ l and 70 μ l) were dispersed on agar-plates containing Ampicillin or Kanamycin in a final concentration of 50 μ g/ml. Plates were incubated o.n. in a sterile incubator at 37°C.

4.11.3.2 Cloning of *PLS3V5* into the *Rosa* targeting vector

Before *PLS3V5* was inserted into the *Rosa* targeting vector, 5' and 3' Asc I restriction overhangs were added via HiFi-Taq PCR and the construct was subcloned into the Zero blunt Topo vector. For the final cloning step into the *Rosa* 26 targeting vector, 5 μ g of the Zero blunt vector containing *PLS3V5* and the empty *Rosa26* targeting vector were digested with Asc I (chapter 4.11.1.9). To prevent self ligation, the targeting vector was alkaline phosphatase treated prior ligation by addition of the respective buffer and enzyme directly to the restriction reaction. The complete restrictions were then separated on a 1 % agarose gel. The restricted *Rosa* targeting vector as well as the 2 kb *PLS3V5* fragment were cut out and purified from the gel using QIAEX II gel extraction kit for the targeting vector and the QIAquick Gel Extraction Kit for the *PLS3V5* fragment. After elution in an adequate volume of H₂O (e.g. 20 – 50 μ l) the concentration of the eluates was determined and the ligation reaction performed using a vector:insert ratio of 1:3 o.n. at 13°C (chapter 4.11.1.10). The next morning, transformation of XL1-Blue chemocompetent cells was performed according to the protocol described for TOP10 cells under 4.11.3.1.

4.11.3.3 Picking and colony PCR for the identification of correct clones

The agar plates containing the respective antibiotic were kept at 37°C o.n. and usually 10 colonies were picked per construct the next morning. For colony PCR, clones were lysed by osmotic shock in 20 μ l dH₂O. 5 μ l of the clone were used for colony PCR, while the other 15 μ l were used to inoculate an 8 ml o.n. culture.

The next morning, 0.5 ml of the culture were mixed with 0.4 ml of 50 % glycerol, snap-frozen and then stored as glycerol stocks at -80°C. The rest of the culture (7.5 ml) was used for the isolation of plasmids with the Qiagen MiniPrep Kit after the manufacturer's instructions. After elution of plasmids in dH₂O, the concentrations were photometrically determined and 150 ng used for sequencing (chapter 4.11.1.8).

4.11.3.4 Maxi preparation of plasmids

To isolate up to 500 μ g of plasmid, the EndoFree Plasmid Maxi Kit (*Qiagen*) was used following the manufacturer's instructions. Usually 250 ml of o.n. culture were used for the experiments. The kit is specifically designed to eliminate any bacterial contaminations, e.g. lipopolysaccharides (LPS) that might interfere with subsequent transfection reactions. The plasmids generated and used in this work are listed in Table 6.

4.12 Protein biochemical and immunological methods

4.12.1 Working with proteins

Since proteins are highly temperature-sensitive, all protein work including thawing was performed on ice. Since proteins can furthermore degrade through protease activity, protease inhibitor was added to the RIPA buffer.

4.12.1.1 Isolation of proteins from mouse tissues

For protein isolation from mouse tissue, a small part of the respective tissue was lysed in 350-600 μ l RIPA buffer, depending on the size of the sample. Prior use, complete mini protease inhibitor (1 pill per 7 ml of RIPA buffer) was added to the RIPA buffer to block protease activity. Soft tissues like spinal cord or brain were homogenized with help of an EPPI-pestle. For compact tissues like muscle, the T 10 basic ULTRA-TURRAX homogenizer was used. Next, protein solutions were centrifuged for 30 min at 13.200 rpm at 4°C. The supernatant containing the dissolved proteins was transferred to a fresh tube and the protein concentration was determined (chapter 4.12.1.3).

4.12.1.2 Isolation of proteins from cells

To harvest proteins, cells were first washed two times in 1 x PBS. Lysis of the cells was performed by adding 50 μ l RIPA buffer containing protease inhibitor (chapter 4.12.1.1) directly on a 10 cm Petri dish (30 μ l per 1 well of a 6 well plate). The dishes were kept on ice for 20 min before a cell scraper was used to collect the solution which was then transferred into a fresh 1.5 ml tube. Following another 20 min of incubation on ice, the tubes were centrifuged for 20 min at 13.200 rpm at 4°C. The supernatant was transferred into a new 1.5 ml tube and the concentration was determined (chapter 4.12.1.3) before it was frozen at -80°C.

4.12.1.3 Determination of protein concentration

The protein concentration was determined using the Bradford method (Bradford, 1976). Bradford dye is able to bind to proteins whereupon it shifts its absorption maximum from 470 to 595 nm. To determine the protein concentration of a sample, 2 μ l of protein lysate were mixed in 498 μ l of Bradford solution and incubated for 20 min at RT. After blank with Bradford dye, the absorption of the sample was measured at a wavelength of 595 nm. The protein concentration of the unknown sample was determined by the machine comparing the measurements to a bovine serum albumin (BSA) standard curve.

4.12.1.4 SDS polyacrylamide gel electrophoresis (SDS PAGE)

When separated by SDS PAGE, proteins need to be denatured in Laemmli buffer and under the influence of heat (95°C). The SDS of the Laemmli buffer and the PAA gel applies a

negative charge to the protein which by far exceeds the intrinsic charge of the protein. This way, SDS page allows the separation of all proteins of a sample by size (Laemmli, 1970).

For SDS PAGE, a 12 % PAA separation gel (chapter 4.7.6) was prepared between two glass plates (0.5 mm thickness). Isopropanole was pipetted on top to cover the gel. After polymerization, the isopropanole was removed and a stacking gel (chapter 4.7.6) was poured on top of the separation gel. A suitable comb was fixed between the glass slides and adjusted using two clamps. Stacking- and separation gel differ by their PAA content and pH. Since the stacking gel contains less PAA it forms bigger pores through which the denatured proteins can migrate easily in between a front of dipolar glycine and Cl^- ions. Therefore, the function of a stacking gel is to concentrate the proteins along the border of stacking and separation gel. Once the proteins migrate into the separation gel, the glycine dissociates due to the increased pH. The separation gel contains a bigger amount of PAA and therefore smaller pores are formed. Thus, bigger proteins are slowed while small proteins can easily migrate through the pores. Due to their overall negative net charge, proteins are separated only by size. Protein samples to be separated (typically 7.5 μg) were supplied with 5 μl of 2x Laemmli buffer to which β -Mercaptoethanol had been added in a ratio of 1:10. After mixing and a short spin to collect the solution at the bottom of the tube, the proteins were heated to 95°C for 5 min for complete denaturation. The heating step was followed by a short centrifugation step at 4°C to collect condensed fluid from the tube seam. Proteins were kept on 4°C until loaded on the gel. Protein size was estimated loading the PAGE Ruler Plus (Fermentas) protein ladder in a separate lane. Gel electrophoresis was performed using the Mini-Protean 3 cell or Protean II xi system (*Biorad*). The proteins were run at 40 V in 1 x electrophoresis buffer (4.7.6) until reaching the separation gel. From this point on, the applied current was increased to 80-120 V.

4.12.1.5 Transfer of proteins to a nitrocellulose membrane (Western blotting)

To transfer proteins on a nitrocellulose membrane by wet blotting, the separation gel was removed from the glass plates and the remaining stacking gel was discarded. Two sponge pads, two filters, the nitrocellulose membrane as well as the gel were equilibrated in transfer buffer (4.7.6) and arranged on top of each other in the following order: Sponge pad, filter, gel, membrane, filter, sponge pad. Possible air bubbles in the sandwich were removed by carefully rolling a small glass pipette over the filter paper. The gel sandwich was then inserted into a transfer cell and a cooling module was added. The transfer cell was placed in a 4°C room and a current of 30 V was applied o.n.. Caused by the negative charge, the proteins migrate in the electric field and finally adhere to the membrane due to hydrophobic interactions, at the same time keeping the separation pattern present in the gel. The next morning, the wet blot was disassembled and the membrane was briefly rinsed in TBST.

Protein transfer was either monitored via reversible Ponceau staining or the membrane was immediately used for subsequent immunological detection.

4.12.1.6 Ponceau staining of proteins on nitrocellulose membranes

To control the protein transfer to the nitrocellulose membrane staining with Ponceau solution is commonly used. Ponceau interacts with positively charged amino acid side chains and since the staining is reversible the membrane can afterwards be used for subsequent immunological detection using antibodies. For Ponceau staining, the membrane was incubated in Ponceau solution for 30 sec. The arising band pattern could be clarified rinsing the membrane in fresh TBST. For further analysis, the membrane was simply washed in TBST until no red signal was present on the membrane any longer.

4.12.1.7 Immunological detection of proteins on nitrocellulose membranes

To detect proteins on a nitrocellulose membrane, primary antibodies are used that specifically recognize the protein of interest. The staining procedure was performed as follows: After wet blotting, the membrane was washed 5 times in TBST to remove any residual MeOH from the transfer buffer. To avoid background, the membrane was next blocked using 6 % non-fat milk powder in TBST for 3 h. The 6 % non-fat milk was discarded and exchanged with 3 % non-fat milk in which the primary antibody had been diluted. After incubation with the primary antibody, the membrane was washed 5 x for 5 min in TBST to remove unbound primary antibody. Following washing, the membrane was incubated with an HRP-conjugated secondary antibody in 3 % non-fat milk that was directed against the species from which the primary antibody was derived. After incubation with the secondary antibody, the membrane was washed again 5 x for 5 min in TBST to remove unspecifically or unbound secondary antibody. To chemiluminescently detect the protein bands, the membrane was incubated for another 5 min in SuperSignal® West Pico Chemiluminescent Substrate (*Pierce*). Lastly, the membrane was carefully wrapped in plastic foil, placed into an developing cassette and exposed to Hyperfilm ECL (*Amersham*). Densitometric analysis of the films was performed using ChemiDOC XRS analysis software.

For a summary of primary and secondary antibodies used in this study and respective dilutions and incubation times see Table 12. For order numbers of the respective antibodies refer to chapter 4.6.

Table 12: Antibodies used in Western blotting

Primary antibodies	Dilution	Incubation time
Rabbit- α -PLS3 (custom made, Eurogentech)	1: 4,000	o.n.
α -SMN (monoclonal)	1:2,000	2 h, alt. o.n.
α -V5 (monoclonal)	1:3,500	o.n.
α -V5-HRP conjugated	1:1,500	2 h
α -Actin (monoclonal)	1:80,000	0.5 h
α -GAPDH (monoclonal)	1:4,000	o.n.
Rabbit- α - β -Tubulin (polyclonal)	1:80,000	0.5 h
Secondary antibodies	Dilution	incubation time
Goat- α -mouse-HRP	1:10,000	1 h
Donkey- α -rabbit-HRP	1:10,000	1 h

4.12.2 Immuno- and histochemical staining procedures

Histochemical stainings were performed to visualize cells of the spinal cord (Nissl stainings) as well as muscle fibers (Hematoxylin and eosin stainings, H&E). While histochemistry describes the staining of tissues using structure specific dyes (e.g. hematoxylin staining nuclei and eosin delineating the cytoplasm), immunohistochemical stainings are based on the use of primary- and secondary antibodies to detect a protein of interest. In a first step, the fixed section is incubated with the primary antibody. After washing steps, the fluorophore-conjugated secondary antibody is applied to indirectly detect the protein. Analysis is then performed under UV light excitation using a microscope equipped with respective filter sets. Alternatively, HRP-conjugated secondary antibodies can be used, whereby HRP converts the substrate 3,3'-Diaminobenzidine (DAB) into an insoluble brown reaction product in the presence of H_2O_2 . The signal can then be detected using a common transmission filter.

4.12.2.1 Nissl stainings

For Nissl stainings the basophilic organic compound Cresyl violet is used to outline nucleic and ribosomal structures of nerve tissue. In this work, Nissl stainings were exclusively performed on 7 μ m thick spinal cord sections. First, spinal cord sections were deparaffinized by incubation in Xylol for 3 min. Via incubation in decreasing EtOH concentrations (100 %, 96 %, 70 %, 50 %, 3 min each) and subsequent incubation for 5 min in PBS, the sections were rehydrated before they were stained in Cresyl violet acetate for 10 min. Following a short wash in H_2O , sections were washed in highly diluted acetic acid (2-3 drops in 100 ml H_2O), dehydrated via increasing EtOH concentrations (50 %, 70 %, 96 %, 100 %, 3 min each), air-dried and embedded in Entellan mounting media.

4.12.2.2 Hematoxylin and eosin (H&E) stainings of muscle fibers

H&E stainings were in this study performed to counter-stain mouse muscle tissue for subsequent fiber size measurements. In order to stain with H&E, muscle sections of 7 μm thickness were deparaffinized by incubation in Xylol for 30 min. Following incubation in decreasing EtOH concentrations (100 %, 96 %, 70 %, 50 %, 3 min each), the sections were quickly washed once in PBS and then incubated in H₂O for 1 min. Next, sections were incubated in Hematoxylin for 6 min and afterwards washed in H₂O for 15 min. The sections were rinsed quickly in H₂O once to remove excess dye and then placed into Eosin solution for 1 min. To clarify the stainings, sections were rinsed in H₂O 6-7 times and then dehydrated in increasing EtOH concentrations. Finally, sections were air dried and embedded in Entellan.

4.12.2.3 Immunohistological stainings of motor neurons

In order to stain motor neurons, 7 μm thick spinal cord sections were deparaffinized for 2 h in Xylol and subsequently rehydrated in decreasing EtOH concentrations (100 % I, 100 % II, 96 %, 70 %, 1 min each). Following an incubation in H₂O for 10 min, antigen retrieval was performed by boiling the sections in citrate buffer for 3 x 5 min at 600 W in a microwave. After boiling, the sections were left in citrate buffer and cooled down to RT for 45 min. To remove citrate buffer, sections were washed once in TBS for 5 min. Blocking of the sections was carried out in 5 % of the secondary antibody's host serum plus 5 % BSA in TBS by directly pipetting the solution on the sections and incubating for 45 min at RT in a wet chamber. Subsequently, sections were washed for 3 x 5 min using TBS in a glass tray. After that, the sections were incubated with primary antibodies diluted in blocking media o.n. at 4°C in a wet chamber (Rabbit α -PLS3 1:40; rabbit α -V5 1:40, goat α -Chat 1:40). The next day, unbound primary antibody was removed from the sections by 3 x 5 min washing steps in TBS. The secondary antibodies were diluted in freshly made blocking solution (Donkey α -goat Alexa 488 1:200, donkey α -rabbit Alexa 568 1:200) and directly pipetted on the sections. Incubation with the secondary antibodies was carried out for 3-4 h at 4°C in a wet chamber. To get rid of unbound secondary antibody, sections underwent 3 more washes for 5 min each. To remove residual salt, sections were briefly rinsed in H₂O and then embedded in Mowiol[®] mounting media.

4.12.2.4 Immunohistological stainings of neuromuscular junctions (NMJ)

Neuromuscular junction (NMJ) stainings were either performed on proximal- (Transversus abdominis, TA) or distal muscle tissue (Gastrocnemius). The isolation of TA- and Gastrocnemius muscle is described in chapter 4.14.2.2. All washing and incubation steps were performed in 24 well plates.

First, the tissue derived from TA muscle was fixed for 10 min and such from Gastrocnemius muscle for 20 min in 4 % PFA at RT. After fixing, the TA muscle could directly be used for stainings. Different from that Gastrocnemius was embedded in 4 % low melting agarose and sliced into 150 μ m thick sections prior the actual staining protocol. From this point on, the staining protocol was the same for TA- and Gastrocnemius muscle. To remove excess PFA, the muscles were washed in 1 x PBS 3 x for 10 min on a rocking platform at RT. To permeabilize the tissue, muscles were incubated in PBS containing 2 % of Triton X for 30 min on a rocking platform. Following permeabilization, blocking was performed in PBS containing 4 % BSA and 1 % Triton. Finally, the antibodies were prepared in blocking solution (Mouse- α -2H3 1:100, mouse- α -SV2 1:100, mouse- α -neurofilament 1:250) and pipetted on the tissue samples. To obtain the best results, incubation with the first antibody was always performed o.n.. To reduce background, the samples were 6 x washed in 1 x PBS for 10 min under constant shaking on a rocking platform. At this point of the protocol, a Bungarotoxin (BTX, labeled with Rhodamine) staining step was included into the protocol. For that, 10 μ l of BTX stock solution (1 M) was diluted in 7 ml of PBS and the samples incubated for 10 min under shaking at RT. In the meanwhile, the secondary antibody (goat α -mouse Alexa 488 1:250) was diluted in PBS. After the BTX staining had completed, the media was exchanged with the secondary antibody in PBS without any intermediate washing step and incubated for 2 h at RT on a rocking platform and wrapped in tin foil.

4.12.2.5 Immunohistological stainings of murine embryonic fibroblasts (MEF)

For staining of murine embryonic fibroblasts, cells were trypsinized and replated in 12 wells provided with sterile cover slips. After settling o.n., MEFs were rinsed in PBS once and afterwards fixed in 4 % PFA for 15 min at RT. Following fixation, the cells were washed once in 1 x PBS for 5 min. To make the epitope better accessible for the antibody, antigen retrieval was conducted by adding 80°C hot citrate buffer (pH 6.0) to the cells and incubating them under constant cooling to RT for 20 min. After another washing step in 1 x PBS, cells were permeabilized in 0.2 % Triton X (alternatively Tween20) in PBS for 5 min. For blocking, cells were incubated in 5 % of the secondary antibody's host serum plus 5 % BSA in PBS for 2 h at RT. Next, the primary antibodies (Rabbit α -PLS3 1:40, mouse α -V5, rabbit α -V5 1:40, mouse α -Vinculin 1:150) were diluted in 5 % BSA in PBS and given to the cells for o.n. incubation. The next day, unbound antibody was removed in 3 washing steps in 1 x PBS for 15 min each. The secondary antibodies (Donkey α -rabbit Alexa 350 1:250, goat α -mouse Alexa 488 1:250) were codiluted with Phalloidin (1:40) in PBS containing 5 % BSA. For an optimum result, the cells were incubated in secondary antibody/phalloidin for 4 h, however, if shorter incubation times were necessary, the time could be reduced to a minimum time of 1 h. To remove residual salt, cover slips were repeatedly dunked in dH₂O before they were

mounted in Vectashield mounting media containing DAPI. Especially when an Alexa 350 conjugated antibody was used, the DAPI of the mounting media could mask all upcoming signals. In this case, DAPI-free Mowiol was used as mounting media.

To save antibodies, in all experiments a 40 μ l droplet of the respective antibody solution was pipetted on parafilm and the cover slips placed on the drop with the cells facing the solution. For washing steps, the cover slips could easily be transferred into 12 wells again.

4.13 Eukaryotic cell culture procedures

To avoid microbial contamination, all cell culture work was performed under sterile conditions in a laminar flow tissue culture hood. Additionally, all equipment was sterilized with Bacillol or 70 % Ethanol. All ES cell work was conducted under antibiotic- as well as fungicide-free conditions, whereas amphotericin B and PenStrep were added to the media used for the work with isolated primary murine fibroblasts (chapter 4.7.2). All cell cultures were stored in sterile cell incubators at normal cultivation growing conditions in an atmosphere with 5 % CO₂ at 37°C.

4.13.1 Common cell-culture techniques

4.13.1.1 Thawing of cells

All cell types used in this work were long-term stored in 2 ml *Nunc* cryo-tubes at either –80°C or in liquid nitrogen. To thaw eukaryotic cells, 1 ml of the respective media was added to the cells and carefully pipetted up and down to slowly resuspend the cells. To dilute toxic DMSO the media containing the cells was then transferred into a 15 ml Falcon tube containing 8 ml of media. Subsequently, cells were pelleted at 1,200 rpm for 5 min and then resuspended in an appropriate volume for further cultivation.

4.13.1.2 Freezing of cells

For freezing, the cells were once rinsed with PBS, then trypsin was added and cells were incubated at 37°C in a sterile incubator for 5 min. The detachment-process was monitored using an inverse microscope since extensive trypsin-treatment might harm the cells. When all cells were detached from the surface, the trypsinization-reaction was stopped adding the equivalent amount of culture media. Cells were harvested into a collection tube of appropriate size and centrifuged at 1,200 rpm for 5 min. The pellet was resuspended in freezing media (chapter 4.7.2) and resuspended cells were distributed into cryo-tubes. Cells were frozen and stored at -80°C for the first 24 h and then transferred to liquid nitrogen.

4.13.1.3 Passaging of cells and cell number estimation

For passaging, cells were first rinsed in PBS and then trypsinized at 37°C in a sterile incubator for 5 min. The trypsinization reaction was interrupted by addition of an equivalent amount of culture media and resuspended cells were transferred into appropriate collection

tubes. The collection tubes were centrifuged at 1200 rpm for 5 min and the pellet was reconstituted in an adequate volume of culture media. The resuspended cells were then split onto fresh cell plates.

Estimation of cell number was a frequently used method, e.g. for plating constant numbers of cells for immunohistochemical stainings (as performed with MEF cells) but also for the transfection procedure of ES cells. To estimate cell number, the cell pellet was resuspended in 10 ml of the respective media. 10 μ l of the suspension were taken and dispersed between a cover slip and a Neubauer counting chamber. The mean value of cells of four squares was determined and multiplied by 10^4 to obtain the total amount of cells per 1 ml of media.

4.13.2 Murine embryonic fibroblasts

Mitotically inactive murine embryonic fibroblasts (MEFs) are commonly used in the culturing of murine embryonic stem cells (ES cells). Since transgenic ES cells are eventually transplanted into host-blastocysts to finally develop the germline of the chimeric animal, it is absolutely necessary to keep them undifferentiated while in culture. In ES cell culturing, MEFs serve as monolayer cell matrix to promote ES cell growth. At the same time, MEFs secrete leukemia inhibitory factor (LIF), a protein needed to maintain the undifferentiated state of ES cells. To further inhibit unwanted differentiation, ES cell media was additionally supplied with recombinant LIF (Smith et al., 1988, Williams et al., 1988).

4.13.2.1 Isolation of murine embryonic fibroblasts

Murine embryonic fibroblasts (MEFs) for ES cell culture were isolated from E13.5 animals. Since ES cells were selected against Neomycin during the transgenesis-procedure, it was important to obtain fibroblasts from Neomycin resistant embryos. For that purpose, Neomycin-resistant male mice of the line IL-4 (Muller et al., 1991) were bred with wt female animals of clean C57BL/6N background. To determine the exact time point of fertilization, females were routinely plug-checked early in the morning. If plug positive, the day of fertilization was considered as day E0.5 of embryonic development. At E13.5, mothers were sacrificed and the embryos carefully prepared from the surrounding uterine tissue. Heart and liver were removed while the head of the embryo was used for subsequent genotyping. The remaining tissue was transferred to a Petri dish where it was rinsed in PBS 2 times. After the washing steps, the embryonic tissue was incubated in 50 ml trypsin/EDTA solution at 37°C for 30 min before the reaction was stopped using MEF media. Cells were then centrifuged at 1,200 rpm for 5 min and the cell pellet was resuspended in MEF media. Finally, the cell-number was determined as described in chapter 4.13.1.3 and 2.5×10^6 cells were plated per 15 cm Petri dish. Cells were grown to confluence under standard cell culture conditions and frozen as aliquots containing 5×10^6 cells. Whenever needed, one aliquot of MEF cells could

be thawed and afterwards plated on three 15 cm Petri dishes. At this stage, MEF cells were considered as so called EF1 cells, the name indicating that they had been passaged once. EF1 cells were then grown to confluence and again split in a 1:3 ratio on three more 15 cm Petri dishes resulting in nine 15 cm Petri dishes of EF2 cells. In a last round, EF2 cells were passaged to another three 15 cm dishes. Via this way, all in all 27 15 cm dishes of EF3 cells could be obtained from one single MEF cell aliquot. EF3 cells could then be mitotically inactivated by MMC treatment for usage in ES cell culture. If not directly needed for ES cell culture, EF2 cells were frozen instead and thawed as EF3 cells, inactivated via MMC treatment and used for ES cell culturing whenever needed.

MEFs that were isolated for immunohistochemical stainings were obtained from E13.5 embryos, too. A wt female of clean C57BL/6N background was bred with a *PLS3V5^{tg/wt}* animal. At E13.5, the mother animal was sacrificed and again heart and liver were removed from the embryos while the head was used for genotyping. Individual embryos were homogenized by pressing the tissue through a cell sieve using the plunger of a 10 ml syringe. The sieve containing the cells was then rinsed with 10 ml of MEF media and the flow-through collected in a 50 ml tube. The cell suspension was centrifuged at 1,200 for 5 min rpm, the resulting pellet was resuspended in an adequate volume of MEF media and the cells plated on 6 cm Petri dishes. MEFs could then be expanded as described above and used for immunohistochemical stainings.

4.13.2.2 Mitomycin C treatment of EF cells

For usage in ES cell culture, it is important to mitotically inactivate EF cells by MMC treatment. Before MMC treatment, EF cells were rinsed once in PBS. After the washing step, 15 ml of sterile-filtered MMC/MEF media of 10 µg/ml concentration were added per one 15 cm Petri dish of EF cells. This way, EF cells were incubated for 2-4 h at 37°C in a sterile incubator. Next, MMC solution was removed from the cells followed by two washing steps in PBS. Finally, normal EF media was added to the cells. Before EF cells were used for ES cell culture, 2 h of incubation were given allowing the EF cells to release intracellular MMC that might inhibit ES cell proliferation. MMC treated EF cells were always prepared on gelatinized Petri dishes. Preceding gelatinization of Petri dishes was performed by incubation of the Petri dishes with 0.1 % gelatin/PBS for 5 min at 37°C. After gelatin-excess was removed EF cells were plated.

4.13.3 Murine embryonic stem cells

Murine embryonic stem cells (ES cells) are derived from the inner cell mass of the blastocysts of an early stage embryo at around 3dpc. ES cells are pluripotent cells, meaning that they have the capacity to differentiate into all derivatives of every of the three germ layers, namely endo-, ecto- and mesoderm. They replicate indefinitely and can be cultured on a

monolayer of mitotically inactivated feeder cells. Feeder cells serve as an ideal substrate to allow proper proliferation of ES cells (Evans and Kaufman, 1981, Martin, 1981). Furthermore, feeder cells secrete leukemia inhibitory factor (LIF), a protein inhibiting the differentiating process of ES cells. Therefore, they are of highest importance to preserve pluripotency of ES cells while culturing. Additionally, the ES cell media is usually supplied with recombinant LIF to preserve an undifferentiated state of the ES cells.

It is possible to genetically manipulate ES cells *in vitro* and to inject these cells afterwards into host-blastocysts. Thereupon, the ES cells can incorporate into the early stage embryo to differentiate into all the various tissues and cellular subtypes, including sperm- or oocytes of the germ line (Bradley et al., 1984, Gossler et al., 1986, Robertson et al., 1986). The resulting animal consists of cells of the host embryo and of donor ES cells and is thus chimeric, whereby the degree of chimerism depends on the proliferative ability and the degree of pluripotency of the injected ES cells. If the germ-line in the Chimera has formed of transgenic ES cells, the respective ES cell genotype can be inherited and a stable founder generation of genetically modified animals be established.

4.13.3.1 Cultivation of murine embryonic ES cells

ES cells were grown on mitotically inactivated fibroblasts under standard culturing conditions of 37°C, 5 % CO₂ and 95 % air humidity. ES cell media was changed daily. When ES cell colonies reached app. 80 % confluence, cells were passaged, usually in a ratio of 1:3.

4.13.3.2 Transfection of ES cells

Transfection of DNA into eucaryotic cells can be accomplished via different methods. Next to methods using lipophilic carrier substrates to deliver DNA into the cell, the transfection via electric pulses has turned out to be a highly efficient technique (Neumann et al., 1982). The so called electroporation-method was used in this work for the targeted transgenesis of ES cells.

For one round of electroporation, a total of 60 µg of *Rosa26* targeting vector was linearized by restriction digestion using *Asi*I. The linearized vector was afterwards phenol/chloroform extracted and could be stored in 70 % ethanol at -20°C until the transfection time point. For transfection, the linearized vector was centrifuged at 13,200 rpm for 10 min, excess 70 % Ethanol was removed from the tube and the pellet was air dried at RT under the sterile hood for 15-20 min. Finally, the targeting construct was resuspended in 400 µl RPMI medium (w/o phenol-red) and was then ready to use. In one round of electroporation, the ES cells (Type V6.5, (Eggan et al., 2002)) of one 10 cm dish (~1x10⁷ cells) were first trypsinized, centrifuged at 1,200 rpm for 5 min and also resuspended in 400 µl of RPMI-media. ES cell- and DNA suspension were mixed together and the whole

approach (800 μ l) was pipetted into the electroporation cuvette. Electroporation was then conducted applying 500 μ F at a current of 240 mV. Immediately after the transfection, 0.7 ml of ES-media was pipetted into the cuvette, the cells were incubated for 10 min and finally resuspended in 40 ml of ES-media. 10 ml of the ES cell suspension were pipetted on one of four 10 cm Petri dishes that had previously been prepared with mitotically inactivated EF3 cells.

4.13.3.3 Selection of recombinant ES cell clones

After the transfection of the targeting construct, the ES cells were positively selected using the Neomycin analogon G418. Since the targeting vector carries the Neomycin resistance gene *Neo^r*, only ES cells that have stably inserted the construct into their genome should survive the selection. Two days after the transfection, positive selection was started by adding G418 to a final concentration of 250 μ g/ml to the ES cell media.

Next to the positive selection, it was also possible to negatively select the ES cells against random insertion of the construct into the genome. For that purpose, the thymidin-kinase gene was cloned downstream of the 3'-homology arm of the *Rosa26* targeting construct. Thymidin-kinase can convert the selection substrate Ganciclovir (nucleoside-analogon) into Ganciclovir-monophosphate. Cellular kinases then phosphorylate the monophosphate into Ganciclovir-triphosphate. This molecule can be incorporated into DNA during the process of replication which is toxic to the cell and finally leads to cell death. Since the Thymidin-kinase-gene was cloned downstream of the 3'-homology arm it should be lost in case of homologous recombination but not if the construct was inserted randomly. As a consequence, only cells in which the construct had inserted via homologous recombination should survive negative selection with Ganciclovir. Negative selection was started at day 5 after transfection. For it Ganciclovir was added to the media to a final concentration of 2 μ M while positive selection was further continued, too. Between 8-10 days after transfection, surviving ES cell colonies were picked into 96 well plates that had been covered with mitotically inactive EF3 cells.

4.13.3.4 Isolation of ES cell clones

Between days 8-10 after transfection, the positive and negatively-selected ES cells had formed nicely oval-shaped colonies with rounded borders. For ES cell colony harvesting, the 10 cm dishes harboring the colonies were rinsed once with cold PBS and then kept in PBS. Using a pipette-tip, single colonies were carefully detached and then sucked up in a total volume of 40 μ l of PBS. The colonies were then transferred into a single u-shaped slot of a 96 well plate. To avoid contamination, this work was performed under a sterile hood using a stereo-microscope. The slots of the 96 well plate had each been provided with 25 μ l of 1 x trypsin solution. Since trypsin can harm the cells, the isolation of a total of 96 clones was

completed in a maximum time of 30 min. After sampling, the 96 well plates were incubated for 5 min at 37°C in a sterile incubator and the reaction was stopped by adding 100 µl of ES cell media. After properly pipetting up- and down, the suspension of each slot (total volume 165 µl) was split (each 50µl) to 3 further 96 well plates with flat bottoms to produce triplicates of each clone. These 96 well plates had been covered with MMC treated EF3 cells before. When these plates were almost confluent two of the three plates were frozen on two consecutive days. For that purpose, plates were first washed 2 x with 100 µl of PBS and then treated with 50 µl of 1 x trypsin solution for 3 min at 37°C in a sterile incubator. The reaction was stopped adding 100 µl ES cell media and 100 µl 2 x freezing media. Plates were accurately sealed using parafilm, properly labeled and frozen in a box at -80°C. The last of the three plates was again split to 3 new gelatinized 96 well plates. When the clones of these plates had grown confluent, the plates were washed twice with 100 µl of 1 x PBS. The PBS was removed and two of the three plates were sealed and then frozen without media for later DNA isolation and subsequent southern blot analysis at -20°C. The third plate was immediately used for DNA isolation (chapter 4.13.3.6)

4.13.3.5 Freezing and passaging of isolated ES cell clones on 96 well plates

After culturing the 96 well plates harboring the individual clones for 2-3 days, 2 of the 3 plates were frozen on following days. For that purpose, cells were rinsed once with 200 µl of 1 x PBS and then treated with 50 µl of trypsin for 5 min at 37°C in a sterile incubator. To stop the reaction, 50 µl of 2 x freezing media were added to the cells (80 % FK, 20 % DMSO). To properly suspend the cells, the solution was pipetted up- and down several times. The plates were sealed with parafilm and frozen at -80°C.

To obtain DNA for Southern blotting the remaining 96 well plate was split on 3 more 96 well plates. Since the cells served only for DNA-isolation, the plates were not prepared with MMC treated EF3 cells but only gelatinized instead.

4.13.3.6 Identification of positive ES cell clones from 96 well plates

Positive ES cell clones were identified via Southern blotting (chapter 4.11.1.11) from 96 well plates. Both, the isolation of DNA and the enzymatic restriction with EcoR I were performed directly on the 96 well plate. To isolate DNA, 50 µl of lysis buffer/Proteinase K were pipetted into each slot and the well was sealed with parafilm. To avoid drying-out, the wells were additionally wrapped in wet paper and placed in a wet chamber for o.n. incubation at 55°C in a water bath. After cooling to RT, 100 µl of EtOH were added to each of the slots and the DNA was allowed to precipitate for 1 h. By carefully inverting the plates over tissue paper, the supernatant EtOH was removed. The remaining DNA pellet was 3 x washed in 70 % EtOH and then air dried for 30 min at 37°C in an incubator. In a next step, DNA was enzymatically restricted by adding 35 µl of restriction solution to each of the slots and

incubating o.n. again in a wet chamber (chapter 4.11.1.9). The following day, the restricted DNA was subjected to Southern blot analysis.

4.13.3.7 Thawing and expansion of positive ES cell clones from 96 well plates

After identification of positive ES cell clones, clones from triplica-96 well plates were thawed to expand the cells for blastocyst injection. For that purpose, 100 μ l RT ES cell media was given to each positive clone and the cell suspension was carefully pipetted up and down. Positive clones were first dispersed in 24 wells that had been covered with MMC treated EF3 cells. To avoid mixing up of positive clones, the neighboring clones were isolated, too. Additionally, these clones served as negative controls in later Southern blot analyses. When subconfluent, clones were further split on 6 cm wells covered with EF3 cells for further expansion. When grown nicely, the clones of one 6 well were finally split on two 10 cm Petri dishes covered with EF3 cells. When subconfluent, the ES cells of one 10 cm dish were frozen as $\frac{1}{4}$ as described in chapter 4.13.1.2. A small amount of every clone was additionally given on a gelatinized 24 well for later DNA isolation and reconfirmation via Southern blotting.

4.13.3.8 *In vitro* Cre mediated deletion of the stop-cassette

ES cells were subjected to *in vitro* Cre-mediated deletion of the stop cassette to analyse functionality of the system and proof proper transgene expression. For *in vitro* deletion of the stop cassette, a modified version of Cre recombinase (HTN-Cre) is used that carries a hydrophobic N-terminal tag including a nuclear localization signal (NLS). This modification of the protein allows HTN-Cre to pass the membrane of cells and to even enter the nucleus (Peitz et al., 2002). In the nucleus, Cre catalyzes site-specific recombination (deletion of the stop cassette) between the two *loxP* sites. *In vitro* Cre-deleted positive ES cell clones were analyzed visually under a microscope and via fluorescent activated cell sorting (FACS) analysis for Green fluorescent protein (GFP) expression (chapter 4.13.3.9). Furthermore, the expression of the *PLS3V5* transgene was demonstrated via Western blotting and immunological detection of the transgene with a V5-antibody.

For *in vitro* HTN-Cre deletion, 2×10^5 cells of positive clones (served as negative controls) were plated on a 6 well and incubated for 5 h. After the incubation phase, the cells were washed once in 1 x PBS and sterile filtered HTN-Cre solutions of molarities ranging from 0.5-8 μ M/DMEM were added to the cells as a total volume of 600 μ l. As negative control, one well of each positive clone was treated with DMEM only. After 20 h of incubation with HTN-Cre, the media was taken off, the cells were washed once in 1 x PBS and fresh ES cell media was added. To allow *GFP* and *PLS3V5* expression, cells were incubated in another 3 days.

4.13.3.9 Fluorescent activated cell sorting of positive ES cell clones (FACS)

FACS is a specialized type of flow cytometry that allows sorting of a mixture of cells based on the fluorescent characteristics of the cells.

For FACS analysis, HTN-Cre deleted cells (chapter 4.13.3.8) were first trypsinized and then sedimented at 1,200 rpm for 5 min. The pellet was reconstituted in 500 µl PBS and pipetted up and down several times to perfectly suspend the cells. Cells were kept on ice until FACS analysis using the BD FACS Vantage SE and CellQuest analysis software. Excess of cells was further used for Western blot analysis.

4.13.3.10 Preparation of ES cells for injection into blastocysts

To prepare positively tested ES cells for injection, one vial of expanded ES cells (4.13.3.7) was thawed on a EF3 cells-covered 10 cm Petri dish and grown to subconfluently for 2-3 d. The cells were then split at different densities on 3 new 10 cm Petri dishes provided with EF3 cells (e.g. 1:3, 1:5, 1:8). At the day of injection, the clones with the optimum density grade and morphology were chosen for the final preparation steps. Cells were first trypsinized as described previously, sedimented at 1,200 rpm and resuspended in 10 ml of ES cell media. The cell suspension was given to a fresh 10 cm dish and cells allowed to settle for 30-40 min. EF-3 cells settle faster than ES cells and therefore ES cells can be enriched in the supernatant media this way. Supernatant ES cells were centrifuged at 1,200 rpm for 5 min and the pellet was resuspended in 500 µl of prechilled injection media. Cells were kept on ice until injection into blastocysts.

4.13.3.11 Injection of positive ES cells into blastocysts

The injection of prepared ES cells (chapter 4.13.3.10) was performed as a service of the centre for mouse genetics of the University of Cologne. In brief: ES cells were sucked into the injection needle fixed to a micro manipulator (*Leica*) and injected into blastocysts derived from CB20 females (white coated). The chimeric blastocysts were then surgically transplanted into the uteri of pseudopregnant females that had been produced by breeding with vasectomized males. In the best case, chimeric animals were born 21 d later. After another 4 weeks, chimeras could be bred with C57BL/6N male and the offspring be analyzed for germline transmission.

4.14 Working with mice

4.14.1 Mouse inbred strains

To exclude the influence of the genetic background on a given phenotype it is essential to use mouse inbred strains of high homozygosity (Silver, 1995). In this work, all experiments were performed using mice on a genetically pure C57 black 6 N (C57BL/6N) background. If not on a C57BL/6N background, mouse mutant- or transgenic lines were backcrossed for at

least 7 generations to 100 % pure C57BL/6N wt animals. Mice were housed in micro-isolation chambers in the mouse facility of the Institute of Genetics, Cologne. All experiments conducted had previously been described in the animal experimental form as such was confirmed by the local animal protection committee under reference number 93.2.10.31.07.186. All mice were humanely euthanized according to protocols set forth by the *Landesamt für Natur, Umwelt und Verbraucherschutz NRW*. In the following, mutant- and transgenic mouse strains used in this study are explained.

4.14.1.1 SMA-mice

The FVB.Cg-Tg(*hSMN2*)2Hung *Smn*^{1tm1Hung}/J were purchased from The Jackson Laboratory (Bar Harbor, Maine (USA), Stock number: 005058) and served as SMA mouse model in this study. In these mice, *Smn* exon 7 is replaced by a targeted insertion of the hypoxanthine phosphoribosyl transferase (HPRT) cassette. Since the homozygous knockout of *Smn* (*Smn*^{-/-}) results in early embryonic lethality, transgenic mice with a 115-kb genomic DNA fragment encompassing the human *SMN2* region from a human BAC library were generated (Hsieh-Li et al., 2000). Importantly, these mice carry 2 *hSMN2* copies per integrate (Riessland et al., 2010). In a next step, the *hSMN2* transgene was crossed into the existing SMA background. This way, normal living and fertile *Smn*^{-/-};*hSMN2*^{tg/tg} animals could be generated. It is then possible to breed *Smn*^{-/-};*hSMN2*^{tg/tg} mice with *Smn*^{+/-} animals to produce 50 % SMA-offspring of the disease genotype *Smn*^{-/-};*hSMN2*^{tg/wt} and 50 % of heterozygous control animals of the genotype *Smn*^{+/-};*hSMN2*^{tg/wt}. In the course of this work this SMA mouse line is termed “Hung SMA” mouse line or the “Taiwanese mouse model” referring to the fact that it was generated by a Taiwanese group (Hsieh-Li et al., 2000). Originally, SMA-Hung mice were obtained on pure FVB genetic background by the Jackson Laboratory. In contrast to that, all used *Cre*-lines and *PLS3V5*-transgenic mice were bred onto a pure C57BL/6N background. To investigate possible disease modifying effects of *PLS3V5* expression on the SMA background, SMA-Hung mice had to be backcrossed against C57BL/6N wt animals for 7 generations to reach 99 % genetic purity.

4.14.1.2 *PLS3V5*-transgenic mice

4.14.1.2.1 *PLS3V5*-floxed mice

In the scope of this work *PLS3V5* transgenic mice were generated. An N-terminally V5-tagged version of human *PLS3* (*PLS3V5*) was first cloned into a murine *Rosa26* locus targeting construct (Kindly provided by Dr. Thomas Wunderlich, Cologne). Targeted transgenesis was performed using the Hybrid ES cell line V6.5 (Eggan et al., 2002). Since this cell line represents a mixture of 129/Sv and C57BL/6 genetic background the resulting *PLS3V5*-floxed line had to be backcrossed against C57BL/6N wt animals for 7 generations to reach 99 % genetic purity. In the targeting construct, the *PLS3V5* coding sequence (cgs) is

located downstream of the CMV enhancer/chicken β -actin (CAG) fusion promoter. However, a *loxP* sites flanked stop-cassette is present between promoter and *PLS3V5* transgene preventing uncontrolled *PLS3V5* expression. By breeding with tissue-specific *Cre*-strains conditional overexpression of the *PLS3V5* transgene can be achieved. For a detailed description of the generation and nomenclature of the *PLS3V5*-floxed line see chapters 5.3.1 and 5.3.2.

4.14.1.2.2 *PLS3V5*-ubi mice

By intercrossing the *PLS3V5*-floxed line with the *Cre*-deleter line cytomegalovirus minimal promoter (*CMV*)-*Cre* (Schwenk et al., 1995), permanent deletion of the stop-cassette between promoter and *PLS3V5*-cds was achieved. In the resulting and from now on termed *PLS3V5*-ubi mice deletion of the stop-cassette resulted in ubiquitous expression of the transgene in nearly all tissues investigated (chapter 5.4.1.1). Neither animals heterozygous nor homozygous for *PLS3V5* displayed any obvious outer phenotypes. *PLS3V5*-ubi animals are fully fertile and show a normal life expectancy. Since *CMV-Cre* mediated deletion includes germ cells, the deletion of the stop-cassette is inherited to further generations also in the absence of the *CMV-Cre* allele. For a detailed description of the generation and nomenclature of the *PLS3V5*-floxed line see chapters 5.3.1 and 5.3.3.

4.14.1.3 *Cre*-lines

4.14.1.3.1 *CMV-Cre*-deleter mice

The *CMV-Cre* deleter line expresses *Cre-Recombinase* under the control of the human cytomegalovirus minimal promoter (*CMV*) (Schwenk et al., 1995). Using this mouse line, deletion of *loxP* flanked genes or stop-cassettes occurs in all tissues, including germ cells. For this reason and because it was available in the mouse facility of the Institute of Genetics (Cologne) the *CMV-Cre* line was chosen to permanently remove the stop-cassette between promoter and *PLS3V5*-cDNA in the *PLS3V5*-floxed line. In this context, it is important to mention that the *CMV-Cre* transgene is located on the X-chromosome (Schwenk et al., 1995). Due to gene silencing effects via X-chromosomal inactivation only *CMV-Cre* homozygous females (*CMV-Cre*^{X-tg/X-tg}) were used to efficiently delete the stop-cassette in F1 male mice of the genotype *PLS3V5*^{fl-st/wt}; *CMV-Cre*^{X-tg/y} (For a detailed explanation see chapter 5.3.3).

4.14.1.3.2 *Hb9-Cre* mice

In the *Hb9-Cre* mouse line the *Cre* gene is expressed under the intrinsic motor neuron-specific promoter of the *Hb9* gene. Since homozygous loss of *Hb9* results in perinatal lethality and because the *Cre* insertion disrupts *Hb9* function (Arber et al., 1999, Yang et al., 2001) it is only possible to keep the *Hb9-Cre* transgene in a heterozygous state. By breeding

the *PLS3V5*-floxed line with *Hb9-Cre* mice, it was possible to delete the stop-cassette specifically in the motor neurons. This technique allows to investigate possible cell autonomous effects of *PLS3V5* overexpression on motor neurons, nerve terminals as well as AChR clustering. The *Hb9-Cre* line was on pure C57BL/6N background.

4.14.2 Preparation of mouse tissues and organs

For the preparation of mouse organs, the animals were euthanized, placed on their dorsal side and arms and legs were fixed using needles. A longitudinal section was cut through the abdominal wall and the rib cage to open the animal. The rib cage and abdominal skin were stretched sideways and also fixed with needles. Organs were isolated into 1.5 ml tubes using ligature scissors and dissecting forceps and could directly be used for isolation of RNA or proteins. Alternatively, organs were snap frozen in liquid nitrogen and placed at -80°C for longer storage.

4.14.2.1 Isolation of the spinal cord

To isolate the spinal cord as a whole, the fur and skin on the dorsal side of the euthanized animal had to be removed. Next, it was cut in posterior to anterior direction along the spine. Head and tail were cut off and the spine was removed by carefully detaching it from ventral connective tissue. Using a scalpel, the tail region of the spinal cord was removed up to where the lumbar region begins. In a next step, PBS was loaded into a 20 ml syringe and the blunt grinded 20G needle inserted into the lumbar end of the spinal cord. Under constant pressure, the spinal cord was flushed out of the spine into a glass containing 1 x PBS. For subsequent staining procedures, the spinal cord was fixed for 2 d in 4 % PFA at 4°C and then embedded into paraffin. When used for RNA or protein isolation, the halves of the spinal cord were separated longitudinally. One half was used for RNA while the other half was used for protein isolation.

4.14.2.2 Preparation of muscle tissue

4.14.2.2.1 *Transversus abdominis* muscle

The isolation of the proximal *Transversus abdominis* (TVA) muscle is laborious and requires working under a stereomicroscope. To open the skin, first a little cut was made above the genitals of the euthanized animal. Next, a careful section once around the belly and immediately under the skin was performed. Using forceps, the animal was skinned over the head so that the underlying abdominal wall was exposed. Before the next steps, the connective- and muscle tissue of the neck and the throat had to be removed. Then, the abdominal wall was opened carefully just above the bladder of the animal. In a next step, it was cut on both sides laterally towards the spine and on the dorsal side of the animal along the spine towards the neck through the dorsal part of the ribcage. To remove the ribcage

from the abdominal cavity, it was sectioned through the diaphragm from both sides. The whole ribcage was then placed on Sylgard-filled Petri dishes, the abdominal wall was stretch-fixed using fine minutien-pins and covered in 1 x PBS. To expose TA muscle, small windows were cut through the first three muscle layers (Rectus abdominis, external oblique muscle and internal oblique muscle) using micro scissors. After fixing the whole rib cage for 20 min in 4 % PFA the windows were excised and stored in 1 x PBS at 4°C for subsequent staining procedures.

4.14.2.2.2 Isolation of *Gastrocnemius* and *Vastus lateralis* muscle

To isolate *Gastrocnemius* and *Vastus lateralis* muscle, the legs were cut off from the euthanized animal just above the pelvises. Using forceps, remaining skin and hair were removed.

For preparation of *Gastrocnemius* muscle, attaching tendons of the femoral bone and Achilles tendon were intersected so that the muscle could easily be isolated. For *Vastus lateralis* isolation, the lower leg was cut off after *Gastrocnemius* preparation. The upper leg was fixed and embedded as whole prior sectioning.

For fixation, muscles were incubated for 10 min in 4 % PFA. *Gastrocnemius* was most of the times immediately used in subsequent neuromuscular junction (NMJ) staining procedures. Alternatively, it was stored for up to one week in 1 x PBS at 4°C. For isolation of protein, *Gastrocnemius* was snap frozen and proteins were isolated whenever needed. *Vastus lateralis* was exclusively used for muscle fiber size determination and therefore dehydrated and subsequently embedded for sectioning.

4.14.2.3 Motoric ability testing and weight measurement

To analyze the motoric ability of animals, the tube test and the righting reflex test were recruited (El-Khodori et al., 2008).

Via the tube test, the proximal hind limb muscle strength, weakness and fatigue in mouse Neonates can be assessed. The test is performed in two consecutive trials, whereby the animal is placed head down into a 50 ml Falcon tube hanging by its hind limbs. In the following, the so called hind limb score (HLS) was evaluated based on the positioning of the hind limbs towards each other (Figure 5).

The righting reflex test is another method to examine muscle strength. For this test, animals were placed on their back on a flat surface. The time to reposition themselves was measured over a 30 sec period. The righting times were related to a score in the following manner: >1 sec = 0, 1-2 sec = 1, 3-4 sec = 2, 5-6 sec = 3, 7-8 sec = 4, 9-10 sec = 5, <10 sec = 6.

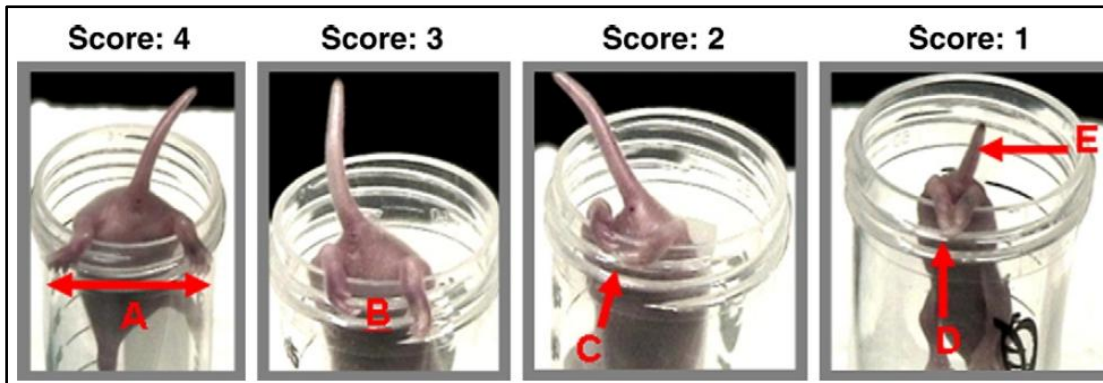


Figure 5: Tube test (El-Khodor et al., 2008): Hind limb scores (HLS) and respective leg positions for motoric ability assessment

4.14.3 The *Cre/loxP* system for conditional gene-deletion or activation

The *Cre/loxP* system is a genetic recombination tool which was developed in the 1980s and patented by DuPont. The system allows the deletion of any kind of DNA sequences located between two *loxP* sequences, which are target sites for the recombinase Cre (Cyclization recombination).

For gene deletion, the *loxP* sites are targeted into the endogenous gene locus flanking the whole gene or only certain parts, e.g., an exon important for proper function of the protein. The targeted mouse line with the so called floxed allele is then crossed with another mouse line expressing *Cre* recombinase under a tissue specific promoter. In the offspring carrying both the floxed allele as well as the *Cre* recombinase the target gene (or exon) will be deleted only in the tissue where *Cre* is active (Figure 6, A).

For conditional transgene expression, as used in the present work, a floxed stop cassette is cloned between a ubiquitously active promoter (e.g. CAG promoter) and the transgene (chapter 5.1.1). When the *LoxP* line is then crossed with another line expressing *Cre* under a tissue specific promoter, the stop cassette is conditionally deleted resulting in tissue specific transcription of the transgene (Figure 6, B). In this work, motor neuron specific activation of *PLS3V5* was established using a *Cre*-line carrying *Cre* under the motor neuron specific *Hb9*-promoter .

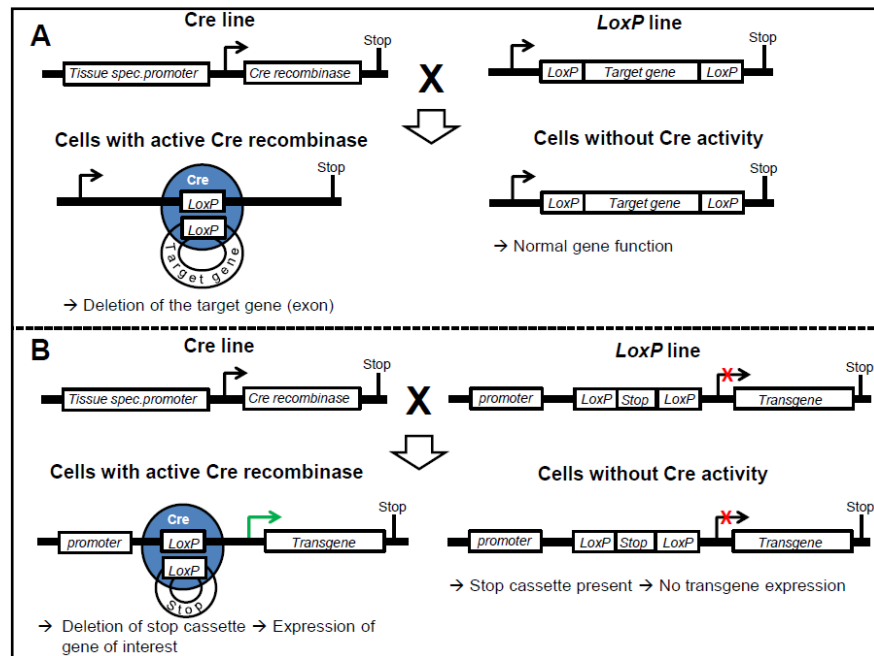


Figure 6 **Cre/loxP system. A:** Cre is expressed under a tissue specific promoter and therefore tissue specifically deletes the floxed target gene. **B:** Cre/loxP system in conditional transgene expression. Cre is expressed under a tissue specific promoter and accomplishes deletion of the floxed stop cassette present between promoter and transgene. This results in tissue specific transgene expression.

4.15 Statistical methods

To test significance of measurements the directional student's t-test was recruited. Three levels of statistical significance were distinguished: $p < 0.05 = *$, $p < 0.01 = **$, and $p < 0.001 = ***$. Furthermore, a Wilcoxon-rank-sum test was performed in order to determine the significance of the survival differences (the shift of the Kaplan-Meier curves) between SMA and *PLS3V5* + SMA mice and SMA mice on different genetic backgrounds.

5 Results

5.1 Generation of the *Rosa26* targeting construct

5.1.1 *Rosa26* targeting and structure of the targeting construct

Currently, the two most common methods for the generation of transgenic animals are (i) pronuclear injection or (ii) gene targeting into a certain locus of the mouse genome. For pronuclear injection, a solution of DNA is directly injected into fertilized oocytes with a micro syringe under a microscope (Costantini and Lacy, 1981, Gordon and Ruddle, 1981). In a next step, the blastocysts are then transplanted into pseudopregnant recipient females. Transgenic founder can be obtained after 3 weeks and be bred with wt animals another 7 weeks later to identify germline transmission. This method of transgenesis offers the advantage of being relatively fast and cost effective. Since the insertion of the transgene into the genome is random, however, the chance exists that it integrates into another gene or its promoter region, thereby disrupting the function of the gene. Insertional mutagenesis can therefore contribute to any observed phenotype and complicate analysis. Furthermore, transgenes are often silenced due to multiple transgene copy number insertions (up to 1000+ tandem copies of the transgene) (Garrick et al., 1998).

To circumvent these problems, targeted transgenesis into the *Rosa26* locus was used in this work. For targeted transgenesis, ES cells were stably transfected with the targeting vector carrying the transgene. After selection of clones that had correctly inserted the targeting construct in the *Rosa26* locus, cells of such clones were injected into blastocysts and these transplanted into pseudopregnant females. After 3 weeks chimeric mice were born, raised to adulthood and bred with wt mice to scan the F1 offspring for transgenic founder animals.

The *Rosa26* locus is frequently used for transgenesis of mice since integration into this site occurs highly efficient, it supports strong and ubiquitous expression of inserted sequences and is not subjected to gene silencing effects (Zambrowicz et al., 1997). Importantly, the murine *Rosa26* locus is located on chromosome 6. Since *Smn*, *hSMN2* and *Hb9-Cre* all map to other chromosomes, it was possible to cross the *PLS3V5* transgene onto the SMA background (Figure 7) or to motor neuron specifically express the transgene. E.g., to study the effect of *PLS3V5* overexpression on the SMA phenotype, *PLS3V5^{tg/wt}; Smn^{-/-}; hSMN2^{tg/wt}* mice were generated. In case, however, that *PLS3V5* and the *Smn* knockout mapped to the same chromosome, it would not be possible to express *PLS3V5* on an *Smn^{-/-}* background since the allele carrying *PLS3V5* carries a wt version of *Smn*.

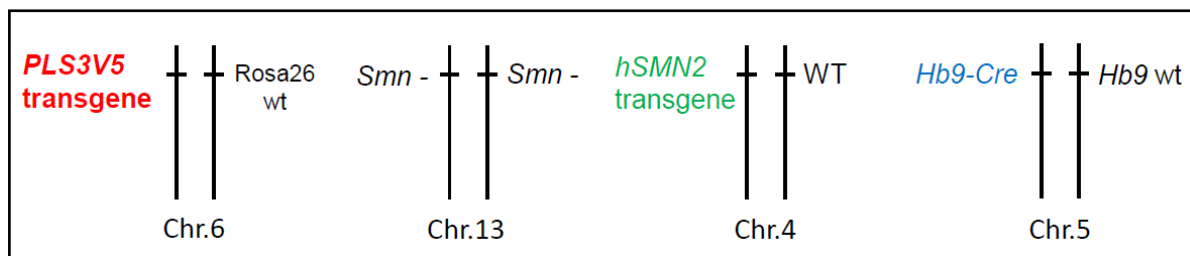


Figure 7: Illustration of the chromosomal location of transgene and knockout alleles important in this work. *Rosa26* maps to chromosome 6 and thus *PLS3V5*, *Smn* is located on chromosome 13, the *hSMN2* transgene is on chromosome 4. *Hb9-Cre* maps to chromosome 5 and has been inserted under the *Hb9*-promoter.

In the *Rosa26* targeting construct (Kindly provided by Dr. Thomas Wunderlich, University of Cologne (Belgardt et al., 2008)) the gene of interest, in this work *PLS3V5*, is cloned via an *Asc I* restriction site and driven by the CMV enhancer/chicken β -actin (CAG) promoter (Figure 8). The Neomycin resistance gene (*Neo'*) and the transcription stop cassette are flanked by *loxP* sites on both sides and are located between promoter and transgene to allow conditional activation of the transgene (*Cre/loxP* system, chapter 4.14.3). 3' of the gene of interest, *green fluorescent protein (GFP)* is cloned behind an internal ribosomal entry site (*IRES*) allowing indirect detection of the transgene *in vivo*. The size of the DNA homology arms was 1.080 and 4.247bp for the short and long arm, respectively. The sequences were cloned 5' and 3' flanking the internal elements to allow targeted homologous recombination. Additionally, *Diphtheria toxin A* was cloned 3' of the long homology arm and served as negative selection marker in case of non homologous random insertion of the construct. The sequence including both homology arms and internal elements has a size of 16.054 bp. The nucleotide sequence of the targeting construct is included in the appendix of this work.

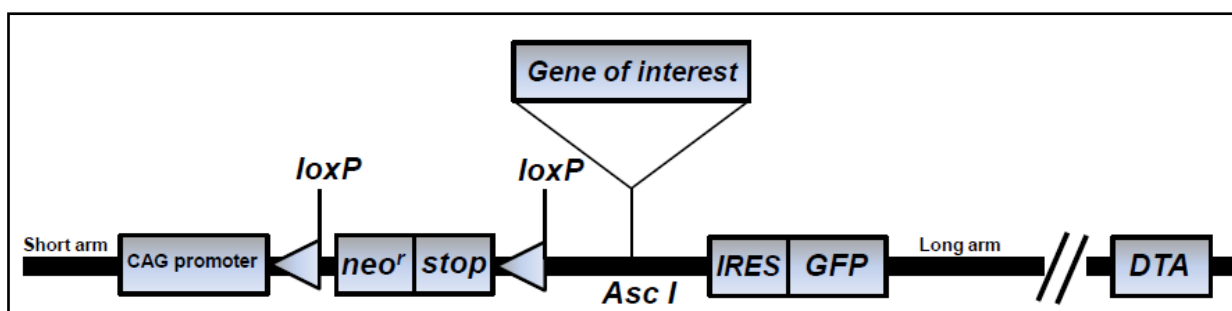


Figure 8: The *Rosa26* targeting construct. (Abbreviations: CAG = CMV enhancer/chicken β -actin promoter, *Neo'* = Neomycin, *IRES* = internal ribosomal entry side, *GFP* = *green fluorescent protein*; *DTA* = *Diphtheria toxin A*).

5.1.2 3 Step (A-C) strategy for cloning *PLS3V5* into the *Rosa26* targeting vector – Overview

Before *PLS3* was inserted into the *Rosa26* targeting vector, a *V5*-tag was cloned in frame with the *PLS3* coding sequence (cds) so that the transgene could be discriminated from murine *Pls3*. For that purpose, *PLS3* cds was inserted into the pcDNA3.1V5/His Topo vector (Figure 9, Step A). After confirmation of the sequence, *Asc I* restriction overhangs were

added to the 5' and 3' ends of *PLS3V5* via HiFi Taq PCR and the product was subcloned into Zero blunt Topo (Step B). The sequence was again confirmed and using enzymatic restriction with *Asc* I, *PLS3V5* was cut out of the vector and finally ligated into the *Rosa26* targeting vector (Step C). The GVO numbers of the sequence-confirmed clones are depicted in Figure 9.

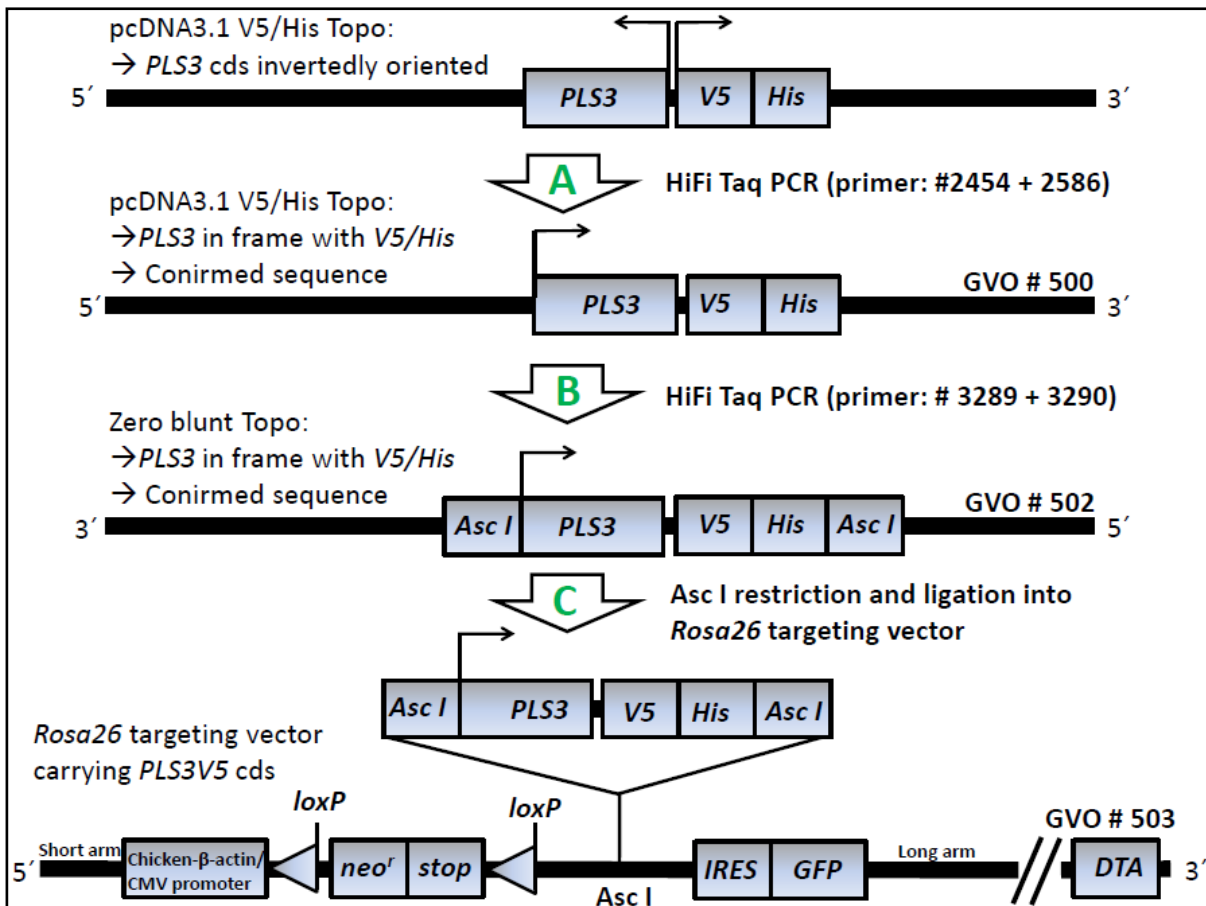


Figure 9: Steps of *PLS3V5* cloning into the targeting vector. **A:** Amplification of *PLS3* and subcloning into pcDNA3.1V5/HIS Topo vector to add the V5-tag. **B:** Amplification of *PLS3V5* using *Asc* I restriction overhang primers and subcloning into Zero blunt Topo. Note that *Asc* I-*PLS3V5*-*Asc* I was reversely cloned as indicated by the 5' and 3' orientation of the vector. **C:** Enzymatic restriction with *Asc* I and ligation into the *Rosa26* targeting vector. (Abbreviations: GVO # = *Gentechnisch veränderter Organismus*)

5.1.2.1 Step A: Subcloning of *PLS3* into the pcDNA3.1V5His Topo vector

At the beginning of this work, *PLS3* cds (1893bp) was present in the pcDNA3.1V5/His Topo vector, however it was inversely oriented. To correctly add the V5-tag 3' of the *PLS3* cds, *PLS3* was first amplified using HiFi Taq, purified via a 1 % agarose gel and again subcloned into the pcDNA3.1V5/His vector (Figure 9). Clones with correct orientation of the *PLS3* insert were identified via colony-PCR, amplified, plasmids isolated and subjected to test restriction using *Xmn* 1 and *Hind* III restriction enzymes (Figure 10).

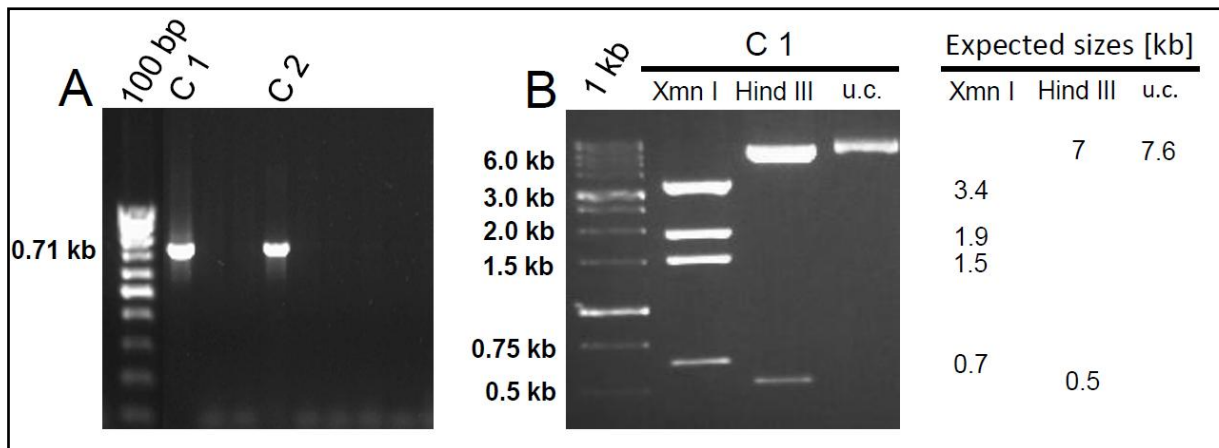


Figure 10: **A:** Colony PCR of *PLS3V5* in pcDNA3.1V5/His (Primer: #1840 + 2457, expected size = 714 bp) **B:** Test restriction of clone 1 of *PLS3V5* in pcDNA3.1V5/His and respective expected sizes. (Abbreviations: C = clone; u.c. = uncut vector)

Clones showing the expected restriction band pattern were analyzed via sequencing to assure that no mutations were present after the PCR-amplification step and that the *V5*-tag was in frame with *PLS3* cds. Clones were backup-frozen in liquid nitrogen under GVO reference number 500.

5.1.2.2 Step B: Addition of *Asc* I restriction overhangs to *PLS3V5* and subcloning into Zero blunt Topo

For inserting *PLS3V5* into the *Rosa26* targeting vector, *Asc* I restriction sites had to be cloned 5' and 3' of *PLSV5*. For this purpose, *PLS3V5* was Hifi Taq-amplified from GVO # 500 (Figure 9) with *Asc* I restriction-overhang primers, gel purified and subcloned into Zero blunt Topo. Since the orientation of *PLS3V5* in this vector was of no relevance, a colony PCR using primers binding in the internal region of *PLS3* was performed. Through test restriction clone one (C 1) was identified as reversely inserted into Zero blunt and afterwards confirmed to be correct by complete sequencing of the insert (Figure 11). Bacteria of this clone were backup-frozen in liquid nitrogen under GVO reference number 502.

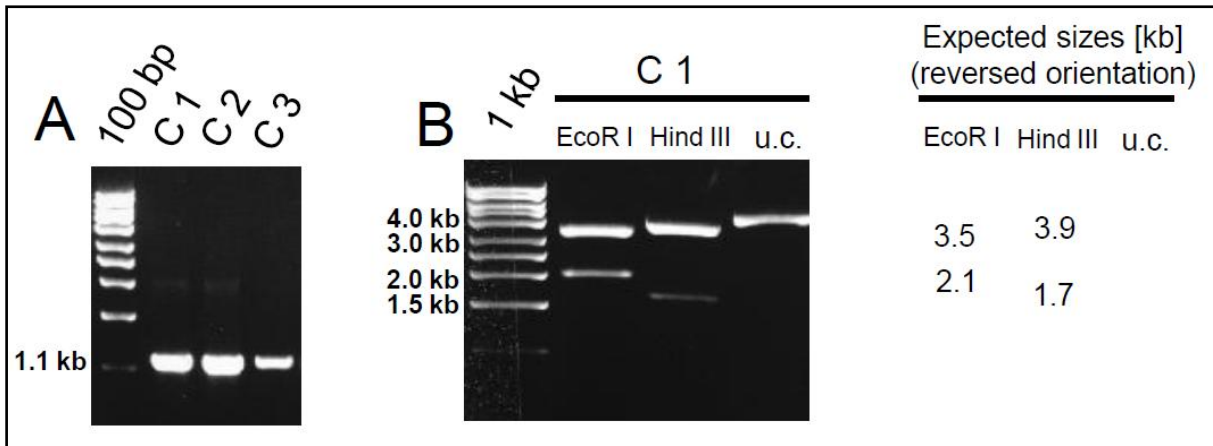


Figure 11: **A:** Colony PCR of *PLS3V5* with *Asc I* restriction sites in Zero blunt Topo (Primer: #2463 + 2456, expected size = 1.1kb). **B:** Test restriction of C 1 using *EcoR I* and *Hind III* revealed a reversed insertion of *Asc I-PLS3V5-Asc I* into Zero blunt Topo. (Abbreviations: C = Clone; u.c. = uncut)

5.1.2.3 Step C: Insertion of *PLS3V5* into the *Rosa26* targeting vector

To insert *PLS3V5* into the *Rosa26* targeting vector, GVO clone # 502 and the empty targeting vector were enzymatically restricted using *Asc I* (Figure 12, A). After restriction was completed, the *PLS3V5* band (~2 kb) and the linearized *Rosa26* targeting vector (~16 kb) were cut out of the gel and purified using QIAquick Gel Extraction Kit. To avoid religation, the linearized targeting vector was alkaline phosphatase treated and subsequently phenol/chloroform extracted. Since transformation of large constructs into bacterial cells can be problematic, XL1-Blue bacteria were used in this approach. Bacteria were selected against Ampicillin, clones picked the next morning and subjected to colony PCR (Figure 12, B). Positive clones were amplified and a test restriction was performed using *EcoR V*, *Xho I* and *Asc I* (Figure 12, C) After observation of the correct band pattern, clone 1 (GVO # 503) was analyzed by sequencing and found to be 100 % correct (Figure 12, D). Since large amounts of *Rosa26* targeting vector were needed for the transfection of ES cells, new media was inoculated with GVO clone # 503 and Maxi preparation of the plasmid was performed using the EndoFree Plasmid Maxi Kit (*Qiagen*). The transfection of ES cells, ES cell selection, clone picking and DNA preparation for subsequent Southern blot analysis were performed as described in the Material and Methods part of this work (chapter 4.13.3).

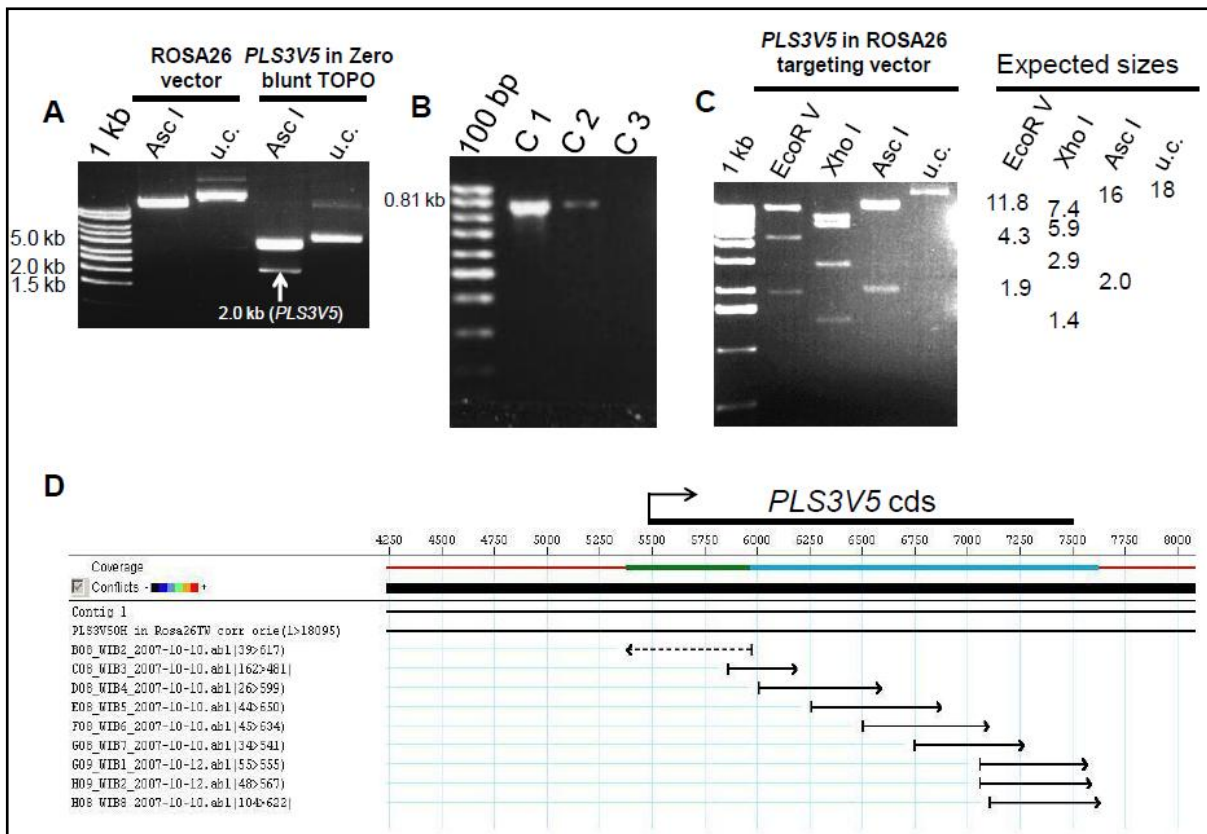


Figure 12: **A:** Enzymatic restriction digestion of the *Rosa26* targeting vector and *PLS3V5* in Zero blunt Topo with *Asc* I. **B:** Colony PCR with clones obtained after ligation of *PLS3V5* into the *Rosa26* targeting vector (Primer: #2533 + 2459, expected size = 817bp). **C:** Test restriction of the targeting vector containing *PLS3V5* demonstrated the correct insertion of *PLS3V5* into the *Rosa26* targeting vector. Note that restriction with *Asc* I results in appearance of the 2 kb *PLS3V5* band. **D:** Snapshot of Seqman sequencing analysis software showing 100 % correct sequence for the ready cloned targeting construct (Abbreviations: C = clone, u.c. = uncut).

5.2 Transgenesis of ES cells

5.2.1 Stable integration of the targeting construct into the genome of ES cells

The transfection of ES cells, ES cell selection, picking of recombinant clones and DNA restriction using *EcoR* I for subsequent Southern blot analysis were performed as described in the Material and Methods part of this work (chapter 4.13.3). In the following chapters, the identification of correctly targeted ES cells via Southern blotting and the evaluation of such clones via *in vitro* Cre-deletion will be described.

5.2.1.1 Southern blotting strategy

The correct insertion of a targeting construct into its destined region is typically investigated and confirmed via Southern blotting. For this purpose, genomic DNA of recombinant clones was enzymatically restricted with *EcoR* I and then transferred on a Hybond XL membrane. To identify recombinant clones with a correctly inserted targeting construct, also termed positive clones, two different radioactively labeled probes were used: (i) An external probe, termed *Rosa* probe, that binds in the genomic region 5' of the short

homology arm of the construct. After restriction of genomic DNA with EcoR I, a 6.8 kb recombinant fragment is observed in the case of correct insertion of the targeting vector (Figure 13, A). Since homologous recombination is a rare event, the targeting construct typically inserts on one chromosome only, while the other chromosome remains wt. On the wt chromosome, restriction with EcoR I then leads to a fragment of 16 kb size (Figure 13, B). (ii) An internal probe, termed *Neo* probe, which is complementary to parts of the *Neo^r* gene and detects the same 6.8 kb fragment as the *Rosa* probe in case of correct homologous recombination into the target site and digestion of DNA with EcoR I enzyme (Figure 13, C). However, random integration of the insert can only be detected by the *Neo* probe: In case of non homologous recombination a fragment of undefined size is observed ranging from the internal EcoR I restriction site in the stop-cassette to the next genomic upstream EcoR I restriction site in the region 5' of the short homology arm (Figure 13, D).

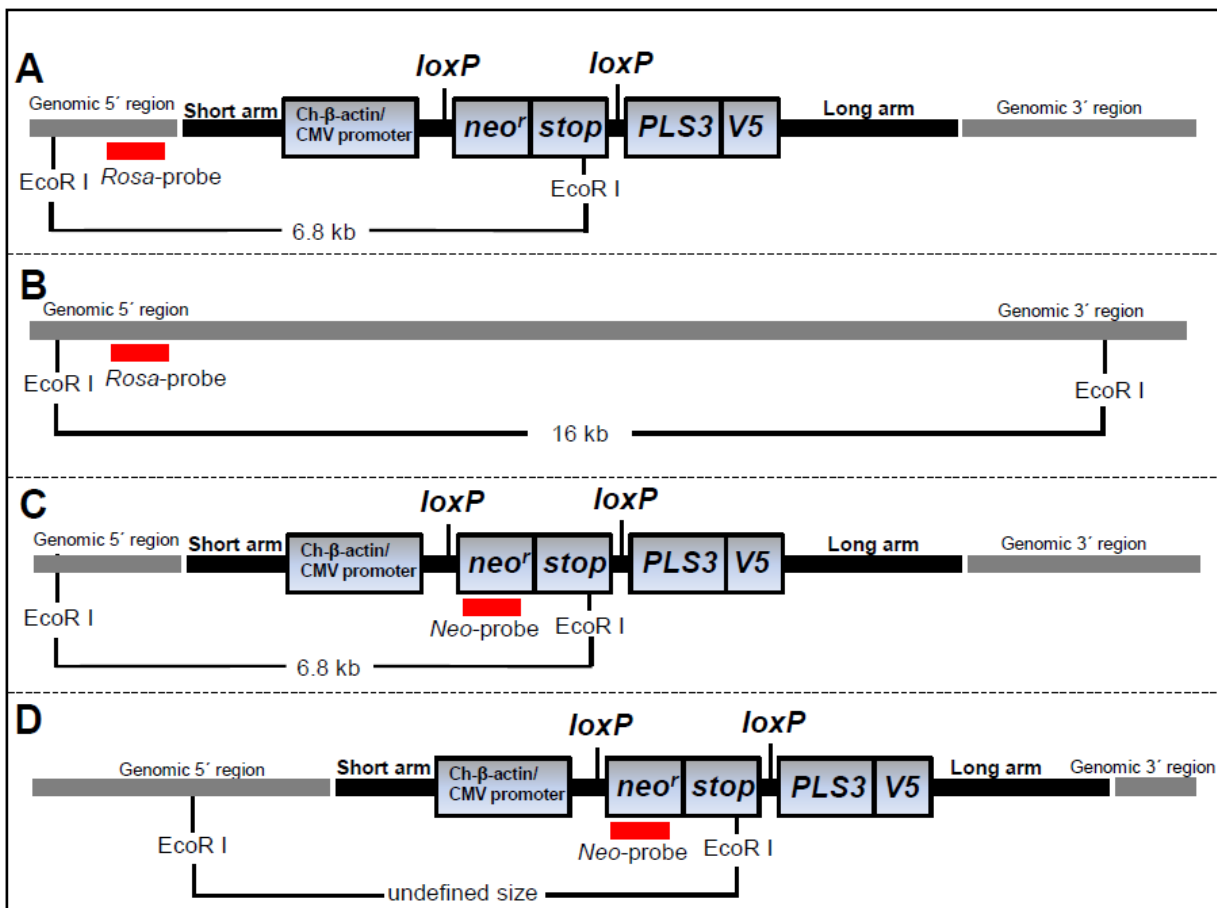


Figure 13: Southern blotting strategy to identify recombinant ES cell clones with correct insertion into the *Rosa26* locus. **A:** In case of homologous recombination of the targeting vector into the *Rosa26* locus, the *Rosa* probe detects a 6.8 kb DNA fragment. **B:** On a wt chromosome, the *Rosa* probe recognizes a 16 kb fragment. **C:** The *Neo* probe binds in the *Neo^r* gene and identifies the same 6.8 kb fragment as the *Rosa* probe in case of homologous recombination. **D:** In case of random integration of the targeting construct, the *Neo* probe will detect a fragment of undefined size

5.2.1.2 Identification of positive clones via Southern blotting

The Southern blot strategy for the identification of positive recombinant ES cell clones with a correctly inserted targeting construct using an external (*Rosa*) as well as internal (*Neo*) probe was described in detail (chapter 5.2.1.1). To identify positive clones, genomic DNA was isolated from 96 well backup plates and enzymatically restricted by *EcoR* I digestion. The genomic DNA of each clone was separated by gel electrophoresis and the DNA blotted on a nylon membrane. In a next step, the membrane was incubated with the radioactively labeled external *Rosa* probe and analyzed using a phosphorimager (Figure 14, A). Of 196 spotted clones, 8 clones were identified as recombinant for the *Rosa26* targeting construct resulting in a recombination efficiency of 4.1 %.

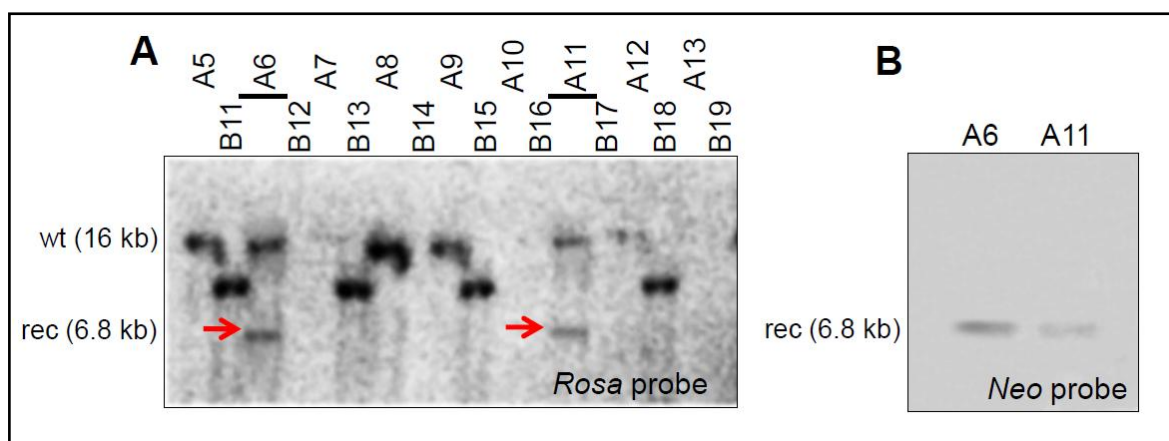


Figure 14: **A:** Snapshot of a membrane of clones from one 96 well plate hybridized with the *Rosa* probe. Clones were loaded next to each other in two vertical rows (E.g., A5-A13, B11-B19). Next to the 16 kb wt band, clones A6 and A11 (underlined) showed the 6.8 kb recombinant band (red arrows) and were identified as positive clones. **B:** Exclusion of random integration of the *Rosa26* targeting construct into the genome in positive clones A6 and A11

All 8 positive clones were thawed from 96 well plates, expanded to 10 cm dishes and finally frozen as $\frac{1}{4}$ aliquots of one 10 cm dish. However, only clones A6 and A11 showed a high proliferation rate and were further analyzed via *in vitro* Cre deletion of the stop cassette (chapter 5.2.1.3). Since the *Rosa* probe does not identify random genomic integration of the targeting construct and to exclude this possibility, clones A6 and A11 were additionally investigated using the *Neo* probe. As expected and considering that homologous recombination is a rare event both clones A6 and A11 showed exclusively the predicted band at a size of 6.8 kb (Figure 14, B).

Therefore, it was concluded that the *Rosa26* targeting vector had correctly integrated into the *Rosa26* genomic locus in clones A6 and A11.

5.2.1.3 *In vitro* Cre deletion and analysis of positive ES cell clones

In vitro Cre deletion is a powerful tool to delete *loxP* flanked sequences in cell culture experiments. The technique makes use of a modified version of *Cre* recombinase (HTN-Cre) that carries a hydrophobic N-terminal tag including a nuclear localization signal (NLS) (Peitz

et al., 2002). If added to the cell media, HTN-Cre can permeate the membrane, be transported into the nucleus and catalyze recombination of *loxP*-flanked sequences. Here, this method was recruited to evaluate the potential of positive ES cell clones to express *PLS3V5* before they were injected into blastocysts. Moreover, any cell toxicity effects caused by the overexpression of the transgene would become obvious. In line with that, such observations would make it necessary to reassess the chances of success in establishing a transgenic *PLS3V5* overexpressing mouse line.

To analyze HTN-Cre-mediated activation of *PLS3V5*, positive ES cell clones A6 and A11 (chapter 5.2.1.2) were thawed from ¼ aliquots of one 10 cm petri dish. After expansion of the clones to 80 % confluence, *in vitro* Cre treatment was conducted (chapter 4.13.3.8). Since *in vitro* HTN-Cre treatment is a rather harsh method that can lead to cell death, ES cells were given 4 days to recover prior analysis.

In vitro Cre-deleted ES cells were first analyzed under a fluorescence microscope. Given that *GFP* is located downstream of the *PLS3V5* cds in the targeting vector (Figure 8), the deletion of the stop-cassette should result in a green fluorescent signal. As anticipated, both recombinant clones (A6 and A11) that were treated with HTN-Cre showed a green fluorescent signal while no signal was detected under UV light for untreated cells (Figure 15, compare A+B with E+F and I+J with M+N). To further support these observations, clones A6 and A11 were trypsinized and subjected to FACS analysis. When gating the ES cell population, a clear peak-shift towards GFP was detected for both clones and only when cells were treated with HTN-Cre (Figure 15, compare D with H and L with P). Additionally, by comparing HTN-Cre treated with untreated cells under transmitted light no morphological differences could be observed. Stop-cassette-deleted clones exhibited the typical ES cell-like shape as untreated controls and appeared to proliferate normally. Taken together, these experiments demonstrate that the deletion of the stop-cassette results in GFP expression and that, accordingly, the *Cre/loxP* expression system of the targeting vector is functional.

Since GFP expression after stop-cassette deletion alone is only a principle proof for the functionality of the *Cre/loxP* expression system, proteins were isolated from the remaining cells and examined for *PLS3V5* expression via Western blotting. Using a V5 antibody for the specific detection of *PLS3V5*, a sharp and clear signal in the calculated size of ~75 kDa could only be observed for HTN-Cre treated cells of both clones, A6 and A11 (Figure 16).

To summarize, via HTN-Cre mediated deletion of the stop-cassette the expression of both, *PLS3V5* and *GFP* could be induced. These findings demonstrate the functionality of Cre-inducible conditional activation of the vector-expression system. Additionally, the absence of any GFP or *PLS3V5* signals in untreated cells, either via FACS as well as in Western blot analysis, proves that the stop-cassette successfully prevents uncontrolled transcription of the transgenes. Based on these findings and in combination with the proof of

correct insertion of the targeting vector into the *Rosa26* locus (chapter 5.2.1.2), clones A6 and A11 were used for the injection into blastocysts (chapter 5.3.2).

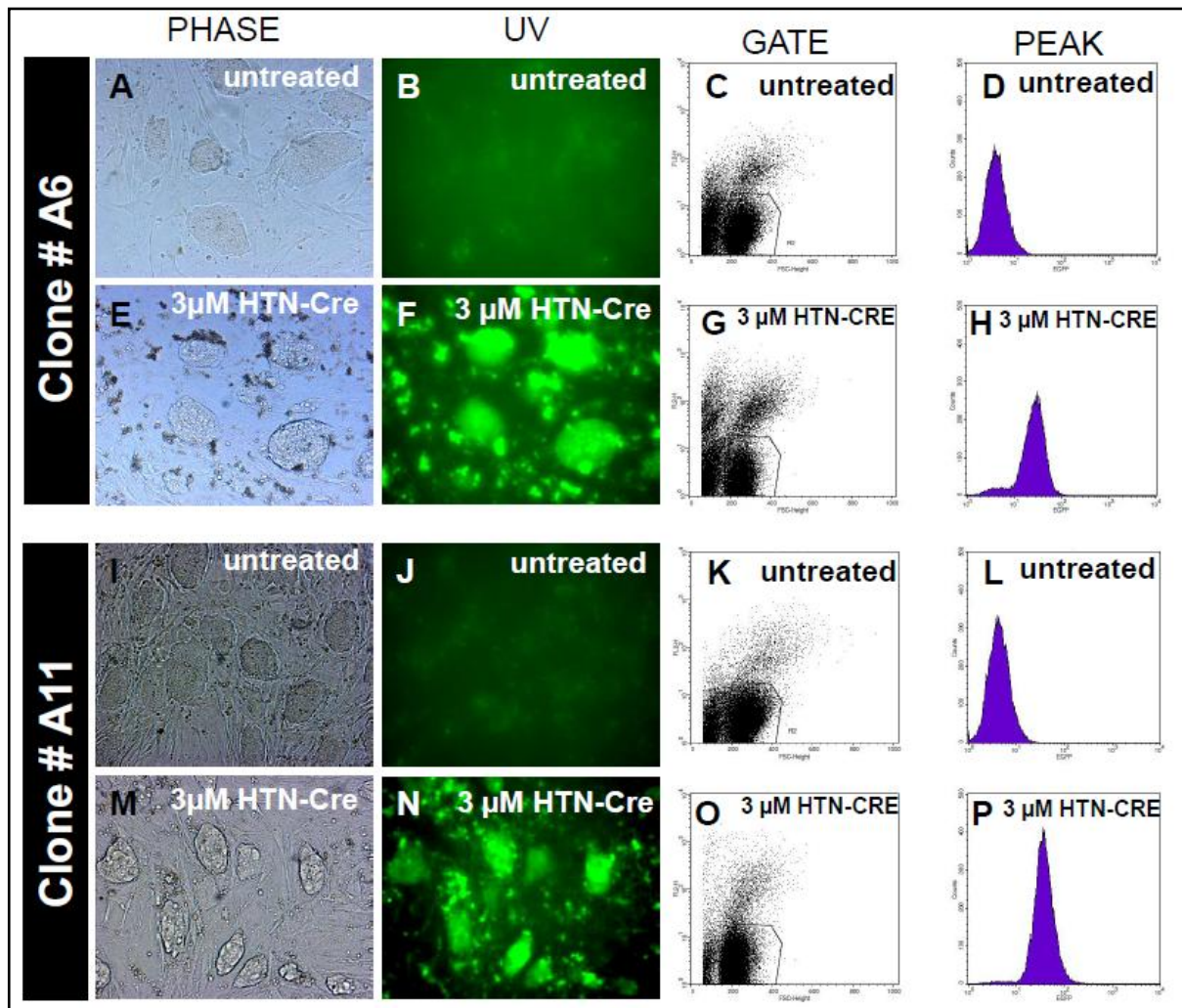


Figure 15: GFP expression after HTN-Cre mediated deletion of the stop-cassette. **A-H:** Microscopical- and FACS detection of GFP fluorescence after stop-cassette deletion in clone A6. **I-P:** Microscopical- and FACS detection of GFP fluorescence after stop-cassette deletion in clone A11. For FACS analysis, the ES cell population was gated and analyzed for GFP expression.

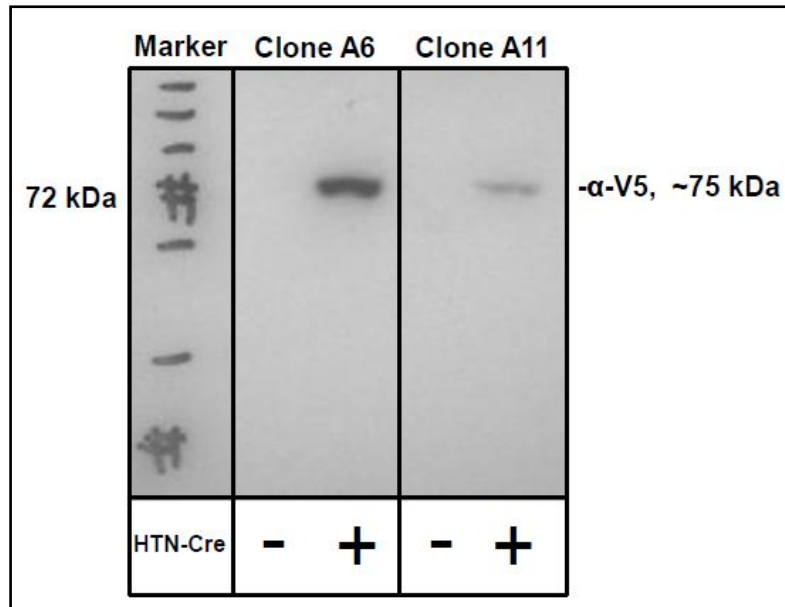


Figure 16: Western blot analysis of ES cell clones A6 and A11 with or without HTN-Cre treatment. Using an antibody directed against the V5-tag of the PLS3V5, only cells treated with HTN-Cre and deleted for the stop-cassette express PLS3V5 and show a sharp signal at the correct size of ~75 kDa

5.3 Generation of PLS3V5 transgenic mice

5.3.1 Nomenclature of the PLS3V5 transgenic mouse lines generated in this thesis - Overview

In the course of this work, first a stable cohort of PLS3V5 transgenic mice was generated that still carried the stop-cassette between promoter and the PLS3V5 cds (chapter 5.3.2). This line is from now on termed the **PLS3V5-floxed** line. To indicate that the stop-cassette is still present between promoter and the PLS3V5 cds in these mice, e.g. heterozygous individuals of this line are from now on defined as **PLS3V5^{fl-st/wt}** (fl = floxed, st = stop) mice. Due to the presence of the stop-cassette in PLS3V5^{fl-st/wt} mice, PLS3V5 is not yet being expressed in such individuals. By breeding PLS3V5^{fl-st/wt} mice with Cre-lines expressing Cre under tissue specific promoters, conditional activation of PLS3V5 can be achieved. In this thesis, PLS3V5^{fl-st/wt} animals were e.g. bred with the motor neuron specific Cre line *Hb9-Cre* (Arber et al., 1999, Yang et al., 2001) to exclusively activate transcription of the PLS3V5 transgene in motor neurons.

To activate PLS3V5 expression ubiquitously, the stop-cassette in PLS3V5^{fl-st/wt} animals was deleted by breeding animals of the PLS3V5-floxed line with the ubiquitously Cre-expressing line *CMV-Cre* (Schwenk et al., 1995). As a result, a stable cohort of PLS3V5 ubiquitously expressing animals was generated (chapter 5.3.3). This line is from now on termed the **PLS3V5-ubi** line. E.g., heterozygous individuals of this line are by now defined as **PLS3V5^{tg/wt}** mice. Once the stop-cassette was genomically deleted via Cre in the germline

and this was inherited to the next generation, the *Cre* allele was no longer necessary to ubiquitously activate *PLS3V5* expression.

In Table 13, an overview about the two different *PLS3V5* transgenic lines and their respective nomenclature is given.

Table 13: Nomenclature of transgenic *PLS3V5* lines generated in this thesis

<i>PLS3V5</i> transgenic line	E.g. heterozygous individual (exemplary)	E.g. homozygous individual (exemplary)	Description
<i>PLS3V5</i> -floxed	<i>PLS3V5</i> ^{fl₋st/wt}	<i>PLS3V5</i> ^{fl₋st/fl₋st}	Stop cassette present, conditional activation of <i>PLS3V5</i> via breeding with <i>Cre</i> -lines.
<i>PLS3V5</i> -ubi	<i>PLS3V5</i> ^{tg/wt}	<i>PLS3V5</i> ^{tg/tg}	Permanent and inherited deletion of stop cassette. Ubiquitous <i>PLS3V5</i> expression.

5.3.2 Generation of chimeras and identification of transgenic *PLS3*-floxed mice

For the generation of chimeric animals in which the germline carries the *PLS3V5* transgene, cells of both positive clones, A6 and A11, were prepared (4.13.3.10) and injected into blastocysts derived from CB20-background females (Table 14). Using ES cells of clone A6, an additional pilot-injection-series using morulae (2-3 dpf) was performed. At morula stage, cells are completely undifferentiated while around blastula stage, first gastrulation events take place and along with that the determination of cell fate precedes. For that reason and because morulae consist of fewer cells, it is assumed that injected ES cells are better integrated and can stronger contribute to the developing embryo.

Table 14: ES cell injection and chimera production

Injected clone (V6.5)	Date	Injected Blastulae / Morulae	Foster / pregnant	Pups / DOB	Chimeras (gender, % chimerism)
A6	11.12.08	29 Blastulae	3 / 3	13 / 28.12.08	7 (6 ♂, 10, 15, 25, 25, 45, 75 (#94); 1 ♀ 20)
	18.12.08	29 Blastulae	3 / 1	3 / 04.01.09	1 (1 ♂, 70 (#97))
	18.12.08	9 Morulae	1 / 1	1 / 05.01.09	1 (1 ♂, 75 (#98))
A11	12.12.08	26 Blastulae	3 / 0	-	-

Even though ES cells of both clones were injected, chimeric animals were only obtained following injection with clone A6 (Table 14). From injections into blastocysts and morulae, all together 9 chimeric mice were produced of which 3 male mice were of higher chimerism

(estimated by the percentage of dark hair contributing to the coat color), namely one 70 % (# 97) and two 75 % (# 94, 98) chimeric animals (Table 14, highlighted in red). Only the 3 higher chimeric animals were used for breeding with wt animals and the offspring screened for the presence of the insertional allele via PCR. (Figure 17).

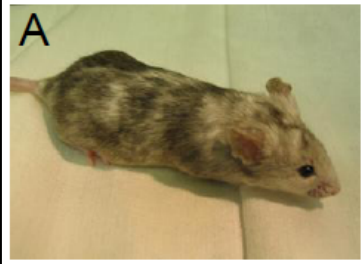
	B Chimera (% chimerism)	Number of litter	Number of offspring	Transgenic offspring
	♂ # 97 (70)	-	-	-
	♂ # 94 (75)	7	53	1
	♂ # 98 (75)	5	39	-

Figure 17: Chimera breedings with wt mice (F0) to obtain transgenic offspring in the F1 generation. **A:** Example of a 90 % chimeric mouse (picture kindly provided by Dr. Ylva Mende). **B:** Numbers of litters, offspring and transgenics obtained. Only a single transgenic female was obtained by chimera # 94.

Of the three chimeric mice used for F0 breedings with wt mice, animal # 97 was infertile and did not produce any offspring. However, chimeras # 94 and 98 were normally fertile and generated potentially transgenic F1 offspring that was screened via PCR for the presence of the targeting construct. Of a total of 92 F1 offspring screened via PCR (Primer see chapter 4.8), only one female mouse showed the recombinant band (Figure 18, A).

Since PCR is in fact a fast but also sensitive method, another PCR was conducted using a forward primer within *PLS3V5* and a reversed primer located in the 3'-V5-tag. Thereupon, a signal of correct size was only observed using DNA of the assumed *PLS3V5*^{fl-st/wt} (explanation of nomenclature see chapter 5.3.1) animal, but not in control wt DNA (Figure 18, B).

To further confirm the transgenic state of the animal, DNA of the tail tip was subjected to Southern blotting using *Rosa*- and *Neo* probes. When compared to wt control DNA, using the *Rosa* probe the recombinant band was only detected in the DNA of the *PLS3V5*^{fl-st/wt} mouse (Figure 18, C). With the *Neo* probe, a single band could be observed at the correct size in the *PLS3V5*^{fl-st/wt} animal.

A picture of the first *PLS3V5*^{fl-st/wt} female is depicted in Figure 18, D.

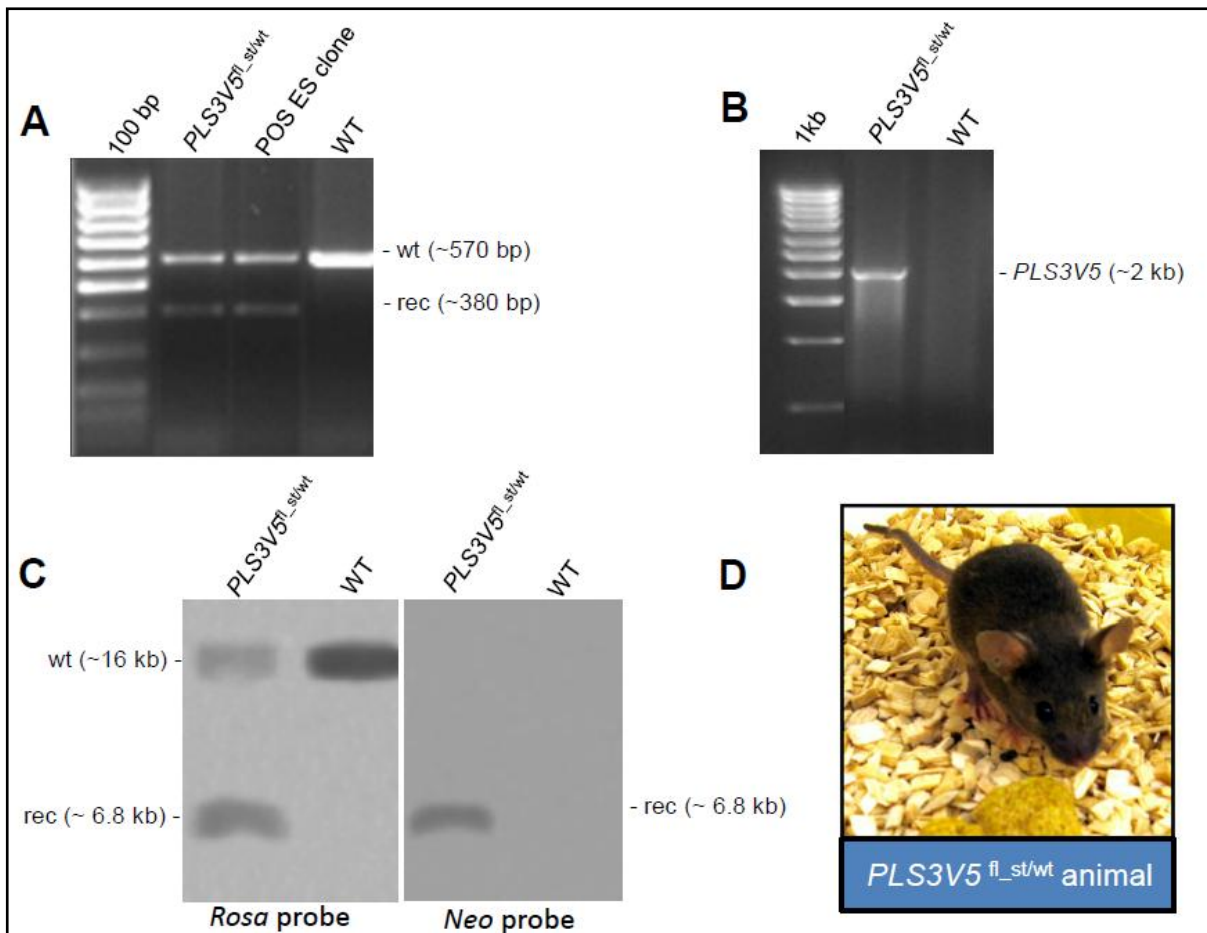


Figure 18: Confirmation of the first $PLS3V5^{fl_st/wt}$ female **A**: Screening (genotyping) PCR (primers # 3648, # 3649 and # 3650), **B**: PCR targeting $PLS3V5$ (primer # 3911 and # 3913), **C**: Southern blot using the *Rosa* probe. **D**: Picture of the first $PLS3V5^{fl_st/wt}$ female

To conclude, ES cells of clones A6 and A11 were injected into blastocysts and morulae and 3 higher percentage chimeras could successfully be produced from clone A6. Of the three chimeras, two males were fertile and one of them, chimera # 94, produced one single transgenic $PLS3V5^{fl_st/wt}$ female. The presence and correct insertion of the targeting construct into the *Rosa26* locus of the female was confirmed via PCR and Southern blotting. By breeding with a C57BL/6N wt male mouse a stable founder generation of the $PLS3V5$ -floxed line was established. Given that the first transgenic female was of 129/Sv and C57BL/6 mixed genetic background, the $PLS3V5$ -floxed line was backcrossed for 7 generations to a clean C57BL/6 background.

5.3.3 Generation of the $PLS3V5$ -ubi line by permanent deletion of the stop cassette in $PLS3V5$ -floxed mice

$PLS3$ has been shown to be expressed in a broad variety of tissues in rat, including liver, lung and heart as well as brain and muscle (Lin et al., 1994). Also in SMA patients, $PLS3$ is highly expressed in brain, spinal cord and muscle tissue, with its highest expression in the spinal cord (Oprea et al., 2008). In blood, however, $PLS3$ was shown to be present in 5 % of the control population only, confirming that $PLS3$ expression in blood is rare. In order to

optimally mimic the situation in unaffected patients, ubiquitous expression of the *PLS3V5* transgene was established.

Since *PLS3V5* expression is inhibited in the *PLS3V5*-floxed line by the presence of the stop-cassette, the ubiquitously *Cre*-expressing line *CMV-Cre* (*Cre* is located on the X-chromosome in these mice, see also 4.14.1.3.1) was used to permanently delete the stop-cassette in the *PLS3V5*-floxed line. For that purpose, male mice of the genotype $PLS3V5^{fl_st/wt}$ were bred with homozygous $CMV-Cre^{X_tg/X_tg}$ female mice (Figure 19, A). In resulting female offspring, one X chromosome originates from the father while the *Cre*-transgenic X chromosomes is derived from the mother. Due to X inactivation, however, one X chromosome is randomly silenced. Accordingly, the female offspring is mosaic for the *Cre* expression and the stop cassette is not deleted in all cells. Yet in the resulting male offspring the *Cre*-carrying X chromosome can only result from the $CMV-Cre^{X_tg/X_tg}$ mother. Because the only X chromosome in $PLS3V5^{fl_st/wt};CMV-Cre^{X_tg/Y}$ male mice is never silenced, *Cre* is active in all cells of the body and consequently, the stop-cassette should be deleted in all cells as well. By breeding a $PLS3V5^{fl_st/wt}$ male with a $CMV-Cre^{X_tg/X_tg}$ female mice, males with the genotype $PLS3V5^{fl_st/wt};CMV-Cre^{X_tg/Y}$ were obtained (Figure 19, A, B).

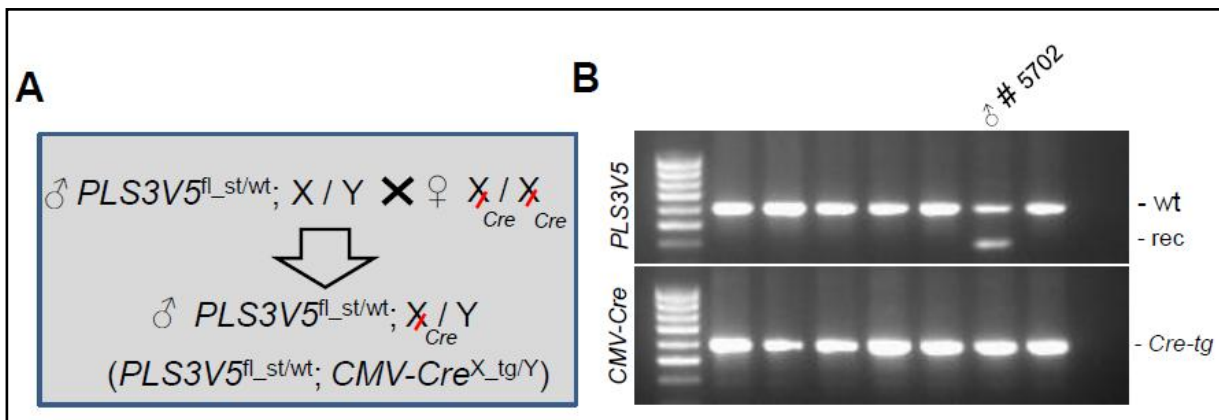


Figure 19: Ubiquitous deletion of the stop cassette. **A:** Breeding scheme for $PLS3V5^{fl_st/wt}$ X $CMV-Cre$ crossings. **B:** Genotyping PCR (Primer: *PLS3V5*: # 3648, # 3649 and # 3650; *CMV-Cre*: # 3104 and # 3105): E.g., male # 5702 showed the recombinant *PLS3V5* band in combination with the *CMV-Cre* allele. (wt = 576 bp; rec = 380 bp; *Cre-tg* = 600 bp)

To investigate the real deletion efficiency of *CMV-Cre* in $PLS3V5^{fl_st/wt};CMV-Cre^{X_tg/Y}$ male mice, a multiplex PCR was designed allowing the simultaneous detection of the stop-cassette-containing allele, here termed “stop-in” allele (band size = 505 bp), and the stop-cassette-deleted allele, termed “stop-out” allele (band size = 412 bp). Multiplex PCR was then performed on genomic tail tip DNA of $PLS3V5^{fl_st/wt};CMV-Cre^{X_tg/Y}$ male mice. Despite carrying the same genotype, big discrepancies could be observed regarding the deletion efficiency between individuals: Beside the complete deletion of the stop-cassette, also mosaic deletion or no deletion at all was observed (Figure 20, A). An analysis of a total of 15

male mice of the genotype $PLS3V5^{fl_st/wt};CMV-Cre^{X_tg/Y}$ revealed that indeed 52 % of animals showed no stop-out signal albeit the presence of Cre (Figure 20, A).

To address whether the variable deletion-efficiencies observed among $PLS3V5^{fl_st/wt};CMV-Cre^{X_tg/Y}$ individuals directly correlated with $PLS3V5$ expression, proteins from one animal completely lacking the stop cassette (Figure 20, A, # 5745) and another animal showing the stop-in signal only (Figure 20, A, # 5732) were compared by Western blot analysis. Using a V5 antibody, $PLS3V5$ protein could be detected in all tissues of the stop-out-only animal # 5745 (Figure 20, B). By contrast, $PLS3V5$ expression was entirely absent in animal # 5732, where only the stop-in signal had been detected by PCR. Thus, the data obtained in Western blot analysis were in line with the results from multiplex PCR and multiplex PCR is a powerful tool to predict whether any $PLS3V5^{fl_st/wt};CMV-Cre^{X_tg/Y}$ mouse would indeed express $PLS3V5$.

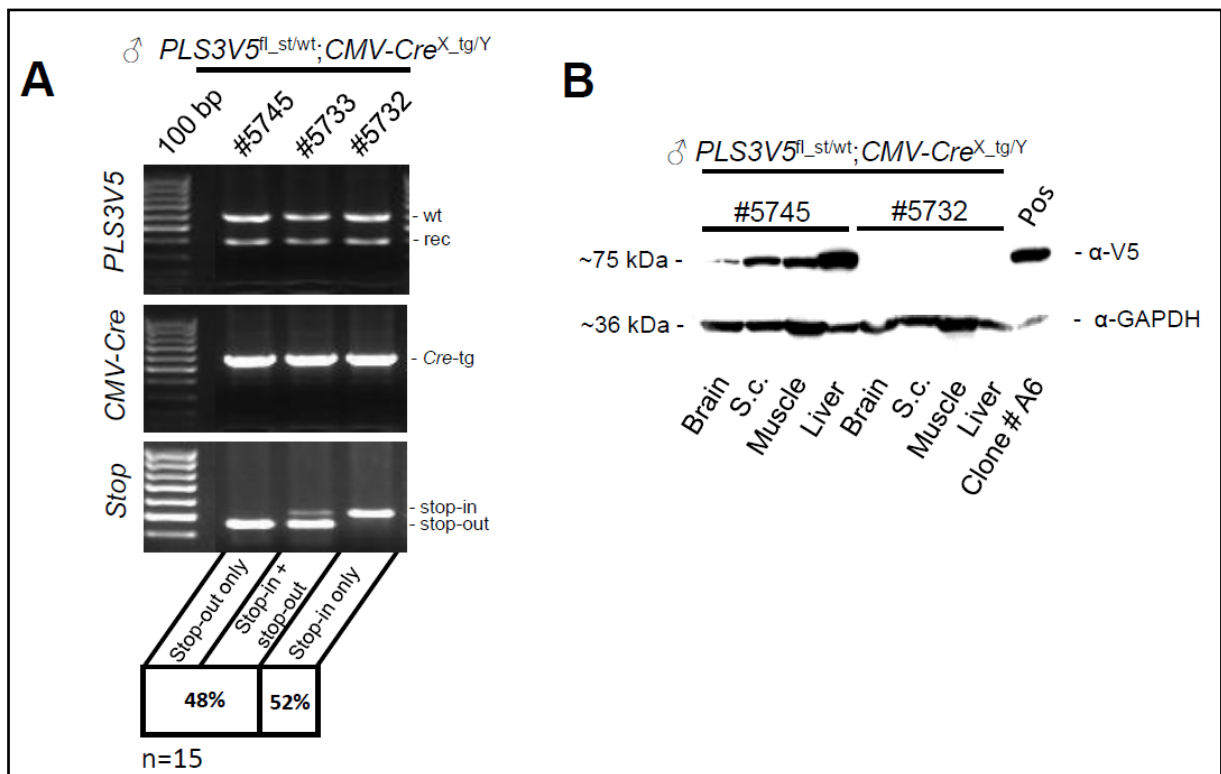


Figure 20: Stop-cassette deletion efficiencies in $PLS3V5^{fl_st/wt};CMV-Cre^{X_tg/Y}$ male mice. **A:** Deletion efficiencies could be classified into three groups: (i) Complete deletion of the stop-cassette (1st lane, stop-out only), (ii) mosaic deletion of the stop cassette (2nd lane, stop-in + stop-out) and (iii) no deletion of stop-cassette despite presence of the Cre-allele (3rd lane, stop-in only). 52 % of a total of 15 $PLS3V5^{fl_st/wt};CMV-Cre^{X_tg/Y}$ males showed no deletion of the stop cassette despite presence of the $CMV-Cre$ allele. **B:** Western blot analysis of one stop-out only animal (# 5745) and one stop-in only animal (# 5732). Using α -V5 antibody, $PLS3V5$ expression could be detected in all tissues investigated of animal # 5745. In animal # 5732, $PLS3V5$ expression was completely absent despite the presence of the $CMV-Cre$ allele. (wt = 576 bp; rec = 380 bp; Cre-tg = 600 bp; stop-in = 505 bp; stop-out = 412 bp. Abbreviations: S.c. = Spinal cord, POS = positive control (ES cell clone # A6))

The knowledge about the deletion efficiency in a certain $PLS3V5^{fl_st/wt};CMV-Cre^{X_tg/Y}$ male was also important from a different perspective: For the generation of mice in which

effectively all cells are deleted for the stop-cassette and that are ubiquitously *PLS3V5* expressing, *PLS3V5^{fl-st/wt};CMV-Cre^{X-tg/Y}* males were further bred with wt females. If the stop-cassette was also deleted in the germ cells of *PLS3V5^{fl-st/wt};CMV-Cre^{X-tg/Y}* males and since *PLS3V5* and *CMV-Cre* are located on different chromosomes, the deletion should be inherited to some of the offspring independently of the *CMV-Cre* allele. Since the deletion efficiency in a certain *PLS3V5^{fl-st/wt};CMV-Cre^{X-tg/Y}* male could be estimated via stop-cassette multiplex PCR, only males solely showing the stop-out signal were used in such breedings. In fact, when mating *PLS3V5^{fl-st/wt};CMV-Cre^{X-tg/Y}*-stop-out-only males with wt females, *PLS3V5* transgenic offspring was identified that did not carry the *CMV-Cre* allele but at the same time showed the stop-out signal only (Figure 21, B).

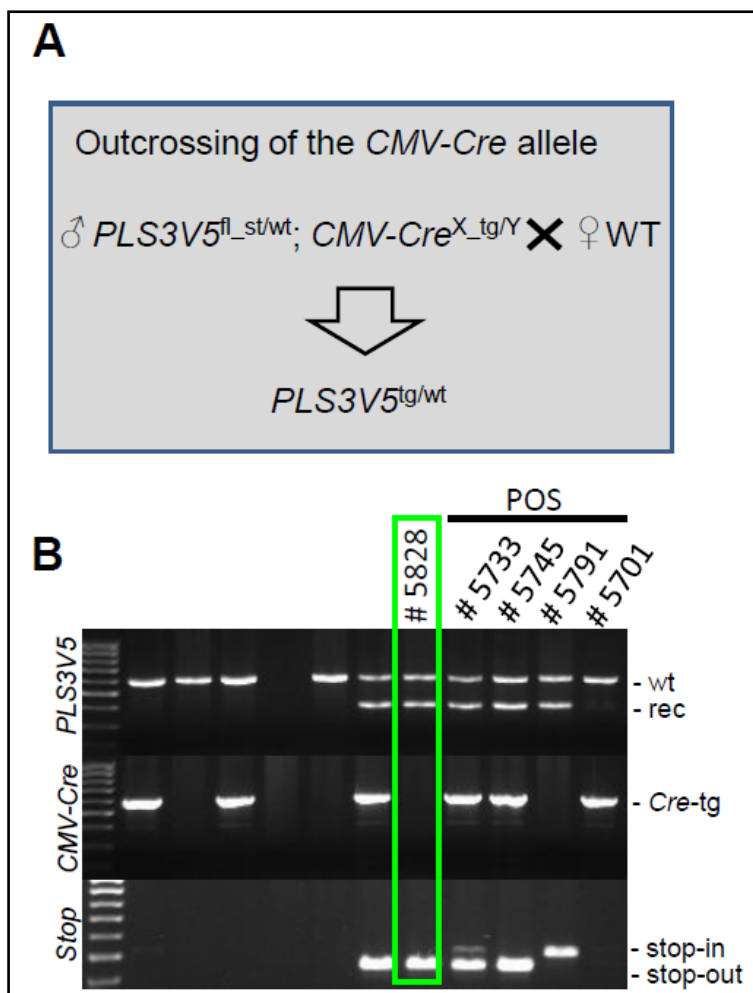


Figure 21: Generation of *PLS3V5*-ubi mice (*PLS3V5^{tg/wt}*). **A:** Breeding scheme for the production of *PLS3V5^{tg/wt}* animals. **B:** In *PLS3V5^{tg/wt}* animals, the stop-cassette is ubiquitously deleted in the absence of the *CMV-Cre* allele. Animal # 5828 showed the recombinant *PLS3V5* band and only the stop-out signal coincidental with the absence of *CMV-Cre*. (wt = 576 bp; rec = 380 bp; *Cre*-tg = 600 bp; stop-in = 505 bp; stop-out = 412 bp. Abbreviations: POS = positive controls. # 5733 = *PLS3V5^{fl-st/wt};CMV-Cre^{X-tg/Y}* (stop-in+stop-out); # 5745 = *PLS3V5^{fl-st/wt};CMV-Cre^{X-tg/Y}* (stop-out only); # 5791 = *PLS3V5^{fl-st/wt}* (stop-in only); 5701 = *CMV-Cre^{tg/wt}* (no stop signal)).

In these mice, the stop cassette is heritably deleted in effectively all body cells resulting in ubiquitous expression of *PLS3V5*. Accordingly, the line was termed *PLS3V5-ubi* and mice e.g. heterozygous for the transgene were defined as *PLS3V5^{tg/wt}* animals.

In summary, *PLSV5* ubiquitously expressing mice (*PLS3V5-ubi* line, genotypic definition *PLS3V5^{tg/wt}*) were successfully generated crossing the *PLS3*-floxed line with the *CMV-Cre* line. In the context of these experiments, the functionality of Cre-mediated activation of the *PLS3V5* transgene was for the first time demonstrated in a Western blot experiment using a V5 antibody to specifically detect *PLS3V5 in vivo* (Figure 20, B). Since a detailed analysis of ubiquitous *PLS3V5* expression in *PLS3V5^{tg/wt}* mice is presented in chapter 5.4.1 and following, it should at this point only be mentioned that Cre-mediated *PLS3V5* overexpression was activated in the mainly through SMA affected tissues, namely brain, spinal cord and muscle. Before *PLS3V5^{tg/wt}* animals were used in *PLS3V5* overexpression experiments on an SMA background (chapter 5.4), the line was bred congenic by backcrossing to wt C57BL/6N animals for 7 generations.

5.4 Ubiquitous expression of *PLS3V5* in an SMA mouse model

When *PLS3V5*-floxed mice were crossed with the *Hb9-Cre* line, *PLS3V5* expression was conditionally activated in the resulting offspring. A detailed analysis of the effects of motor neuron specific overexpression of *PLS3V5* in wt background is given in chapter 5.5 and following.

In the *PLS3V5-ubi* line, the stop-cassette is permanently deleted resulting in ubiquitous expression of the *PLS3V5* transgene. Since *PLS3* is expressed in all SMA-affected tissues in human (Oprea et al., 2008), ubiquitous overexpression of *PLS3V5* in a murine SMA background would resemble the situation in human best possible. To study the effects of *PLS3V5* expression on the SMA phenotype, the *PLS3V5-ubi* line was therefore crossed into the Hung SMA background (chapter 5.4.2.1).

5.4.1 Quantitative and qualitative assessment of *PLS3V5* ubiquitous expression on wt background

Prior to studying the effects of *PLS3V5* expression on the murine SMA phenotype, quantitative expression analysis using qRT-PCR and Western blotting was performed in the *PLS3V5-ubi* line. Furthermore, to prove functionality of the *PLS3V5* protein, murine embryonic fibroblast cells (MEFs) were isolated from *PLS3V5^{tg/wt}* animals to investigate the cellular localization of *PLS3V5* compared to wt murine *Pls3* (m*Pls3*) via immunohistochemical detection.

5.4.1.1 Total *plastin 3* mRNA (*PLS3V5* + *mPls3* mRNA) levels are significantly increased in various tissues of *PLSV5-ubi* mice

To assess the fold overexpression of *plastin 3* mRNA in *PLS3V5-ubi* animals, mRNA from various tissues of wt and *PLS3V5*^{tg/wt} mice (n=3 each) was isolated and quantitative real time PCR (qRT-PCR) performed. The amount of total *plastin 3* mRNA was quantified as the sum of transgenic *PLS3V5* plus murine *Pls3* (*mPls3*) mRNA by using primers detecting both genes and standardizing to endogenous *Hprt1* expression. Due to drastic discrepancies in housekeeper expression between different tissue types, only the fold upregulation for a certain tissue could be determined. For this purpose, wt *mPls3* mRNA level was set to 100 % and excess *plastin 3* amount in *PLS3V5*^{tg/wt} mice assumed to be caused by additional transgene expression. For all of the tissues investigated, total *plastin 3* mRNA levels were significantly increased in *PLS3V5*^{tg/wt} animals compared to wt basal expression (Figure 22, A). While in brain and spinal cord only moderate changes of 3.6 and 3.4 fold were detected, the level of *plastin 3* expression was remarkably elevated to 206 fold over endogenous level in blood. In this context, it is important to mention that *mPls3* is naturally almost absent in blood. Since total *plastin 3* levels in *PLS3V5*^{tg/wt} mice resemble *PLS3V5* + *mPls3* expression relative to endogenous *mPls3* levels in wt this might explain the immense increase observed in blood tissue.

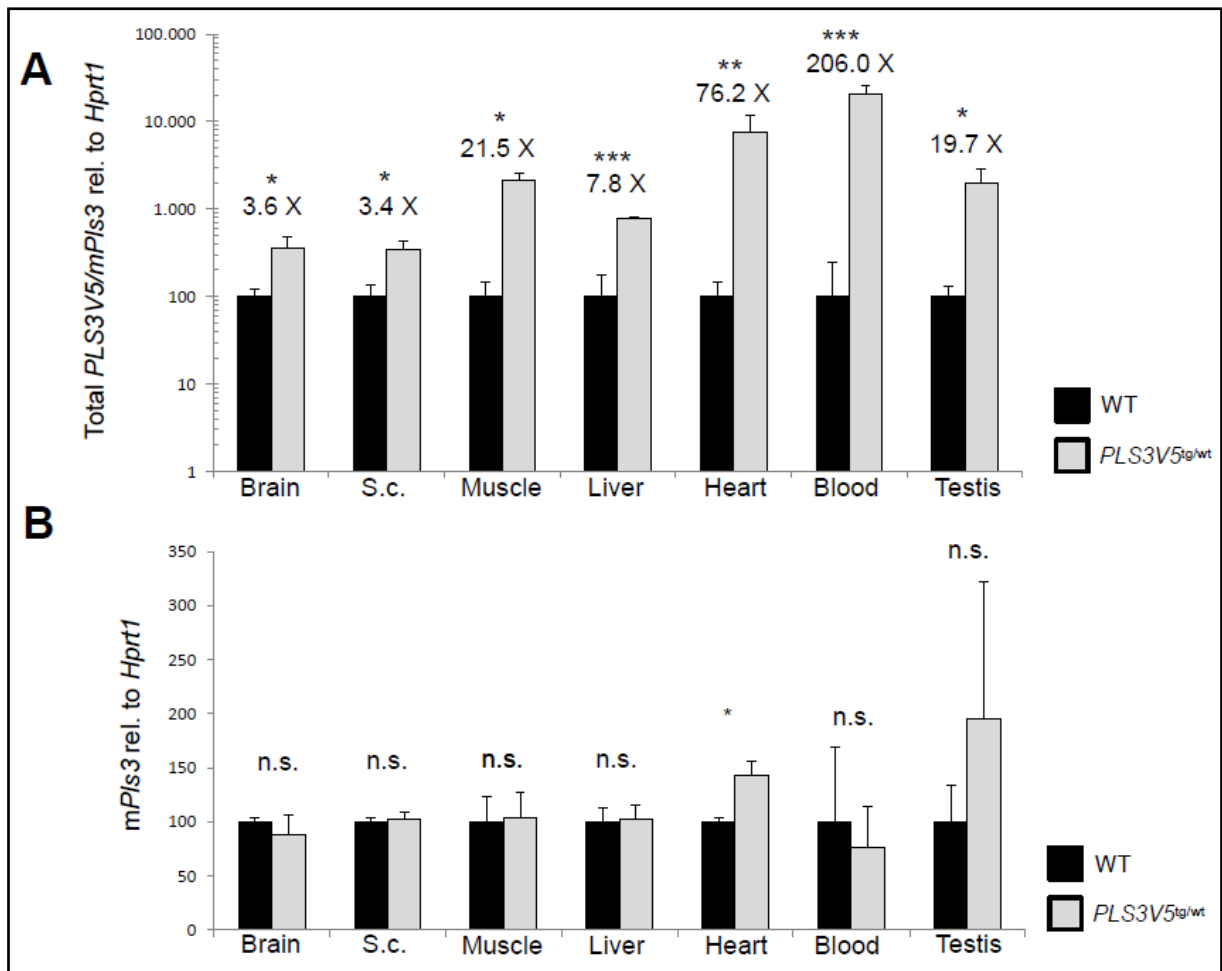


Figure 22: Assessment of fold overexpression of T-plastin mRNA in *PLS3V5*^{tg/wt} versus wt animals. **A** Logarithmic scale: Using primers detecting both, *PLS3V5* and *mPls3*, a significant increase of T-plastin expression was observed in *PLS3V5*^{tg/wt} animals compared to wt. **B**: murine *Pls3* mRNA levels (*mPls3*) were not changed in *PLS3V5*^{tg/wt} compared to wt animals, suggesting that the measured excess of total T-plastin (*PLS3V5* + *mPls3*) in Figure 22 A reflects the true *PLS3V5* overexpression. (Animal numbers of both experiments: *PLS3V5*^{tg/wt} = 3 and Wt = 3; * = $p < 0.05$; ** = $p < 0.01$; *** = $p < 0.001$; Abbreviations: S.c. = Spinal cord)

As mentioned, by setting the wt *mPls3* expression to 100 % all measured excess in *PLS3V5*^{tg/wt} animals should be attributed to the additional expression of the *PLS3V5* transgene. This idea holds true except in the presence of regulatory feedback mechanisms of *PLS3V5* on *mPls3* expression. To exclude this possibility, *mPls3* mRNA levels were analyzed in *PLS3V5*^{tg/wt} and wt animals using primers solely detecting endogenous *mPls3*. Strikingly, no significant differences were noticed, except for heart tissue where only a very slight increase of up to 1.4 fold in *PLS3V5*^{tg/wt} animals could be observed. These findings showed that *PLS3V5* has no feedback on endogenous *mPls3* expression, legitimizing the methodology as well as confirming the measurements of total T-plastin mRNA levels.

Taken together, total *plastin 3* mRNA levels are significantly increased in all tissue types investigated in *PLS3V5*^{tg/wt} animals, including brain, spinal cord and muscle (Figure 22, A). Since *PLS3V5* expression does not influence endogenous *mPls3* levels (Figure 22, B), it can

be concluded that the excess of measured total *plastin 3* in *PLS3V5^{tg/wt}* animals is indeed attributable to *PLS3V5* overexpression.

5.4.1.2 PLS3V5 protein is detected in nearly all tissues of *PLS3V5^{tg/wt}* mice using a V5 antibody, but quantification of total T-plastin expression on protein level is not in line with mRNA measurements

In the targeting construct, *PLS3V5* is located downstream of the CMV enhancer/chicken β -actin (CAG) fusion promoter (Figure 8). This promoter is frequently used for driving strong and ubiquitous expression of transgenes in the mouse (Niwa et al., 1991, Xu et al., 2001). To qualitatively and quantitatively analyze *PLS3V5* protein expression in the *PLS3V5-ubi* line, proteins of various tissues from *PLS3V5^{tg/wt}* mice were isolated and the lysates investigated by Western blot analysis using V5 antibody to specifically detect *PLS3V5* protein. In order to compare *PLS3V5* expression levels between individual tissues, standardization of *PLS3V5* protein to a subset of housekeeper proteins was carried out (e.g. actin, rpl13a1, tubulin). However, this attempt failed due to immense discrepancies of housekeeper expression in the different tissues. Therefore, simply the total protein amount of 15 μ g of each of the tissues was loaded on an SDS-Gel, Western blotting was performed and *PLS3V5* detected with the V5 antibody. To confirm loading of equal protein amounts for *PLS3V5^{tg/wt}* and wt control animals, Ponceau staining was conducted prior immunological detection using the V5 antibody (Figure 23, A). As expected, apart from kidney all other tissues investigated showed a clear V5 signal at the expected size of \sim 75kDa in *PLS3V5^{tg/wt}* but not in wt animals. This way, strongest expression of *PLS3V5* was detected in liver while in brain, spinal cord and muscle moderate expression levels were observed (Figure 23, B). To exemplarily demonstrate the heterogeneous housekeeper expression found in the different tissues, the membrane was costained with an antibody directed against β -tubulin. While in brain, spinal cord and lung strong to moderate β -tubulin levels were detected, respectively, the β -tubulin signal was completely absent in the rest of the tissues for the chosen exposure time. Even if rather imprecise, loading equal protein amounts to compare *PLS3V5* expression was therefore the only appropriate method to estimate expression intensities between the different tissues.

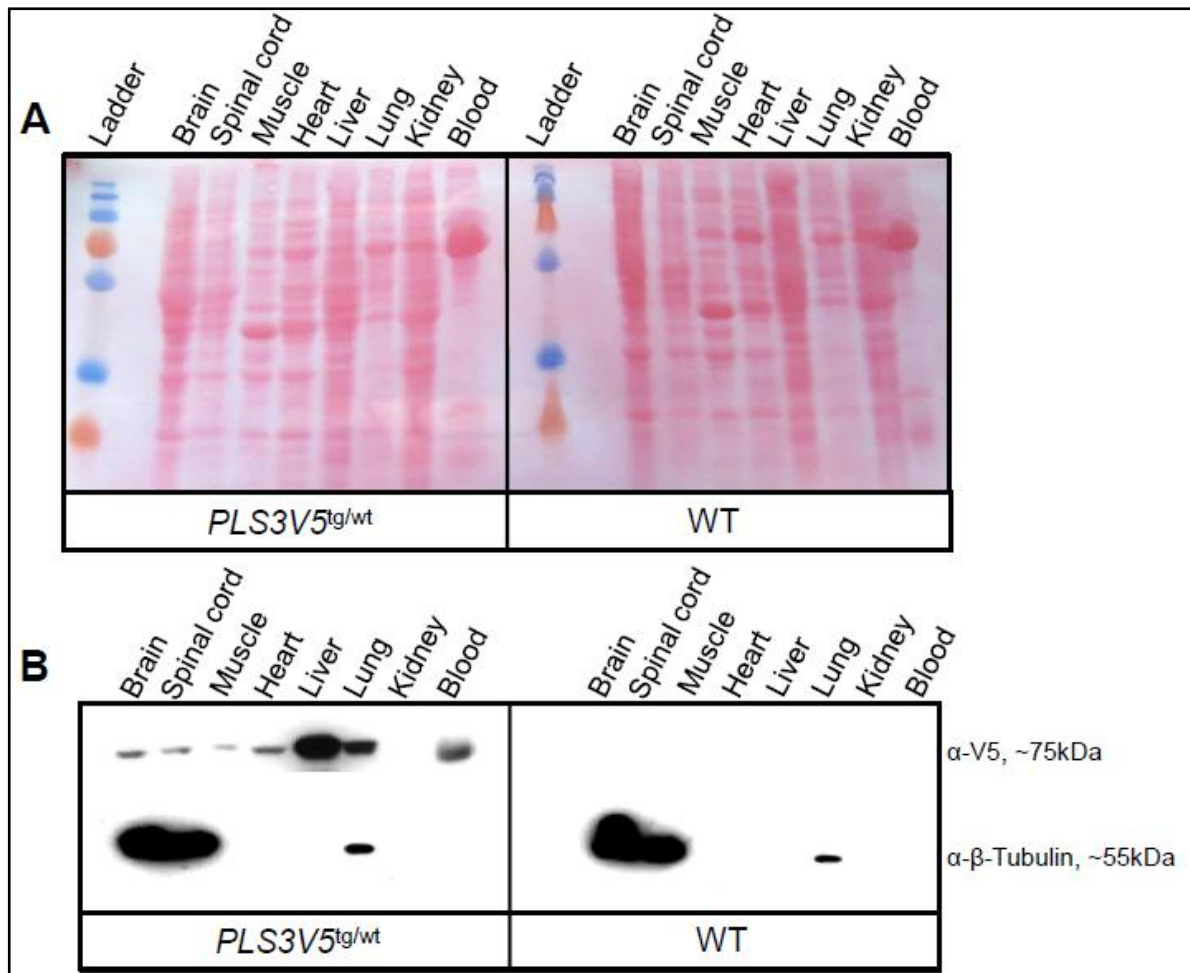


Figure 23: Analysis of PLS3V5 expression in various tissues of *PLS3V5^{tg/wt}* and wt animals. **A:** To demonstrate loading of equal protein amounts for *PLS3V5^{tg/wt}* and wt animals, Ponceau staining was performed prior to immunological detection of PLS3V5. Note that for all tissues loaded *PLS3V5^{tg/wt}* and wt animals show approximately the same band intensities. **B:** Using V5 antibody PLS3V5 protein was detected in almost all tissues of *PLS3V5^{tg/wt}* animals, but not in wt.

Similar to the analysis performed on mRNA level (chapter 5.4.1.1), it was tried to determine the fold upregulation of plastin 3 (PLS3V5 + mPls3) expression relative to endogenous mPls3 level in brain and spinal cord tissue of *PLS3V5^{tg/wt}* animals. Protein lysates of *PLS3V5^{tg/wt}* and wt animals (n=3 each) were blotted and subsequently incubated with PLS3 antibody that recognizes an N-terminal region in the coding sequence of both, mPls3 and PLS3V5. Since the molecular mass of PLS3V5 (~75kDa) is slightly increased due to the V5-tag compared to mPls3 (~70kDa), transgenic and murine plastin 3 were expected to run as two adjacent bands. Using the PLS3 antibody, however, apart from the signal for endogenous mPls3 (~70kDa), no additional PLS3V5 band could be detected in *PLS3V5^{tg/wt}* mice for both brain and spinal cord (Figure 24, A and B, lane II.). Only when the PLS3 antibody was used in combination with V5 antibody, two separate bands appeared for mPls3 and PLS3V5 exclusively in *PLS3V5^{tg/wt}* mice (Figure 24, A and B, lane I.). These findings together with an only moderate *plastin 3* increase in spinal cord and brain of *PLS3V5^{tg/wt}* mice on mRNA level (Figure 22, A) led to the assumption that PLS3V5 protein concentration in

these tissues might be too low for immunological detection. Since for liver a bigger increase in *plastin* expression was detected in $PLS3V5^{tg/wt}$ mice on mRNA (Figure 22, A) and protein level (Figure 23, B) as compared to brain and spinal cord, liver protein of $PLS3V5^{tg/wt}$ mice was analyzed with the PLS3 antibody. Indeed, for liver both mPls3 and PLS3V5 were detected using the PLS3 antibody solely (Figure 24, C', lane I.). While for liver an almost 8 fold increase of total *plastin 3* (*mPls3* + *PLS3V5*) was observed in $PLS3V5^{tg/wt}$ animals on mRNA level (Figure 22), quantification of total *plastin 3* protein revealed an only 2 fold increase over endogenous mPls3 level (Figure 24, C', lane I.). Therefore, it is to consider that also in brain and spinal cord of $PLS3V5^{tg/wt}$ mice the *plastin 3* upregulation on protein level is rather below the observed increase on RNA level (Figure 22) and that PLS3V5 was therefore not detected in Western blot analysis using the PLS3 antibody.

Another explanation for the absence of the PLS3V5 band in brain and spinal cord of $PLS3V5^{tg/wt}$ mice (Figure 24, A and B, lane II.) could be a different binding affinity of the PLS3 antibody to mPls3 and PLS3V5. It has previously been shown that the homologue L-plastin can be phosphorylated at Serin 7 in the N-terminus of the protein, regulating the actin bundling activity of L-plastin (Lin et al., 1998). Serin 7 is highly conserved and also present in the epitope region of *plastin 3* recognized by the PLS3 antibody (H2N-MATTQISKDELDELKC-CONH2). However, at least in fibroblasts and leukocytes no equivalent phosphorylation of the Serin 7 residue could be observed for *plastin 3* (Lin et al., 1998). Nevertheless, an effect of the recombinant V5 tag on the phosphorylation properties of PLS3V5 could not entirely be excluded. Therefore, proteins of spinal cord and brain were investigated using another PLS3 antibody (*Santa Cruz*), accordingly termed PLS3-sc antibody, that was raised against a different epitope located between amino acids 482 and 516 in the C-terminal region of PLS3. Due to strong and unspecific background obtained when using the PLS3-sc antibody, however, this question could not further be studied (data not shown).

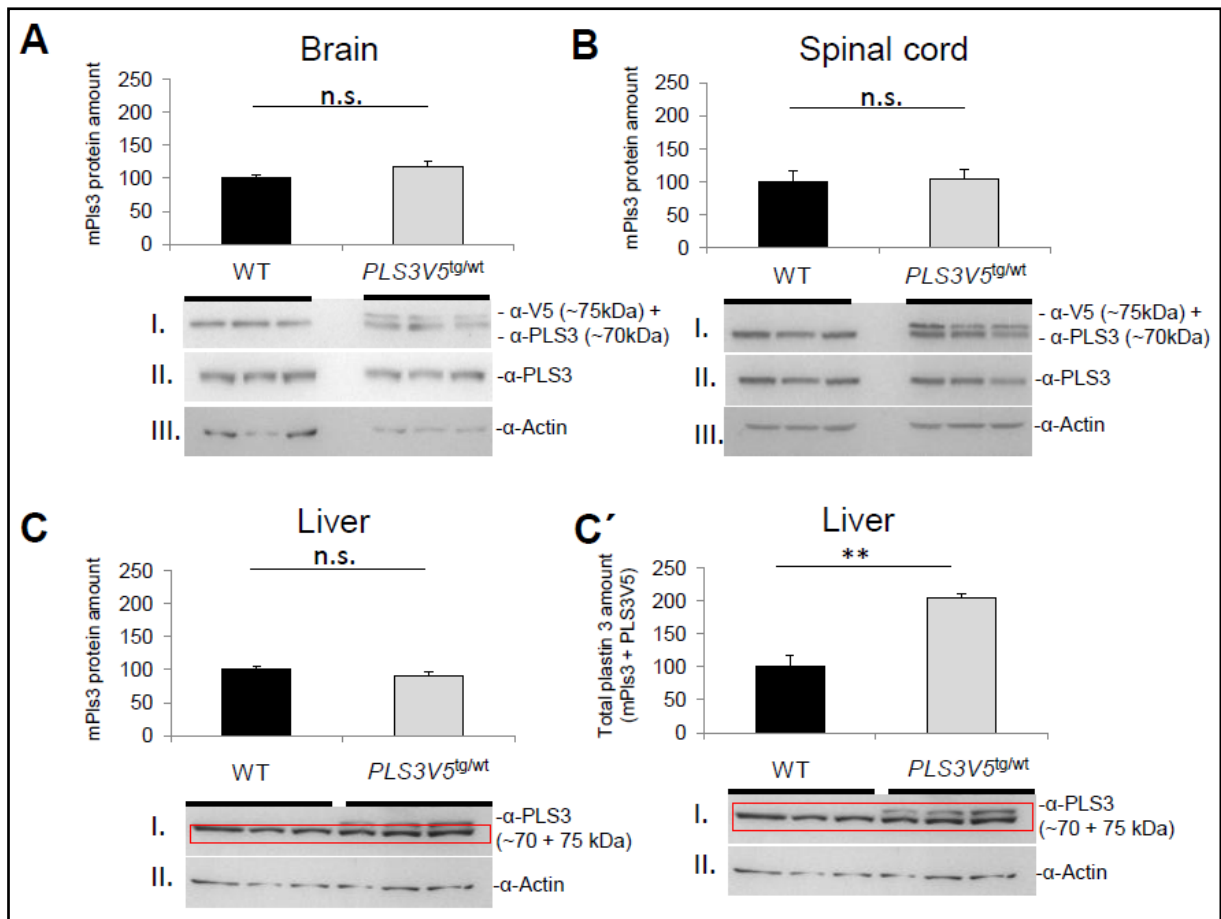


Figure 24: Assessment of total plastin 3 (PLs3V5^{tg/wt} + mPLs3) protein levels in brain, spinal cord and liver of *PLS3V5^{tg/wt}* and wt animals. **A + B**: Analysis of total plastin 3 in brain and spinal cord using the α-PLS3 antibody resulted in the detection of the mPLs3 band only (lane II. in A and B). In combination with the α-V5 antibody signals for both, mPLs3 (~70 kDa) and PLS3V5 (~75kDa) were obtained (lane I. in A and B). Quantifying mPLs3 expression levels (lane II.) and standardizing to Actin, no changes in endogenous mPLs3 levels were detected between *PLs3V5^{tg/wt}* and wt animals in brain and spinal cord. **C**: In liver both mPLs3 and PLS3V5 were recognized by the PLS3 antibody leading to two bands of 70 and 75 kDa size, respectively. Quantification of only endogenous mPLs3 (indicated by the red square in lane I.) revealed no significant changes between *PLS3V5^{tg/wt}* and wt animals as it was also observed in brain and liver. **C'**: Quantification of total plastin 3 protein amount (indicated by the red square in lane I.) revealed a significant 2 fold upregulation in *PLS3V5^{tg/wt}* compared to wt animals. (All quantifications were standardized to actin expression; * = p < 0.05; ** = p < 0.01; ***)

Furthermore, endogenous mPLs3 protein levels were quantitatively assessed in brain, spinal cord and liver of *PLS3V5^{tg/wt}* and wt mice (Figure 24, A, B and C). As was the case on mRNA level (Figure 22, B), no significant changes in mPLs3 protein amount were measured between *PLS3V5^{tg/wt}* and wt animals.

To summarize, using V5 antibody PLS3V5 expression was proven in almost all tissues investigated, that is brain, spinal cord, muscle, heart, liver, lung and blood while only in kidney PLS3V5 was absent for the given exposure time (Figure 23). Since the PLS3V5 transgenic band (~75 kDa) was not recognized by the PLS3 antibody in brain and spinal cord (Figure 24, A and B), it was not possible to determine the fold upregulation of total plastin 3

protein levels in these tissues of *PLS3V5^{tg/wt}* mice. Using liver proteins showing a stronger upregulation of PLS3V5 on mRNA (Figure 22) and protein level (Figure 23) it was possible to detect PLS3V5 by PLS3 antibody and to estimate the fold upregulation of plastin 3 protein to ~2 fold in this tissue (Figure 24, C'). Since the total plastin 3 upregulation was only ~2 fold on protein as compared to ~8 fold on mRNA level in liver, it is to assume that also in brain and spinal cord PLS3V5 protein upregulation is comparatively low considering the only moderate upregulation of 3.6 and 3.4 fold on mRNA level in these tissues, respectively (Figure 22).

5.4.1.3 Transgenic PLS3V5 colocalizes with actin filaments, shows wt localization and results in extensive filopodial outgrowth in murine embryonic fibroblasts (MEFs)

To confirm the functionality of transgenic PLS3V5 protein, murine embryonic fibroblasts (MEFs) were isolated from *PLS3V5^{tg/wt}* and wt control embryos and immunohistochemistry was performed.

To study the capability of PLS3V5 to colocalize with and bundle actin filaments, the V5 antibody was used together with phalloidin stainings on MEFs of *PLS3V5^{tg/wt}* animals. This way, a strong colocalization of PLS3V5 (green) with actin filaments (red) could be observed predominantly in the area of filopodial growth (Figure 25, A + A'). In this regard, PLS3V5/actin colocalization did not occur along the entire actin filament but was rather restricted to regions of filament consolidation, the region-specific localization pointing out the functionality of the PLS3V5 protein (Figure 25, white arrow in C, C' and C''). To ascertain the specificity of the antibody, wt MEFs were incubated with α -V5 antibody using the same concentration, incubation condition as well as exposure time in microscopic analysis as for *PLS3V5^{tg/wt}* MEFs. As expected, no green signals were observed using the V5 antibody in wt MEFs proving specificity of all signals observed in *PLS3V5^{tg/wt}* MEFs (Figure 25, B and B').

Furthermore, a diffuse PLS3V5 staining was detected all over the cell body with slightly increased intensities around the cell nucleus. However, the increase around the nucleus might only be a secondary effect caused by an intensity overlay due to a thicker three dimensional cell structure in this area.

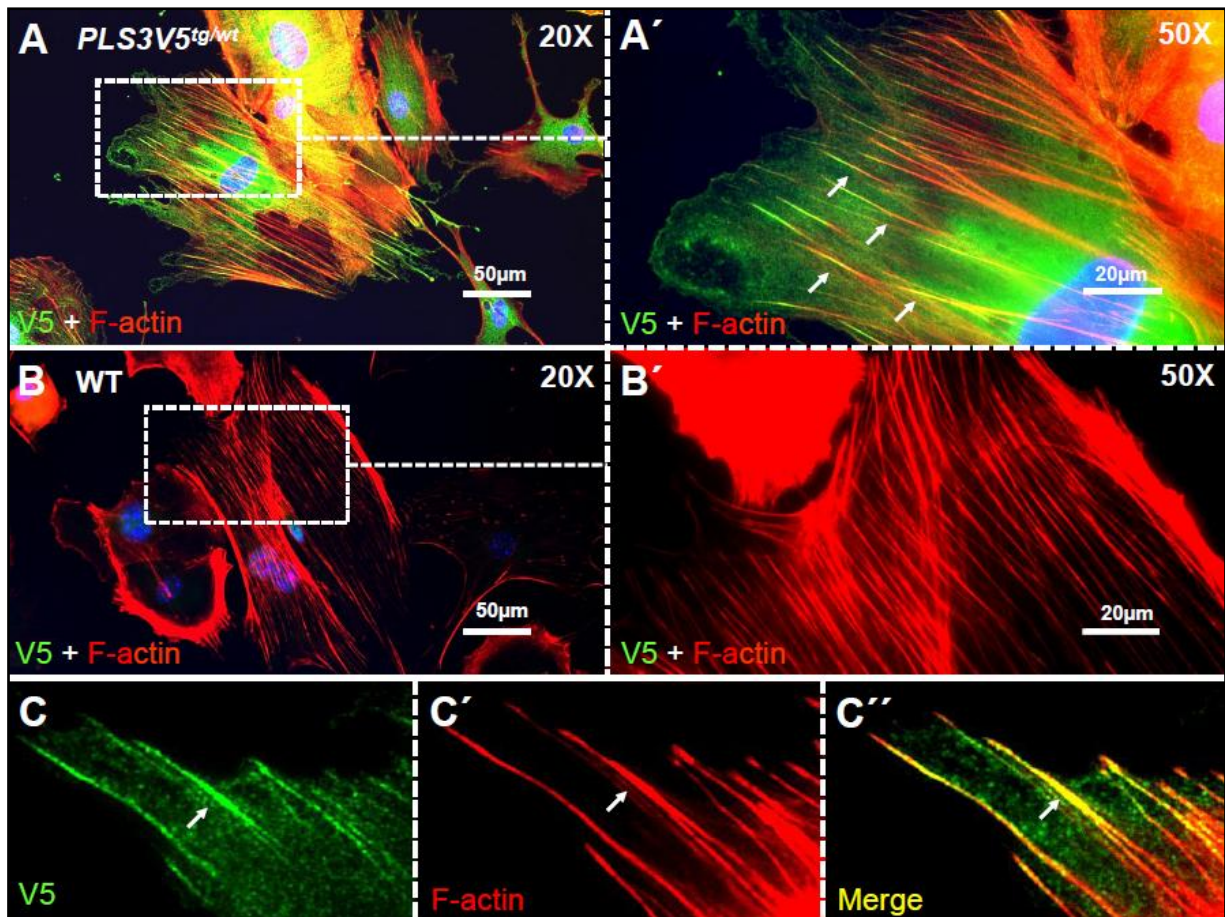


Figure 25: *PLS3V5* transgene expression in murine embryonic fibroblasts (MEFs). **A + A'**: Different magnifications (20x and 50x) of *PLS3V5* staining using V5 antibody in MEFs of *PLS3V5^{tg/wt}* animals. *PLS3V5* colocalizes with actin filaments predominantly in regions of filopodial growth (white arrows in A'). **B + B'**: No green signal was obtained when wt MEFs were stained with the α -V5 antibody, proving specificity of the signals in A and A'. **C, C' + C''**: Detailed view of an actin filament branch point. *PLS3V5* accumulates where actin filaments overlap (white arrow in C, C' and C'') but is not present on isolated actin filaments. (Green = *PLS3V5*, red = F-actin (Phalloidin), blue = DAPI)

After *PLS3V5* turned out to be functional as based on its very specific localization in regions of actin filament consolidation, costainings of *PLS3V5* and wt mPls3 in MEFs of *PLS3V5^{tg/wt}* animals were performed to investigate whether the V5 tagged transgene and the wt protein share overlapping expression domains (Figure 26, A – A''). The *PLS3* antibody was used to detect both mPls3 and *PLS3V5* (Figure 26, A'). Additionally, the V5 antibody was recruited to detect exclusively *PLS3V5* (Figure 26, A''). Since the individual stainings overlapped completely and no extra staining domains were observed for mPls3 when the *PLS3* antibody was used, it is to conclude that transgenic *PLS3V5* shows a totally wt localization in MEF cells.

It has previously been reported that plastin 3 colocalizes with vinculin in integrin mediated focal adhesions of fibroblast like cells (Arpin et al., 1994). To further support the finding of wt localization of transgenic *PLS3V5*, mPls3 and *PLS3V5* were costained with vinculin in wt and *PLS3V5^{tg/wt}* MEFs, respectively. In line with previously published data, mPls3 was observed to colocalize with vinculin also in wt MEFs (Figure 26, white arrows in B, B' and B'').

Importantly, also transgenic PLS3V5 showed a strong overlay with vinculin in focal adhesions of *PLS3V5^{tg/wt}* MEFs (Figure 26, white arrows in C, C' and C'''). These observations further underline that PLS3V5 localizes wildtypic and that the C-terminal V5-tag does not interfere with normal PLS3 function.

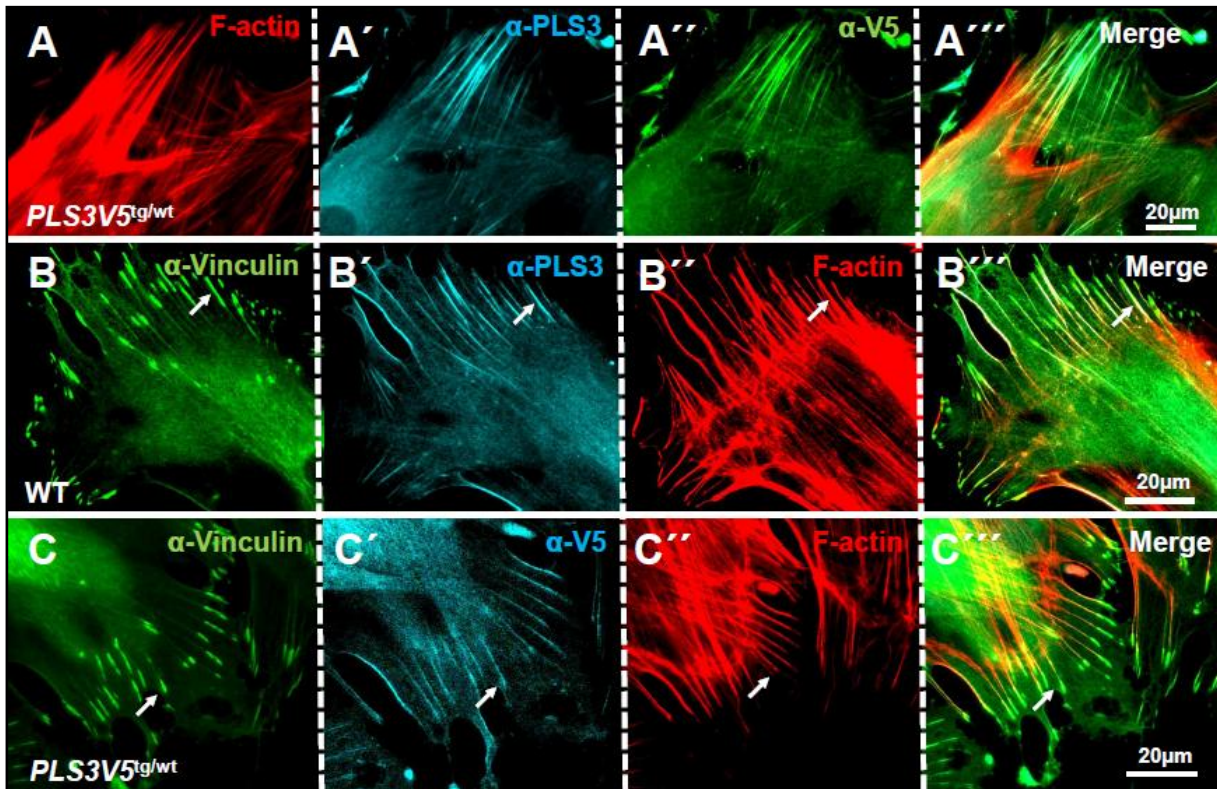


Figure 26: PLS3V5 localization analysis. **A-A'''**: *PLS3V5^{tg/wt}* MEFs were stained with either PLS3 antibody detecting both, mPLS3 and *PLS3V5^{tg/wt}* (A', blue) or V5 antibody to stain PLS3V5 protein only (A'', green). Because no additional expression domains for mPLS3 were observed in A' compared to PLS3V5 in A'', transgenic PLS3V5 displays fully normal and *wt* localization. **B-B'''**: Colocalization of vinculin and mPLS3 is demonstrated in *wt* MEFs by using vinculin (B, green) and PLS3 antibodies (blue). Arrows in B-B''' indicate vinculin/mPLS3 overlapping regions. **C-C'''**: Also for PLS3V5 colocalization with vinculin was proven by combined stainings using vinculin (B, green) and V5 antibodies (blue).

Moreover, it has been shown that *plastin 3* overexpression leads to changes in cell morphology of polarized epithelial cells (LLC-PK1) (Arpin et al., 1994). When overexpressed, *plastin 3* resulted in the formation of thicker microvilli on the surface of LLC-PK1 cells, resembling a phenotype similar to that observed after overexpression of Villin, another actin bundling protein (Friederich et al., 1989). Besides that, *PLS3V5* overexpression led to extensive axonal outgrowth in *in vitro* experiments with PC12 cells and murine primary motor neurons (Oprea et al., 2008). Therefore, MEFs derived from *wt* and *PLS3V5^{tg/wt}* animals were morphologically compared using immunohistochemistry and focusing on filopodial protrusions. Such membrane protrusions are continuously initiated at the leading edge of migrating fibroblasts in a process that is highly dependent on actin dynamics (Mitchison and Cramer, 1996). Typically, filopodia contain a thick stretch of actin that is held together by actin bundling proteins such as PLS3. Based on that, it was speculated that PLS3V5 might

have a stabilizing effect on filopodia of MEFs from *PLS3V5^{tg/wt}* mice. When analyzing MEF cell structure microscopically, filopodial outgrowth was markedly enhanced in MEFs derived from *PLS3V5^{tg/wt}* animals (Figure 27, compare A and A' as well as B and B'). Additionally, while wt MEFs appeared completely normal, the biggest proportion of *PLS3V5^{tg/wt}* MEFs exhibited an elongated, polarized shape as it is typically observed for migrating fibroblasts. According to its function in cytoskeletal regulation, it can therefore be stated that PLS3V5 overexpression has a severe impact on the cell structure also in MEF cells.

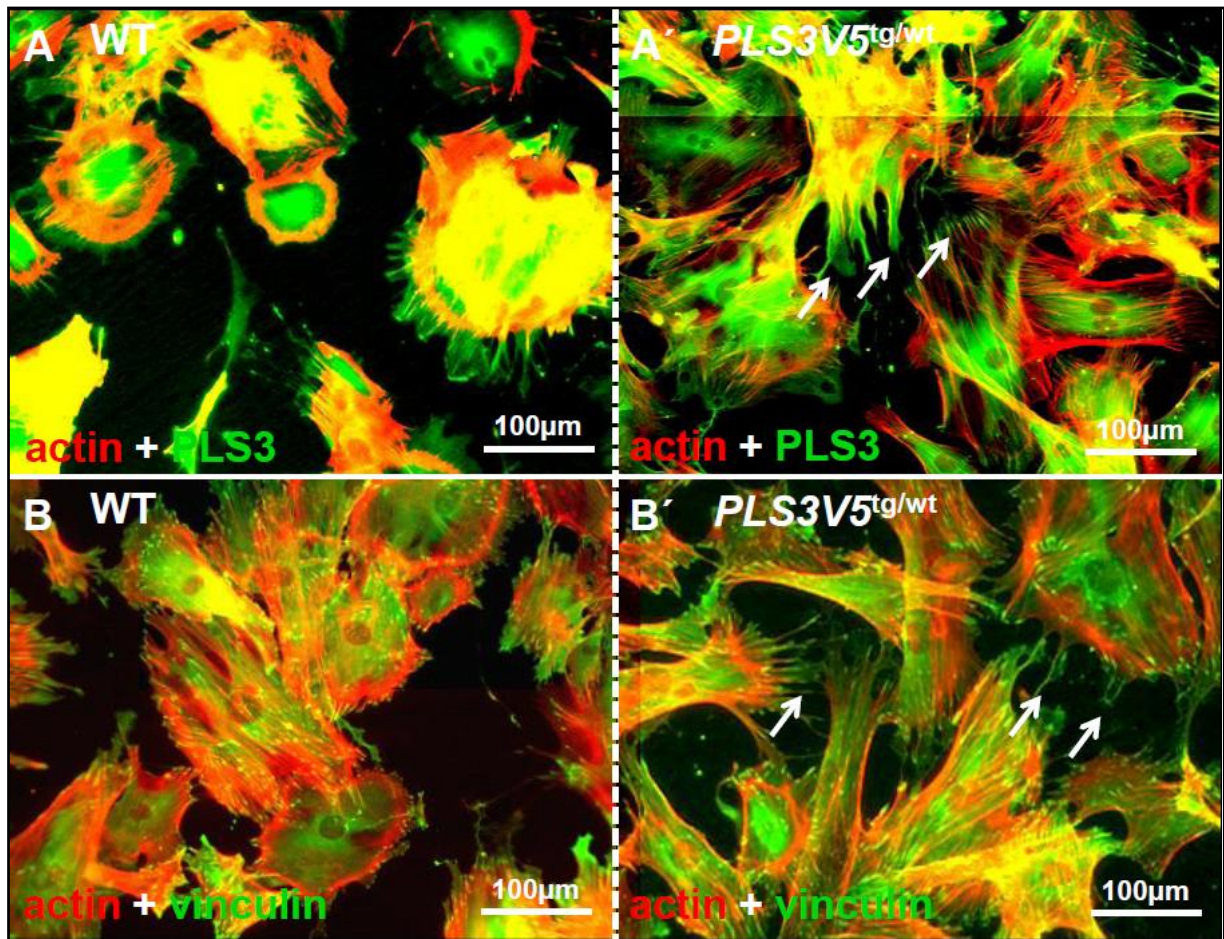


Figure 27: PLS3V5 overexpression leads to structural changes in MEFs derived from *PLS3V5^{tg/wt}* animals. **A + A'**: actin (Phalloidin, red) and PLS3 (green) costainings reveal a drastic increase in filopodial growth in *PLS3V5^{tg/wt}* MEFs (white arrows in A'). **B + B'**: Enhanced filopodial outgrowth was also confirmed in actin (red) and vinculin (green) costainings (note white arrows in B').

To summarize, by using immunofluorescence it was demonstrated that PLS3V5 specifically accumulates at distal ends of lamellipodia and filopodia at actin filament branch points, proving that PLS3V5 is functional (Figure 25). By costaining with its endogenous orthologue mPls3 and vinculin, PLS3V5 was confirmed to entirely colocalize with endogenous Pls3 in MEFs (Figure 26). Moreover, PLS3V5 overexpression results in excessive filopodial growth in MEFs derived from *PLS3V5^{tg/wt}* animals (Figure 27). These results are in line with previously published data after which PLS3 is important in microvilli formation as well as axonal outgrowth in PC12 cells as well as motor neurons (Arpin et al.,

1994, Oprea et al., 2008). The here presented results anticipate a role of PLS3 in the regulation of axon growth in the context of NMJ maturation (chapter 5.4.3 and following).

5.4.2 Generation of an SMA mouse model for the overexpression analysis of *PLS3V5*

To ubiquitously express *PLS3V5* on an SMA background and to investigate possible rescuing effects it was important to select an appropriate SMA mouse model. The Taiwanese SMA mouse model (chapter 4.14.1.1), also termed Hung SMA mouse model here, appeared to be the most suitable model for three reasons:

(i) The distribution of the alleles on different chromosomes allows uncomplicated breedings (*Smn* = chromosome 13, human *SMN2* transgene (*hSMN2*) = chromosome 4, *PLS3V5* = chromosome 6, *Hb9-Cre* transgene = chromosome 5). E.g., the homozygous expression of *PLS3V5* on the Hung SMA background (chapter 5.2) resulting in the genotype *Smn*^{-/-};*hSMN2*^{tg/wt};*PLS3V5*^{tg/tg} would not be possible if *PLS3V5* mapped to the same chromosome as either the *Smn* knockout or the *hSMN2* transgene.

(ii) Hung SMA mice display a life expectancy that is long enough to study effects of *PLS3V5* expression in postnatal stages. As will be outlined in the following chapters, Hung SMA mice on a pure C57BL/6N background live ~15d, allowing e.g. motoric ability testing or analysis of possible NMJ phenotypes.

(iii) As will be described in chapter 5.4.2.1, breedings of the Hung mouse model result in 50 % of affected SMA animals and 50 % control animals. Since the limitations in time and space during daily laboratory routine often interfere with fast analysis progression, the Hung SMA line displays an excellent model to overcome these issues.

Since at the beginning of this work the Hung SMA model was only available on an FVB genetic background it had to be backcrossed with C57BL/6N animals to reach 100 % genetic purity. It is commonly accepted, that the genetic background of mouse strains can have an enormous modifying impact on the severity of a given phenotype. This has also been reported for the Hung SMA model: When on pure FVB background, Hung SMA animals show a mean survival of ~10d (Riessland et al., 2010). However, on a clean C57BL/6J background Hung SMA animals were reported to survive ~13 months, showing first signs of spinal motor neuron degeneration from 6 months of age (Tsai et al., 2008). Knowing that Hung SMA animals on the closely related C57BL/6J background survive for more than 1 year, it appeared questionable if Hung SMA mice on C57BL/6N background would show earlier signs of SMA symptoms and with a survival time similar to that of FVB-SMA animals.

Backcrossing is very time consuming. Assuming 7 generations of backcrossing and considering the 10 weeks generation time of mice, it was calculated that backcrossing of Hung SMA mice to a clean C57BL/6N background would take at least 17.5 months. However, a possibly strong ameliorative impact of the C57BL/6N background on the SMA

phenotype, e.g. an extremely extended life expectancy, was expected to become apparent already after some rounds of backcrossing. Therefore, Hung SMA animals with a statistic proportion of 87.5 % C57BL/6N / 12.5 % FVB mixed background, short “mixed background”, were phenotypically analyzed and compared to Hung SMA mice on a pure FVB background. This way, the Hung SMA phenotype on a relatively high C57BL/6N background was analyzed while backcrossings were still ongoing, giving an early first impression whether Hung SMA mice on pure C57BL/6N background would be appropriate for subsequent analysis at all.

As will be outlined in the next chapters, the comparison of the phenotype of Hung SMA mice on either FVB or mixed background suggests that the SMA phenotype is severely influenced by the genetic background, underlining the importance of genetic purity for accurate phenotypic analysis.

5.4.2.1 Nomenclature of Hung SMA mice and breeding scheme for the production of SMA mice

As was mentioned, the Hung SMA mouse model was selected to serve for the analysis of *PLS3V5* overexpression on an SMA background. In this mouse line, *hSMN2* is homozygously present on *Smn* null background. These animals, here defined as *Smn*^{-/-}; *hSMN2*^{tg/tg}, carry 2 *SMN2* copies per integrate, thus homozygous transgenic mice have 4 *SMN2* copies. They do not develop an SMA phenotype, are fully fertile and live for > 1 year but develop a shortened and thick tail as well as necrotic ears (Riessland et al., 2010). By breeding *Smn*^{-/-}; *hSMN2*^{tg/tg} mice with animals heterozygous for the *Smn* knockout (*Smn*^{+/-}), in each litter 50 % of SMA mice (*Smn*^{-/-}; *hSMN2*^{tg/wt}) and 50 % of control carriers (*Smn*^{+/-}; *hSMN2*^{tg/wt}) were produced. In the following, for reasons of simplicity SMA mice of the genotype *Smn*^{-/-}; *hSMN2*^{tg/wt} are abbreviated with “SMA animals” and control carriers of the genotype *Smn*^{+/-}; *SMN2*^{tg/wt} are termed “HET animals” (derived from heterozygously for the *Smn* knockout). An overview about the breeding scheme to produce SMA offspring and the nomenclature used for SMA animals as well as control carriers is given in Figure 28.

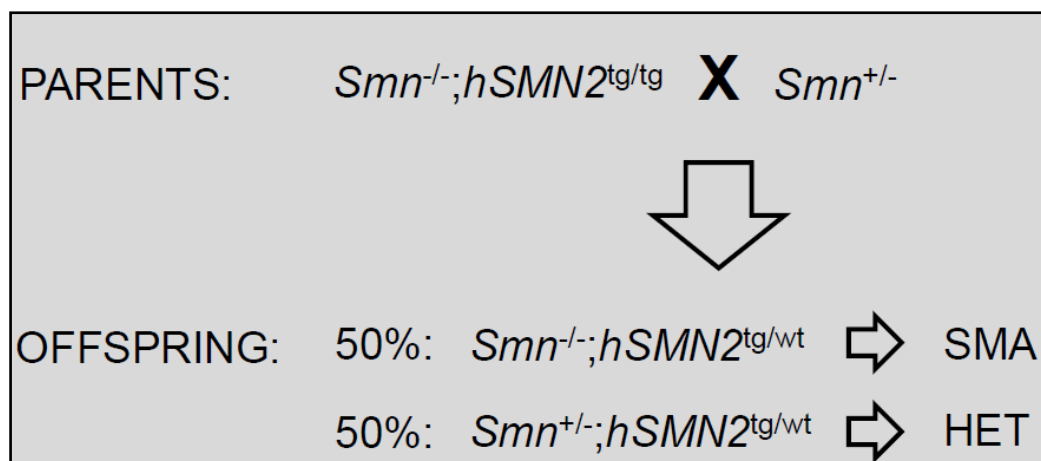


Figure 28: Breeding scheme and nomenclature of Hung SMA mice. Breeding of $Smn^{-/-};hSMN2^{tg/tg}$ with $Smn^{+/-}$ mice produces 50 % of SMA offspring of the genotype $Smn^{-/-};hSMN2^{tg/wt}$ and 50 % of control carriers of the genotype $Smn^{+/-};hSMN2^{tg/wt}$. SMA and control carriers are abbreviated as “SMA” and “HET” animals, respectively

5.4.2.2 Survival, weight and motoric ability of Hung SMA mice are strongly dependent on the genetic background

In order to get an impression of the influence of the C57BL/6N genetic background on the SMA phenotype, SMA animals ($Smn^{-/-};hSMN2^{tg/wt}$) of the mixed background (87.5 % C57BL/6N / 12.5 % FVB) were analyzed and compared with SMA mice from a clean FVB background. First survival, weight gain and motoric ability of SMA animals were compared, before also morphological differences were analyzed (Endplate occupancy, endplate area, muscle fiber size, chapter 5.4.2.3). Since at the end of this work data for survival, weight and motoric ability were available for pure C57BL/6N SMA animals and HET controls, these were included into the respective diagrams. Regarding morphological analyses, only data of FVB and mixed background animals were available and could thus be compared with each other.

SMA animals on the different backgrounds showed highly significant differences in survival, as revealed by Student’s t-test. While FVB SMA mice show a mean survival of 9.9 d, mixed background SMA animals survive only ~ 9 d longer, namely ~19.2 d, despite the relative high proportion of 87 % C57BL/6N background (Figure 29, A). It was therefore assumed that also further backcrossing to C57BL/6N background would not increase the survival of mixed background SMA animals to such extent as it was observed when the Hung SMA model was backcrossed onto clean C57BL/6J background (Mean survival ~13 mo) (Tsai et al., 2008).

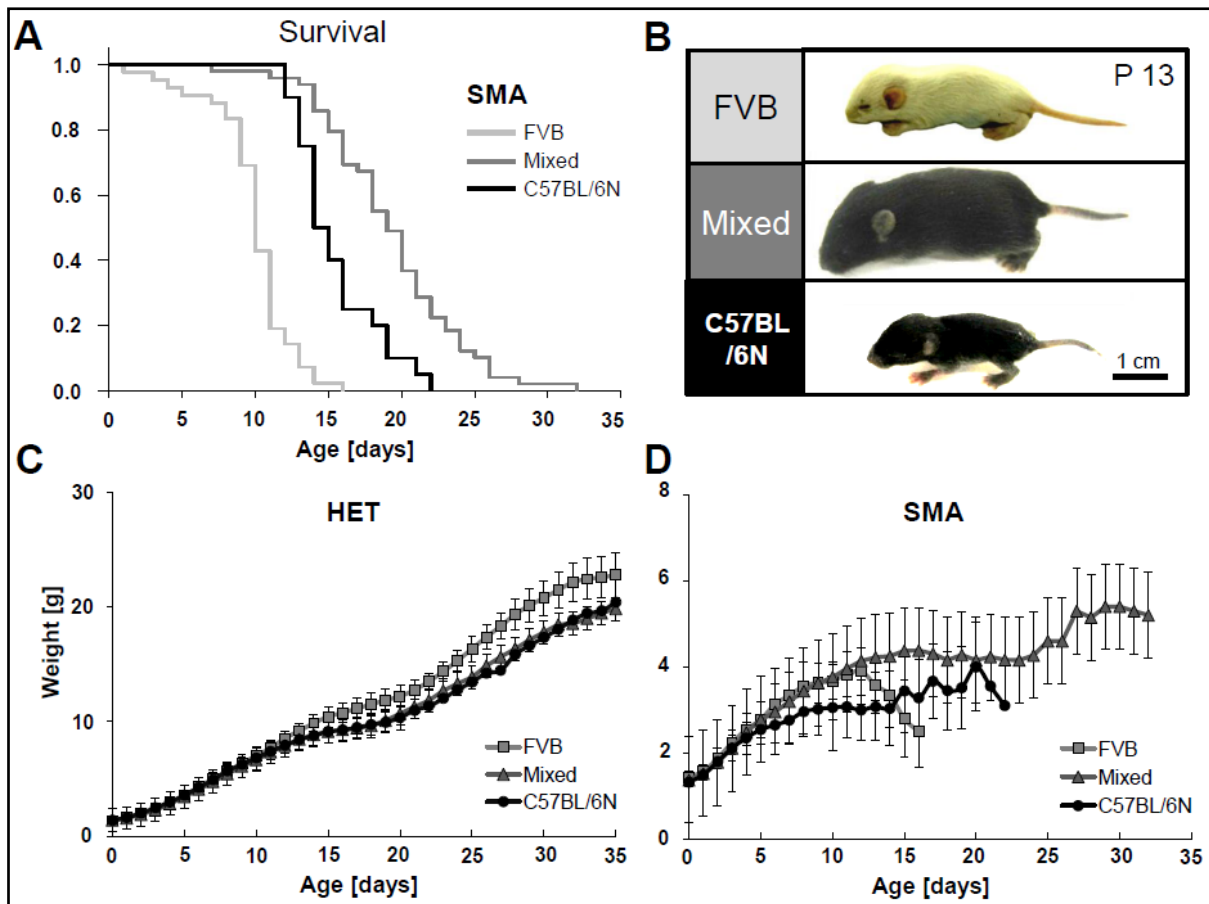


Figure 29: Survival and weight analysis of Hung SMA mice ($Smn^{-/-};hSMN2^{tg/wt}$) on different genetic backgrounds (100 % FVB, mixed (87 % C57BL/6N + 13 % FVB) and 100 % C57BL/6N). **A:** SMA mice on pure FVB background show a mean survival of 9.9 d, mixed background SMA animals have a mean life expectancy of 19.2 days and SMA animals on clean C57BL/6N background survive for 15.5 days. **B:** Example of P13 SMA animals on the three different backgrounds: FVB, mixed and C57BL/6N. Note the size differences. **C:** Weight diagram of HET controls ($Smn^{+/-};hSMN2^{tg/wt}$) of all three genetic backgrounds. **D:** Weight progression in SMA animals of all three genetic backgrounds. C57BL/6N animals weigh less than pure FVB or mixed background mice. (Animal numbers for weight and survival measurements: HET animals: $n_{FVB}=29$, $n_{mixed}=51$, $n_{C57BL/6N}=23$; SMA animals: $n_{FVB}=33$, $n_{mixed}=44$, $n_{C57BL/6N}=22$)

Based on this assumption, backcrossing to C57BL/6N background was continued in order to produce an appropriate SMA model for *PLS3V5* overexpression studies. It was found, that SMA mice of clean C57BL/6N background had an again reduced mean life expectancy of 15.5 d as compared to mixed SMA animals (Figure 29, A). The fact that Hung SMA mice show reduced survival on both pure FVB and C57BL/6N background if compared to mixed SMA animals suggests an ameliorative effect through heterogeneity on the disease phenotype. Furthermore, the increase in survival observed for C57BL/6N SMA mice (15.5 d) when compared to FVB SMA animals (9.9 d) may indicate the presence of background specific modifiers in the C57BL/6N background.

The general picture of SMA mice on different backgrounds did not forcedly correlate with the observed survival. Around P13, mixed SMA mice, that lived longest, showed a significant increase in weight when compared to FVB or C57BL/6N SMA animals (Figure 29, D).

Additionally, they were visibly larger and seemed more robust than FVB or C57BL/6N SMA mice of the same age (Figure 29, B). In contrast to that, between FVB and C57BL/6N SMA mice the disease picture did not correlate with the survival data: Even though C57BL/6N SMA live ~5 d longer than FVB SMA animals, C57BL/6N SMA mice weighed significantly less at P13 and are by far smaller compared to FVB SMA mice of the same age (Figure 29, B and D). One possible explanation for this contradictive observation could be that even when smaller and lighter, C57BL/6N mice possess an increased muscle/fat tissue ratio compared to FVB SMA animals. Noteworthy, HET animals ($Smn^{+/-};HSMN2^{tg/wt}$) of all genetic backgrounds showed no significant weight differences at P13 (Figure 29, C).

To investigate the motoric ability of SMA animals on the different backgrounds, mice were subjected to the tube test. In this test, SMA animals of mixed background showed the best motoric ability from P0 until P15 again pointing at an ameliorative effect of heterogeneity on the SMA phenotype (Figure 30, B). Between P15 and P30, the motoric ability of mixed background SMA animals improved to almost the level of HET animals (Figure 30, A). In this context it is important to mention that only a few mixed SMA animals survived P25 ($n=3$). Therefore, it is to keep in mind that these animals displayed exceptional motoric abilities but were not representative for the gross of mixed SMA mice. In the time period between P5 and P11 and similar to the weight results, FVB SMA mice displayed a tendency towards better motoric performance compared to C57BL/6N SMA animals (Figure 30, B), even though they live significantly shorter than C57BL/6N mice (Figure 29, A). At around P10, however, the curve steeply decreases for FVB SMA animals, reflecting the progression of SMA pathology.

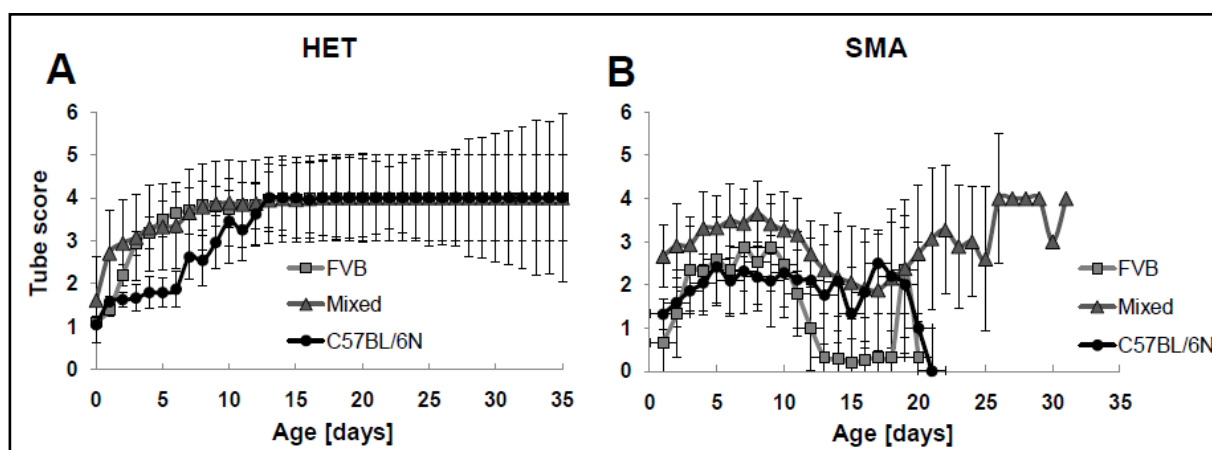


Figure 30: Motoric evaluation of HET ($Smn^{+/-};hSMN2^{tg/wt}$) and SMA mice ($Smn^{-/-};hSMN2^{tg/wt}$) using the tube test. **A:** Motoric ability of HET mice over a time period of 35 days. **B:** Motoric ability curve of SMA animals over a time period of 35 days. (Used animal numbers: HET animals: $n_{FVB}=29$, $n_{mixed}=51$, $n_{C57BL/6N}=23$; SMA animals: $n_{FVB}=33$, $n_{mixed}=44$, $n_{C57BL/6N}=22$)

HET animals of mixed and FVB background behaved similar reaching the maximum tube score of 4 at around P9. Interestingly, however, HET mice on clean C57BL/6N background displayed significantly weaker performance between P2 and P12 ($p=0.0003$). This finding might indicate that C57BL/6N animals do principally exhibit reduced motoric abilities in early

stages. On the other hand, the weight of HET C57BL/6N mice did not significantly differ from FVB and mixed background animals in this time period. Additionally, the overall size and appearance of HET animals on C57BL/6N was by all means comparable to that of FVB and mixed background mice.

Taken together, SMA mice show significantly different survival times, weight gain and motoric abilities depending on the genetic background. In this regard heterogeneity seems to have a positive influence on the SMA phenotype since mixed background SMA mice were the longest living and motorically fitter compared to clean FVB or C57BL/6N SMA mice.

5.4.2.3 Hung SMA mice on pure FVB and mixed genetic background show highly significant differences regarding endplate area size and occupancy as well as muscle fiber size

The vertebrate neuromuscular junction (NMJ) consists of the terminal part of the motor neuron, the so called presynapse, and the muscular accumulation of acetyl cholinesterase receptors (AChR), called endplate. It has previously been demonstrated that the maturation of the NMJ is seriously impaired in SMA-like mice, including poor arborization of presynaptic motor neuron terminals as well as reduction of the endplate area size in SMA mice compared to control littermates (Kariya et al., 2008).

Taking these characteristics of SMA pathology as criteria, NMJs of *Gastrocnemius* muscle of SMA mice on FVB and mixed genetic background were compared with each other. For this purpose, muscle sections were prepared and nerve terminals stained using an antibody against neurofilament-M (green) and endplates using rhodamine labeled bungarotoxin (red).

The arborization degree of incoming motor neuron terminals was assessed in P5 SMA and HET mice by allocating the observed phenotypic appearance of NMJs to one of 4 different branching types (Figure 31, A). For each respective genotype (SMA or HET) and background (FVB or mixed) 100 NMJs of a total of 3 animals were analyzed. When comparing HET animals on FVB and mixed background, no significant differences regarding the distribution of branching types could be observed (Figure 31, B), as was confirmed by Student's t-test. In contrast to that when comparing SMA animals on FVB and mixed genetic background, mixed SMA animals showed a significantly reduced number of type I ($p=0.039$) and a significantly increased number of type III NMJs ($p=0.02$). These results suggest that endplates of SMA mice on a mixed genetic background display a stronger occupation by nerve terminals compared to FVB mice.

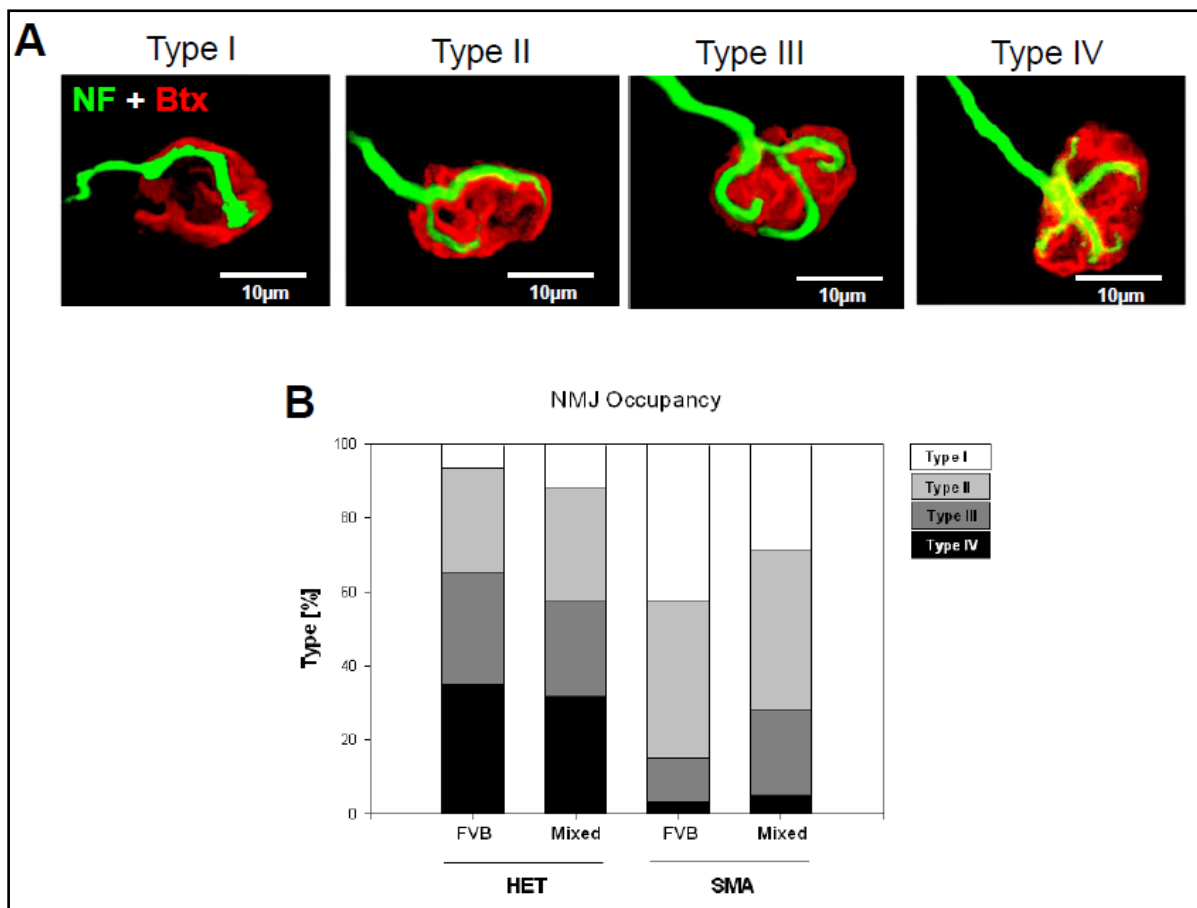


Figure 31: Analysis of NMJ occupancy in *Gastrocnemius* muscle of P5 SMA and HET mice on pure FVB and mixed genetic background. **A**: Categorization scheme depicting the 4 different branching types: Type I like endplates display one, Type II two, Type III three and Type 4 four or more nerve branchings per endplate. **B**: Assessment of the percentages of the different occupancy types (A) in HET and SMA mice of FVB and mixed background. While HET mice exhibited no significant changes among the different genetic backgrounds, mixed SMA mice displayed a significantly lower proportion of type I but instead increased number of type III occupied endplates. (Used animal numbers : HET animals: $n_{FVB}=3$, $n_{mixed}=3$; SMA animals: $n_{FVB}=3$, $n_{mixed}=3$; Stainings: Red = bungarotoxin (Btx); Green = α -neurofilament (NF); 100 NMJs were classified per animal)

Next the endplate area size of SMA and HET animals was determined in a time course experiment for both genetic backgrounds, FVB and mixed. For this purpose, endplates were visualized using rhodamine labeled Bungarotoxin and the sizes of AChR clusters were measured with help of Axio Vision computer software (Zeiss) under a fluorescent microscope.

Including P1, P5 and P10 time points it was found that HET animals on FVB or mixed genetic background exhibited no significant differences in their endplate sizes (Figure 32, B). However, when SMA animals of FVB and mixed background were compared a significant increase in endplate size was observed for SMA mice of mixed background starting at P5 ($SMA_{FVB} = 100,29 \pm 36,53 \mu m^2$, $SMA_{mixed} = 129,37 \pm 33,93 \mu m^2$; $p=0.00193$) and becoming even more evident at P10 ($SMA_{FVB} = 120,30 \pm 38,45 \mu m^2$, $SMA_{mixed} = 169,28 \pm 84,16 \mu m^2$; $p=0.00066$). To visualize the measurements, the difference in endplate size of FVB and

mixed SMA animals is additionally depicted in Figure 32, A. These findings are in line with the observed increase in endplate occupancy in mixed SMA animals. In the past, numerous studies have identified a broad spectrum of diffusible and non diffusible factors provided by the presynapse that are important for AChR clustering, one of the most important effectors in AChR clustering being the secreted MuSK receptor ligand Agrin (Wu et al., 2010). Assuming that a higher degree of arborization of nerve terminals in mixed SMA animals results in elevated secretory vesicle release it seems plausible that motor endplate size of mixed SMA animals increases simultaneously.

Together with the data from the occupancy studies, the increase of endplate size in mixed SMA animals points at an improved NMJ maturation process compared to FVB SMA animals.

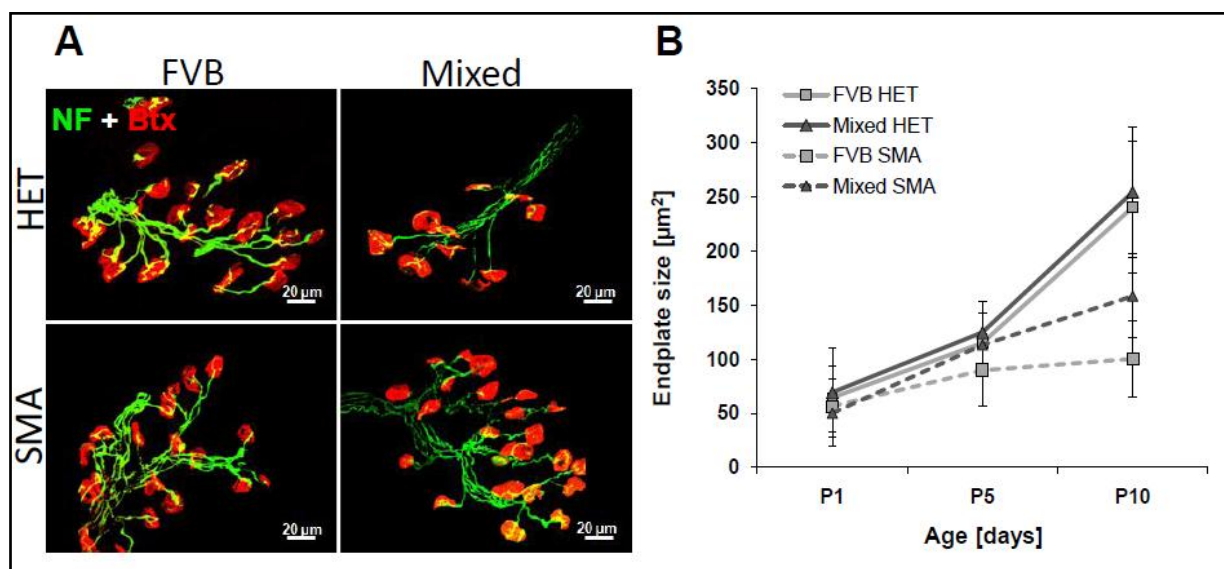


Figure 32: Analysis of endplate size in *Gastrocnemius* muscle of SMA and HET mice on FVB and mixed genetic background. **A:** Representative picture of NMJ sizes in P10 SMA and HET animals on FVB and mixed genetic background. The endplate size of mixed SMA animals is markedly increased compared with SMA mice on FVB background. **B:** Time course experiment (P1, P5 and P10) depicting NMJ sizes of SMA and HET mice on FVB and mixed genetic background. While FVB and mixed HET mice show nearly the same endplate size at the various time points, the endplates of mixed SMA animals are clearly enlarged compared to FVB SMA mice starting at P5 ($p=0.00193$) and becoming even more evident at P10 ($p=0.00066$). (Used animal numbers: HET animals: $n_{FVB}=3$, $n_{mixed}=3$; SMA animals: $n_{FVB}=3$, $n_{mixed}=3$; Stainings: Red = bungarotoxin (Btx); Green = α -NF; 100 endplates were measured per animal)

To investigate whether the improved NMJ maturation process observed for mixed SMA mice resulted in increased muscle fiber size compared to FVB SMA animals, cross sections of *Vastus lateralis* muscle from mouse upper legs were produced and H&E stainings performed. As could be observed HET animals of both, FVB and mixed background displayed no significant differences in muscle fiber size at the various time points, as evaluated by the Student's t-test. However, muscle fiber size of mixed SMA mice was highly significantly increased at P1 ($SMA_{mixed} = 111.00 \pm 49.00 \mu m^2$, $SMA_{FVB} = 87.38 \pm 30.02 \mu m^2$; $p=2.2 \times 10^{-12}$), P5 ($SMA_{mixed} = 129.37 \pm 33.93 \mu m^2$, $SMA_{FVB} = 100.29 \pm 36.53 \mu m^2$; $p=2.3 \times 10^{-12}$).

²³) and P10 ($SMA_{\text{mixed}} = 169.28 \pm 84.16 \mu\text{m}^2$, $SMA_{\text{FVB}} = 120.30 \pm 38.45 \mu\text{m}^2$; $p=8.5 \times 10^{-15}$) time points when compared to SMA mice of FVB genetic background animals. These results are highly consistent with the previous findings of improved motoric ability (chapter 5.4.2.2) as well as NMJ maturation in mixed background SMA animals.

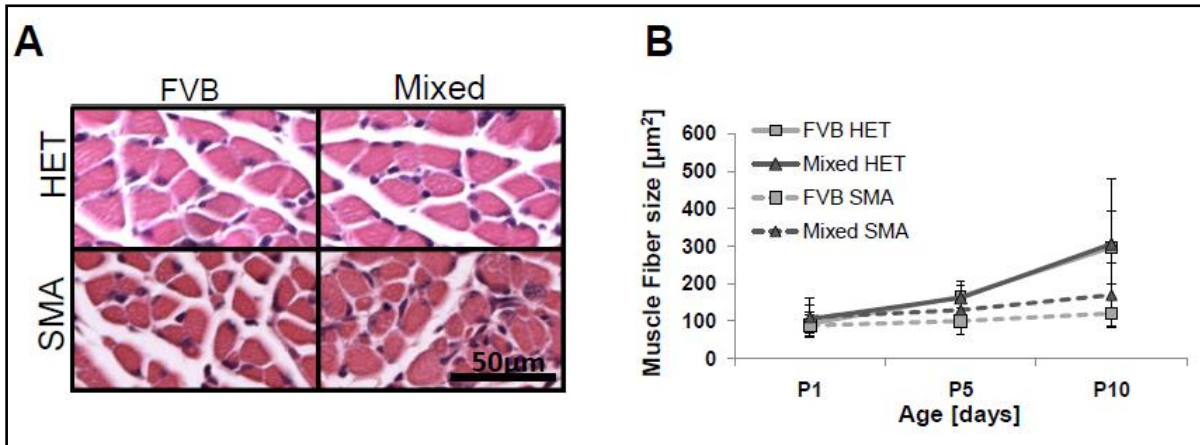


Figure 33: H&E staining to determine *Vastus lateralis* muscle fiber size in SMA and HET controls on FVB and mixed genetic background. **A:** Cross section through *Vastus lateralis* muscle of P10 SMA and HET mice of FVB and mixed background to illustrate muscle fiber size differences. **B:** Time course experiment (P1, P5 and P10) depicting muscle fiber sizes of SMA and HET mice on FVB and mixed genetic background. While HET mice on FVB and mixed background display identical muscle fiber sizes at the various time points, mixed SMA mice show an increase of muscle fiber size at P1 ($p=2.2 \times 10^{-12}$), P5 ($p=2.3 \times 10^{-23}$) and P10 ($p=8.5 \times 10^{-15}$) when compared with FVB SMA mice. (Used animal numbers: HET animals: $n_{\text{FVB}}=3$, $n_{\text{mixed}}=3$; SMA animals: $n_{\text{FVB}}=3$, $n_{\text{mixed}}=3$, 100 muscle fibers were measured per animal)

To summarize, mixed SMA were found to exhibit longer survival and improved motoric abilities compared to SMA animals on pure FVB or C57BL/6N background. The assumption that heterogeneity causes an amelioration of the SMA phenotype was further confirmed by morphological analyzes of mixed and FVB SMA animals: In this context, mixed SMA mice when compared with FVB SMA animals showed clear improvement of the NMJ maturation process, as demonstrated by occupancy as well as endplate size measurements. Furthermore, improved NMJ maturation in mixed SMA mice was accompanied by an increase in muscle fiber size strengthening the view of an ameliorative effect of heterogeneity on the SMA phenotype.

Finally, SMA animals on pure C57BL/6N background showed a ~5 days prolonged mean survival compared to SMA mice on pure FVB background. Since heterogeneity can be excluded, this suggests the presence of background specific SMA ameliorative modifiers in C57BL/6N SMA mice.

5.4.3 Functional analysis of PLS3V5 expression on the SMA phenotype

To study a possible rescuing effect of PLS3V5 expression on the SMA phenotype, the ubiquitously *PLS3V5* expressing *PLS3V5-ubi* line (chapter 5.3.1) was crossed onto the Hung

SMA background. Since the genetic background had been demonstrated to markedly influence the severity of the SMA phenotype (chapters 5.4.2.2 and 5.4.2.3) both, the *PLS3V5-ubi* as well as the SMA line were first backcrossed on pure C57BL/6N background.

Functional analysis of *PLS3V5* overexpression effects comprised survival, weight and motoric ability assessment of *PLS3V5* expressing SMA mice and controls (chapter 5.4.3.2). Furthermore, morphological studies were performed with particular focus on the development and integrity of the NMJ. In a previous study, transient *PLS3V5* expression has been shown to rescue axonal outgrowth defects observed in primary motor neurons from SMA mice and in zebrafish, in which *Smn* was knocked down by morpholino injection (Oprea et al., 2008). Moreover, in chapter 5.4.1.3 of this work *PLS3V5* overexpression was shown to result in the stabilization of filopodial protrusions in MEF cells (chapter 5.4.1.3). Therefore, it was assumed that *PLS3V5* overexpression might also in the mouse play an important role for axonal integrity at the level of NMJ formation *in vivo*.

5.4.3.1 Crossing *PLS3V5* onto the SMA background and nomenclature of animals

To facilitate *PLS3V5* expression on the SMA background, heterozygous *Smn* knockout mice were crossed with *PLS3V5^{tg/wt}* mice in a first step to obtain *Smn^{+/-};PLS3V5^{tg/wt}* offspring (Figure 34). *Smn^{+/-};PLS3V5^{tg/wt}* mice were then bred with *Smn^{-/-};hSMN2^{tg/tg}* animals. The resulting offspring was made up of 4 different genotypes, each occurring with a statistically equal incidence of 25 %:

- *Smn^{-/-};hSMN2^{tg/wt}*: SMA mice
- *Smn^{-/-};hSMN2^{tg/wt};PLS3V5^{tg/wt}*: SMA mice expressing *PLS3V5*
- *Smn^{+/-};hSMN2^{tg/wt}*: HET mice
- *Smn^{+/-};hSMN2^{tg/wt};PLS3V5^{tg/wt}*: HET mice expressing *PLS3V5*

Since all resulting offspring could be used for further examinations, the 100 % outcome of this breeding scheme accelerated the process of analysis.

For reasons of simplicity, in the next chapters all genotypes of SMA and *PLS3V5* expressing SMA animals as well as the HET and *PLS3V5* expressing HET mice are abbreviated as is defined in Figure 34.

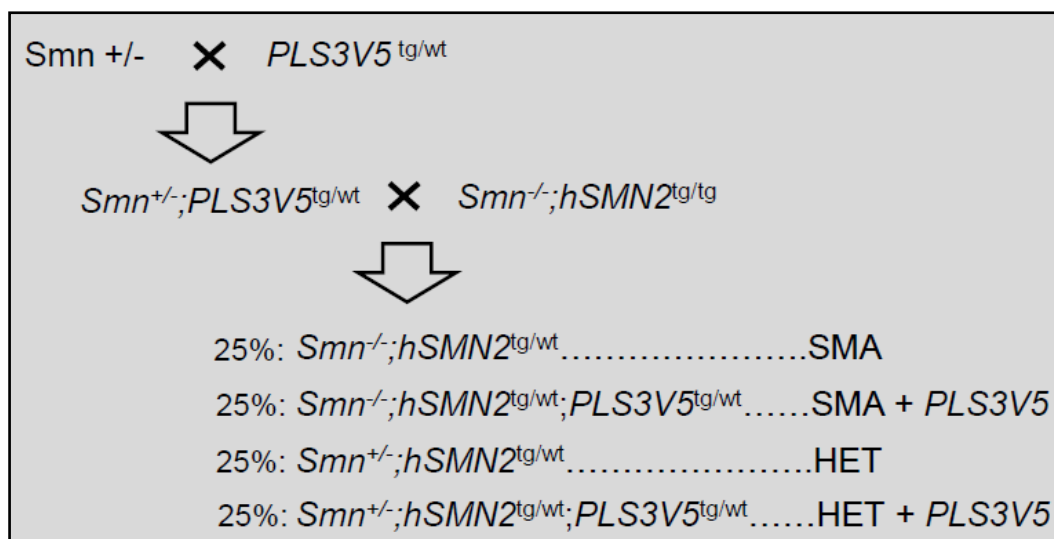


Figure 34: Breeding scheme for the production of *PLS3V5* overexpressing Hung SMA mice

5.4.3.2 *PLS3V5* expression does not improve survival, weight or motoric ability of Hung SMA mice

Since *SMN1*-deleted unaffected siblings of discordant SMA families, who are highly expressing *PLS3*, are fully asymptomatic (Oprea et al., 2008), it was nearby to first investigate the survival of SMA animals compared to SMA mice expressing *PLS3V5* (SMA + *PLS3V5* mice). A total of 20 animals were analyzed for each genotype, whereby the group consisted always of 10 males and 10 females to exclude any gender specific effects. Unexpectedly, SMA + *PLS3V5* mice displayed no different life expectancy compared to SMA animals (Figure 35, A): While SMA animals showed a mean survival of 15.5 ± 2.9 d, SMA + *PLS3V5* animals have a mean life expectancy of 14.6 ± 3.4 d. However, the slight divergence of 0.9 d between the two genotypes was not significant ($p=0.529$). Since only female patients were observed to be protected by high levels of *PLS3* (Oprea et al., 2008), it was plausible to ask if also in mice a possible rescuing effect was restricted to female mice only. To answer this question, the mean survival of female SMA and SMA + *PLS3V5* mice was separately compared. While female SMA mice exhibited a mean survival of 15.9 ± 3.1 d, the mean life expectancy of SMA + *PLS3V5* females was reduced to 13.7 ± 3.1 d. However, when applying Student's t-test, this difference turned out to not be significant ($p=0.148$). Also male SMA and SMA + *PLS3V5* mice did not display obvious changes in their survival times: While male SMA animals have a mean survival of 15.1 ± 2.6 d, male SMA + *PLS3V5* mice live for an average of 15.5 ± 4.0 d, the observed differences again not being significant ($p=0.777$). Since no changes regarding survival time were observed in the groupwise comparison of females and males this indicates that there is no gender specific ameliorative effect on the SMA phenotype in mice.

The absence of survival differences between SMA + *PLS3V5* and SMA animals was also reflected in the general phenotypical picture of these mice. During the developmental

process from birth until death, SMA and SMA + *PLS3V5* mice were not at all distinguishable (Figure 35, B). Also HET + *PLS3V5* animals did not phenotypically differ from HET mice by any means. Additionally, also the analysis of weight revealed no differences between SMA and SMA + *PLS3V5* animals as well as HET and HET + *PLS3V5* mice (Figure 35, C).

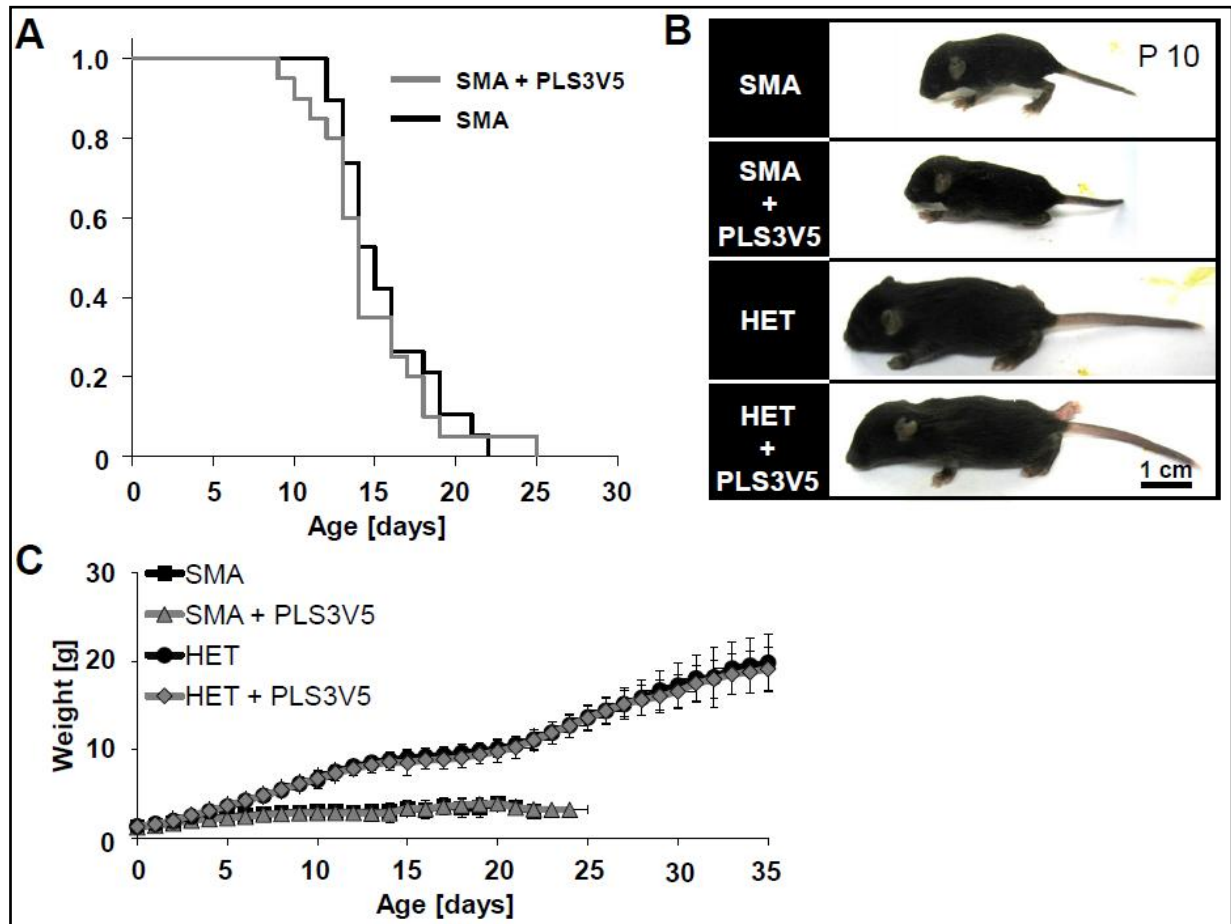


Figure 35: Survival, gross appearance and weight analysis of *PLS3V5* expressing SMA animals and HET controls. **A**: Kaplan Meier curve of SMA and SMA + *PLS3V5* animals, demonstrating no beneficial effect of *PLS3V5* expression on survival (Mean survival times: SMA = 15.5 d, SMA + *PLS3V5* = 14.6 d ($p=0.529$)). HET and HET + *PLS3V5* animals are not depicted since they showed normal survival **B**: Gross appearance of SMA and SMA + *PLS3V5* mice as well as HET and HET *PLS3V5* control mice. **C**: Weight progression of SMA and SMA + *PLS3V5* as well as HET and HET + *PLS3V5* mice. (Animal numbers: In survival as well as weight progression analysis 20 animals (10 males and 10 females) were analyzed for each genotype)

Next, a possible effect of *PLS3V5* overexpression on the motor function of SMA animals was investigated by applying the tube test and the righting reflex test. As has been described by others, SMA mice showed in the tube test a highly significant decrease in motor function compared to HET mice starting around P10 ($p=0.0009$) (Figure 36, A). However, no improvement of motoric ability was detected in SMA + *PLS3V5* animals compared to SMA mice and also HET + *PLS3V5* mice did not display any functional changes when compared with HET animals.

These results were further confirmed by the righting reflex test. While SMA animals displayed a highly significant weakening in motor function compared with HET mice starting

at P10 ($p = 3.7 \times 10^{-5}$), the presence of *PLS3V5* once again had no positive impact on motor function in SMA mice: As confirmed by Student's t-test, no significant changes in their ability to right could be measured between SMA + *PLS3V5* and SMA animals over the whole life span (Figure 36, B).

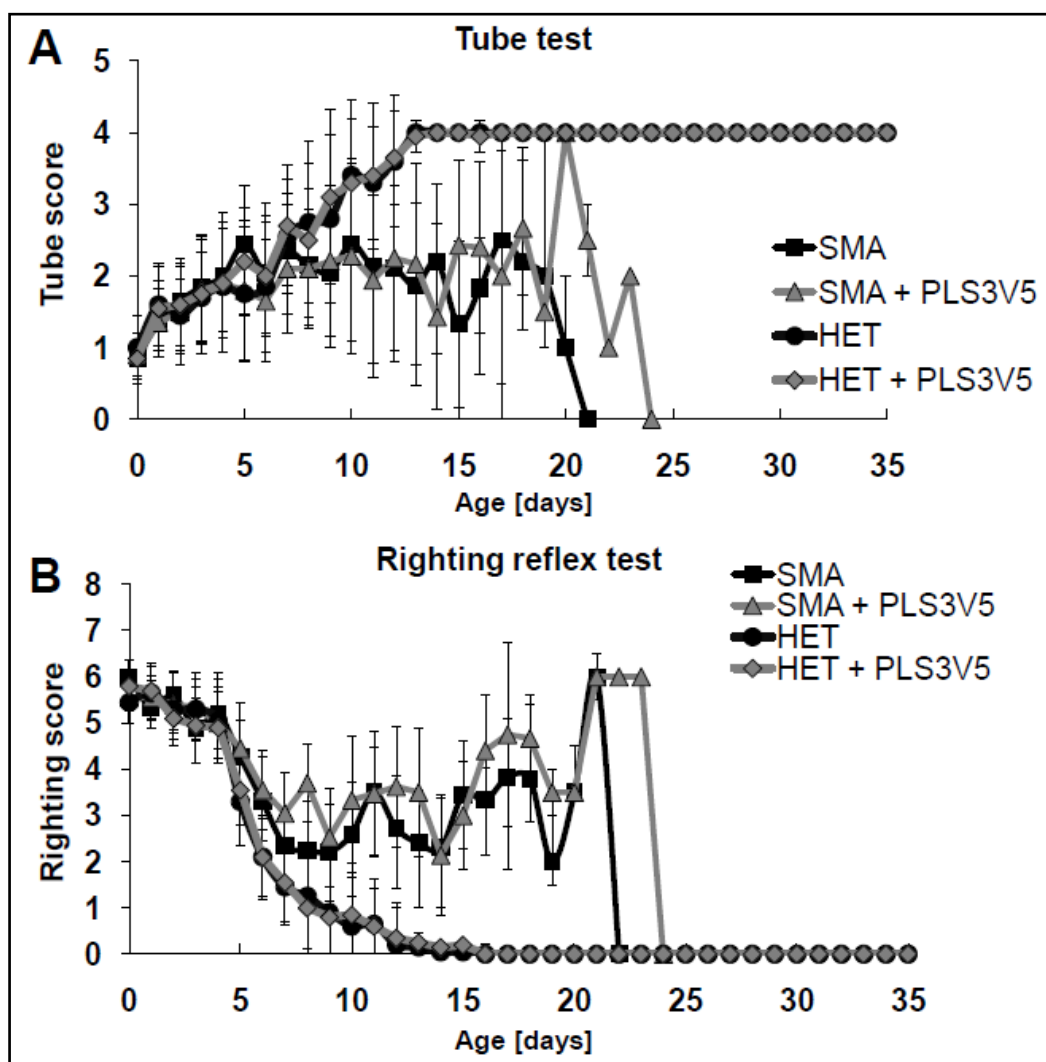


Figure 36: Evaluation of motoric ability in SMA and SMA + *PLS3V5* as well as HET and HET + *PLS3V5* controls by tube and righting reflex test. **A:** The tube test did not reveal any changes in motoric ability between SMA and SMA + *PLS3V5* animals. **B:** Also in the righting reflex test, SMA and SMA + *PLS3V5* animals performed similar and did not display any significant differences. (Animal numbers: In both tube- and righting reflex test, 20 animals (10 males and 10 females) were analyzed for each genotype)

Taken together, no ameliorative effects of *PLS3V5* overexpression were observed on neither survival, nor on weight or the general clinical picture of SMA mice. Furthermore, SMA + *PLS3V5* mice did not show any improvement in their motoric ability as assessed by tube and righting reflex test. These data are not in line with the previous findings in human, where high *PLS3V5* levels had a fully rescuing effect on the SMA phenotype. In this context, it is important to mention that unaffected human siblings in most cases carried 3 *hSMN2* copies, reflecting Type III SMA while Hung SMA mice display a very severe form of SMA. Therefore,

one might speculate that a high PLS3 level exerts its ameliorative effect only in the presence of certain amounts of SMN/Smn protein.

5.4.3.3 NMJ endplate area but not muscle fiber size is increased in the distal *Gastrocnemius* muscle of ubiquitously *PLS3V5* expressing P10 SMA mice

Unexpectedly, *PLS3V5* overexpression had no influence on the survival or motoric abilities of SMA mice (chapter 5.4.3.2). Nevertheless, it was observed before that *PLS3V5* overexpression results in extensive filopodial protrusions in MEF cells derived from *PLS3V5*^{tg/wt} animals (chapter 5.4.1.3). Additionally, a positive effect of *PLS3V5* on the outgrowth of axons from Smn depleted PC12 cells as well as murine primary motor neurons has been reported before (Oprea et al., 2008). Therefore, the focus of further analysis lay on studying a potential effect of *PLS3V5* expression on the integrity of the neuromuscular junctions (NMJ).

To investigate on that, NMJs of *Gastrocnemius* muscle sections from 6 animals (3 males and 3 females) of SMA, SMA + *PLS3V5*, HET and HET + *PLS3V5* mice were analyzed using an antibody directed against neurofilament and bungarotoxin. Next, AxioVision Rel.4.7 software was employed to measure the surface area size of muscular acetylcholine receptor (AChR) clusters (also termed “endplates”). As depicted in Figure 37 (A and B), SMA + *PLS3V5* animals demonstrated markedly increased endplates when compared with SMA mice (SMA = $121.28 \pm 8.31 \mu\text{m}^2$; SMA + *PLS3V5* = $141.75 \pm 2.76 \mu\text{m}^2$; $p = 2.8 \times 10^{-38}$). However, the endplate size in SMA + *PLS3V5* mice was not restored to that of HET mice (HET = $162.15 \pm 2.99 \mu\text{m}^2$), highlighting the importance of Smn protein in the process of proper NMJ formation. Moreover, this effect of *PLS3V5* overexpression became also apparent in healthy HET + *PLS3V5* mice when compared with HET mice (HET + *PLS3V5* = $190.48 \pm 7.22 \mu\text{m}^2$; $p = 1.9 \times 10^{-50}$).

Noticeably, endplate measurements of male and female mice of each genotype did not reveal any gender specific differences. For that reason and in combination with the finding that no survival differences were detectable between sexes (chapter 5.4.3.2) the gender was no longer considered in further analyzes.

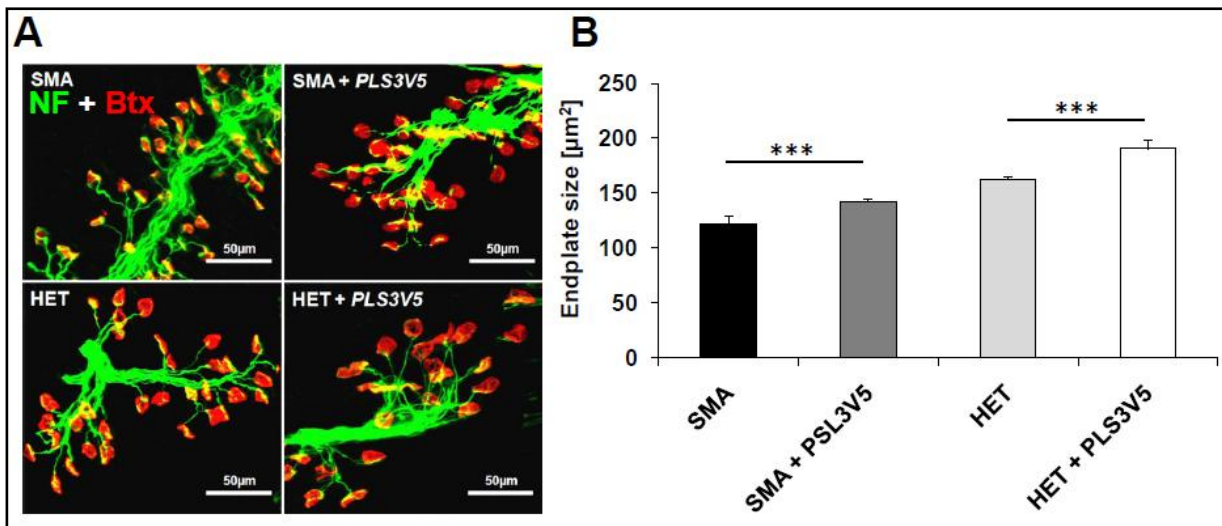


Figure 37: Endplate measurements in *Gastrocnemius* muscle of SMA, SMA + *PLS3V5*, HET and HET + *PLS3V5* controls. **A**: Endplate size differences as visualized by confocal microscopy. **B**: Quantification of endplate sizes found in the different genotypes. SMA + *PLS3V5* possess enlarged endplates than SMA mice. Also in HET animals, the endplate size increased highly significant upon *PLS3V5* expression. (Animal numbers: For endplate measurements, 6 animals (3 males and 3 females) were analyzed for each genotype; Stainings: Red = Bungarotoxin (Btx); Green = α -Neurofilament (NF); * = $p < 0.05$; ** = $p < 0.01$; *** = $p < 0.001$; 100 endplates were measured per animal)

In view of the fact that these results pointed towards improved NMJ integrity, next cross sections of *Vastus lateralis*, a proximal muscle, were prepared and the muscle fiber size of the same animals was determined. Different from what was expected, SMA + *PLS3V5* and HET + *PLS3V5* animals showed no increase in muscle fiber size compared to SMA or HET mice, respectively (Figure 38, B; SMA = $142.66 \pm 51.54 \mu\text{m}^2$; SMA + *PLS3V5* = $147.02 \pm 66.1 \mu\text{m}^2$; HET = 179.10 ± 55.91 ; HET + *PLS3V5* = 181.71 ± 54.53). At the same time, however, these results are in line with the observation that SMA + *PLS3V5* animals were not displaying any signs of improved motoric function compared to SMA mice (Figure 36).

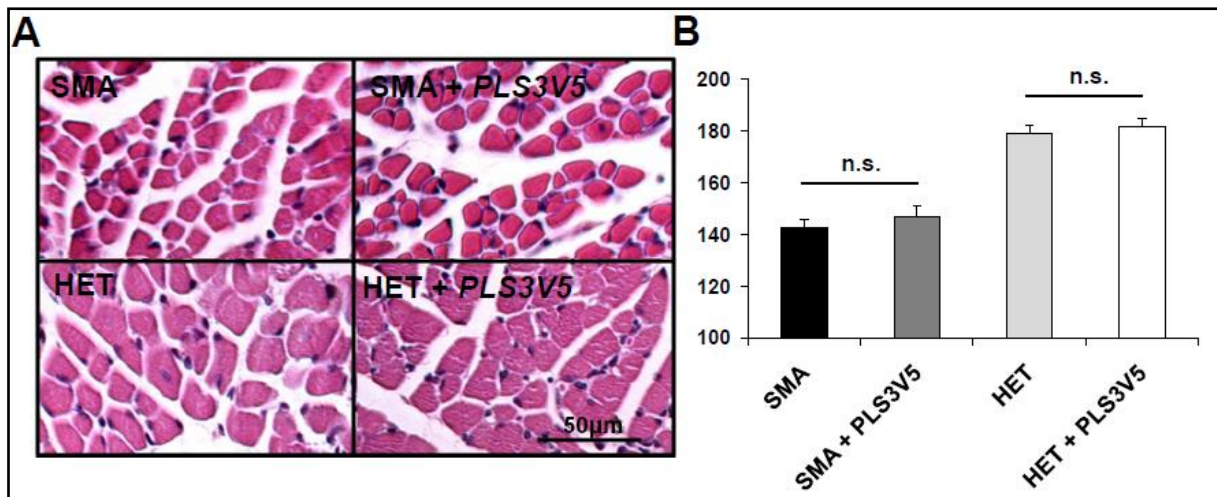


Figure 38: H&E stainings to determine *Vastus lateralis* muscle fiber size in SMA, SMA + *PLS3V5*, HET and HET + *PLS3V5* mice. **A:** Cross section through *Vastus lateralis* muscle of P10 animals of the 4 different genotypes. No obvious size differences were observable **B:** Quantification of muscle fiber size found in the different genotypes. SMA + *PLS3V5* and SMA mice as well as HET and HET + *PLS3V5* display no significant differences regarding muscle fiber size. (Animal numbers: 3 animals were analyzed for each genotype; Abbreviations: n.s.= not significant; 100 muscle fibers were measured per animal)

In summary, *PLS3V5* led to an increase of endplate size in SMA or HET animals compared to the respective controls, independent of the gender. Since these results pointed towards improved NMJ integrity in *PLS3V5* expressing mice, it was assumed that this might result in increased muscle fiber size in the same animals. However, muscle fiber size was unchanged between SMA + *PLS3V5* and SMA mice as well as HET + *PLS3V5* and HET control animals at P10 time point.

5.4.3.4 Ubiquitous *PLS3V5* expression leads to improved axonal connectivity in the proximal *Transversus abdominis* (TVA) muscle of SMA animals

PLS3V5 expression resulted in an increased postsynaptic endplate size in P10 SMA animals. Since factors secreted by presynaptic terminals regulate AChR clustering, e.g. Agrin (Nitkin et al., 1987), an improved axonal integrity might explain this observation. The actin cytoskeleton plays an important role in axon growth, branching and retraction, but also in synapse formation and stability (Luo, 2002). Particularly in motor neurons, *Smn* has a function in promoting presynaptic differentiation by contributing to the translocation of β -actin mRNA to the presynaptic compartment (Rossoll et al., 2003). In another work, the lack of presynaptic β -actin protein has been linked to defective clustering of voltage-gated Ca^{2+} channels in motor neurons isolated from SMA animals (Jablonka et al., 2007). The authors speculate that this, in turn, could impair transmitter release from the axon terminals (Zhong and Zucker, 2004), finally leading to NMJ degeneration. Furthermore, *PLS3V5* transient overexpression has been demonstrated to rescue axon outgrowth defects caused by *Smn* depletion in PC12 cells and primary motor neurons derived from SMA animals (Oprea et al.,

2008). Moreover, as was reported before (Arpin et al., 1994) and was additionally shown in this work for MEF cells, *PLS3V5* expression led to extensive filopodial outgrowth (chapter 5.4.1.3), reflecting its function in actin bundling and cytoskeletal stabilization.

Together, these findings highlight the importance of cytoskeleton integrity in presynaptic development. Therefore, a possible effect of *PLS3V5* expression on the stability of terminal motor axons *in vivo* was assumed. To investigate on that, the process of axonal pruning was studied in a time course experiment at P1, P4 and P8 time points. The process of vertebrate nervous system development results in an overabundance of axonal connections. In this context, axonal pruning is a strategy to selectively remove exuberant neuronal branches and connections in the immature nervous system to ensure the proper formation of functional circuitry (Low and Cheng, 2006). The vertebrate NMJ has been a perfect model to study NMJ disassembly for a long time. During early postnatal stages, each muscle fiber is innervated by multiple axons or terminal arbors (Sanes and Lichtman, 1999). In a process of fine tuning, axon collaterals and axon arbors are removed or remodeled over time. Then, with ongoing maturation, postsynaptic endplates finally become innervated by only one terminal arbor from a single motor neuron (Low and Cheng, 2006). To find out whether *PLS3V5* has any “stabilizing” effect on axons in the process of axonal pruning, the number of axons innervating individual endplates was determined in SMA, SMA + *PLS3V5*, HET and HET + *PLS3V5* animals via fluorescent microscopy at P1, P4 and P8 time points. For this purpose, proximal *Transversus abdominis* (TVA) muscle was prepared from 3 animals for each of the described genotypes and time points and co-stained with neurofilament + Synaptic vesicle 2 (SV2) antibodies and bungarotoxin to outline incoming axon terminals of the NMJ. The number of axons was then counted for 100 endplates as is exemplarily depicted in Figure 39, A.

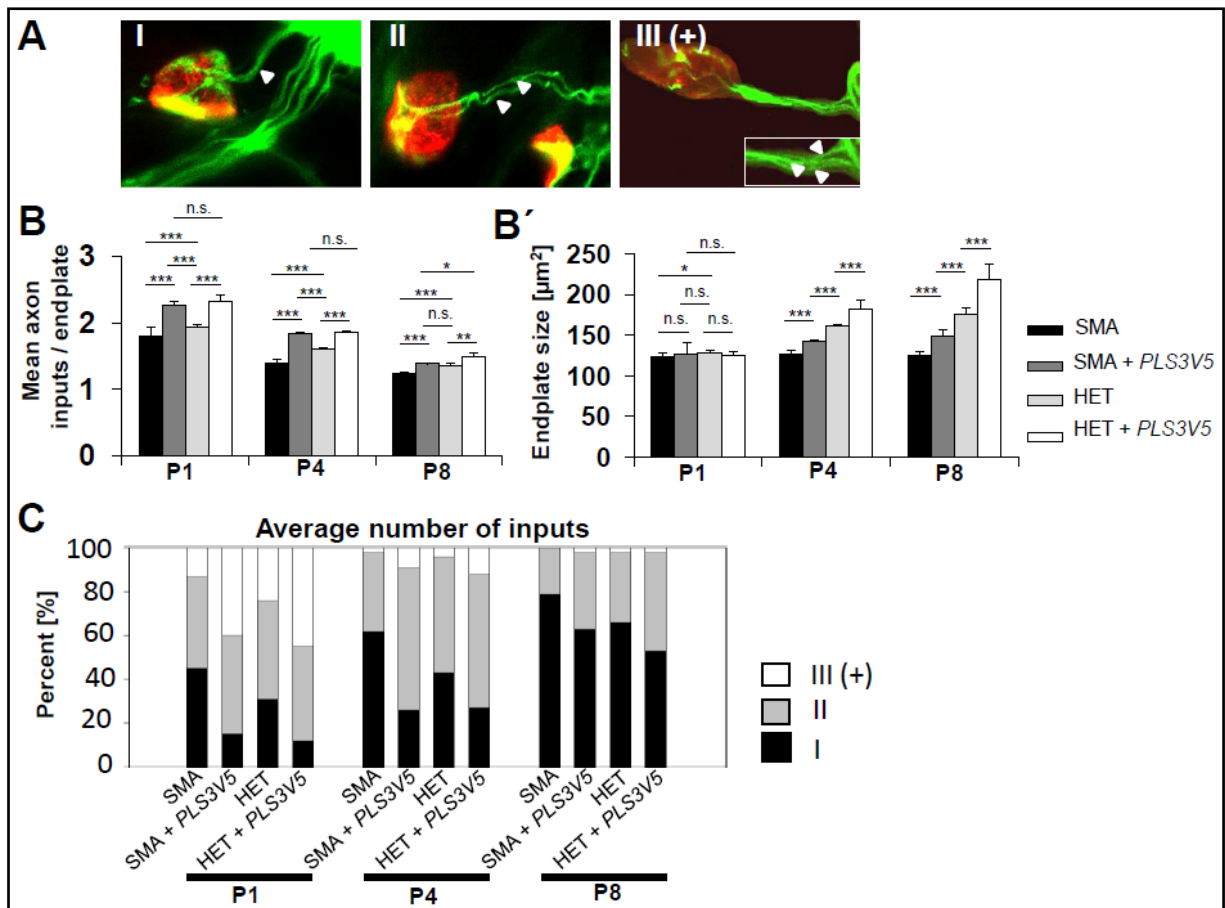


Figure 39: PLS3V5 delays axon withdrawal in the process of axonal pruning in *Transversus abdominis* muscle (P1 – P8). **A**: Exemplary pictures for axon counting. The number of axonal inputs of 100 endplates in 3 mice of each genotype (SMA, SMA + *PLS3V5*, HET and HET + *PLS3V5*) were determined and classified as I = 1 axon, II = 2 axons, III (+) = 3 or more axons. **B**: Calculation of the mean axon input number of all four genotypes revealed that *PLS3V5* expressing SMA and HET animals show an increased mean number of axonal inputs per endplate at all given time points compared with SMA and HET mice. **B'**: Endplate size of all four different genotypes. First significant differences in endplate size get obvious around P4 and manifest at P8, whereby *PLS3V5* expressing SMA and HET mice show an increase in endplate size compared with SMA or HET mice, respectively. **C**: Different representation of the data given in B, depicting the distribution of either I, II or III(+) axonal inputs / endplate (in percent) for each genotype at the respective time points P1, P4 and P8. (Animal numbers: 3 animals were analyzed for each genotype and time point; Stainings: Red = bungarotoxin; Green: neurofilament + SV2; * = $p < 0.05$; ** = $p < 0.01$; *** = $p < 0.001$; 100 NMJs were classified per animal)

As is shown in Figure 39 B and C, the mean number of axons innervating one single endplate decreased constantly from P1 until P8 in all genotypes investigated. Importantly, during the whole developmental phase of 8 days, HET animals showed a significantly higher mean number of axons per endplate compared to SMA mice, indicating poorer neuromuscular connectivity in TVA muscle of SMA animals. Interestingly, this result is contrary to findings by others, who were not able to observe a significant disturbance of the axonal pruning process in SMA mice (Kariya et al., 2008). However, a possible explanation for this could be that Kariya et al. investigated the distal and thus less affected

Gastrocnemius muscle, whereby in this thesis the proximal *Transversus abdominis* muscle was analyzed.

Furthermore, and most strikingly, SMA + *PLS3V5* mice displayed a highly increased mean number of axons per endplate compared to SMA animals at all given time points (Figure 39, B and C). These findings strongly suggest that *PLS3V5* expression causes a delay in the axonal pruning process and exerts a “stabilizing” effect on axons, as it was similarly observed for filopodial protrusions in MEF cells before (chapter 5.4.1.3). Moreover, the observation of increased axon number was not only restricted to SMA + *PLS3V5* mice but could also be seen in HET + *PLS3V5* animals. Compared to HET mice, HET + *PLS3V5* mice displayed significantly more axons reaching the endplates at all time points. Importantly, the number of incoming axons was almost identical between SMA + *PLS3V5* and HET + *PLS3V5* mice over the whole time course, indicating that the axon “stabilizing” effect of *PLS3V5* is likely independent of *Smn*.

Measurement of the endplate size in *PLS3V5* expressing SMA and HET animals previously revealed that *PLS3V5* has a positive effect on the endplate size at P10 (chapter 5.4.3.3). Also in the time course experiment, *PLS3V5* expression in SMA and HET animals resulted in highly significantly increased endplates when compared to SMA or HET animals, respectively (Figure 39, B'). This observation was first detectable around P4 and manifested at P8, whereas at P1 almost no significant differences in endplate size were observable in the different genotypes. At P1, however, the mean axon number per endplate was already highly significantly increased in *PLS3V5* expressing SMA and HET mice. This observation indicates that the increase in endplate size timely follows improved axonal connectivity observed in *PLS3V5* expressing animals and implicates that enhanced AChR clustering might be a consequence of stronger innervation. Even though the mean axon number per endplate in SMA + *PLS3V5* mice significantly exceeded the level of HET controls at P1 and P4, this was not sufficient to restore endplate size in SMA + *PLS3V5* mice to the level of HET mice (Compare B and B' in Figure 39).

This result highlights the importance of *Smn* in correct NMJ formation and suggests that *PLS3V5* alone, at least at heterozygous expression levels, is not sufficient to compensate endplate defects observed in SMA animals. As shown in unaffected siblings of discordant families, who in most cases possess three or four *hSMN2* copies, a certain amount of SMN protein seems to be required for full rescue.

It has been demonstrated in the past that actin filament assembly in the muscle is a necessary pre-requisite for Agrin induced AChR clustering (Dai et al., 2000). Since *PLS3V5* was ubiquitously expressed in the here described experiments, including muscle tissue, an influence of *PLS3V5* on the endplate size by stabilizing actin filaments in the muscle must be considered. In order to dissect the impact of presynaptic *PLS3V5* expression on the endplate

size, experiments in which PLS3V5 was motor neuron specifically activated will be presented in the course of this work (chapter 5.5.).

Taken together, it was shown that the presence of PLS3V5 results in a “stabilization” of incoming motor axons in SMA and HET animals during the process of axonal pruning. Since the extend of axon “stabilization” mediated by PLS3V5 was similar between SMA and HET animals, this indicates an *Smn* independent mechanism. The increase in axonal input number was accompanied by enhanced AChR clustering, whereby SMA + *PLS3V5* mice displayed a highly significant increase in endplate size when compared to SMA animals. At least when heterozygously expressed, PLS3V5 was not able to fully restore endplate size in *Gastrocnemius* muscle of SMA animals to the level of HET controls, pointing at the indispensability of *Smn* protein in the process of proper NMJ maturation.

5.4.3.5 Ubiquitous *PLS3V5* expression results in highly occupied endplates and extensive presynaptic branching at the NMJ

It was studied next, whether PLS3V5 had a direct influence on the occupancy level of postsynaptic endplates. For this purpose, the degree of nerve occupation at the NMJ was estimated for 100 NMJs of 3 P4 animals of each of the genotypes SMA, SMA + *PLS3V5*, HET and HET + *PLS3V5* regarding to the reference given in Figure 40, A. As has been reported before (Cifuentes-Diaz et al., 2002), the comparison between HET and SMA mice revealed less occupied endplates in SMA animals, with 68 % of all investigated NMJs reflecting Type I (poorly occupied) AChR cluster (Figure 40, A). In contrast to that, *PLS3V5* expressing SMA as well as HET animals displayed hyperinnervated endplates with the main proportion of NMJs reflecting Type III (fully occupied) AChR clusters (63 and 67 %, respectively) when compared to SMA or HET animals, respectively. No significant differences were found regarding occupancy level between *PLS3V5* expressing SMA and HET animals, further supporting the view that PLS3V5 mediated “stabilization” of presynaptic structures occurs *Smn* independently. Moreover, careful microscopical analysis of *PLS3V5* expressing SMA and HET mice revealed generally stronger arborized and branched presynaptic nerve terminals, reflecting the positive impact of PLS3V5 on axon outgrowth as was observed in PC12 as well as isolated murine motor neurons (Oprea et al., 2008) (Figure 40, B).

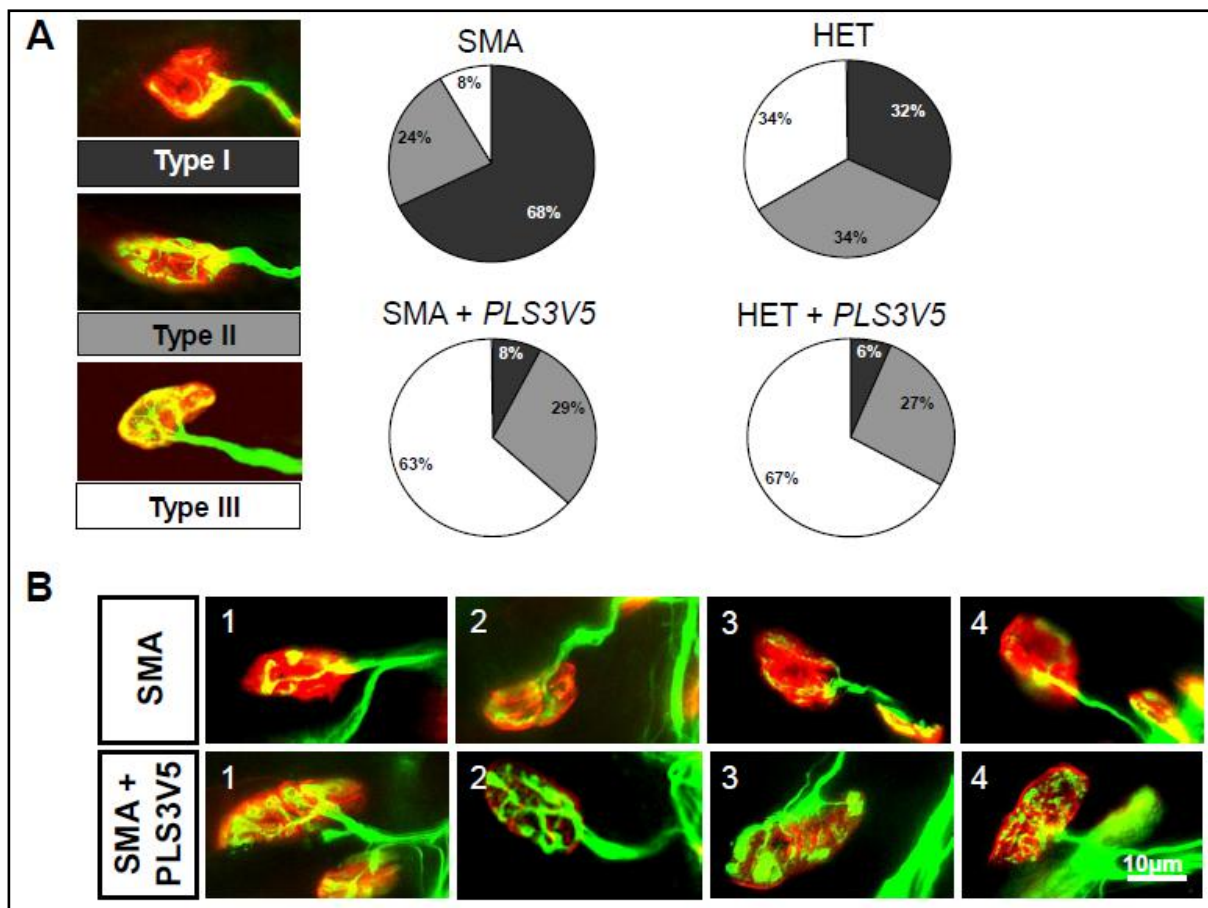


Figure 40 Increased NMJ occupancy and nerve terminal sprouting in *Transversus abdominis* muscle of PLS3V5 expressing SMA and HET mice. **A:** Classification of occupancy level into poorly occupied (Type I), medium occupied (Type II) and fully occupied (Type III) endplates. SMA + PLS3V5 and HET + PLS3V5 mice displayed a higher degree of fully occupied endplates compared to SMA and HET animals, respectively. **B:** Presynaptic nerve terminals are strongly arborized and branched in SMA + PLS3V5 and HET + PLS3V5 mice compared to SMA and HET animals, respectively. Four representative examples (1-4) are given per genotype. (Animal numbers: 3 P4 animals were analyzed for each genotype ;Stainings: Red = Bungarotoxin; Green = α -Neurofilament + SV2; 100 NMJs were classified per animal).

In summary, PLS3V5 expressing SMA and HET animals show highly increased endplate occupancy as well as presynaptic branching when compared to non expressing animals. These findings are in line with the observed axon stabilization phenotype during the process of axonal pruning (chapter 5.4.3.4) and implicate that an increased endplate size in the presence of PLS3V5 might be caused by enhanced presynaptic release, e.g. Agrin.

5.4.3.6 PLS3V5 protein has no stabilizing effect on Smn protein and vice versa

Via 2-dimensional gel electrophoresis Pls3 and Smn were shown to exist in a 200- and in a 500 kDa complex in murine spinal cord (Oprea et al., 2008). Furthermore, via Co-immunoprecipitation experiments it was found that Pls3 and Smn indirectly interact with each other. These observations led to the assumption that Pls3 and Smn might have a stabilizing effect on each other. In line with this idea, it was previously reported that Pls3 levels were significantly reduced in brain and spinal cord of SMA mice, as shown by quantitative Western

blotting and immunohistochemistry (Bowerman et al., 2009). Similar results were obtained when Smn was knocked down via morpholino (MO) injection in zebrafish: Also here, pls3 protein levels were significantly reduced when smn was depleted, whereas restoration of smn resulted in a simultaneous normalization of pls3 levels (Oral presentation Dr. Christine Beattie at the 15th FSMA meeting, San Francisco, USA).

To investigate whether the loss of Smn protein affects Pls3 levels also in the here used SMA mouse model, proteins were isolated from brain and spinal cord tissue of 3 animals of HET controls and SMA mice and subjected to semi-quantitative Western blotting detecting Pls3. As was found for both brain and spinal cord Pls3 protein levels were not significantly changed between SMA and HET mice (Figure 41, A). In the inverse experiment, Smn levels were measured in *PLS3V5^{tg/wt}* mice of the *PLS3V5-ubi* line and compared with wt animals. It was speculated that in case of PLS3V5/Smn interaction PLS3V5 might have a stabilizing effect on Smn protein, however, no increase in Smn protein could be detected in *PLS3V5^{tg/wt}* animals (Figure 41, B). Together, these data do not confirm the observations made by others ((Bowerman et al., 2009) and Dr. Christine Beattie) who reported a correlation of Pls3/pls3 and Smn/smn protein amounts in mouse and zebrafish.

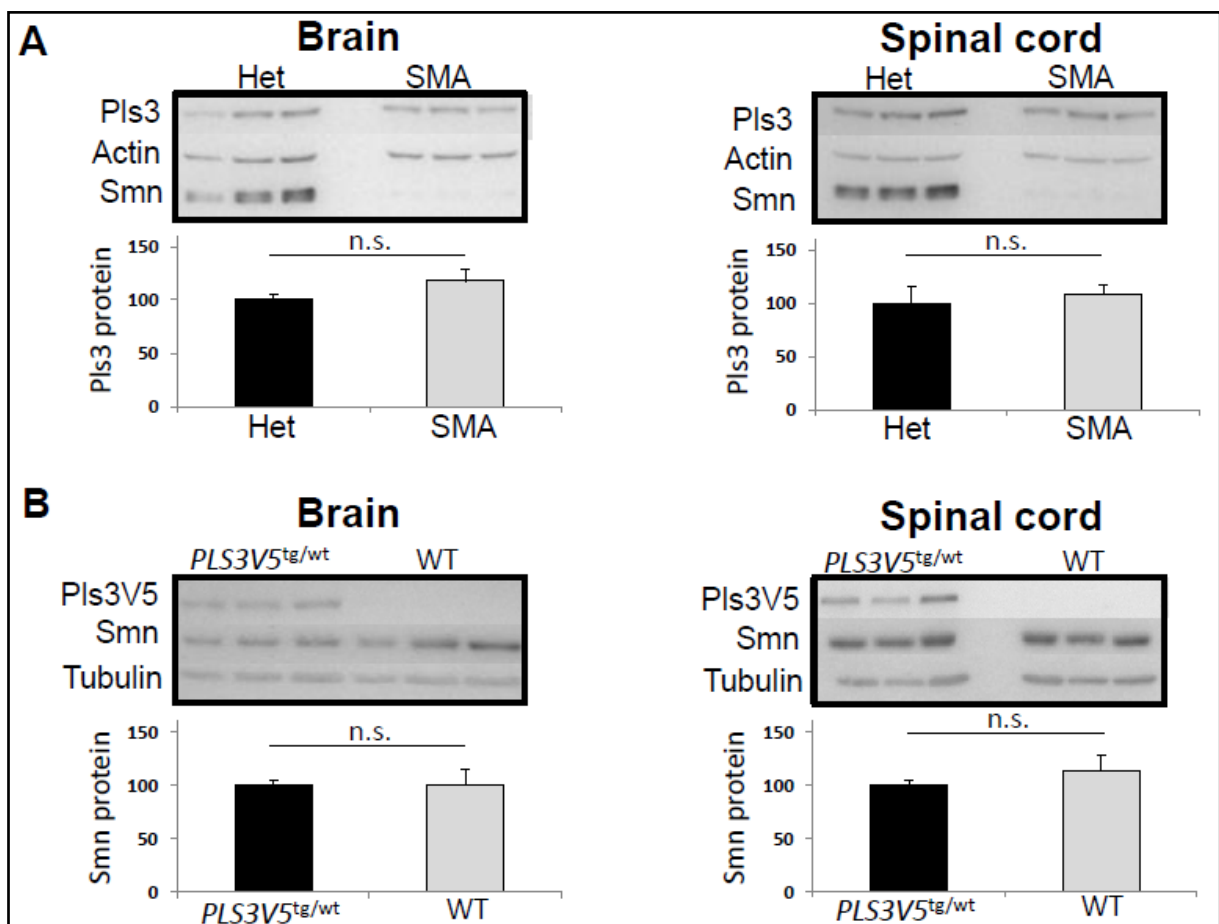


Figure 41 Pls3 expression analysis in the SMA background and Smn protein expression analysis in *PLS3V5^{tg/wt}* mice of the *PLS3V5-ubi* line. **A:** Pls3 protein amount was not changed between HET and SMA mice. **B:** Smn protein amount did not change in the presence of *PLS3V5*.

5.5 Motor neuron specific expression of *PLS3V5* on a wt background

In the last few years, diverse publications have proven a direct involvement of actin polymerization in the process of AChR clustering (Dai et al., 2000, Campagna and Fallon, 2006, Stetzkowski-Marden et al., 2006, Willmann et al., 2006, Zhu et al., 2006, Pato et al., 2008, Lee et al., 2009). To address the question whether the observed positive effect of ubiquitous *PLS3V5* expression on endplate size (chapters 5.4.3.3 and 5.4.3.4) is driven by *PLS3V5* present in the muscle or whether motor neuron specific expression is sufficient, *PLS3V5* was overexpressed specifically in motor neurons on a wt background. For this purpose, *PLS3V5*^{fl_{-st}/wt} mice of the *PLS3V5*-floxed line were crossed with the motor neuron specific *Cre* expressing line *Hb9-Cre* (Arber et al., 1999) (Figure 42). Resulting offspring was then analyzed via immunohistological methods for the effect of motor neuron specific *PLS3V5* expression on motor neuron-, endplate- and muscle fiber size.

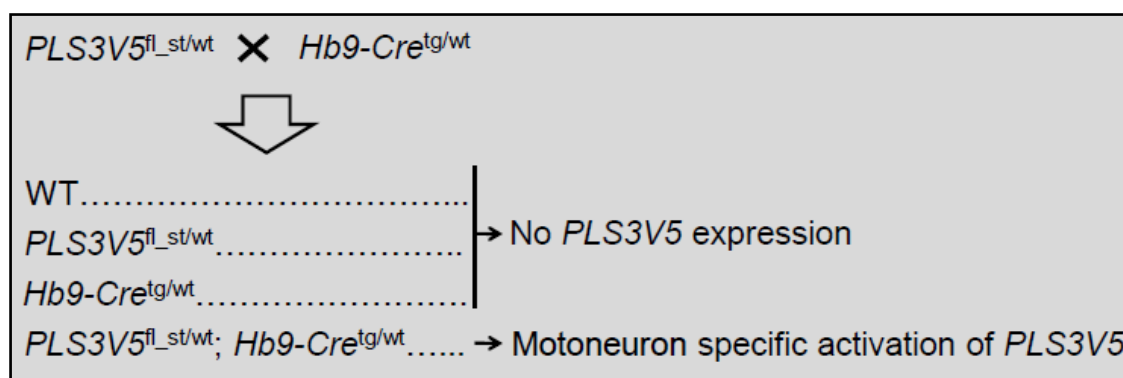


Figure 42 Breeding scheme for the production of motor neuron specific *PLS3V5* expressing mice: In *PLS3V5*^{tg/wt}; *Hb9-Cre*^{tg/wt} animals, *Cre* is motor neuron specifically expressed and leads to the deletion of the Stop-cassette between promoter and *PLS3V5* transgene. In WT, *PLS3V5*^{tg/wt} and *Hb9-Cre*^{tg/wt} control animals, *PLS3V5* is not expressed.

5.5.1 Effects of motor neuron specific expression of *PLS3V5*

5.5.1.1 *PLS3V5* is motor neuron specifically expressed in *PLS3V5*^{fl_{-st}/wt}; *Hb9-Cre*^{tg/wt} mice and leads to an increase of motor neuron cell body size

To analyze whether *Hb9-Cre* mediated deletion of the stop-cassette between promoter and *PLS3V5* transgene was successful and resulted in motor neuron specific *PLS3V5* expression in *PLS3V5*^{fl_{-st}/wt}; *Hb9-Cre*^{tg/wt} mice, immunohistological stainings were performed. For this purpose, spinal cord sections from lumbar regions 4 to 5 of P10 *PLS3V5*^{fl_{-st}/wt}; *Hb9-Cre*^{tg/wt} mice were stained using V5 antibody to specifically detect *PLS3V5* protein. In this approach, WT, *PLS3V5*^{fl_{-st}/wt} and *Hb9-Cre*^{tg/wt} mice were used as negative controls to exclude false positive signals due to unspecific binding of the antibody. Importantly, *PLS3V5* protein was only detectable in motor neurons of *PLS3V5*^{fl_{-st}/wt}; *Hb9-Cre*^{tg/wt} mice but not in WT, *PLS3V5*^{fl_{-st}/wt} or *Hb9-Cre*^{tg/wt} controls (Figure 43).

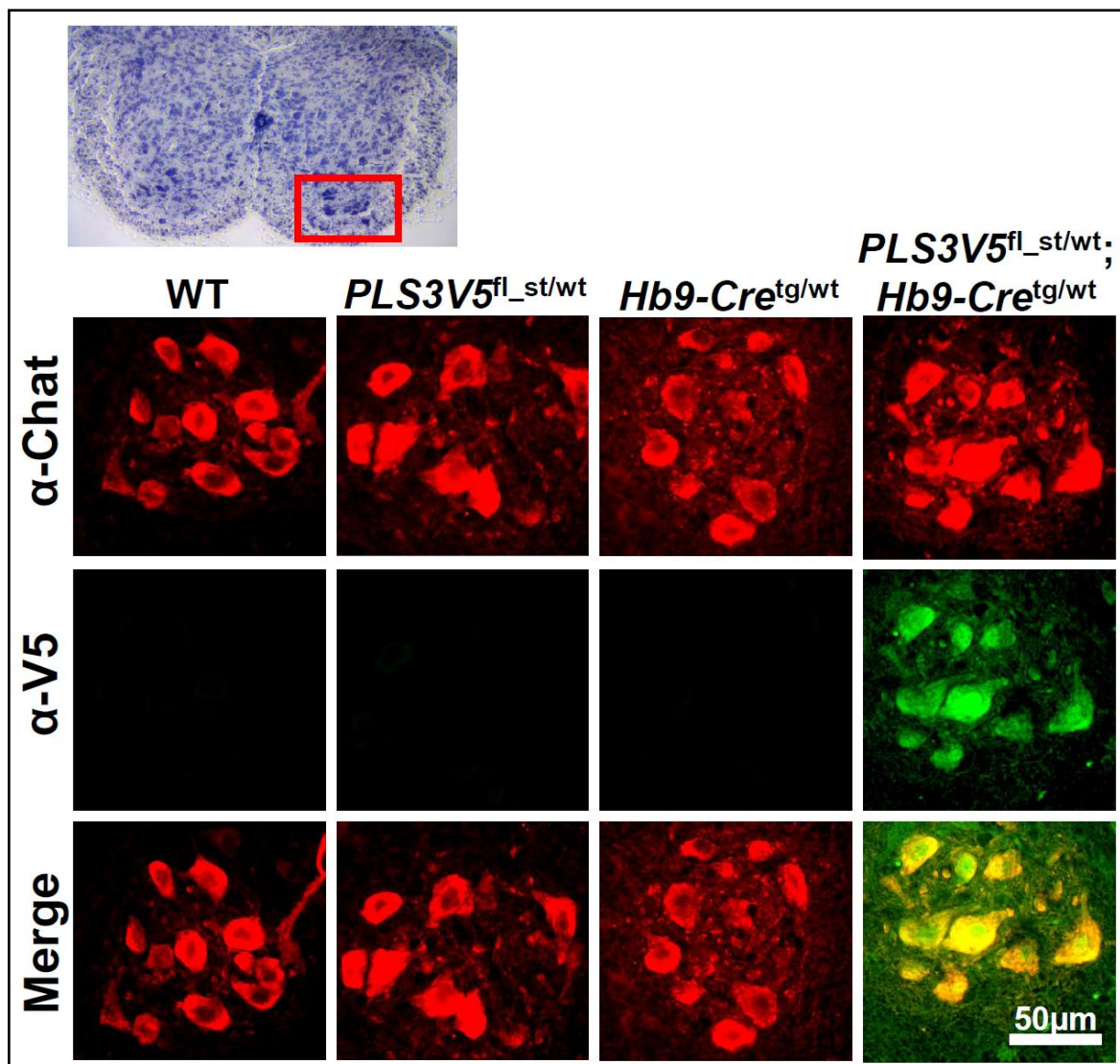


Figure 43 *PLS3V5* is motor neuron specifically expressed in *PLS3V5*^{fl-st/wt};*Hb9-Cre*^{tg/wt} mice, but not in *PLS3V5*^{fl-st/wt} and *Hb9-Cre*^{tg/wt} controls. For a better orientation, the respective ventral horn area is delineated in the above Nissl overview. (Stainings: Red = Chat staining; Green = V5)

Since it is known from MEF cells that *PLS3V5* overexpression can lead to morphological changes (chapter 5.4.1.3), it was next asked whether *PLS3V5* overexpression might have an influence on motor neuron cell shape also *in vivo*. To investigate on that, AxioVision Rel.4.7 software was used to determine the motor neuron soma size in spinal cord sections of P21 *PLS3V5*^{fl-st/wt};*Hb9-Cre*^{tg/wt} animals as well as *PLS3V5*^{fl-st/wt} and *Hb9-Cre*^{tg/wt} controls. As depicted in Figure 44, *PLS3V5*^{fl-st/wt};*Hb9-Cre*^{tg/wt} animals showed a highly significant increase in motor neuron size compared to *PLS3V5*^{fl-st/wt} and *Hb9-Cre*^{tg/wt} controls ($p = 3.52 \times 10^{-40}$ and $p = 3.62 \times 10^{-34}$, respectively; *PLS3V5*^{fl-st/wt};*Hb9-Cre*^{tg/wt} = $931.44 \pm 24.64 \mu\text{m}^2$, *PLS3V5*^{fl-st/wt} = $726.70 \pm 55.6 \mu\text{m}^2$, *Hb9-Cre*^{tg/wt} = $754.24 \pm 11.75 \mu\text{m}^2$), whereby motor neuron size between *PLS3V5*^{fl-st/wt} and *Hb9-Cre*^{tg/wt} animals did not significantly differ ($p = 0.05263$). The finding of increased motor neuron size in *PLS3V5*^{fl-st/wt};*Hb9-Cre*^{tg/wt} animals is of particular interest since reduced proprioceptive reflexes of motor neurons have recently been

correlated with decreased number and function of synaptic connections between motor neurons and muscle spindle afferents in SMA mice (Mentis et al., 2011). Since an increased motor neuron soma might provide extra surface area for afferent synapses this could possibly have a positive impact on spinal circuit function.

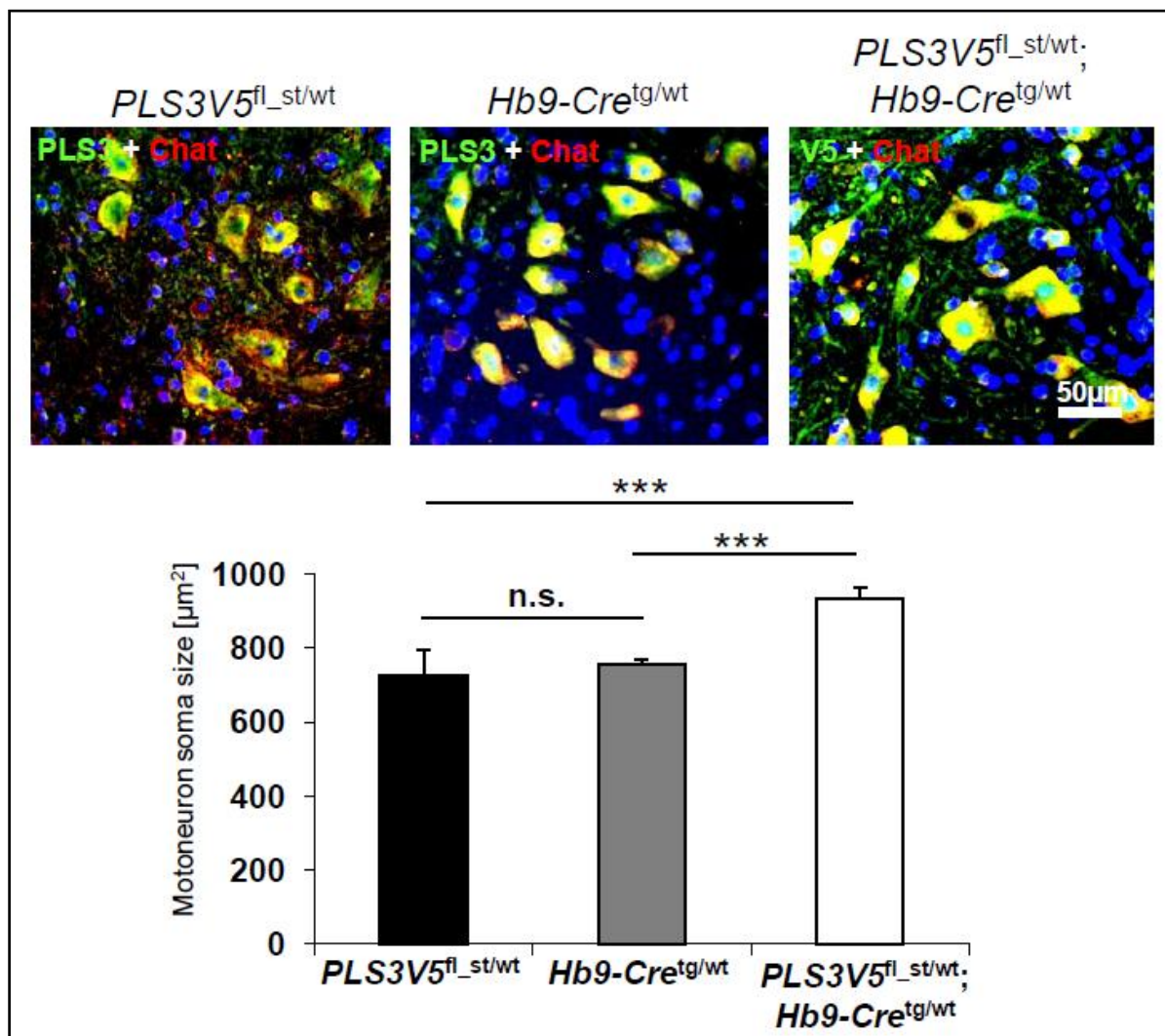


Figure 44 Measurement of motor neuron size revealed highly significantly increased motor neuron soma size in *PLS3V5^{fl}/st/wt; Hb9-Cre^{tg}/wt* compared to *PLS3V5^{fl}/st/wt* and *Hb9-Cre^{tg}/wt* controls. (Animal numbers: 3 animals were analyzed for each genotype; Stainings: Red: Chat; Green: PLS3 or PLS3V5; * = $p < 0.05$; ** = $p < 0.01$; *** = $p < 0.001$; 100 motor neurons were counted per animal)

Here it was shown that *PLS3V5* is activated specifically and exclusively in motor neurons of *PLS3V5^{fl}/st/wt; Hb9-Cre^{tg}/wt* mice. These findings allowed to investigate, whether motor neuron specific expression of *PLS3V5* is sufficient to increase endplate size or if improved AChR clustering is solely regulated by muscular *PLS3V5* protein (chapter 5.5.1.2.) Furthermore, in P21 *PLS3V5^{fl}/st/wt; Hb9-Cre^{tg}/wt* animals *PLS3V5* expression lead to a highly significant increase in motor neuron soma size compared to control mice.

5.5.1.2 Motor neuron specific expression of *PLS3V5* is able to rescue endplate defects observed in *Hb9-Cre^{tg/wt}* p10 and p21 animals and leads to a highly significant muscle fiber size increase in p21 *PLS3V5^{fl-st/wt};Hb9-Cre^{tg/wt}* mice.

As was speculated in chapter 5.5, *PLS3V5* in the muscle might account for the observed increase in endplate size in P10 *PLS3V5* ubiquitously expressing SMA and HET mice (chapters 5.4.3.3 and 5.4.3.4.). To assess if also motor neuron specific expression of *PLS3V5* was sufficient to increase endplate size in *Gastrocnemius* muscle, *PLS3V5* was motor neuron specifically activated on a wt background by crossing with the *Hb9-Cre* line (chapter 5.5). In *Hb9-Cre* mice, Cre recombinase is inserted in the intrinsic *Hb9* gene causing loss of function. In 1999, Arber et al. reported that the homozygous loss of *Hb9* in *Hb9-Cre^{tg/tg}* mice resulted in total absence of motor axons and consequentially perinatal lethality. Furthermore, severe AChR clustering defects were observed as the process of pre patterning and the individual shape of early endplates was disturbed (Arber et al., 1999).

In line with these observations, P10 *Hb9-Cre^{tg/wt}* mice showed a highly significant reduction in endplate size when compared to *PLS3V5^{fl-st/wt}* and *PLS3V5^{fl-st/wt};Hb9-Cre^{tg/wt}* mice (Figure 45, A; $p = 3.09 \times 10^{-39}$ and 3.46×10^{-44} , respectively; P10 *Hb9-Cre^{tg/wt}* = $136.66 \pm 10.09 \mu\text{m}^2$, *PLS3V5^{fl-st/wt}* = $160.08 \pm 4.14 \mu\text{m}^2$, *PLS3V5^{fl-st/wt};Hb9-Cre^{tg/wt}* = $162.96 \pm 5.66 \mu\text{m}^2$). The fact that the endplate size in *PLS3V5^{fl-st/wt};Hb9-Cre^{tg/wt}* mice was restored to that of *PLS3V5^{fl-st/wt}* animals demonstrated that motor neuron specific overexpression of *PLS3V5* was sufficient to rescue endplate size defects of *Hb9-Cre^{tg/wt}* animals. Nevertheless, an involvement of muscular *PLS3V5* protein in the process of AChR clustering cannot be excluded based on these findings. Furthermore, when comparing muscle fiber diameter of *Vastus lateralis* muscle, *PLS3V5^{fl-st/wt}*, *Hb9-Cre^{tg/wt}* and *PLS3V5^{fl-st/wt};Hb9-Cre^{tg/wt}* mice did not display any differences at P10 (Figure 45, A').

At later time point P21, *PLS3V5* expression in *PLS3V5^{fl-st/wt};Hb9-Cre^{tg/wt}* led to a highly significant increase in endplate size relative to *PLS3V5^{fl-st/wt}* and *Hb9-Cre^{tg/wt}* animals in *Gastrocnemius* muscle (Figure 45, B; $p = 5.16 \times 10^{-5}$ and $p = 0.00081$, respectively; *PLS3V5^{fl-st/wt};Hb9-Cre^{tg/wt}* = $372.62 \pm 15.02 \mu\text{m}^2$, *PLS3V5^{fl-st/wt}* = $306,49 \pm 6.02 \mu\text{m}^2$; *Hb9-Cre^{tg/wt}* = $319.03 \pm 5.17 \mu\text{m}^2$). In addition and most strikingly, the bigger endplate size in *PLS3V5^{fl-st/wt};Hb9-Cre^{tg/wt}* animals was accompanied by the observation of a highly significant increase in muscle fiber size (*Vastus lateralis*) compared to *PLS3V5^{fl-st/wt}* and *Hb9-Cre^{tg/wt}* controls (Figure 45, B', $p = 3.15 \times 10^{-11}$ and $p = 5.81 \times 10^{-15}$, respectively; *PLS3V5^{fl-st/wt};Hb9-Cre^{tg/wt}* = 539.53 ± 16.85 , *PLS3V5^{fl-st/wt}* = $408.87 \pm 9.36 \mu\text{m}^2$; *Hb9-Cre^{tg/wt}* = $382.48 \pm 9.94 \mu\text{m}^2$). These findings strongly suggest that the observed improvement in axonal connectivity and NMJ occupation in *PLS3V5* expressing mice (chapters 5.4.3.4 and 5.4.3.5) is indeed functional. However, since endplate size and muscle fiber size were determined in different

muscles, further experiments will include endplate size measurements in *Vastus lateralis* muscle as well as muscle fiber size determination in *Gastrocnemius* muscle.

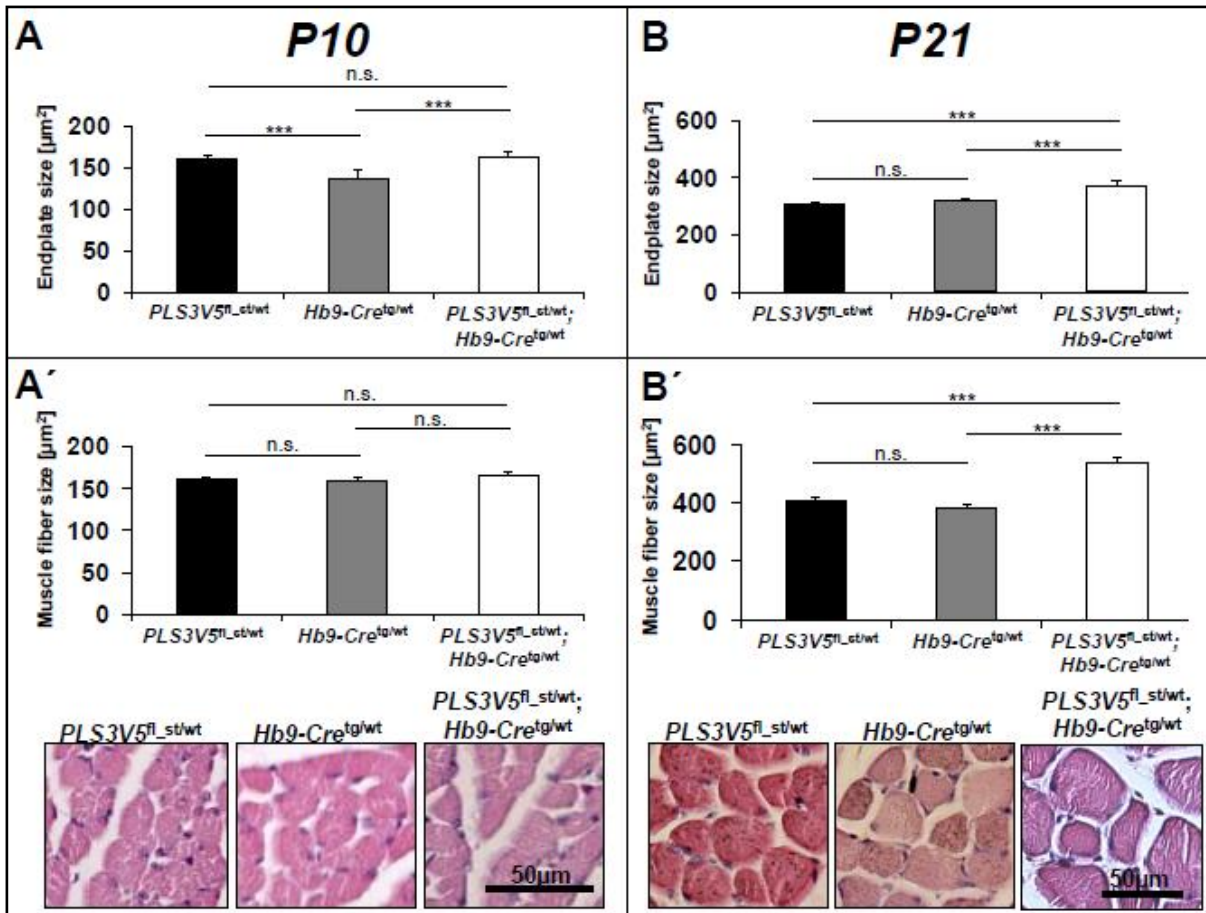


Figure 45: Motor neuron specific expression of *PLS3V5* at P10 and P21 time points and its effects on endplate (*Gastrocnemius* muscle) as well as muscle fiber size (*Vastus lateralis* muscle). **A and A'**: *PLS3V5* expression in P10 *PLS3V5^{fl-st/wt}; Hb9-Cre^{tg/wt}* mice is able to compensate endplate size defects observed in *Hb9-Cre^{tg/wt}* animals, whereby muscle fiber size did not differ between *PLS3V5^{fl-st/wt}*, *Hb9-Cre^{tg/wt}* and *PLS3V5^{fl-st/wt}; Hb9-Cre^{tg/wt}* mice. **B and B'**: At P21, *PLS3V5* expression in *PLS3V5^{fl-st/wt}; Hb9-Cre^{tg/wt}* resulted in highly increased endplate- and muscle fiber size compared to *PLS3V5^{fl-st/wt}* and *Hb9-Cre^{tg/wt}* mice. (Animal numbers: 5 animals were analyzed for each genotype at P10 and 3 animals for each genotype at P21; * = $p < 0.05$; ** = $p < 0.01$; *** = $p < 0.001$, 100 endplates and 100 muscle fibers were counted per animal in the respective tissue)

To summarize, conditional expression of *PLS3V5* exclusively in motor neurons was sufficient to increase endplate size at both time points, P10 and P21. These results support the view that enhanced axonal connectivity and endplate occupancy observed in *PLS3V5* expressing SMA and HET animals directly augmented AChR clustering, possibly through improved presynaptic release. Importantly, motor neuron specific *PLS3V5* expression was able to highly significantly increase *Vastus lateralis* muscle fiber size in *PLS3V5^{fl-st/wt}; Hb9-Cre^{tg/wt}* mice at P21 time point. This finding demonstrates that improved axonal connectivity and endplate occupancy in *PLS3V5* expressing animals is functional. The finding of increased muscle fiber size at P21 but not at P10 suggests that *PLS3V5* effects on muscle fiber size become obvious first at later time points. However, severe Hung SMA mice die

already around P15. Therefore, SMA mice might just die too early to profit from *PLS3V5* overexpression.

6 Discussion

6.1 Generation of a *PLS3V5* expressing mouse

PLS3 has previously been proven to be a fully protective modifier in unaffected *SMN1*-deleted siblings of discordant SMA families (Oprea et al., 2008). Therefore, it was the main aim of the present study to investigate, whether *PLS3* overexpression is also able to rescue the phenotype of an SMA mouse model.

PLS3-overexpressing mice were produced by targeting a V5-tagged version of the human *PLS3* gene (*PLS3V5*) controlled by the CMV enhancer/chicken β -actin (CAG) fusion promoter into the *Rosa26* locus. Since a *LoxP* sites flanked stop-cassette was present between promoter and transgene (Figure 8), *PLS3V5* expression could be driven either ubiquitously or tissue specifically. We induced a motor neuron specific expression by breeding *PLS3V5*-floxed mice with the *Cre*-expressing line *Hb9-Cre* (Arber et al., 1999).

For transgenesis, the hybrid ES cell line V6.5 (SV129 and C57BL/6N) was used in this study (Eggan et al., 2002). V6.5 ES cells offer the big advantage of being insensitive and robust in handling. Furthermore, favorable germline transmission rates have been reported for those cells by various laboratories. Altogether, two rounds of ES cell transgenesis (chapter 5.2) and injection into blastocysts were performed using V6.5 ES cells before a single *PLS3V5*^{fl-st/wt} transgenic female could be identified by genotyping PCR. Nevertheless, to study a possible modifying function of *PLS3V5*, a clean genetic background was required. Therefore, resulting *PLS3V5*^{fl-st/wt} founder animals had to be backcrossed for more than 7 generations to reach a statistical genetic purity of 100 % prior to further analysis.

While constantly backcrossing *PLS3V5*^{fl-st/wt} mice onto a clean C57BL/6N background, the same line was bred with the ubiquitously *Cre*-expressing line *CMV-Cre* (Schwenk et al., 1995) in order to permanently delete the stop cassette between CAG promoter and transgene. Importantly, the *Cre* transgene is located on the X-chromosome in *CMV-Cre* mice. In animals of the genotype *PLS3V5*^{fl-st/wt};*CMV-Cre*^{X-tg/Y} the transgene was expected to be expressed ubiquitously in every cell type (chapter 5.3.3). However, using a PCR allowing to detect the presence or absence of the stop cassette, it was found that the stop cassette was present in ~50 % of *PLS3V5*^{fl-st/wt};*CMV-Cre*^{X-tg/Y} mice despite the presence of *Cre*, likely due to insufficient penetrance of the *Cre* enzyme (Figure 20, A). In line with this, the presence of the stop cassette in *PLS3V5*^{fl-st/wt};*CMV-Cre*^{X-tg/Y} mice was correlated with an absence of *PLS3V5* expression on protein level (Figure 20, B). Importantly, this finding proved that the stop cassette between CAG promoter and *PLS3V5* transgene successfully prevents uncontrolled transgene expression. This observation was of particular importance with respect to motor neuron specific overexpression of the *PLS3V5* transgene.

Cre expression has been shown to act toxic on cells in a dose dependent manner in various organisms and should therefore be outcrossed for further analyzes whenever

possible (Silver and Livingston, 2001). Moreover, Cre recombinase has been shown to induce proliferation disturbances in *Drosophila melanogaster*, resulting in phenotypic aberrations (Heidmann and Lehner, 2001). Finally, mice expressing Cre at high levels in spermatids display chromosome scrambling after meiosis II, causing complete male sterility (Schmidt et al., 2000). Since Cre was not necessary to activate *PLS3V5* expression once the stop cassette had been deleted in the germline and to avoid unspecific side effects of Cre, *PLS3V5* was outcrossed by breeding *PLS3V5^{fl-st/wt};CMV-Cre^{X-tg/Y}* mice with C57BL/6N wt animals (chapter 5.3.3).

This way, heterozygous *PLS3V5^{tg/wt}* animals of the so termed *PLS3V5*-ubi line (Table 13) were established, invariably carrying the stop-cassette-deleted allele in every cell and tissue. Notably, *PLS3V5^{tg/wt}* animals displayed completely normal behavior, motoric ability, weight gain and fertility and were indistinguishable by their wt littermates. This suggested that *PLS3V5* overexpression, at least when driven by the CAG promoter, is not *per se* toxic to cells. Additionally, the absence of toxic effects of *PLS3V5* transgene expression allowed to model the situation in unaffected SMA siblings best possible, namely by ubiquitously overexpressing *PLS3V5* in the murine SMA background.

PLS3V5^{tg/wt} animals on C57BL/6N wt background were further analyzed for *PLS3V5* expression on mRNA and protein level. By comparing total *plastin 3* mRNA levels (here defined as the sum of *PLS3V5* + endogenous *Pls3*) between wt and *PLS3V5^{tg/wt}* mice, it was shown that *plastin 3* is significantly overexpressed in all examined tissues affected by SMA, including brain, spinal cord and muscle (Figure 22, A). However, total *plastin 3* mRNA levels were only moderately increased in brain, spinal cord and muscle to 3.6, 3.4 and 21.5 fold of endogenous level, respectively. In other tissue types, e.g. heart or blood, *plastin 3* levels were more significantly increased, with 76.2 and 206 fold overexpression. Notice that the fold-expression reflects the difference compared to the endogenous level. Since there is usually no *Pls3* expression in blood, a 200 fold increase is easy to be achieved. On the other hand, endogenous *Pls3* is highly expressed in spinal cord or muscle, which means that the total *plastin 3* level observed in spinal cord or muscle of transgenic mice might still exceed the level in blood. To ultimately compare *plastin 3* overexpression levels between different tissue types, an absolute quantification would be necessary.

On protein level, *PLS3V5* was neither detectable in brain, nor in spinal cord of *PLS3V5^{tg/wt}* mice using a PLS3 antibody recognizing both, endogenous *Pls3* as well as *PLS3V5* (Figure 24, A, B). In this regard, it was only possible to obtain the endogenous *Pls3* protein band and only in combination with V5 antibody, also *PLS3V5* was detectable. Together, these findings indicated that *PLS3V5* is present in brain and spinal cord of *PLS3V5^{tg/wt}* animals, however, in lower concentrations as was indicated on mRNA level. This finding gets further support from experiments with liver proteins, where total *plastin 3* mRNA amount was 7.8 fold increased

compared to endogenous level (Figure 22, A). Concomitantly with an increased PLS3V5 expression on mRNA level, PLS3V5 protein was indeed detectable by using the PLS3 antibody (Figure 24, C). Nevertheless, as assessed by densitometric analysis, the expression of total plastin 3 protein in liver of *PLS3V5^{tg/wt}* mice was only ~2 fold increased compared to wt level. Therefore, it is likely that also in brain, spinal cord and muscle the real *plastin 3* upregulation is far below the levels indicated by mRNA expression analysis. These findings suggest that *PLS3V5* mRNA is not likewise converted into PLS3V5 protein, indicating translational regulation of the transgene or other possible negative feedback mechanisms on its own expression. In this context it might be possible that 5' and 3' sequence elements of the targeting vector might account for lower translation rates. Furthermore, the V5-tag of the human *PLS3* transgene might negatively impact on protein folding or stability and might thus induce degradation via the ubiquitin-proteasome system.

Additionally, *PLS3V5* was successfully activated specifically in motor neurons by crossing *PLS3V5^{fl-st/wt}* mice with the motor neuron specific *Cre* line *Hb9-Cre*. Via qRT-PCR and Western blotting it was tried to detect *PLS3V5* expression on mRNA and protein level in spinal cord of *PLS3V5^{fl-st/wt};Hb9-Cre^{tg/wt}* mice. Unexpectedly, *PLS3V5* expression was detectable neither on mRNA, nor on protein level (data not shown). It is known that only a small percentage, in the range of 3-5 % of the total cell population, of spinal cord consists of motor neurons (Arce et al., 1999, Wiese et al., 2010). Therefore, it must be considered that in spinal cord lysate *PLS3V5* mRNA and protein also hold only a very small percentage of total transcripts and proteins. Since no expression differences were detectable between *PLS3V5^{fl-st/wt};Hb9-Cre^{tg/wt}* animals and *PLS3V5^{fl-st/wt}* as well as *Hb9-Cre^{tg/wt}* controls, it was concluded that qRT-PCR and Western blotting methods are not sensitive enough to detect such low levels of *PLS3V5* mRNA and protein, respectively. A similar observation has been made in the context of motor neuron specific deletion of the splicing factor *Sfrs10* in *Sfrs10^{fl/fl};Hb9-Cre^{tg/wt}* mice by our group (Mende et al., 2010). Finally, motor neuron specific expression of *PLS3V5* was proven via immunohistochemical stainings using a V5 antibody on spinal cord sections of *PLS3V5^{fl-st/wt};Hb9-Cre^{tg/wt}* mice.

6.2 The genetic background influences the phenotypic severity in Hung SMA mice

The *PLS3V5* transgenic lines were backcrossed onto pure C57BL/6N background in this thesis while the *Hb9-Cre* line for motor neuron specific overexpression was already present on pure C57BL/6N. It is commonly accepted that genetic purity is absolutely essential for the reliability and consistency of precise analysis. For that reason, also Hung SMA mice, at that time only present on FVB background, were backcrossed for at least 7 generations to C57BL/6N wt animals. Hung SMA mice on FVB background show a mean survival of 9.9 d (Riessland et al., 2010), while SMA mice on a C57BL/6N background live for 15.5 d.

Interbred SMA mice containing a statistical portion of 87 % C57BL/6N and 13 % FVB (mixed background), however, displayed the longest mean survival with 19.2 d. Because mice on pure C57BL/6N background live longer compared to SMA mice on FVB background, this suggests the presence of genomic modifying factors. Furthermore, the fact that mixed SMA mice survive longer than SMA animals on either of the two clean backgrounds indicates that genetic heterogeneity mitigates phenotypic severity. In contrast to the short survival time of only 15.5 d in Hung SMA mice on pure C57BL/6N background found here, Tsai et al. found that Hung SMA mice on pure C57BL/6J background survived for ~13 months (Tsai et al., 2008).

How can these huge discrepancies between genetically distinct backgrounds, but in particular between the relatively close two C57BL/6 substrains (“N” and “J”), be explained? Of the two strains mentioned, C57BL/6J was the “original” strain, whereby subline C57BL/6N originated at the National Institute of Health (NIH) and was separated by C57BL/6J in 1951 (Zurita et al., 2011). Until today, the individual lines were kept over many generations by various investigators and vendors. Due to genetic drift, it is supposed that each of these sublines is genetically distinct, although externally, they are very similar (Zurita et al., 2011). Genetic differences comprise a whole consortium of minor or major genomic alterations, among these single nucleotide polymorphisms (SNPs), microsatellites, copy number variations but also genomic rearrangements as well as mutations in genes or promoter regions of genes. E.g., with regard to the latter, most substrains derived from C57BL/6J mice carry a mutation in the nicotinamide nucleotide transhydrogenase (*Nnt*) gene, resulting in inappropriate glucose homeostasis (Freeman et al., 2006, Zurita et al., 2011). Up to now, only little information is available on the differences between various substrains. In a screen applying an Illumina[®] Mouse Medium Density (MD) Linkage mapping panel, one study comprised altogether 1.449 SNPs selected from 20 mouse chromosomes and compared these between different C57BL/6 substrains (Zurita et al., 2011). In this study, only 12 SNPs were found to be polymorphic between the C57BL/6J and C57BL/6N substrains. Although 5 of the 12 SNPs mapped to boundaries of known genes (*Naaladl2*, *Fgf14*, *Lims1*, *Aplp2*, *Snap29*), it appears unlikely that the enormous survival differences between Hung SMA mice on C57BL/6J and C57BL/6N can be explained by only those variants. Moreover, considering a mean coverage of 3 SNPs per 5 Mb interval when using only 1.449 SNPs, it seems even more obvious that further genetic differences must be present among the two substrains that account for the phenotypical discrepancies.

Last but not least, it must be mentioned that also environmental factors can have a major impact on the severity of SMA-pathology. Besides different animal care and health standards, e.g. also nutrition has been demonstrated to significantly influence the course of disease in the SMNΔ7 mouse model. In this regard, combining Trichostatin A (TSA, an

HDAC inhibitor) treatment with nutritional support extended the median life span of SMA mice to about 170 %, compared to only 40 % when TSA was given alone (Narver et al., 2008).

6.3 The effects of *PLS3V5* overexpression on the morphology of murine embryonic fibroblasts

In the present study, murine embryonic fibroblasts (MEFs) were isolated from *PLS3V5*^{tg/wt} animals and the transgene detected using an antibody against the V5-tag. By comparing the localization pattern of wt PLS3 with *PLS3V5*, it was found that transgenic protein localizes completely normal and specifically at sites of actin filament consolidation. Moreover, *PLS3V5* overexpression led to significant changes in MEF cell morphology as was implicated by a significantly increased number of filopodial and lamellipodial structures compared to wt cells.

In the year 1980, *PLS3* was first described as a 68 kDa protein colocalizing with actin filaments and being present in membrane ruffles, microspikes and microvilli of chicken fibroblast cells (Bretscher and Weber, 1980). Based on these observations, further analysis revealed that *PLS3* is an F-actin bundling protein with main function in cytoskeletal organization (Bretscher, 1981, Glenney et al., 1981). By overexpressing *PLS3* in fibroblast like CV-1 cells and in the polarized epithelial cell line LLC-PK1, it was found that high levels of *PLS3* exert significant effects on cell morphology (Arpin et al., 1994). In CV-1 cells, *PLS3* overexpression led to the reorganization of F-actin filaments into polygonal networks around the cell surface and consequentially to a rounding up of cells, structural properties reminiscent of rat embryo cells just before spreading (Lazarides, 1976). Moreover, *PLS3* overexpression was associated with a partial loss of adherence in CV-1 cells as concluded by the observation of a diminution of focal contacts. In contrast, *PLS3* overexpression induced the formation of thickened and elongated microvilli in LLC-PK1 cells. Also, when overexpressed in stereocilia of developing auditory hair cells, *PLS3* led to an increase in length, width, and density of microvilli (Daudet and Lebart, 2002). Together, these results suggest an important role for *PLS3* in the rearrangement of cytoskeletal structures towards membrane outgrowth. Accordingly, in the present study overexpression of *PLS3V5* in MEFs derived from *PLS3V5*^{tg/wt} mice led to a significant stabilization of lamellipodial as well as filopodial structures when compared to wt cells.

The observation of stabilized filopodia in *PLS3V5* overexpressing MEFs raises the question how an actin bundling protein might affect the length of an actin microfilament. In the yeast null-mutant of fimbrin (*SAC6Δ*) cytoplasmic actin filaments are completely absent (Belmont and Drubin, 1998). The other way around, in yeast strains expressing the V159N mutant form of actin (*act1-159*), filaments depolymerize approximately three times slower than in wt filaments and are more abundant than in wt (Belmont and Drubin, 1998). However, in the *sac6Δ act1-159* double mutant the number of F-actin cables is restored to almost wt

level while filaments seemed mislocalized and displayed an abnormal organization. Furthermore, by a rhodamine-phalloidin-binding assay as well as G-actin measurement in permeabilized yeast *sac6Δ* mutant cells, F-actin was found to be decreased, G-actin to be increased while no change in total actin levels compared with wt was observed (Karpova et al., 1995). Also in lymphoblastoid as well as HEK cells, overexpression of PLS3 led to increased F-actin levels (Oprea et al., 2008). Together, these findings suggest that PLS3 has multiple roles in stabilizing F-actin by inhibiting depolymerization and directing F-actin filament orientation. However, in order to find out how PLS3 mechanistically prevents F-actin depolymerization further biochemical investigations are required.

6.4 Effects of *PLS3V5* overexpression at NMJ level

The main goal of this study was to investigate a possible rescuing effect of *PLS3V5* overexpression on the murine SMA phenotype. As outlined previously, *PLS3V5* overexpression did not have a positive impact on survival and motoric ability of the severe Hung SMA mouse model (chapter 5.4.3.2). Nevertheless, careful morphological analysis revealed a very prominent phenotype at the neuromuscular junction (NMJ) of ubiquitously *PLS3V5* expressing SMA and HET control mice (Figure 39 and Figure 40). Additionally, to further dissect pre- and postsynaptic effects of *PLS3V5* expression on AChR clustering, *PLS3V5* was motor neuron specifically activated on a wt background (chapter 5.5). In the next chapters, the effects of *PLS3V5* overexpression on NMJ morphology and the implications for SMA pathology will be discussed.

6.4.1 Increased AChR clusters – effect of pre- or postsynaptic *PLS3V5* action?

Since no improvement in survival and motoric ability were detected in *PLS3V5* overexpressing SMA mice, morphological analysis was performed on muscle sections to investigate whether *PLS3V5* overexpression affects NMJ morphology. Thereupon, it was found that the size of postsynaptic AChR clusters was highly significantly increased in the *Gastrocnemius* muscle of P10 SMA + *PLS3V5* and HET + *PLS3V5* animals when compared to SMA and HET mice (Figure 37). At early time points of mouse development and still preceding axon arrival, patches of AChR spontaneously assemble along the midline of muscles in a process termed AChR-prepatterning (Lin et al., 2001, Yang et al., 2001). Upon nerve arrival, synaptogenic factors are released that further trigger and refine AChR clustering to sites of nerve innervation. In this context, the most important presynaptic factor known to trigger AChR clustering is the proteoglycan and MuSK receptor ligand Agrin (Wu et al., 2010). Since in the initial experiments *PLS3V5* was ubiquitously expressed in SMA + *PLS3V5* and HET + *PLS3V5* animals, the question was raised whether PLS3V5 at pre- or postsynaptic sites accounts for the increase in endplate size of P10 animals.

Noteworthy, addressing this question was of particular interest since a presynaptic effect of *PLS3V5* expression on AChR clustering would point at improved presynaptic signaling in transgenic mice. Initial support for the view of a presynaptic contribution of *PLS3V5* overexpression on AChR cluster size came from a time course experiment: Here, it was found that the endplate size between SMA, SMA + *PLS3V5*, HET and HET + *PLS3V5* animals did not significantly differ at the early time point P1 (Figure 39). Importantly, endplate size differences between *PLS3V5* expressing and control mice were first seen around P4. However, the CAG promoter driving *PLS3V5* expression is ubiquitously active already very early during development, also in the muscle (Sakai and Miyazaki, 1997). Therefore, in case of a muscle specific effect of *PLS3V5* on AChR cluster size, one would expect an effect of *PLS3V5* on AChR clustering already during the AChR prepatterning process, just before first nerve terminals arrive. In line with that, an increase in endplate size should also be detectable at P1. Around P4, significant morphological changes take place in the context of mouse NMJ maturation. Principally, these changes comprise synapse elimination (axonal pruning) and concomitant conversion of the uniform patch-like shape of AChR cluster into a perforated pretzel-like appearance (Kariya et al., 2008, Murray et al., 2008). In this context, postnatal endplate maturation is known to be dependent on excitation from motor nerve terminals (Misgeld et al., 2002). The fact that endplate size increase in *PLS3V5* transgenic mice falls together with motor axon rearrangement processes further suggests a presynaptic role for *PLS3V5* in AChR clustering. At this point it should be remembered that *PLS3V5* overexpression indeed results in significant changes of presynaptic organization, such as delayed axonal pruning as well as hyperinnervation of endplates. Therefore, these effects of *PLS3V5* on presynaptic organization might well account for the observed increase in endplate size.

To further analyze the influence of presynaptic presence of *PLS3V5* on endplate size, *PLS3V5* was motor neuron specifically overexpressed in *PLS3V5^{fl-st/wt};Hb9-Cre^{tg/wt}* mice. In heterozygous *Hb9-Cre^{tg/wt}* mice, *Cre* is located in the endogenous *Hb9* locus, resulting in heterozygous knockout of *Hb9* (Arber et al., 1999). Moreover, homozygous *Hb9-Cre^{tg/tg}* mice are even perinatally lethal and display a complete loss of motor neuron axons (Yang et al., 2001). Furthermore, AChR prepatterning has been shown to be clearly disturbed in *Hb9-Cre^{tg/tg}* mice with abnormal scattered distribution of AChR clusters across the diaphragm muscle at the early time point E12-E18.5. Although postsynaptic prepatterning defects of homozygous *Hb9-Cre^{tg/tg}* are long known, until now no study has ever focused on later time points in living heterozygous *Hb9-Cre^{tg/wt}* mice. In the present study, it was found that also *Hb9-Cre^{tg/wt}* mice exhibit AChR clustering defects by means of reduced endplate size in *Gastrocnemius* muscle as compared to controls at P10. This finding highlights the essential role of *Hb9* for normal motor neuron development (Yang et al., 2001). Furthermore, these

findings underline the importance of normal motor neuron development and nerve innervation for proper AChR clustering. Most strikingly, endplate size was restored to normal level in *PLS3V5^{fl-st/wt};Hb9-Cre^{tg/wt}* mice. As muscular *PLS3V5* expression can be excluded in *PLS3V5^{fl-st/wt};Hb9-Cre^{tg/wt}* animals, it seems plausible that presynaptic changes must account for the observed increase in endplate size. Since *PLS3V5* overexpression led to an amelioration of the endplate size defects not only in SMA but also in *Hb9-Cre* mice, these findings together point at a general *PLS3V5* neuroprotective effect, which might in turn impact on endplate size.

Nevertheless, despite clear evidence for presynaptic contribution of *PLS3V5* overexpression to enhanced AChR clustering, an additional muscle specific effect of *PLS3V5* from P4 time point on cannot be excluded. Many studies have focused on the relationship between the actin cytoskeletal organisation and AChR clustering in the past. In myotubes, F-actin filament formation clearly precedes Agrin induced AChR clustering (Dai et al., 2000). Additionally, it has been shown in the same study, that AChR clusters did not form in the presence of Latrunculin, a toxin that sequesters globular (G)-actin and prevents F-actin assembly. From these experiments, it can be concluded that F-actin assembly is a prerequisite for the formation of Agrin induced AChR clusters. Furthermore, AChR clustering involves signaling by positive regulators of actin polymerization and filament growth, e.g. Rho-family GTPases (regulate actin polymerization-driven processes) (Weston et al., 2003, Hall, 2005), p21-activated kinase 1 (effector of the GTPase Cdc42, which in turn regulates actin polymerization) (Luo et al., 2002) or geranylgeranyl transferase (enhances the membrane association and activation of GTPases) (Luo et al., 2003). Additionally, cortactin, which is an activator of the Arp 2/3 complex, has been shown to be important for AChR clustering (Madhavan et al., 2009). Most interestingly, however, many F-actin-associated proteins with impact on filament organization have been found to colocalize with AChR clusters at the mature or developing NMJ, such as vinculin (links integrins to the actin cytoskeleton) or filamin as well as α -actinin (function in F-actin bundling and interconnection) (Bloch and Hall, 1983, Cartaud et al., 2011). α -actinin has been shown to inhibit the rate of F-actin depolymerization, thereby stabilizing F-actin (Cano et al., 1992). This observation is in line with findings for PLS3 which, when overexpressed in LB or HEK cells, increases the F-actin to G-actin ratio (Oprea et al., 2008). Although mechanics of PLS3-mediated F-actin stabilization have not yet been sufficiently studied, the findings together indicate that F-actin filament stabilization through inhibition of depolymerization might be a feature common to actin bundling proteins. Assuming that PLS3 exerts a stabilizing effect on F-actin and on the background that F-actin formation is essential for AChR clustering and maintenance, muscle specific PLS3 might hence be positively involved in endplate maturation. To examine possible muscle specific contribution of PLS3, it would be interesting to compare AChR

cluster size between motor neuron specifically and ubiquitously *PLS3V5* expressing mice. Any increase in endplate size in *PLS3V5* ubiquitously expressing animals compared to motor neuron specifically expressing mice would then indicate muscle specific effects.

6.4.2 Delayed axonal pruning in *PLS3V5* overexpressing mice

Based on the fact that presynaptic *PLS3V5* overexpression influences AChR cluster size (chapter 6.4.1), it was speculated whether improved nerve connectivity in *PLS3V5* expressing mice might account for the bigger endplates. It has previously been reported that smn-depleted zebrafish as well as cultured motor neurons derived from SMA mice exhibit severe axon outgrowth defects. Since no defects in initial axon outgrowth have ever been observed in mice *in vivo*, it is assumed that loss of nerve connectivity at the NMJ results rather from a dying-back mechanism (McWhorter et al., 2003, Rossoll et al., 2003, McGovern et al., 2008, Sleight et al., 2011). Nevertheless, severe SMA mice have been shown to exhibit a significant reduction of axonal inputs per endplate during the axonal pruning process in proximal TVA muscle (Murray et al., 2008). In order to analyze the impact of *PLS3V5* on axonal integrity, the process of axonal pruning was studied in time course experiment (Figure 39). Including P1, P4 and P8 time points, it was demonstrated that SMA animals showed a reduced number of axonal inputs at all given time points compared to HET controls. However, in SMA + *PLS3V5* animals, the mean number of axonal inputs was highly significantly increased compared to SMA controls and exceeded even that of HET animals. These findings suggested that *PLS3V5* might exert a positive effect on the integrity of existing axons. At later time point P11, however, the number of axons per endplate adapted between *PLS3V5* expressing and non-expressing animals and approached a nearly singular innervation pattern (preliminary data and thus not shown). Therefore, rather a retraction-delaying than a “stabilizing” function of *PLS3V5* on axons during the axonal pruning process must be assumed.

Nevertheless, the observations raise the questions about the mechanism of *PLS3V5*-mediated delay in axon retraction. The observation of delayed axonal pruning is highly reminiscent of the analogous finding from MEF cells, where *PLS3V5* overexpression led to an increase in filopodial structures. Additionally, it was observed in MEF cells that *PLS3V5* specifically localizes to sites of actin filament consolidation in filopodia as well as lamellipodia. Since the localization pattern of *PLS3V5* in motor neurons has not yet been resolved, it can only be speculated whether *PLS3V5* is enriched in axonal filopodia and lamellipodia as well and exerts similar function there as well. It is known that actin dynamics play an essential role in regulating axon growth, branching ability as well as motility and guidance of the growth cone (Luo, 2002, Dent et al., 2003). Ultimately, the term actin dynamics comprises a variety of processes including actin polymerization and depolymerization, filament branching, bundling and interaction of actin polymers with other

components of the cytoskeleton, such as the microtubule network. Particularly, a balanced rate of F-actin polymerization and depolymerization is an important prerequisite for axon dynamics, including formation and withdrawal of growth cone filopodia. This has e.g. been demonstrated by experiments in which the effect of the drug jasplakinolide (jasp), a cell-permeable macrocyclic peptide that inhibits F-actin turnover, was tested on retinal and dorsal root ganglion (DRG) neuron cultures (Gallo et al., 2002). When neurons were treated with jasp, growth cone motility, defined as lamellipodial and filopodial extension, stopped, the growth cones contracted and the axons began to retract. In their experiments, the authors observed that actin depolymerization was absent in the central zone (C domain) of the growth cone. Since polymerization of F-actin at the leading edge of the growth cone (P domain) requires G actin release by filament turnover in the C domain (Cramer, 1999), a lack of G actin supply might explain axon retraction after jasp treatment. In line with this observation, inhibiting actin polymerization using drugs like Cytochalasin or Latrunculin also interferes with normal axon growth. At high doses, Cytochalasin treatment has been shown to result in the disassembly of F-actin and subsequent defects in neurite outgrowth (Letourneau et al., 1987). Furthermore, axons in the developing grass hopper nervous system have been shown to lose all pathfinding capabilities upon treatment with Cytochalasin (Bentley and Toroian-Raymond, 1986). Interestingly, it was reported in another study that neurons form multiple axons upon Cytochalasin and Latrunculin treatment in moderate concentrations, suggesting that high actin turnover rates support axon outgrowth (Bradke and Dotti, 1999). Based on these findings it appears obvious that actin dynamics and turnover, rather than overall cytoskeletal rigidity, are essential for axon elongation and growth. As it was already mentioned earlier, α -actinin has been shown to inhibit the rate of F-actin depolymerization, thereby indirectly stabilizing F-actin (Cano et al., 1992). Similarly, also *PLS3* overexpression has been demonstrated to increase the F-actin to G-actin ratio in lymphoblastoid (LB) and HEK cells (Oprea et al., 2008). Therefore, it might be possible that *PLS3* prevents F-actin depolymerization and thus exerts a stabilizing effect on axons and growth cones, however, without shifting the equilibrium of actin poly- and depolymerization towards a critical end.

In this context, it would be interesting to further investigate the substructural location of *PLS3V5* in growth cones. In MEF cells, *PLS3V5* is generally more abundant in filopodia and lamellipodia. Nevertheless, a rather weak staining was also detected throughout the entire cell body. In the axonal growth cone, F-actin is mainly present in filopodia and lamellipodia of the P domain, while C and transition (T) domains represent areas of G-actin regeneration. Given that *PLS3* binds only filamentous actin and has no intrinsic actin polymerizing activity, a possible actin filament-stabilizing effect is therefore likely to be restricted to axonal filopodia and lamellipodia. Nevertheless, stabilizing effects of *PLS3V5* on F-actin filaments migrating

into T and C domain, a normal process during axon dynamics, might consequentially reduce regeneration of G-actin in the C domain of the growth cone. Similar to the observations under jasp treatment, insufficient regeneration of G-actin would be expected to result in axon retraction and withdrawal. In the complainant's view, this raises the question how *PLS3V5* overexpression can result in exactly the opposite effect, namely a delay in axon withdrawal from the NMJ? In order to investigate the role of *PLS3V5* in actin dynamics of the growth cone, high resolution confocal microscopy might be an adequate tool. In a vice versa experiment, it would also be interesting to precisely analyze the consequences of *Pls3* depletion for growth cone motility in mouse motor neurons.

6.4.3 Innervation defects in Hung SMA mice and hyperinnervation of endplates in *PLS3V5* expressing animals

Besides delayed axonal pruning, hyperinnervated endplates were found at P4 in SMA + *PLS3V5* and HET + *PLS3V5* mice compared to SMA and HET mice (Figure 40, A). Furthermore, SMA + *PLS3V5* animals displayed highly arborized nerve terminals at the same time point, while nerve terminals of age matched SMA littermates exhibited significantly reduced terminal sprouting when compared to HET controls (Figure 40, B). Most strikingly, the observed effects of *PLS3V5* overexpression at NMJ level seem to be functional, since mice specifically overexpressing *PLS3V5* in the motor neurons showed a highly significant increase in muscle fiber size.

The finding of reduced endplate occupancy in Hung SMA mice is consistent with previous findings from other mouse models (Murray et al., 2008, Kong et al., 2009). In 2008, Kariya et al. have been the first to extensively investigate NMJ pathology in the *SMN Δ 7* SMA mouse model (Kariya et al., 2008). In their studies, they have been able to show that SMA mice display severe structural abnormalities at the NMJ level in *Gastrocnemius* muscle, including massive neurofilament accumulations and a failure of axons to form fine terminal arbors. However, Kariya et al. were unable to observe complete endplate denervation in the distal *Gastrocnemius* muscle of postnatal *SMN Δ 7* SMA mice. In humans, SMA usually affects the proximal muscles first. In line with this, others have detected the presence of 51 % unoccupied AChR clusters already at E18.5 and 49 % at P2 in the proximal intercostal muscles of the *SMN Δ 7* mouse (McGovern et al., 2008). Similarly, in late symptomatic SMA mice of the very severe Monani model (*Smn*^{-/-}; *SMN2(89Ahmb)*^{tg/tg}, survival ~ 5 d, (Monani et al., 2000)), ~15 % of endplates have been shown to be completely denervated in proximal TVA muscle (Murray et al., 2008). Interestingly, the authors have observed denervated endplates also in distal muscles of the lumbricals in Monani SMA animals, however, at significantly lower percentage. Therefore, as above findings suggest, NMJs display highly variable phenotypic severity among diverse muscles in one and the same SMA model, but also between different SMA mouse models. Despite a reduction in presynaptic coverage of

endplates, completely denervated endplates were more or less absent in proximal TVA muscle of Hung SMA mice in the present study (Figure 40). Surprisingly, however, it has been published before that in the distal *Gastrocnemius* muscle of Hung SMA mice around 9 % of endplates showed a denervation phenotype (Riessland et al., 2010). Together, these observations are not in line with the findings from human, where proximal rather than distal muscles are severely affected by SMA. One possible explanation for these findings is that the Hung SMA mice analyzed here were on pure C57BL/6N background, while Riessland et al. have used Hung SMA mice on pure FVB background in their work. As was found in the present study, Hung SMA mice on C57BL/6N background show a five days prolonged mean life span (15.5 d) compared to Hung SMA mice on pure FVB background (9.9 d). As it was discussed before (chapter 6.2), the C57BL/6N background obviously exerts an ameliorative effect on disease severity, which might explain the observation of better nerve connectivity in proximal TVA (C57BL/6N) compared to distal *Gastrocnemius* muscle (FVB) in Hung SMA mice.

As mentioned, P4 SMA and HET animals expressing *PLS3V5* displayed increased endplate occupancy and extensive sprouting of nerve terminals compared to SMA and HET littermates, respectively (Figure 40). What implication do these observations have with regards to NMJ maturation and better neurotransmission? Since reduced nerve occupancy is a hallmark of SMA, stronger nerve coverage of endplates has frequently been taken as positive criteria to verify beneficial effects of various drugs, e.g. in studies investigating the therapeutic potential of the HDACi VPA, SAHA or TSA (Narver et al., 2008, Tsai et al., 2008, Riessland et al., 2010). In the present work, an increase in endplate occupancy and nerve terminal arborization was observed at P4, however, *PLS3V5* expressing mice at earlier (P1) or later (P8, P11) time points showed similar effects at the NMJ. Therefore, observed effects at the NMJ might impact on both endplate maturation and signal transduction of established NMJs. It is well known that synaptogenic factors, such as Agrin and ACh, direct endplate maturation by refining areas of AChR clustering (Wu et al., 2010). While Agrin positively triggers the recruitment, assembly and maintenance of AChR at sites of innervation, ACh negatively impacts on AChR clustering, suppresses AChR expression and destabilizes AChR clusters globally in entire muscle fibers. During endplate maturation, the patch-like structure of AChR clusters gets perforated and clusters only remain at sites of presynaptic innervation. In the present work, motor neuron specific *PLS3V5* expressing animals showed an increase in endplate size (Figure 45). Therefore, one possible explanation for the bigger endplates could be that the increased nerve occupancy and terminal arborization leads to a higher release of pro-AChR-clustering factors such as Agrin.

In line with this idea, *PLS3V5* overexpression and concomitant cytoskeletal rearrangements might have an influence on the location and the release of synaptic vesicles

and thus on neurotransmission. In two studies using the *SMN Δ 7* mouse model, an abnormal synaptic vesicle number and location was accompanied with defects in neurotransmission as assessed by detailed electrophysiological analyzes (Kariya et al., 2008, Kong et al., 2009). Two pools of vesicles exist in motoric presynapses: Readily releasable vesicles (RRVs), which are in proximity to or already docked with the presynaptic membrane and vesicles of the reserve pool (RPV), which are located farther from the membrane (Dillon and Goda, 2005). Kong et al. have observed a 36 % reduction of RRVs in TVA muscle of the *SMN Δ 7* mouse (Kong et al., 2009). Moreover, the transmitter per single vesicle (quantal content, QC) (QA) was unchanged between SMA and control mice, while a significantly reduced number of synaptic vesicles was released after nerve stimulation in SMA mice (quantal amplitude, QA). Therefore, the authors assumed that reduced density of synaptic vesicles may contribute to declined QC at SMA NMJs. As mentioned, not only the number of vesicles was found to be reduced, but also overall location of vesicles in the presynapse was disturbed. Therefore, the authors further speculated whether the commonly observed neurofilament (NF) accumulations are indicative for a more generally disturbed neuronal cytoskeleton. A disruption of cytoskeletal structures, in turn, might then result in displacement of vesicles, and consequentially in impaired neurotransmission. Interestingly, the idea of cytoskeletal disorganization as a pathological feature of SMA also matches the observation of significantly impaired *β -actin* mRNA transport into growth cones of SMA motor neurons (Rossoll et al., 2002). Additionally, also many other findings highlight the importance of a functional actin cytoskeleton for presynaptic function: E.g., it is well accepted that F-actin plays important roles in both recycling and transport of synaptic vesicles (Shupliakov et al., 2002, Bloom et al., 2003). Furthermore, after a current model synaptic vesicles are tethered near the membrane by F-actin via phosphorylation-dependent interaction with the vesicular molecule synapsin (Dillon and Goda, 2005). Upon depolymerization, Synapsin undergoes a conformational change, thereby freeing synaptic vesicles for release (Li et al., 2010). Last not least, F-actin regulates the availability of RPV by surrounding the vesicle cluster, thus providing a corralling function by forming a physical barrier to impede vesicle dispersion (Dillon and Goda, 2005). Taken together, these observations underline the importance of F-actin in synaptic vesicle organization and release. Therefore, by influencing F-actin dynamics *PLS3V5* might act as a regulator of synaptic release, compensating for presynaptic dysfunction in SMA nerve terminals.

6.5 Why does *PLS3V5* overexpression not ameliorate the survival of SMA mice? *SMN* and *PLS3V5* protein amounts as limiting factors

In 6 discordant families *PLS3* has been demonstrated to act as a fully protective modifier of SMA in *SMN1*-deleted unaffected siblings (Oprea et al., 2008). In the present study, the goal was to investigate a possible rescuing effect of *PLS3* overexpression on the murine

SMA phenotype. To analyze the effect of ubiquitous *PLS3V5* overexpression on the SMA phenotype, *PLS3V5* was heterozygously overexpressed in the severe Hung SMA background (chapter 5.4 and following). However, differently from the situation in SMA patients, where high PLS3 levels had previously been reported to result in a full rescue of SMA symptoms, *PLS3V5* overexpression did not affect survival in the murine system: While SMA mice showed a mean survival of 15.5 d, SMA + *PLS3V5* animals lived for 14.6 d ($p = 0.529$). Interestingly, despite the absence of any positive effects of *PLS3V5* overexpression on survival of SMA mice, the observed pre- as well as postsynaptic morphological changes in *PLS3V5* overexpressing animals seem to be functional. This assumption is based on the fact that motor neuron specific activation of the transgene on wt background led to an increase in muscle fiber size at the late time point P21. However, at P10 time point, *PLS3V5* overexpression had no significant effect on muscle fiber size, suggesting that *PLS3V5* effects on muscle fiber size get obvious only at later time points.

In recent times, it became more and more clear that the severe form of SMA is not simply a motor neuron disease, but that also other neuronal (e.g. proprioceptive neurons, hippocampus) and non

neuronal tissues (e.g. heart, bone, blood vessels, liver) are affected (Finsterer and Stollberger, 1999, Kelly et al., 1999, Hsieh-Li et al., 2000, Felderhoff-Mueser et al., 2002, Arai et al., 2005, Hachiya et al., 2005, Bach, 2007, Shanmugarajan et al., 2007, Khatri et al., 2008, Rudnik-Schoneborn et al., 2008, Araujo Ade et al., 2009, Meyer et al., 2009, Shanmugarajan et al., 2009, Bevan et al., 2010, Gogliotti

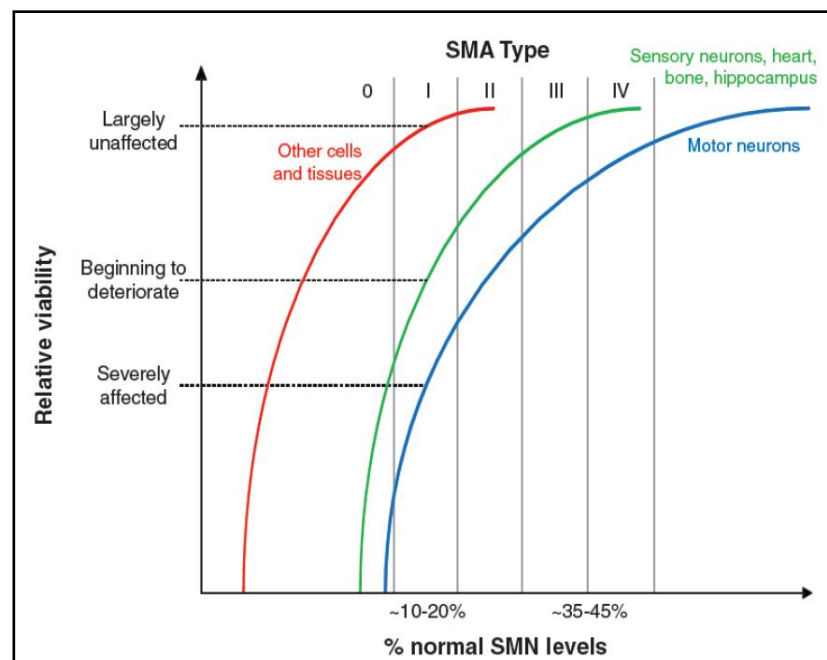


Figure 46: Differential susceptibility of cell and tissue types to SMN reduction (Sleigh et al., 2011)

et al., 2010, Heier et al., 2010, Hua et al., 2010, Michaud et al., 2010, Riessland et al., 2010, Shababi et al., 2010). The observation of pathological features in cell types other than motor neurons has led to the development of the so called threshold theory. This hypothesis proposes that there is a differential susceptibility of cells to SMN depletion: While motor neurons are affected at already relatively weakly reduced SMN levels, other cells and tissues such as the heart, bone and finally all tissue types get affected as SMN levels further

decrease or are even completely absent (Sleigh et al., 2011). Consequentially, in the severe Hung SMA model any positive effects of *PLS3V5* on survival through improved axonal connectivity, NMJ maturation and muscle fiber size might be limited by defects in other tissues, which finally result in early death of SMA mice. In other words: An amelioration of the survival phenotype by *PLS3V5* overexpression might require relatively high SMN levels.

Importantly, there are two observations strongly supporting this idea. The first hint comes from discordant families themselves: It has been found here, that all *SMN1*-deleted unaffected siblings of the 6 discordant families harbored 3 or 4 *SMN2* copies, accordingly leading to type III SMA in their affected siblings.

Further support for this idea comes from a study investigating the effects of the Rho-kinase (ROCK) inhibitor Fasudil on the murine SMA phenotype. Rho/ROCK signaling is a major regulatory pathway of actin dynamics and has been demonstrated to be upregulated in *Smn*-depleted PC12 cells and SMA mice (Bowerman et al., 2007, Bowerman et al., 2010). Accordingly, Rho/ROCK activation has been implicated in dendritic simplification, reduced spine length and density (Nakayama et al., 2000, Govak et al., 2004). In their studies, Bowerman et al. have shown that treatment of severe *SMNΔ7* SMA mice with Fasudil results in increased AChR cluster and TA myofiber size. Most interestingly and very similar to our results, despite the positive effect of Fasudil treatment on endplate and muscle fiber size no improvements of survival could be detected in severe *SMNΔ7* animals. In further experiments, the authors treated the intermediate *Smn*^{2B/-} mouse SMA model (Bowerman et al., 2009) with Fasudil and subsequently investigated the effects on survival. Most strikingly, Fasudil treatment of *Smn*^{2B/-} mice led to a significant increase in survival. These findings suggest that the improvements at NMJ and muscle level upon Fasudil treatment have an ameliorative effect solely in the presence of higher *Smn* threshold levels.

Similar to the results obtained upon Fasudil treatment, it might be possible that high *PLS3* levels only improve the SMA survival phenotype in the presence of relatively higher *Smn* levels, too. Since *Smn*^{2B/-} mice represent an intermediate SMA model with a mean survival of ~4 weeks (Bowerman et al., 2009), these animals might be appropriate to study possible effects of *PLS3V5* overexpression on survival as well. However, *Smn*^{2B/-} mice are currently maintained on C57BL/6×CD1 mixed background resulting in a broad distribution in survival time of individuals from the same litter. Therefore, to analyze the impact of *PLS3V5* overexpression on the SMA survival phenotype, backcrossing *Smn*^{2B/-} mice to a clean C57BL/6N background would be required first. Additionally, considering that the genetic background has a major impact on survival of SMA mice (chapter 6.2), purification of *Smn*^{2B/-} mice to clean C57BL/6N background might result in a significant alteration of mean survival in these animals. Finally, it must be considered that *Smn*^{2B/-} mice are not available at the Institute of Genetics, Cologne, and would need to be imported via embryo transfer first,

which is time and cost intensive. Another possibility to study the consequences of *PLS3* expression in a milder SMA model would be to cross *PLS3V5* onto the homozygous Hung *Smn^{-/-};hSMN2^{tg/tg}* background. *Smn^{-/-};hSMN2^{tg/tg}* mice carry a total of 4 *hSMN2* copies (2 per integrate) and show only very mild SMA symptoms, e.g. necrosis of ears and tail with subcutaneous edema. Moreover, *Smn^{-/-};hSMN2^{tg/tg}* mice display normal fertility slightly reduced life span of ~1.5 years. Nonetheless, an exact description of the pathological features of this model has not been performed yet and therefore bears further analyses (e.g. motor neuron count, NMJ pathology, degeneration of muscle). Additionally, due to the extremely weakened phenotype of *Smn^{-/-};hSMN2^{tg/tg}* mice, subtle improvements upon *PLS3V5* expression might be hard to detect. To investigate the effect of *PLS3V5* overexpression on a milder SMA background, it would also be possible to make use of the fact that a mixed genetic background has an ameliorative effect on survival of Hung SMA mice. As it has been demonstrated in the present work, SMA animals of 87 % C57BL/6N / 23 % FVB mixed background have a prolonged life span of 19.2 d as compared to 15.5 d and 9.9 d in pure C57BL/6N or FVB background animals, respectively. In this context, *Smn^{-/-};SMN2^{tg/tg}* animals on pure FVB background could be mated with *Smn^{+/-};PLS3V5^{tg/wt}* mice on pure C57BL/6N background, according to the breeding scheme presented in Figure 28. As the resulting offspring represents genetically mixed animals of 50 % C57BL/6N and 50 % FVB background, an accompanying increase in life span is expected. Furthermore, Hung SMA mice expressing *PLS3V5* on pure or mixed background could additionally be treated with histone deacetylase inhibitors (HDACi) to increase SMN levels. Due to their ability to increase *SMN2* expression and in combination with the fact that ~10 % of full length SMN protein are being produced by *SMN2*, a collection of HDACi has been proven to effectively counteract SMA pathology in the mouse model, e.g. Sodium butyrate (NaBu), Valproic acid (VPA), Trichostatin A (TSA) and suberoylanilide hydroxamic acid (SAHA) (Chang et al., 2001, Avila et al., 2007, Narver et al., 2008, Tsai et al., 2008, Riessland et al., 2010). An increase of SMN in Hung SMA mice might also be accomplished by antisense oligonucleotides (ASOs) treatment. Via binding to *SMN2* pre-mRNA, ASOs have been shown to redirect the incorrect splicing of *SMN2*, resulting in the production of predominantly functional SMN (Passini et al., 2011). Moreover, Passini et al. have shown that early postnatal delivery of ASOs into the lateral ventricle led to improvements in muscle physiology, motor function and survival of *SMNΔ7* SMA mice. Therefore, by titrating the injected ASO amount in early Hung SMA mice it might be possible to generate an intermediate mouse model appropriate for studying *PLS3V5* modifying effects in the presence of relatively high SMN levels. Both, treatment with HDACi or ASO injection to increase SMN levels, however, require high methodological reliability and expertise.

It needs to be mentioned that also only moderate *PLS3V5* expression levels in transgenic animals might explain the absence of ameliorative effects on survival in severe Hung SMA animals. It was demonstrated that *PLS3V5* is overexpressed in all tissues affected by SMA of transgenic animals, namely brain, spinal cord and muscle (chapter 5.4.1.2). However, despite significant, total plastin 3 (endogenous *Pls3* + *PLS3V5*) mRNA levels were only moderately increased in *PLS3V5* transgenic compared to wt mice with 3.6 fold in brain, 3.4 fold in spinal cord and 21.5 fold in muscle tissue (chapter 5.4.1.1). Since it was assumed that *PLS3V5* mRNA is not likewise converted into *PLS3V5* protein (previously discussed in chapter 6.1), an even lower increase of total plastin 3 in *PLS3V5* transgenic mice must be expected on protein level. In Epstein Barr virus (EBV) transfected lymphoblastoid (LB) cell lines of unaffected siblings from discordant families, *PLS3* was shown to be ~40 fold upregulated on mRNA level (Oprea et al., 2008). This observation, however, does not reflect the situation in the actual target tissue of SMA, namely motor neurons. Since only LB as well as fibroblast cell lines of discordant families are available, it is unknown to what extent *PLS3* is upregulated in spinal cord or even motor neurons of unaffected *SMN1*-deleted individuals. This information, however, might provide important information on the quantitative requirement of *PLS3* to exert rescuing effects on the survival of SMA patients. As spinal cord tissue of unaffected siblings is not available, redifferentiation of fibroblast cells into induced pluripotent stem (IPS) cells and subsequent differentiation into motor neurons would be a way to address this question. The effort to obtain such cultures is currently being undertaken in our laboratory and in cooperation with *iPierian* (CA, US). While fibroblasts have already been successfully redifferentiated into IPS cells, the next steps will include differentiation into motor neurons and subsequent confirmation via marker analysis and gene expression profiling. Furthermore, motor neuron specific *PLS3V5*-expressing mice (*PLS3V5*^{fl.st/fl};*Hb9-Cre*^{tg/wt}) might help to investigate the *PLS3* amount required for SMA protection. Notice that *GFP* is cloned downstream of *PLS3V5* in the targeting construct and is co-activated via an internal ribosomal entry site together with *PLS3V5* (Figure 8). This might enable to specifically isolate motor neurons from *PLS3V5*^{fl.st/fl};*Hb9-Cre*^{tg/wt} mice, e.g. via FACS, and to compare total *plastin 3* expression levels with those from respective controls (e.g. motor neuron specific *GFP* expressing mice, available at Jacksons laboratories).

6.6 Does *PLS3V5* act together with or independent of *Smn*?

It has previously been shown via co-immunoprecipitation (Co-IP) that *PLS3* and *SMN* are both present together with Actin in a 500 kDa complex (Oprea et al., 2008). These findings were further supported by the fact that *Pls3* colocalizes with *Smn* in growth cones of differentiated PC12 cells. Moreover, it has been previously assumed that *Smn* exerts stabilizing function on *Pls3*. This idea comes from experiments in the *Smn*^{2b/-} and *SMNΔ7* mouse models, where a low level of *Smn* was found to be associated with reduced *Pls3*

protein amounts ((Bowerman et al., 2009) and Dr. Christine Beattie, oral presentation at the 15th FSMA meeting, Orlando, USA). Beattie et al. further showed that also in zebrafish *smn* depletion is correlated with a reduction in *pls3* amount. In turn, however, restoration of *pls3* did not result in simultaneous increase in *smn* protein. Therefore, Beattie et al. suppose that *smn* might positively act on translation of *pls3* mRNA.

In the present study, a possible interaction between *Smn* and *Pls3/PLS3V5* was investigated in Hung SMA and *PLS3V5* transgenic mice. In a scenario where *Smn* and *Pls3* interact and based on the above mentioned findings by other groups, *Smn* and *Pls3/PLS3V5* might exert stabilizing function on each other. In contrast to the results obtained in *Smn*^{2b/-} and *SMNΔ7* mice, however, endogenous *Pls3* was not downregulated in Hung SMA animals. In the *vice versa* experiment, also *Smn* levels were not increased in *PLS3V5* transgenic mice compared to wt (Figure 41). These results suggested, that at least in Hung SMA mice *Smn* and *Pls3* do not exert a stabilizing effect on each other. Further support for an *Smn*-independent working mechanism of *PLS3* comes from the time course experiment, which was in this thesis performed to investigate the process of axonal pruning in *PLS3V5* expressing SMA mice (Figure 39). Here, it was found that SMA animals expressing *PLS3V5* display an increased number of axons compared to SMA mice at P1, P4 and P8. Also in HET + *PLS3V5* animals, the number of axons was significantly increased compared to HET animals at all time points. Importantly, however, the number of incoming axons was almost identical between SMA + *PLS3V5* and HET + *PLS3V5* mice over the whole time course. More or less the same was observed regarding nerve occupancy at the endplates. Also in this experiment, no difference regarding occupancy status was detected between SMA and HET mice expressing *PLS3V5*. Together, these findings indicate that at least in Hung SMA mice *Smn* and *Pls3/PLS3V5* do not act stabilizing on each other. Furthermore, the results suggest that the axon retraction-delaying effect of *PLS3V5* is likely independent of *Smn*.

One explanation for these opposing findings could be that Dr. Bowerman and Dr. Beattie used different mouse models (*Smn*^{2B/-} and *SMNΔ7*) than was used in this study (Hung SMA). Additionally, at least in the case of *Smn*^{2B/-} mice, animals were kept on C57BL/6xCD1 hybrid background, giving rise to the assumption that background depending factors might influence the stability of *Pls3* in an *Smn* dependent manner. Similarly, species-specific differences might account for the observation of *smn/pls3* protein level correlation made by Beattie et al. in the zebrafish system.

6.7 Future prospects and next steps

In order to investigate the mechanisms underlying *PLS3* protection in *SMN1*-deleted unaffected siblings, transgenic *PLS3V5* expressing mice were generated in this study. It could be shown that *PLS3V5* exerts wt function by localizing the transgene in MEF cells of transgenic mice. Furthermore, it was demonstrated that *PLS3V5* overexpression supports

the formation of lamellipodial/filopodial structures in MEF cells and results in increased occupancy of endplates and highly arborized nerve terminals at the NMJ *in vivo*. Moreover, by investigating the process of axonal pruning, it was revealed that PLSV5 overexpression is able to delay axon withdrawal from NMJs, indicating an important role for PLS3 in the maintenance of axonal integrity. Most strikingly, the observed changes at NMJ level seem to be functional, as motor neuron specific overexpression of PLS3V5 resulted in a highly significant increase in AChR cluster and muscle fiber size.

Despite first insight into PLS3 working mechanisms, several questions remain open or require further investigations. In the following, the next steps to address these questions will be outlined briefly:

- I. *PLS3V5* overexpression did neither ameliorate survival nor motoric ability of the severe Hung SMA mouse model. As previously discussed in chapter 6.5, it might be possible that *PLS3V5* effects can not compensate the severe and lethal global defects of the here used SMA model. Of the different options to investigate *PLS3V5* effects in a milder SMA background depicted (chapter 6.5), *PLS3V5* overexpression in Hung SMA mice on mixed background is the most time and cost effective method and is therefore currently being performed.
- II. Since *PLS3V5* was only heterozygously overexpressed in the SMA background, also *PLS3V5* expression levels might not be sufficiently high to ameliorate the survival phenotype. In order to increase *PLS3V5* levels, breedings are currently ongoing with the goal to homozygously overexpress *PLS3V5*.
- III. Upon *PLS3V5* overexpression, improved axonal connectivity was observed in *PLS3V5* expressing mice. Additionally, muscle fiber size was significantly increased in motor neuron specific *PLS3V5*-expressing mice. In this context, it is important to mention that the observed increase in endplate size in *PLS3V5^{fl-st/wt};Hb9-Cre^{tg/wt}* mice was measured in *Gastrocnemius* muscle, however, muscle fiber size increase was assessed in *Vastus lateralis* muscle. Since distinct muscles are differently affected in SMA mice, a potential muscle fiber size increase has to be reassessed in *Gastrocnemius* muscle of *PLS3V5^{fl-st/wt};Hb9-Cre^{tg/wt}* animals. Furthermore, to confirm functionality of the observed morphological changes at NMJ level, more precise analyzes, e.g. quantal content measurements or Motor Unit Number Estimate (MUNE) are required and will be performed in the future.
- IV. Until now, no information is available on the PLS3 amount required for SMA protection in motor neurons of unaffected discordant siblings. Therefore, approaches to redifferentiate human embryonic fibroblasts into iPS cells and

subsequently differentiate these into motor neurons are currently being performed in our laboratory and in cooperation with iPierian (CA, US).

- V. Pls3 has been described to be enriched in growth cones of PC12 cells and primary motor neurons (Oprea et al., 2008). However, no detailed analysis has been performed on the exact subcellular localization of Pls3 within growth cones. In order to understand the impact of PLS3 action on neurocytoskeletal organization in growth cones, high resolution confocal in combination with electron microscopy will be performed.
- VI. Based on the findings of the present study, PLS3V5 might exert an SMN independent neuroprotective function. Therefore, it would be interesting to test the effects of *PLS3V5* overexpression on other motor neuron diseases, e.g. amyotrophic lateral sclerosis (ALS). In most familial ALS forms (~20%), mutations in the superoxide dismutase 1 (*SOD1*) gene account for disease development (Ticozzi et al., 2011). Since mutated *Sod1* resembles the ALS phenotype in mouse (Gurney et al., 1994), *PLS3V5* transgenic mice might be crossed on a *Sod1* mutant background.

7 Summary

Spinal muscular atrophy (SMA) is a neurodegenerative disease characterized by the loss of α -motor neurons in the ventral horn of the spinal cord. Depending on the severity, the clinical spectrum of SMA ranges from early infant death to normal adult life with only mild muscle weakness. To date, no cure is available. SMA is caused by the homozygous loss of the *survival motor neuron gene 1* (*SMN1*). Besides *SMN1*, another nearly identical copy of the gene is present in the human genome, thus called *SMN2*. In the *SMN2* gene, a C to T transition in exon 7 leads to the disruption of an exonic splicing enhancer, resulting in alternative splicing of *SMN2* pre-mRNA and skipping of exon 7 in 90 % of total transcript. However, about 10 % of full length (FL) transcripts are still being produced by *SMN2*. Through gene duplication events, *SMN2* is present in varying copy numbers in the human population, ranging from the total absence to a maximum of 4 *SMN2* copies per allele. Since every copy produces about 10 % FL transcript, SMA severity is inversely correlated with *SMN2* copy number.

For a long time, *SMN2* was the only known modifying gene and has therefore been target for the development of therapeutic strategies. The observation of *SMN1*-deleted patients with either extremely weakened or even absent symptoms in the presence of only a small number of *SMN2* copies has in the past been associated with the existence of SMA-modifying genes. Finally, in 2008 the Actin-bundling protein Plastin 3 (*PLS3*) has been identified as a protective modifying gene showing high expression in asymptomatic homozygously *SMN1*-deleted siblings of discordant SMA families in our group (Oprea et al., 2008). Cell culture as well as *in vivo* experiments in a zebrafish SMA model revealed that *PLS3* overexpression rescues the axonal outgrowth phenotype.

The goal of the present study was to address the question whether *PLS3* overexpression is able to rescue the phenotype in an existing SMA mouse model. Furthermore, it was asked which effect *PLS3* overexpression has on the development of neuromuscular junctions (NMJ) as well as muscle development and function.

Using the *Cre/loxP* system, transgenic mice were generated expressing a V5-tagged version of human *PLS3* (*PLS3V5*) either ubiquitously or motor neuron specifically (*Hb9* promoter). In a next step, *PLS3V5* transgenic mice were crossed onto the SMA background using the Hung mouse model. All mice were crossed congenic onto clean C57BL/6N background to exclude any background modifying effects. Transgenic *PLS3V5* mice on wildtype (wt) as well as on SMA background were histologically (Motor neurons, NMJs, muscle) and functionally (Motoric tests, weight, survival) analyzed in detail.

Ubiquitous as well as motor neuron specific *PLS3V5* expression was proven by qRT-PCR, Western blot analysis and immunohistochemistry. *PLS3V5* transgenic mice on wt as well as on SMA background showed remarkable influence of *PLS3* overexpression on motor neuron

and NMJ phenotype: The motor neuron and Acetylcholine receptor (AChR) cluster size was highly increased as compared to wt or SMA littermates. Time course measurements of presynaptic sprouting during the process of axonal pruning revealed highly improved axonal connectivity. These findings raised the question whether the increase of AChR cluster size in transgenic animals is an effect of pre- or postsynaptic *PLS3V5* overexpression. To address this issue, motor neuron specific *PLS3V5* overexpression was analyzed in wt mice. Strikingly, motor neuron specific overexpression of *PLS3V5* was sufficient to increase AChR cluster and muscle fiber size, further strengthening the positive impact of neuronal *PLS3V5* expression on neurotransmission. Moreover, electrophysiological analyzes (NMJ quantal content measurements, Motor Unit Number Estimate (MUNE)) will be performed in the future and correlated with the recent findings.

Despite this positive impact on axon biology, *PLS3* overexpression neither increased survival nor improved motoric ability in the severe type I-like SMA mouse model used in this study. Therefore, it was hypothesized that a certain amount of SMN is required – similar to asymptomatic humans, who own at least 3 *SMN2* copies – to rescue the SMA phenotype. To test this hypothesis, the *PLS3V5* transgene is currently crossed onto a milder SMA background. Additionally, *PLS3V5* was up to now only heterozygously overexpressed in SMA mice. Since also higher *PLS3V5* levels might be necessary to finally improve SMA symptoms, *PLS3V5* will be homozygously expressed in the SMA background in the future.

8 Zusammenfassung

Die spinale Muskelatrophie (SMA) ist eine neurodegenerative Erkrankung und kennzeichnet sich durch den Verlust der α -Motoneurone in den ventralen Hörnern des Rückenmarks aus. Abhängig vom Schweregrad der SMA, für die es derzeit noch keine Heilmethode gibt, reicht das klinische Erscheinungsbild vom frühkindlichen Tod bis zu einer normalen Lebenserwartung in Begleitung einer milden Form der Muskelschwäche. SMA wird durch den homozygoten Verlust des *survival motor neuron* Gens 1 (*SMN1*) verursacht. Neben *SMN1* existiert beim Menschen noch ein weiteres, sehr ähnliches Gen: *SMN2*. Das *SMN2* Gen besitzt eine C zu T Nukleotidtransition in Exon 7. Durch die Transition wird ein exonischer Spleißverstärker (*engl. exonic splicing enhancer* (ESE)) in seiner Sequenz verändert, was zu alternativem Spleißen der *SMN2* prä-mRNA und Verlust von Exon 7 in 90 % der Gesamttranskriptmenge führt. Dennoch produziert auch *SMN2* noch rund 10 % Vollängetranskripte. Durch Genkonversion bedingt, kommt *SMN2* in der menschlichen Population in unterschiedlicher Kopienzahl vor, wobei die Anzahl zwischen null und maximal vier Kopien pro Allel schwanken kann. Da von *SMN2* noch rund 10 % Vollängetranskripte gebildet werden, korreliert der Schweregrad der Erkrankung invers mit der Anzahl vorhandener *SMN2* Kopien.

Eine lange Zeit war *SMN2* das einzige bekannte SMA-modifizierende Gen und daher Ziel zahlreicher Therapieansätze. Interessanterweise jedoch wurden in der Vergangenheit immer wieder *SMN1*-deletierte Patienten beschrieben, die trotz geringer *SMN2* Kopienzahl eine nur sehr schwache bis gar nicht ausgeprägte Symptomatik zeigen. Diese Beobachtungen wurden auf das Vorhandensein anderer modifizierender Faktoren in nichtbetroffenen Patienten solcher sogenannten diskordanten Familien zurückgeführt. Im Jahr 2008 wurde in unserer Arbeitsgruppe schließlich das Aktinfilament bündelnde Protein *Plastin 3* (*PLS3*) als stark hochreguliert und vor SMA schützend in asymptotischen *SMN1* homozygot deletierten Geschwistern diskordanter Familien identifiziert (Oprea et al., 2008). An neuronalen Zellkulturen und in einem Zabrafish-SMA Modell wurde gezeigt, dass *PLS3*-Überexpression Defekte im axonalen Auswachsen kompensieren kann.

Im Sinne eines klassischen Rettungsexperiments war das Ziel der hier vorgelegten Arbeit die Untersuchung der Frage, ob die *PLS3*-Überexpression zu deutlicher Verbesserung der SMA-Symptomatik in einem bestehenden SMA-Mausmodell (Hung SMA Mäuse) führt. Weiterhin wurde untersucht, welchen Einfluss die *PLS3*-Überexpression auf die Entwicklung der neuromuskulären Endplatte (NME) sowie der Muskulatur und deren Funktion hat.

Zur Beantwortung dieser Fragen wurden im Rahmen dieser Arbeit unter Zuhilfenahme des *Cre/loxP* Systems transgene Mäuse hergestellt, die eine *V5*-markierte Version des humanen *PLS3* entweder Motoneuronen-spezifisch (*Hb9* Promotor), oder ubiquitär exprimieren. Im nächsten Schritt wurde das *PLS3V5*-Transgen dann auf den SMA-

Hintergrund des Hung Mausmodells gekreuzt. Um modifizierende Einflüsse des genetischen Hintergrunds auszuschließen, wurden alle Mäuse durch Rückkreuzung über mindestens 7 Generationen auf einen reinen C57BL/6N-Hintergrund gebracht. Transgene *PLS3V5*-Mäuse auf wt und SMA Hintergrund wurden dann histologisch (Motoneuronen, NME, Muskel) und funktional (Motorische Tests, Gewichtsmessung, Überlebensdauer) detailliert analysiert.

Zunächst wurde die Motoneuronen-spezifische sowie ubiquitäre *PLS3V5*-Expression mittels quantitativer reverser Transkription (qRT) PCR, Western blot Analyse sowie Immunohistochemie bestätigt. Bei der anschließenden Untersuchung *PLS3V5* transgener Mäuse auf wt und SMA Hintergrund wurde ein signifikanter Einfluss der *PLS3* Überexpression auf den Motoneuronen und NME Phänotyp festgestellt: Im Vergleich zu wt oder SMA Kontrolltieren waren Motoneurone und Acetylcholinrezeptoren (AChR) Cluster stark vergrößert. Die Untersuchung präsynaptischer Verästelungen zu unterschiedlichen Zeitpunkten während der axonalen Spezifizierung ergab eine stark verbesserte axonale Verknüpfung in *PLS3V5* exprimierenden Tieren. Diese Ergebnisse ließen die Frage aufkommen, ob die beobachtete Vergrößerung der AChR Cluster auf prä- oder postsynaptische Effekte der *PLS3V5* Expression zurückzuführen sei. Um diese Frage zu beantworten, wurde *PLS3V5* im folgenden motoneuronenspezifisch im wt Hintergrund überexprimiert und die AChR Cluster Größe bestimmt. Dabei konnte festgestellt werden, dass die motoneuronenspezifische Überexpression von *PLS3V5* ausreichend für die Vergrößerung der AChR Cluster ist. Darüber hinaus konnte in solchen Tieren sogar eine signifikante Zunahme des Muskelfibrillen-Durchmessers festgestellt werden. Diese Beobachtungen scheinen einen positiven Effekt der *PLS3V5*-Überexpression auf die neuronale Weiterleitung zu bestätigen. Dennoch müssen weitere elektrophysiologische Untersuchungen (z.B. Bestimmung des „quantal content“, *Motor Unit Number Estimate* (MUNE)) durchgeführt werden, um ein detaillierteres Bild der Auswirkungen einer *PLS3V5*-Überexpression auf die Reizweiterleitung zu gewinnen.

Trotz der genannten positiven Effekte auf die axonale Entwicklung konnte in *PLS3V5* exprimierenden SMA Tieren weder eine verlängerte Lebenszeit, noch eine verbesserte Motorik beobachtet werden. Darum wurde die Hypothese aufgestellt, dass *PLS3V5* möglicherweise nur in Gegenwart einer gewissen SMN Menge den SMA-Phänotyp verbessern oder retten kann, ähnlich der Situation in asymptomatischen Menschen, die immer mindestens 3 *SMN2* Kopien trugen. Um diese Hypothese zu überprüfen, wird das *PLS3V5*-Transgen derzeit bereits auf einen milderen SMA-Hintergrund gebracht. Außer einer nicht ausreichenden SMN Menge könnte auch eine zu niedrige *PLS3V5*-Konzentration für das Ausbleiben von krankheitsverbessernden Effekten sein. Da in allen bisherigen Versuchen *PLS3V5* lediglich heterozygot überexprimiert wurde, werden aktuell

Verpaarungen zur homozygoten Überexpression von *PLS3V5* auf dem SMA Hintergrund durchgeführt.

9 Publications, presentations, posters and awards

Original publications:

Ackermann B., Nölle A.

Conference report of the “14th Spinal Muscular Atrophy Research meeting”, Santa Clara, USA, 2010

Website: <http://www.initiative-sma.de>

Direct link: <http://www.initiative-sma.de/menu/menu.php?id=5&choice=1&archiv=0&aid=204>

Riessland M, **Ackermann B.**, Förster A, Jakubik M, Hauke I, Garbes L, Fritzsche I, Mende Y, Blumcke I, Hahnen E, Wirth B, 2010

SAHA ameliorates the SMA phenotype in two mouse models for spinal muscular atrophy
Hum Mol Genet.

Sieger, D., **Ackermann B.**, Winkler C., Tautz D., Gajewski M., 2006

her1 and *her13.2* are jointly required for somitic border specification along the entire axis of the fish embryo

Dev. Biol. 293, 242-251

Oral Presentations:

21.06. – 26.06.2011

15th Spinal Muscular Atrophy Research meeting, Orlando, Florida, USA

Titel: *PLS3 overexpression rescues synaptic defects in a mouse model of Spinal Muscular Atrophy*

13.05.2011

Annual Human Genetics meeting, Universität zu Köln, Cologne, Germany

Titel: *PLS3 overexpression rescues synaptic defects in a mouse model of Spinal Muscular Atrophy*

28.05.2010

23rd Meeting of Medical Genetics, Bologna, Italy

Titel: *PLS3 – a modifying factor of Spinal Muscular Atrophy*

Poster presentations

24.06. – 26.06.2010

14th Spinal Muscular Atrophy Research Group meeting”, Santa Clara, California, USA

Titel: *PLS3 overexpression in the mouse increases Motoneuron- and Neuromuscular junction size*

B.Ackermann, S. Kröber, B.Wirth

09.10.2009

Annual Human Genetics meeting, Universität zu Köln, Cologne, Germany

Titel: *Characterization and Identification of Modifying Factors of Spinal Muscular Atrophy*

B.Ackermann, S. Kröber, M. Riessland, A. Förster, B.Wirth

10.09. – 14.09.2008

Axon guidance, Synaptogenesis & Neural Plasticity meeting”, New York / USA

Titel: *Overexpression study of human T-Plastin (PLS3) to rescue the mouse SMA phenotype*

B.Ackermann, S. Kröber, M. Riessland, A. Förster, B.Wirth

21.02.2008

Annual Human Genetics meeting, Universität zu Köln, Cologne, Germany

Titel: *Overexpression study of human T-Plastin (PLS3) to rescue the mouse SMA phenotype*

B.Ackermann, G. Oprea, B. Wirth

12.07 – 15.07.2007

5th European Zebrafish Genetics and Development meeting”, Amsterdam / Niederlande

Titel: *The role of E-Cadherin in the Danio rerio thyroid developmental process*

B.Ackermann, B. Alt, K. Rohr

13.07 – 16.07.2005

4th European Zebrafish Genetics and Development meeting, Dresden, Germany

Titel: *Analysis of the function of Ol-her1/11 und Ol-her13/2 during the somitogenesis process in Medaka (Oryzias latipes)*

B.Ackermann, Dirk Sieger, Martin Gajewski

Awards

June 2011:

Travel grant for the Families of SMA families (FSMA) conference in Orlando, Florida, USA, permitted by Families of SMA (FSMA), USA

June 2010

Travel grant for the Families of SMA families (FSMA) conference in Santa Clara, California, permitted by Initiative SMA and Förderverein für die Deutsche Gesellschaft für Muskelkranke e.V.

May 2010

„Best Poster Award“, 23rd Meeting of Medical Genetics”, Bologna, Italy

10 References

- Aberle H, Haghighi AP, Fetter RD, McCabe BD, Magalhaes TR, Goodman CS (wishful thinking encodes a BMP type II receptor that regulates synaptic growth in *Drosophila*. *Neuron* 33:545-558.2002).
- Abicht A, Lochmuller H (Congenital Myasthenic Syndromes.1993).
- Adam T, Arpin M, Prevost MC, Gounon P, Sansonetti PJ (Cytoskeletal rearrangements and the functional role of T-plastin during entry of *Shigella flexneri* into HeLa cells. *J Cell Biol* 129:367-381.1995).
- Alias L, Bernal S, Fuentes-Prior P, Barcelo MJ, Also E, Martinez-Hernandez R, Rodriguez-Alvarez FJ, Martin Y, Aller E, Grau E, Pecina A, Antinolo G, Galan E, Rosa AL, Fernandez-Burriel M, Borrego S, Millan JM, Hernandez-Chico C, Baiget M, Tizzano EF (Mutation update of spinal muscular atrophy in Spain: molecular characterization of 745 unrelated patients and identification of four novel mutations in the SMN1 gene. *Hum Genet* 125:29-39.2009).
- Amalnath DS, Subrahmanyam DK, Sridhar S, Dutta TK (Escobar syndrome in three male patients of same family. *Indian J Hum Genet* 17:22-25.2011).
- Anderton RS, Meloni BP, Mastaglia FL, Greene WK, Boulos S (Survival of motor neuron protein over-expression prevents calpain-mediated cleavage and activation of procaspase-3 in differentiated human SH-SY5Y cells. *Neuroscience* 181:226-233.2011).
- Andreassi C, Angelozzi C, Tiziano FD, Vitali T, De Vincenzi E, Boninsegna A, Villanova M, Bertini E, Pini A, Neri G, Brahe C (Phenylbutyrate increases SMN expression in vitro: relevance for treatment of spinal muscular atrophy. *Eur J Hum Genet* 12:59-65.2004).
- Angelini C (Diagnosis and management of autoimmune myasthenia gravis. *Clin Drug Investig* 31:1-14.2011).
- Antonarakis SE, Beckmann JS (Mendelian disorders deserve more attention. *Nat Rev Genet* 7:277-282.2006).
- Arai H, Tanabe Y, Hachiya Y, Otsuka E, Kumada S, Furushima W, Kohyama J, Yamashita S, Takanashi J, Kohno Y (Finger cold-induced vasodilatation, sympathetic skin response, and R-R interval variation in patients with progressive spinal muscular atrophy. *J Child Neurol* 20:871-875.2005).
- Araujo Ade Q, Araujo M, Swoboda KJ (Vascular perfusion abnormalities in infants with spinal muscular atrophy. *J Pediatr* 155:292-294.2009).
- Arber S, Han B, Mendelsohn M, Smith M, Jessell TM, Sockanathan S (Requirement for the homeobox gene Hb9 in the consolidation of motor neuron identity. *Neuron* 23:659-674.1999).
- Arce V, Garces A, de Bovis B, Filippi P, Henderson C, Pettmann B, deLapeyriere O (Cardiotrophin-1 requires LIFRbeta to promote survival of mouse motoneurons purified by a novel technique. *J Neurosci Res* 55:119-126.1999).
- Argov Z (Management of myasthenic conditions: nonimmune issues. *Curr Opin Neurol* 22:493-497.2009).
- Arnold AS, Gueye M, Guettier-Sigrist S, Courdier-Fruh I, Coupin G, Poindron P, Gies JP (Reduced expression of nicotinic AChRs in myotubes from spinal muscular atrophy I patients. *Lab Invest* 84:1271-1278.2004).
- Arpin M, Friederich E, Algrain M, Vernel F, Louvard D (Functional differences between L- and T-plastin isoforms. *J Cell Biol* 127:1995-2008.1994).
- Astro V, Asperti C, Cangini MG, Doglioni C, de Curtis I (Liprin-alpha1 regulates breast cancer cell invasion by affecting cell motility, invadopodia and extracellular matrix degradation. *Oncogene* 30:1841-1849.2011).

- Avila AM, Burnett BG, Taye AA, Gabanella F, Knight MA, Hartenstein P, Cizman Z, Di Prospero NA, Pellizzoni L, Fischbeck KH, Sumner CJ (Trichostatin A increases SMN expression and survival in a mouse model of spinal muscular atrophy. *J Clin Invest* 117:659-671.2007).
- Baas PW (Microtubule transport in the axon. *Int Rev Cytol* 212:41-62.2002).
- Bach JR (Medical considerations of long-term survival of Werdnig-Hoffmann disease. *Am J Phys Med Rehabil* 86:349-355.2007).
- Barisic N, Chaouch A, Muller JS, Lochmuller H (Genetic heterogeneity and pathophysiological mechanisms in congenital myasthenic syndromes. *Eur J Paediatr Neurol* 15:189-196.2011).
- Barisic N, Muller JS, Paucic-Kirincic E, Gazdik M, Lah-Tomulic K, Pertl A, Sertic J, Zurak N, Lochmuller H, Abicht A (Clinical variability of CMS-EA (congenital myasthenic syndrome with episodic apnea) due to identical CHAT mutations in two infants. *Eur J Paediatr Neurol* 9:7-12.2005).
- Baumer D, Lee S, Nicholson G, Davies JL, Parkinson NJ, Murray LM, Gillingwater TH, Ansorge O, Davies KE, Talbot K (Alternative splicing events are a late feature of pathology in a mouse model of spinal muscular atrophy. *PLoS Genet* 5:e1000773.2009).
- Bebee TW, Gladman JT, Chandler DS (Generation of a tamoxifen inducible SMN mouse for temporal SMN replacement. *Genesis*.2011).
- Bechade C, Rostaing P, Cisterni C, Kalisch R, La Bella V, Pettmann B, Triller A (Subcellular distribution of survival motor neuron (SMN) protein: possible involvement in nucleocytoplasmic and dendritic transport. *Eur J Neurosci* 11:293-304.1999).
- Beeson D, Hantai D, Lochmuller H, Engel AG (126th International Workshop: congenital myasthenic syndromes, 24-26 September 2004, Naarden, the Netherlands. *Neuromuscul Disord* 15:498-512.2005).
- Beeson D, Higuchi O, Palace J, Cossins J, Spearman H, Maxwell S, Newsom-Davis J, Burke G, Fawcett P, Motomura M, Muller JS, Lochmuller H, Slater C, Vincent A, Yamanashi Y (Dok-7 mutations underlie a neuromuscular junction synaptopathy. *Science* 313:1975-1978.2006).
- Belgardt BF, Husch A, Rother E, Ernst MB, Wunderlich FT, Hampel B, Klockener T, Alessi D, Kloppenburg P, Bruning JC (PKD1 deficiency in POMC-expressing cells reveals FOXO1-dependent and -independent pathways in control of energy homeostasis and stress response. *Cell Metab* 7:291-301.2008).
- Belmont LD, Drubin DG (The yeast V159N actin mutant reveals roles for actin dynamics in vivo. *J Cell Biol* 142:1289-1299.1998).
- Bentley D, Toroian-Raymond A (Disoriented pathfinding by pioneer neurone growth cones deprived of filopodia by cytochalasin treatment. *Nature* 323:712-715.1986).
- Bernal S, Also-Rallo E, Martinez-Hernandez R, Alias L, Rodriguez-Alvarez FJ, Millan JM, Hernandez-Chico C, Baiget M, Tizzano EF (Plastin 3 expression in discordant spinal muscular atrophy (SMA) siblings. *Neuromuscul Disord* 21:413-419.2011).
- Bertrand S, Bulet P, Clermont O, Huber C, Fondrat C, Thierry-Mieg D, Munnich A, Lefebvre S (The RNA-binding properties of SMN: deletion analysis of the zebrafish orthologue defines domains conserved in evolution. *Hum Mol Genet* 8:775-782.1999).
- Bevan AK, Hutchinson KR, Foust KD, Braun L, McGovern VL, Schmelzer L, Ward JG, Petruska JC, Lucchesi PA, Burghes AH, Kaspar BK (Early heart failure in

- the SMN Δ 7 model of spinal muscular atrophy and correction by postnatal scAAV9-SMN delivery. *Hum Mol Genet* 19:3895-3905.2010).
- Bezakova G, Helm JP, Francolini M, Lomo T (Effects of purified recombinant neural and muscle agrin on skeletal muscle fibers in vivo. *J Cell Biol* 153:1441-1452.2001).
- Bishop DL, Misgeld T, Walsh MK, Gan WB, Lichtman JW (Axon branch removal at developing synapses by axosome shedding. *Neuron* 44:651-661.2004).
- Bloch RJ, Hall ZW (Cytoskeletal components of the vertebrate neuromuscular junction: vinculin, alpha-actinin, and filamin. *J Cell Biol* 97:217-223.1983).
- Bloom O, Evergren E, Tomilin N, Kjaerulff O, Low P, Brodin L, Pieribone VA, Greengard P, Shupliakov O (Colocalization of synapsin and actin during synaptic vesicle recycling. *J Cell Biol* 161:737-747.2003).
- Bowerman M, Anderson CL, Beauvais A, Boyl PP, Witke W, Kothary R (SMN, profilin IIa and plastin 3: a link between the deregulation of actin dynamics and SMA pathogenesis. *Mol Cell Neurosci* 42:66-74.2009).
- Bowerman M, Beauvais A, Anderson CL, Kothary R (Rho-kinase inactivation prolongs survival of an intermediate SMA mouse model. *Hum Mol Genet* 19:1468-1478.2010).
- Bowerman M, Shafey D, Kothary R (Smn depletion alters profilin II expression and leads to upregulation of the RhoA/ROCK pathway and defects in neuronal integrity. *J Mol Neurosci* 32:120-131.2007).
- Bradford MM (A rapid and sensitive method for the quantitation of microgram quantities of protein utilizing the principle of protein-dye binding. *Anal Biochem* 72:248-254.1976).
- Bradke F, Dotti CG (The role of local actin instability in axon formation. *Science* 283:1931-1934.1999).
- Bradley A, Evans M, Kaufman MH, Robertson E (Formation of germ-line chimaeras from embryo-derived teratocarcinoma cell lines. *Nature* 309:255-256.1984).
- Bradley WG, Taylor R, Rice DR, Hausmanowa-Petruzewicz I, Adelman LS, Jenkinson M, Jedrzejowska H, Drac H, Pendlebury WW (Progressive myopathy in hyperkalemic periodic paralysis. *Arch Neurol* 47:1013-1017.1990).
- Brahe C (Copies of the survival motor neuron gene in spinal muscular atrophy: the more, the better. *Neuromuscul Disord* 10:274-275.2000).
- Brahe C, Servidei S, Zappata S, Ricci E, Tonali P, Neri G (Genetic homogeneity between childhood-onset and adult-onset autosomal recessive spinal muscular atrophy. *Lancet* 346:741-742.1995).
- Brahe C, Vitali T, Tiziano FD, Angelozzi C, Pinto AM, Borgo F, Moscato U, Bertini E, Mercuri E, Neri G (Phenylbutyrate increases SMN gene expression in spinal muscular atrophy patients. *Eur J Hum Genet* 13:256-259.2005).
- Brandon EP, Lin W, D'Amour KA, Pizzo DP, Dominguez B, Sugiura Y, Thode S, Ko CP, Thal LJ, Gage FH, Lee KF (Aberrant patterning of neuromuscular synapses in choline acetyltransferase-deficient mice. *J Neurosci* 23:539-549.2003).
- Braun S, Croizat B, Lagrange MC, Warter JM, Poindron P (Constitutive muscular abnormalities in culture in spinal muscular atrophy. *Lancet* 345:694-695.1995).
- Bretscher A (Fimbrin is a cytoskeletal protein that crosslinks F-actin in vitro. *Proc Natl Acad Sci U S A* 78:6849-6853.1981).
- Bretscher A, Weber K (Fimbrin, a new microfilament-associated protein present in microvilli and other cell surface structures. *J Cell Biol* 86:335-340.1980).
- Brichta L, Hofmann Y, Hahnen E, Siebzehnrubl FA, Raschke H, Blumcke I, Eyupoglu IY, Wirth B (Valproic acid increases the SMN2 protein level: a well-known drug

- as a potential therapy for spinal muscular atrophy. *Hum Mol Genet* 12:2481-2489.2003).
- Brichta L, Holker I, Haug K, Klockgether T, Wirth B (In vivo activation of SMN in spinal muscular atrophy carriers and patients treated with valproate. *Ann Neurol* 59:970-975.2006).
- Briese M, Esmaili B, Fraboulet S, Burt EC, Christodoulou S, Towers PR, Davies KE, Sattelle DB (Deletion of *smn-1*, the *Caenorhabditis elegans* ortholog of the spinal muscular atrophy gene, results in locomotor dysfunction and reduced lifespan. *Hum Mol Genet* 18:97-104.2009).
- Briese M, Esmaili B, Sattelle DB (Is spinal muscular atrophy the result of defects in motor neuron processes? *Bioessays* 27:946-957.2005).
- Brzustowicz LM, Lehner T, Castilla LH, Penchaszadeh GK, Wilhelmsen KC, Daniels R, Davies KE, Leppert M, Ziter F, Wood D, et al. (Genetic mapping of chronic childhood-onset spinal muscular atrophy to chromosome 5q11.2-13.3. *Nature* 344:540-541.1990).
- Bulman DE, Scoggan KA, van Oene MD, Nicolle MW, Hahn AF, Tollar LL, Ebers GC (A novel sodium channel mutation in a family with hypokalemic periodic paralysis. *Neurology* 53:1932-1936.1999).
- Burghes AH (When is a deletion not a deletion? When it is converted. *Am J Hum Genet* 61:9-15.1997).
- Burghes AH, Beattie CE (Spinal muscular atrophy: why do low levels of survival motor neuron protein make motor neurons sick? *Nat Rev Neurosci* 10:597-609.2009).
- Burglen L, Lefebvre S, Clermont O, Burlet P, Viollet L, Cruaud C, Munnich A, Melki J (Structure and organization of the human survival motor neurone (SMN) gene. *Genomics* 32:479-482.1996).
- Burlet P, Huber C, Bertrand S, Ludosky MA, Zwaenepoel I, Clermont O, Roume J, Delezoide AL, Cartaud J, Munnich A, Lefebvre S (The distribution of SMN protein complex in human fetal tissues and its alteration in spinal muscular atrophy. *Hum Mol Genet* 7:1927-1933.1998).
- Campagna JA, Fallon J (Lipid rafts are involved in C95 (4,8) agrin fragment-induced acetylcholine receptor clustering. *Neuroscience* 138:123-132.2006).
- Cano ML, Cassimeris L, Fechheimer M, Zigmond SH (Mechanisms responsible for F-actin stabilization after lysis of polymorphonuclear leukocytes. *J Cell Biol* 116:1123-1134.1992).
- Capriotti E, Vonderheid EC, Thoburn CJ, Wasik MA, Bahler DW, Hess AD (Expression of T-plastin, FoxP3 and other tumor-associated markers by leukemic T-cells of cutaneous T-cell lymphoma. *Leuk Lymphoma* 49:1190-1201.2008).
- Carissimi C, Saieva L, Baccon J, Chiarella P, Maiolica A, Sawyer A, Rappsilber J, Pellizzoni L (Gemin8 is a novel component of the survival motor neuron complex and functions in small nuclear ribonucleoprotein assembly. *J Biol Chem* 281:8126-8134.2006).
- Carrel TL, McWhorter ML, Workman E, Zhang H, Wolstencroft EC, Lorson C, Bassell GJ, Burghes AH, Beattie CE (Survival motor neuron function in motor axons is independent of functions required for small nuclear ribonucleoprotein biogenesis. *J Neurosci* 26:11014-11022.2006).
- Cartaud A, Stetzkowski-Marden F, Maoui A, Cartaud J (Agrin triggers the clustering of raft-associated acetylcholine receptors through actin-cytoskeleton reorganization. *Biol Cell*.2011).

- Cartegni L, Krainer AR (Disruption of an SF2/ASF-dependent exonic splicing enhancer in SMN2 causes spinal muscular atrophy in the absence of SMN1. *Nat Genet* 30:377-384.2002).
- Cartegni L, Krainer AR (Correction of disease-associated exon skipping by synthetic exon-specific activators. *Nat Struct Biol* 10:120-125.2003).
- Carvalho T, Almeida F, Calapez A, Lafarga M, Berciano MT, Carmo-Fonseca M (The spinal muscular atrophy disease gene product, SMN: A link between snRNP biogenesis and the Cajal (coiled) body. *J Cell Biol* 147:715-728.1999).
- Chan YB, Miguel-Aliaga I, Franks C, Thomas N, Trulzsch B, Sattelle DB, Davies KE, van den Heuvel M (Neuromuscular defects in a Drosophila survival motor neuron gene mutant. *Hum Mol Genet* 12:1367-1376.2003).
- Chang HC, Dimlich DN, Yokokura T, Mukherjee A, Kankel MW, Sen A, Sridhar V, Fulga TA, Hart AC, Van Vactor D, Artavanis-Tsakonas S (Modeling spinal muscular atrophy in Drosophila. *PLoS One* 3:e3209.2008).
- Chang HC, Hung WC, Chuang YJ, Jong YJ (Degradation of survival motor neuron (SMN) protein is mediated via the ubiquitin/proteasome pathway. *Neurochem Int* 45:1107-1112.2004).
- Chang JG, Hsieh-Li HM, Jong YJ, Wang NM, Tsai CH, Li H (Treatment of spinal muscular atrophy by sodium butyrate. *Proc Natl Acad Sci U S A* 98:9808-9813.2001).
- Chari A, Paknia E, Fischer U (The role of RNP biogenesis in spinal muscular atrophy. *Curr Opin Cell Biol* 21:387-393.2009).
- Chevessier F, Faraut B, Ravel-Chapuis A, Richard P, Gaudon K, Bauche S, Prioleau C, Herbst R, Goillot E, loos C, Azulay JP, Attarian S, Leroy JP, Fournier E, Legay C, Schaeffer L, Koenig J, Fardeau M, Eymard B, Pouget J, Hantai D (MUSK, a new target for mutations causing congenital myasthenic syndrome. *Hum Mol Genet* 13:3229-3240.2004).
- Cifuentes-Diaz C, Nicole S, Velasco ME, Borra-Cebrian C, Panozzo C, Frugier T, Millet G, Roblot N, Joshi V, Melki J (Neurofilament accumulation at the motor endplate and lack of axonal sprouting in a spinal muscular atrophy mouse model. *Hum Mol Genet* 11:1439-1447.2002).
- Cobben JM, Lemmink HH, Snoeck I, Barth PA, van der Lee JH, de Visser M (Survival in SMA type I: a prospective analysis of 34 consecutive cases. *Neuromuscul Disord* 18:541-544.2008).
- Cobben JM, van der Steege G, Grootsholten P, de Visser M, Scheffer H, Buys CH (Deletions of the survival motor neuron gene in unaffected siblings of patients with spinal muscular atrophy. *Am J Hum Genet* 57:805-808.1995).
- Cohan CS, Weinhofer EA, Zhao L, Matsumura F, Yamashiro S (Role of the actin bundling protein fascin in growth cone morphogenesis: localization in filopodia and lamellipodia. *Cell Motil Cytoskeleton* 48:109-120.2001).
- Corti S, Nizzardo M, Nardini M, Donadoni C, Salani S, Ronchi D, Simone C, Falcone M, Papadimitriou D, Locatelli F, Mezzina N, Gianni F, Bresolin N, Comi GP (Embryonic stem cell-derived neural stem cells improve spinal muscular atrophy phenotype in mice. *Brain* 133:465-481.2010).
- Costantini F, Lacy E (Introduction of a rabbit beta-globin gene into the mouse germ line. *Nature* 294:92-94.1981).
- Cramer LP (Role of actin-filament disassembly in lamellipodium protrusion in motile cells revealed using the drug jasplakinolide. *Curr Biol* 9:1095-1105.1999).
- Croxen R, Vincent A, Newsom-Davis J, Beeson D (Myasthenia gravis in a woman with congenital AChR deficiency due to epsilon-subunit mutations. *Neurology* 58:1563-1565.2002).

- Cutting GR (Modifier genes in Mendelian disorders: the example of cystic fibrosis. *Ann N Y Acad Sci* 1214:57-69.2010).
- Czeizel A, Hamula J (A Hungarian study on Werdnig-Hoffmann disease. *J Med Genet* 26:761-763.1989).
- D'Angelo MG, Bresolin N (Cognitive impairment in neuromuscular disorders. *Muscle Nerve* 34:16-33.2006).
- Da Silva JS, Hasegawa T, Miyagi T, Dotti CG, Abad-Rodriguez J (Asymmetric membrane ganglioside sialidase activity specifies axonal fate. *Nat Neurosci* 8:606-615.2005).
- Da Silva JS, Medina M, Zuliani C, Di Nardo A, Witke W, Dotti CG (RhoA/ROCK regulation of neuritogenesis via profilin IIa-mediated control of actin stability. *J Cell Biol* 162:1267-1279.2003).
- Dachs E, Hereu M, Piedrafita L, Casanovas A, Caldero J, Esquerda JE (Defective neuromuscular junction organization and postnatal myogenesis in mice with severe spinal muscular atrophy. *J Neuropathol Exp Neurol* 70:444-461.2011).
- Dai Z, Luo X, Xie H, Peng HB (The actin-driven movement and formation of acetylcholine receptor clusters. *J Cell Biol* 150:1321-1334.2000).
- Darzacq X, Jady BE, Verheggen C, Kiss AM, Bertrand E, Kiss T (Cajal body-specific small nuclear RNAs: a novel class of 2'-O-methylation and pseudouridylation guide RNAs. *Embo J* 21:2746-2756.2002).
- Daudet N, Lebart MC (Transient expression of the t-isoform of plastins/fimbrin in the stereocilia of developing auditory hair cells. *Cell Motil Cytoskeleton* 53:326-336.2002).
- de Arruda MV, Watson S, Lin CS, Leavitt J, Matsudaira P (Fimbrin is a homologue of the cytoplasmic phosphoprotein plastin and has domains homologous with calmodulin and actin gelation proteins. *J Cell Biol* 111:1069-1079.1990).
- De Mendonca Neto EC, Kumar A, Shadick NA, Michon AM, Matsudaira P, Eaton RB, Kumar P, Schur PH (Antibodies to T- and L-isoforms of the cytoskeletal protein, fimbrin, in patients with systemic lupus erythematosus. *J Clin Invest* 90:1037-1042.1992).
- DeChiara TM, Bowen DC, Valenzuela DM, Simmons MV, Poueymirou WT, Thomas S, Kinetz E, Compton DL, Rojas E, Park JS, Smith C, DiStefano PS, Glass DJ, Burden SJ, Yancopoulos GD (The receptor tyrosine kinase MuSK is required for neuromuscular junction formation in vivo. *Cell* 85:501-512.1996).
- Delanote V, Vandekerckhove J, Gettemans J (Plastins: versatile modulators of actin organization in (patho)physiological cellular processes. *Acta Pharmacol Sin* 26:769-779.2005).
- Dent EW, Gertler FB (Cytoskeletal dynamics and transport in growth cone motility and axon guidance. *Neuron* 40:209-227.2003).
- Dent EW, Tang F, Kalil K (Axon guidance by growth cones and branches: common cytoskeletal and signaling mechanisms. *Neuroscientist* 9:343-353.2003).
- Dickson A, Osman E, Lorson C (A Negatively-Acting Bifunctional RNA Increases Survival Motor Neuron in vitro and in vivo. *Hum Gene Ther.*2008).
- DiDonato CJ, Chen XN, Noya D, Korenberg JR, Nadeau JH, Simard LR (Cloning, characterization, and copy number of the murine survival motor neuron gene: homolog of the spinal muscular atrophy-determining gene. *Genome Res* 7:339-352.1997).
- Dillon C, Goda Y (The actin cytoskeleton: integrating form and function at the synapse. *Annu Rev Neurosci* 28:25-55.2005).
- Dimitriadi M, Sleight JN, Walker A, Chang HC, Sen A, Kalloo G, Harris J, Barsby T, Walsh MB, Satterlee JS, Li C, Van Vactor D, Artavanis-Tsakonas S, Hart AC

- (Conserved genes act as modifiers of invertebrate SMN loss of function defects. *PLoS Genet* 6:e1001172.2010).
- Dobbins GC, Luo S, Yang Z, Xiong WC, Mei L (alpha-Actinin interacts with rapsyn in agrin-stimulated AChR clustering. *Mol Brain* 1:18.2008).
- Dobbins GC, Zhang B, Xiong WC, Mei L (The role of the cytoskeleton in neuromuscular junction formation. *J Mol Neurosci* 30:115-118.2006).
- Dodds E, Dunckley MG, Roberts RG, Muntoni F, Shaw CE (Overexpressed human survival motor neurone isoforms, SMN Δ exon7 and SMN+exon7, both form intranuclear gems but differ in cytoplasmic distribution. *FEBS Lett* 495:31-38.2001).
- Dominguez E, Marais T, Chatauret N, Benkhalifa-Ziyyat S, Duque S, Ravassard P, Carcenac R, Astord S, de Moura AP, Voit T, Barkats M (Intravenous scAAV9 delivery of a codon-optimized SMN1 sequence rescues SMA mice. *Hum Mol Genet* 20:681-693.2011).
- Donger C, Krejci E, Serradell AP, Eymard B, Bon S, Nicole S, Chateau D, Gary F, Fardeau M, Massoulié J, Guicheney P (Mutation in the human acetylcholinesterase-associated collagen gene, COLQ, is responsible for congenital myasthenic syndrome with end-plate acetylcholinesterase deficiency (Type Ic). *Am J Hum Genet* 63:967-975.1998).
- Ebert AD, Yu J, Rose FF, Jr., Mattis VB, Lorson CL, Thomson JA, Svendsen CN (Induced pluripotent stem cells from a spinal muscular atrophy patient. *Nature* 457:277-280.2009).
- Eggan K, Rode A, Jentsch I, Samuel C, Hennek T, Tintrup H, Zevnik B, Erwin J, Loring J, Jackson-Grusby L, Speicher MR, Kuehn R, Jaenisch R (Male and female mice derived from the same embryonic stem cell clone by tetraploid embryo complementation. *Nat Biotechnol* 20:455-459.2002).
- Eggert C, Chari A, Lagerbauer B, Fischer U (Spinal muscular atrophy: the RNP connection. *Trends Mol Med*.2006).
- El-Khodor BF, Edgar N, Chen A, Winberg ML, Joyce C, Brunner D, Suarez-Farinas M, Heyes MP (Identification of a battery of tests for drug candidate evaluation in the SMN Δ 7 neonate model of spinal muscular atrophy. *Exp Neurol* 212:29-43.2008).
- Emery AE (Population frequencies of inherited neuromuscular diseases--a world survey. *Neuromuscul Disord* 1:19-29.1991).
- Engel AG, Ohno K, Milone M, Wang HL, Nakano S, Bouzat C, Pruitt JN, 2nd, Hutchinson DO, Brengman JM, Bren N, Sieb JP, Sine SM (New mutations in acetylcholine receptor subunit genes reveal heterogeneity in the slow-channel congenital myasthenic syndrome. *Hum Mol Genet* 5:1217-1227.1996).
- Engel AG, Sine SM (Current understanding of congenital myasthenic syndromes. *Curr Opin Pharmacol* 5:308-321.2005).
- Evans MJ, Kaufman MH (Establishment in culture of pluripotential cells from mouse embryos. *Nature* 292:154-156.1981).
- Fallini C, Zhang H, Su Y, Silani V, Singer RH, Rossoll W, Bassell GJ (The survival of motor neuron (SMN) protein interacts with the mRNA-binding protein HuD and regulates localization of poly(A) mRNA in primary motor neuron axons. *J Neurosci* 31:3914-3925.2011).
- Fan L, Simard LR (Survival motor neuron (SMN) protein: role in neurite outgrowth and neuromuscular maturation during neuronal differentiation and development. *Hum Mol Genet* 11:1605-1614.2002).

- Felderhoff-Mueser U, Grohmann K, Harder A, Stadelmann C, Zerres K, Buhner C, Obladen M (Severe spinal muscular atrophy variant associated with congenital bone fractures. *J Child Neurol* 17:718-721.2002).
- Feldkotter M, Schwarzer V, Wirth R, Wienker TF, Wirth B (Quantitative analyses of SMN1 and SMN2 based on real-time lightCycler PCR: fast and highly reliable carrier testing and prediction of severity of spinal muscular atrophy. *Am J Hum Genet* 70:358-368.2002).
- Finsterer J, Stollberger C (Cardiac involvement in Werdnig-Hoffmann's spinal muscular atrophy. *Cardiology* 92:178-182.1999).
- Fischer U, Liu Q, Dreyfuss G (The SMN-SIP1 complex has an essential role in spliceosomal snRNP biogenesis. *Cell* 90:1023-1029.1997).
- Foust KD, Wang X, McGovern VL, Braun L, Bevan AK, Haidet AM, Le TT, Morales PR, Rich MM, Burghes AH, Kaspar BK (Rescue of the spinal muscular atrophy phenotype in a mouse model by early postnatal delivery of SMN. *Nat Biotechnol* 28:271-274.2010).
- Freeman HC, Hugill A, Dear NT, Ashcroft FM, Cox RD (Deletion of nicotinamide nucleotide transhydrogenase: a new quantitative trait locus accounting for glucose intolerance in C57BL/6J mice. *Diabetes* 55:2153-2156.2006).
- Friederich E, Huet C, Arpin M, Louvard D (Villin induces microvilli growth and actin redistribution in transfected fibroblasts. *Cell* 59:461-475.1989).
- Fu AK, Ip FC, Fu WY, Cheung J, Wang JH, Yung WH, Ip NY (Aberrant motor axon projection, acetylcholine receptor clustering, and neurotransmission in cyclin-dependent kinase 5 null mice. *Proc Natl Acad Sci U S A* 102:15224-15229.2005).
- Fuentes JL, Strayer MS, Matera AG (Molecular determinants of survival motor neuron (SMN) protein cleavage by the calcium-activated protease, calpain. *PLoS One* 5:e15769.2010).
- Galkin VE, Orlova A, Cherepanova O, Lebart MC, Egelman EH (High-resolution cryo-EM structure of the F-actin-fimbrin/plastin ABD2 complex. *Proc Natl Acad Sci U S A* 105:1494-1498.2008).
- Gallo G, Yee HF, Jr., Letourneau PC (Actin turnover is required to prevent axon retraction driven by endogenous actomyosin contractility. *J Cell Biol* 158:1219-1228.2002).
- Gamstorp I (Adynamia episodica hereditaria and myotonia. *Acta Neurol Scand* 39:41-58.1963).
- Garbes L, Riessland M, Holker I, Heller R, Hauke J, Trankle C, Coras R, Bluemcke I, Hahnen E, Wirth B (LBH589 induces up to 10-fold SMN protein levels by several independent mechanisms and is effective even in cells from SMA patients non-responsive to valproate. *Human Molecular Genetics* 18:3645-3658.2009).
- Garchon HJ, Djabiri F, Viard JP, Gajdos P, Bach JF (Involvement of human muscle acetylcholine receptor alpha-subunit gene (CHRNA) in susceptibility to myasthenia gravis. *Proc Natl Acad Sci U S A* 91:4668-4672.1994).
- Garrick D, Fiering S, Martin DI, Whitelaw E (Repeat-induced gene silencing in mammals. *Nat Genet* 18:56-59.1998).
- Garvalov BK, Flynn KC, Neukirchen D, Meyn L, Teusch N, Wu X, Brakebusch C, Bamburg JR, Bradke F (Cdc42 regulates cofilin during the establishment of neuronal polarity. *J Neurosci* 27:13117-13129.2007).
- Gaudon K, Penisson-Besnier I, Chabrol B, Bouhour F, Demay L, Ben Ammar A, Bauche S, Vial C, Nicolas G, Eymard B, Hantai D, Richard P (Multiexon

- deletions account for 15% of congenital myasthenic syndromes with RAPSN mutations after negative DNA sequencing. *J Med Genet* 47:795-796.2010).
- Gautam M, Noakes PG, Moscoso L, Rupp F, Scheller RH, Merlie JP, Sanes JR (Defective neuromuscular synaptogenesis in agrin-deficient mutant mice. *Cell* 85:525-535.1996).
- Gavrilina TO, McGovern VL, Workman E, Crawford TO, Gogliotti RG, DiDonato CJ, Monani UR, Morris GE, Burghes AH (Neuronal SMN expression corrects spinal muscular atrophy in severe SMA mice while muscle-specific SMN expression has no phenotypic effect. *Hum Mol Genet* 17:1063-1075.2008).
- Gay S, Dupuis D, Faivre L, Masurel-Paulet A, Labenne M, Colombani M, Soichot P, Huet F, Hainque B, Sternberg D, Fontaine B, Gouyon JB, Thauvin-Robinet C (Severe neonatal non-dystrophic myotonia secondary to a novel mutation of the voltage-gated sodium channel (SCN4A) gene. *Am J Med Genet A* 146:380-383.2008).
- Gesemann M, Denzer AJ, Ruegg MA (Acetylcholine receptor-aggregating activity of agrin isoforms and mapping of the active site. *J Cell Biol* 128:625-636.1995).
- Giganti A, Plastino J, Janji B, Van Troys M, Lentz D, Ampe C, Sykes C, Friederich E (Actin-filament cross-linking protein T-plastin increases Arp2/3-mediated actin-based movement. *J Cell Sci* 118:1255-1265.2005).
- Glass DJ, Bowen DC, Stitt TN, Radziejewski C, Bruno J, Ryan TE, Gies DR, Shah S, Mattsson K, Burden SJ, DiStefano PS, Valenzuela DM, DeChiara TM, Yancopoulos GD (Agrin acts via a MuSK receptor complex. *Cell* 85:513-523.1996).
- Glennay JR, Jr., Kaulfus P, Matsudaira P, Weber K (F-actin binding and bundling properties of fimbrin, a major cytoskeletal protein of microvillus core filaments. *J Biol Chem* 256:9283-9288.1981).
- Gogliotti RG, Hammond SM, Lutz C, DiDonato CJ (Molecular and phenotypic reassessment of an infrequently used mouse model for spinal muscular atrophy. *Biochem Biophys Res Commun* 391:517-522.2010).
- Goldberg DJ, Burmeister DW (Stages in axon formation: observations of growth of Aplysia axons in culture using video-enhanced contrast-differential interference contrast microscopy. *J Cell Biol* 103:1921-1931.1986).
- Goldsmith SC, Pokala N, Matsudaira P, Almo SC (Crystallization and preliminary crystallographic analysis of the N-terminal actin binding domain of human fimbrin. *Proteins* 28:452-453.1997).
- Gomez CM, Maselli RA, Vohra BP, Navedo M, Stiles JR, Charnet P, Schott K, Rojas L, Keeseey J, Verity A, Wollmann RW, Lasalde-Dominicci J (Novel delta subunit mutation in slow-channel syndrome causes severe weakness by novel mechanisms. *Ann Neurol* 51:102-112.2002).
- Gordon JW, Ruddle FH (Integration and stable germ line transmission of genes injected into mouse pronuclei. *Science* 214:1244-1246.1981).
- Gossler A, Doetschman T, Korn R, Serfling E, Kemler R (Transgenesis by means of blastocyst-derived embryonic stem cell lines. *Proc Natl Acad Sci U S A* 83:9065-9069.1986).
- Govek EE, Newey SE, Akerman CJ, Cross JR, Van der Veken L, Van Aelst L (The X-linked mental retardation protein oligophrenin-1 is required for dendritic spine morphogenesis. *Nat Neurosci* 7:364-372.2004).
- Gubitza AK, Feng W, Dreyfuss G (The SMN complex. *Exp Cell Res* 296:51-56.2004).
- Guettier-Sigrist S, Hugel B, Coupin G, Freyssinet JM, Poindron P, Warter JM (Possible pathogenic role of muscle cell dysfunction in motor neuron death in spinal muscular atrophy. *Muscle Nerve* 25:700-708.2002).

- Guptill JT, Sanders DB (Update on muscle-specific tyrosine kinase antibody positive myasthenia gravis. *Curr Opin Neurol* 23:530-535.2010).
- Gurney ME, Pu H, Chiu AY, Dal Canto MC, Polchow CY, Alexander DD, Caliendo J, Hentati A, Kwon YW, Deng HX, et al. (Motor neuron degeneration in mice that express a human Cu,Zn superoxide dismutase mutation. *Science* 264:1772-1775.1994).
- Hachiya Y, Arai H, Hayashi M, Kumada S, Furushima W, Ohtsuka E, Ito Y, Uchiyama A, Kurata K (Autonomic dysfunction in cases of spinal muscular atrophy type 1 with long survival. *Brain Dev* 27:574-578.2005).
- Hahnen E, Forkert R, Marke C, Rudnik-Schoneborn S, Schonling J, Zerres K, Wirth B (Molecular analysis of candidate genes on chromosome 5q13 in autosomal recessive spinal muscular atrophy: evidence of homozygous deletions of the SMN gene in unaffected individuals. *Hum Mol Genet* 4:1927-1933.1995).
- Hall A (Rho GTPases and the control of cell behaviour. *Biochem Soc Trans* 33:891-895.2005).
- Hanein D, Volkmann N, Goldsmith S, Michon AM, Lehman W, Craig R, DeRosier D, Almo S, Matsudaira P (An atomic model of fimbrin binding to F-actin and its implications for filament crosslinking and regulation. *Nat Struct Biol* 5:787-792.1998).
- Hao le T, Burghes AH, Beattie CE (Generation and Characterization of a genetic zebrafish model of SMA carrying the human SMN2 gene. *Mol Neurodegener* 6:24.2011).
- Hauke J, Riessland M, Lunke S, Eyupoglu IY, Blumcke I, El-Osta A, Wirth B, Hahnen E (Survival motor neuron gene 2 silencing by DNA methylation correlates with spinal muscular atrophy disease severity and can be bypassed by histone deacetylase inhibition. *Hum Mol Genet* 18:304-317.2009).
- Heidmann D, Lehner CF (Reduction of Cre recombinase toxicity in proliferating Drosophila cells by estrogen-dependent activity regulation. *Dev Genes Evol* 211:458-465.2001).
- Heier CR, Satta R, Lutz C, DiDonato CJ (Arrhythmia and cardiac defects are a feature of spinal muscular atrophy model mice. *Hum Mol Genet* 19:3906-3918.2010).
- Helmken C, Wirth B (Exclusion of Htra2-beta1, an up-regulator of full-length SMN2 transcript, as a modifying gene for spinal muscular atrophy. *Hum Genet* 107:554-558.2000).
- Herbst R, Burden SJ (The juxtamembrane region of MuSK has a critical role in agrin-mediated signaling. *Embo J* 19:67-77.2000).
- Higuchi Y, Kita K, Nakanishi H, Wang XL, Sugaya S, Tanzawa H, Yamamori H, Sugita K, Yamaura A, Suzuki N (Search for genes involved in UV-resistance in human cells by mRNA differential display: increased transcriptional expression of nucleophosmin and T-plastin genes in association with the resistance. *Biochem Biophys Res Commun* 248:597-602.1998).
- Hisano T, Ono M, Nakayama M, Naito S, Kuwano M, Wada M (Increased expression of T-plastin gene in cisplatin-resistant human cancer cells: identification by mRNA differential display. *FEBS Lett* 397:101-107.1996).
- Hoffmann K, Muller JS, Stricker S, Megarbane A, Rajab A, Lindner TH, Cohen M, Chouery E, Adaimy L, Ghanem I, Delague V, Boltshauser E, Talim B, Horvath R, Robinson PN, Lochmuller H, Hubner C, Mundlos S (Escobar syndrome is a prenatal myasthenia caused by disruption of the acetylcholine receptor fetal gamma subunit. *Am J Hum Genet* 79:303-312.2006).

- Holt CE, Bullock SL (Subcellular mRNA localization in animal cells and why it matters. *Science* 326:1212-1216.2009).
- Hoogenraad CC, Bradke F (Control of neuronal polarity and plasticity--a renaissance for microtubules? *Trends Cell Biol* 19:669-676.2009).
- Hsieh-Li HM, Chang JG, Jong YJ, Wu MH, Wang NM, Tsai CH, Li H (A mouse model for spinal muscular atrophy. *Nat Genet* 24:66-70.2000).
- Hua Y, Sahashi K, Hung G, Rigo F, Passini MA, Bennett CF, Krainer AR (Antisense correction of SMN2 splicing in the CNS rescues necrosis in a type III SMA mouse model. *Genes Dev* 24:1634-1644.2010).
- Huze C, Bauche S, Richard P, Chevessier F, Goillot E, Gaudon K, Ben Ammar A, Chaboud A, Grosjean I, Lecuyer HA, Bernard V, Rouche A, Alexandri N, Kuntzer T, Fardeau M, Fournier E, Brancaccio A, Ruegg MA, Koenig J, Eymard B, Schaeffer L, Hantai D (Identification of an agrin mutation that causes congenital myasthenia and affects synapse function. *Am J Hum Genet* 85:155-167.2009).
- Ikeda H, Sasaki Y, Kobayashi T, Suzuki H, Mita H, Toyota M, Itoh F, Shinomura Y, Tokino T, Imai K (The role of T-fimbrin in the response to DNA damage: silencing of T-fimbrin by small interfering RNA sensitizes human liver cancer cells to DNA-damaging agents. *Int J Oncol* 27:933-940.2005).
- Jablonka S, Bandilla M, Wiese S, Buhler D, Wirth B, Sendtner M, Fischer U (Co-regulation of survival of motor neuron (SMN) protein and its interactor SIP1 during development and in spinal muscular atrophy. *Hum Mol Genet* 10:497-505.2001).
- Jablonka S, Beck M, Lechner BD, Mayer C, Sendtner M (Defective Ca²⁺ channel clustering in axon terminals disturbs excitability in motoneurons in spinal muscular atrophy. *J Cell Biol* 179:139-149.2007).
- Jady BE, Darzacq X, Tucker KE, Matera AG, Bertrand E, Kiss T (Modification of Sm small nuclear RNAs occurs in the nucleoplasmic Cajal body following import from the cytoplasm. *Embo J* 22:1878-1888.2003).
- Janji B, Giganti A, De Corte V, Catillon M, Bruyneel E, Lentz D, Plastino J, Gettemans J, Friederich E (Phosphorylation on Ser5 increases the F-actin-binding activity of L-plastin and promotes its targeting to sites of actin assembly in cells. *J Cell Sci* 119:1947-1960.2006).
- Jing L, Lefebvre JL, Gordon LR, Granato M (Wnt signals organize synaptic prepattern and axon guidance through the zebrafish unplugged/MuSK receptor. *Neuron* 61:721-733.2009).
- Jones G, Meier T, Lichtsteiner M, Witzemann V, Sakmann B, Brenner HR (Induction by agrin of ectopic and functional postsynaptic-like membrane in innervated muscle. *Proc Natl Acad Sci U S A* 94:2654-2659.1997).
- Kariya S, Park GH, Maeno-Hikichi Y, Leykekhman O, Lutz C, Arkovitz MS, Landmesser LT, Monani UR (Reduced SMN protein impairs maturation of the neuromuscular junctions in mouse models of spinal muscular atrophy. *Hum Mol Genet* 17:2552-2569.2008).
- Karpova TS, Tatchell K, Cooper JA (Actin filaments in yeast are unstable in the absence of capping protein or fimbrin. *J Cell Biol* 131:1483-1493.1995).
- Kawasaki Y, Senda T, Ishidate T, Koyama R, Morishita T, Iwayama Y, Higuchi O, Akiyama T (Asef, a link between the tumor suppressor APC and G-protein signaling. *Science* 289:1194-1197.2000).
- Kelley LC, Hayes KE, Ammer AG, Martin KH, Weed SA (Cortactin phosphorylated by ERK1/2 localizes to sites of dynamic actin regulation and is required for carcinoma lamellipodia persistence. *PLoS One* 5:e13847.2010).

- Kelly TE, Amoroso K, Ferre M, Blanco J, Allinson P, Prior TW (Spinal muscular atrophy variant with congenital fractures. *Am J Med Genet* 87:65-68.1999).
- Kerr DA, Nery JP, Traystman RJ, Chau BN, Hardwick JM (Survival motor neuron protein modulates neuron-specific apoptosis. *Proc Natl Acad Sci U S A* 97:13312-13317.2000).
- Keshishian H, Broadie K, Chiba A, Bate M (The drosophila neuromuscular junction: a model system for studying synaptic development and function. *Annu Rev Neurosci* 19:545-575.1996).
- Khatri IA, Chaudhry US, Seikaly MG, Browne RH, Iannaccone ST (Low bone mineral density in spinal muscular atrophy. *J Clin Neuromuscul Dis* 10:11-17.2008).
- Kim N, Stiegler AL, Cameron TO, Hallock PT, Gomez AM, Huang JH, Hubbard SR, Dustin ML, Burden SJ (Lrp4 is a receptor for Agrin and forms a complex with MuSK. *Cell* 135:334-342.2008).
- Kim SK (Common aging pathways in worms, flies, mice and humans. *J Exp Biol* 210:1607-1612.2007).
- Klein MG, Shi W, Ramagopal U, Tseng Y, Wirtz D, Kovar DR, Staiger CJ, Almo SC (Structure of the actin crosslinking core of fimbrin. *Structure* 12:999-1013.2004).
- Kong L, Wang X, Choe DW, Polley M, Burnett BG, Bosch-Marce M, Griffin JW, Rich MM, Sumner CJ (Impaired synaptic vesicle release and immaturity of neuromuscular junctions in spinal muscular atrophy mice. *J Neurosci* 29:842-851.2009).
- Kugelberg E, Welander L (Heredofamilial juvenile muscular atrophy simulating muscular dystrophy. *AMA Arch Neurol Psychiatry* 75:500-509.1956).
- Kunda P, Paglini G, Quiroga S, Kosik K, Caceres A (Evidence for the involvement of Tiam1 in axon formation. *J Neurosci* 21:2361-2372.2001).
- Laemmli UK (Cleavage of structural proteins during the assembly of the head of bacteriophage T4. *Nature* 227:680-685.1970).
- Lajoie WJ (Paramyotonia congenita, clinical features and electromyographic findings. *Arch Phys Med Rehabil* 42:507-512.1961).
- Lazarides E (Actin, alpha-actinin, and tropomyosin interaction in the structural organization of actin filaments in nonmuscle cells. *J Cell Biol* 68:202-219.1976).
- Le TT, Pham LT, Butchbach ME, Zhang HL, Monani UR, Coover DD, Gavrilina TO, Xing L, Bassell GJ, Burghes AH (SMNDelta7, the major product of the centromeric survival motor neuron (SMN2) gene, extends survival in mice with spinal muscular atrophy and associates with full-length SMN. *Hum Mol Genet* 14:845-857.2005).
- Leavitt J (Discovery and characterization of two novel human cancer-related proteins using two-dimensional gel electrophoresis. *Electrophoresis* 15:345-357.1994).
- Leavitt J, Kakunaga T (Expression of a variant form of actin and additional polypeptide changes following chemical-induced in vitro neoplastic transformation of human fibroblasts. *J Biol Chem* 255:1650-1661.1980).
- Lebart MC, Hubert F, Boiteau C, Venteo S, Roustan C, Benyamin Y (Biochemical characterization of the L-plastin-actin interaction shows a resemblance with that of alpha-actinin and allows a distinction to be made between the two actin-binding domains of the molecule. *Biochemistry* 43:2428-2437.2004).
- Lee CW, Han J, Bamburg JR, Han L, Lynn R, Zheng JQ (Regulation of acetylcholine receptor clustering by ADF/cofilin-directed vesicular trafficking. *Nat Neurosci* 12:848-856.2009).

- Lefebvre S, Burglen L, Reboullet S, Clermont O, Burlet P, Viollet L, Benichou B, Cruaud C, Millasseau P, Zeviani M, et al. (Identification and characterization of a spinal muscular atrophy-determining gene. *Cell* 80:155-165.1995).
- Letourneau PC, Shattuck TA (Distribution and possible interactions of actin-associated proteins and cell adhesion molecules of nerve growth cones. *Development* 105:505-519.1989).
- Letourneau PC, Shattuck TA, Ressler AH ("Pull" and "push" in neurite elongation: observations on the effects of different concentrations of cytochalasin B and taxol. *Cell Motil Cytoskeleton* 8:193-209.1987).
- Li YC, Bai WZ, Zhou L, Sun LK, Hashikawa T (Nonhomogeneous distribution of filamentous actin in the presynaptic terminals on the spinal motoneurons. *J Comp Neurol* 518:3184-3192.2010).
- Lichtman JW, Colman H (Synapse elimination and indelible memory. *Neuron* 25:269-278.2000).
- Lim SR, Hertel KJ (Modulation of survival motor neuron pre-mRNA splicing by inhibition of alternative 3' splice site pairing. *J Biol Chem* 276:45476-45483.2001).
- Lin CS, Aebersold RH, Kent SB, Varma M, Leavitt J (Molecular cloning and characterization of plastin, a human leukocyte protein expressed in transformed human fibroblasts. *Mol Cell Biol* 8:4659-4668.1988).
- Lin CS, Chen ZP, Park T, Ghosh K, Leavitt J (Characterization of the human L-plastin gene promoter in normal and neoplastic cells. *J Biol Chem* 268:2793-2801.1993a).
- Lin CS, Lau A, Lue TF (Analysis and mapping of plastin phosphorylation. *DNA Cell Biol* 17:1041-1046.1998).
- Lin CS, Park T, Chen ZP, Leavitt J (Human plastin genes. Comparative gene structure, chromosome location, and differential expression in normal and neoplastic cells. *J Biol Chem* 268:2781-2792.1993b).
- Lin CS, Shen W, Chen ZP, Tu YH, Matsudaira P (Identification of I-plastin, a human fimbrin isoform expressed in intestine and kidney. *Mol Cell Biol* 14:2457-2467.1994).
- Lin W, Burgess RW, Dominguez B, Pfaff SL, Sanes JR, Lee KF (Distinct roles of nerve and muscle in postsynaptic differentiation of the neuromuscular synapse. *Nature* 410:1057-1064.2001).
- Lin W, Dominguez B, Yang J, Aryal P, Brandon EP, Gage FH, Lee KF (Neurotransmitter acetylcholine negatively regulates neuromuscular synapse formation by a Cdk5-dependent mechanism. *Neuron* 46:569-579.2005).
- Ling KK, Lin MY, Zingg B, Feng Z, Ko CP (Synaptic defects in the spinal and neuromuscular circuitry in a mouse model of spinal muscular atrophy. *PLoS One* 5:e15457.2010).
- Liu Q, Dreyfuss G (A novel nuclear structure containing the survival of motor neurons protein. *Embo J* 15:3555-3565.1996).
- Lorson CL, Hahnen E, Androphy EJ, Wirth B (A single nucleotide in the SMN gene regulates splicing and is responsible for spinal muscular atrophy. *Proc Natl Acad Sci U S A* 96:6307-6311.1999).
- Lorson CL, Strasswimmer J, Yao JM, Baleja JD, Hahnen E, Wirth B, Le T, Burghes AH, Androphy EJ (SMN oligomerization defect correlates with spinal muscular atrophy severity. *Nat Genet* 19:63-66.1998).
- Low LK, Cheng HJ (Axon pruning: an essential step underlying the developmental plasticity of neuronal connections. *Philos T R Soc B* 361:1531-1544.2006).

- Lowery LA, Van Vactor D (The trip of the tip: understanding the growth cone machinery. *Nat Rev Mol Cell Biol* 10:332-343.2009).
- Lundquist EA, Herman RK, Shaw JE, Bargmann CI (UNC-115, a conserved protein with predicted LIM and actin-binding domains, mediates axon guidance in *C. elegans*. *Neuron* 21:385-392.1998).
- Luo L (Actin cytoskeleton regulation in neuronal morphogenesis and structural plasticity. *Annu Rev Cell Dev Biol* 18:601-635.2002).
- Luo L, O'Leary DD (Axon retraction and degeneration in development and disease. *Annu Rev Neurosci* 28:127-156.2005).
- Luo ZG, Je HS, Wang Q, Yang F, Dobbins GC, Yang ZH, Xiong WC, Lu B, Mei L (Implication of geranylgeranyltransferase I in synapse formation. *Neuron* 40:703-717.2003).
- Luo ZG, Wang Q, Zhou JZ, Wang J, Luo Z, Liu M, He X, Wynshaw-Boris A, Xiong WC, Lu B, Mei L (Regulation of AChR clustering by Dishevelled interacting with MuSK and PAK1. *Neuron* 35:489-505.2002).
- MacLeod MJ, Taylor JE, Lunt PW, Mathew CG, Robb SA (Prenatal onset spinal muscular atrophy. *Eur J Paediatr Neurol* 3:65-72.1999).
- Madhavan R, Gong ZL, Ma JJ, Chan AW, Peng HB (The function of cortactin in the clustering of acetylcholine receptors at the vertebrate neuromuscular junction. *PLoS One* 4:e8478.2009).
- Markowitz JA, Tinkle MB, Fischbeck KH (Spinal muscular atrophy in the neonate. *J Obstet Gynecol Neonatal Nurs* 33:12-20.2004).
- Marques G, Bao H, Haerry TE, Shimell MJ, Duchek P, Zhang B, O'Connor MB (The *Drosophila* BMP type II receptor Wishful Thinking regulates neuromuscular synapse morphology and function. *Neuron* 33:529-543.2002).
- Martin GR (Isolation of a pluripotent cell line from early mouse embryos cultured in medium conditioned by teratocarcinoma stem cells. *Proc Natl Acad Sci U S A* 78:7634-7638.1981).
- Maselli RA, Arredondo J, Cagney O, Ng JJ, Anderson JA, Williams C, Gerke BJ, Soliven B, Wollmann RL (Mutations in MUSK causing congenital myasthenic syndrome impair MuSK-Dok-7 interaction. *Hum Mol Genet* 19:2370-2379.2010).
- McGovern VL, Gavrulina TO, Beattie CE, Burghes AH (Embryonic motor axon development in the severe SMA mouse. *Hum Mol Genet* 17:2900-2909.2008).
- McWhorter ML, Monani UR, Burghes AH, Beattie CE (Knockdown of the survival motor neuron (*Smn*) protein in zebrafish causes defects in motor axon outgrowth and pathfinding. *J Cell Biol* 162:919-931.2003).
- Meister G, Buhler D, Pillai R, Lottspeich F, Fischer U (A multiprotein complex mediates the ATP-dependent assembly of spliceosomal U snRNPs. *Nat Cell Biol* 3:945-949.2001).
- Meister G, Eggert C, Fischer U (SMN-mediated assembly of RNPs: a complex story. *Trends Cell Biol* 12:472-478.2002).
- Melki J, Abdelhak S, Sheth P, Bachelot MF, Burlet P, Marcadet A, Aicardi J, Barois A, Carriere JP, Fardeau M, et al. (Gene for chronic proximal spinal muscular atrophies maps to chromosome 5q. *Nature* 344:767-768.1990).
- Mende Y, Jakubik M, Riessland M, Schoenen F, Rossbach K, Kleinridders A, Kohler C, Buch T, Wirth B (Deficiency of the splicing factor *Sfrs10* results in early embryonic lethality in mice and has no impact on full-length SMN/*Smn* splicing. *Hum Mol Genet* 19:2154-2167.2010).

- Mentis GZ, Blivis D, Liu W, Drobac E, Crowder ME, Kong L, Alvarez FJ, Sumner CJ, O'Donovan MJ (Early functional impairment of sensory-motor connectivity in a mouse model of spinal muscular atrophy. *Neuron* 69:453-467.2011).
- Mercuri E, Bertini E, Messina S, Solari A, D'Amico A, Angelozzi C, Battini R, Berardinelli A, Boffi P, Bruno C, Cini C, Colitto F, Kinali M, Minetti C, Mongini T, Morandi L, Neri G, Orcesi S, Pane M, Pelliccioni M, Pini A, Tiziano FD, Villanova M, Vita G, Brahe C (Randomized, double-blind, placebo-controlled trial of phenylbutyrate in spinal muscular atrophy. *Neurology* 68:51-55.2007).
- Meyer K, Marquis J, Trub J, Nlend Nlend R, Verp S, Ruepp MD, Imboden H, Barde I, Trono D, Schumperli D (Rescue of a severe mouse model for spinal muscular atrophy by U7 snRNA-mediated splicing modulation. *Hum Mol Genet* 18:546-555.2009).
- Michalk A, Stricker S, Becker J, Rupps R, Pantzar T, Miertus J, Botta G, Naretto VG, Janetzki C, Yaqoob N, Ott CE, Seelow D, Wiczorek D, Fiebig B, Wirth B, Hoopmann M, Walther M, Korber F, Blankenburg M, Mundlos S, Heller R, Hoffmann K (Acetylcholine receptor pathway mutations explain various fetal akinesia deformation sequence disorders. *Am J Hum Genet* 82:464-476.2008).
- Michaud M, Arnoux T, Bielli S, Durand E, Rotrou Y, Jablonka S, Robert F, Giraudon-Paoli M, Riessland M, Mattei MG, Andriambeloson E, Wirth B, Sendtner M, Gallego J, Pruss RM, Bordet T (Neuromuscular defects and breathing disorders in a new mouse model of spinal muscular atrophy. *Neurobiol Dis.*2010).
- Miguel-Aliaga I, Culetto E, Walker DS, Baylis HA, Sattelle DB, Davies KE (The *Caenorhabditis elegans* orthologue of the human gene responsible for spinal muscular atrophy is a maternal product critical for germline maturation and embryonic viability. *Hum Mol Genet* 8:2133-2143.1999).
- Mihaylova V, Muller JS, Vilchez JJ, Salih MA, Kabiraj MM, D'Amico A, Bertini E, Wolffe J, Schreiner F, Kurlemann G, Rasic VM, Siskova D, Colomer J, Herczegfalvi A, Fabriciova K, Weschke B, Scola R, Hoellen F, Schara U, Abicht A, Lochmuller H (Clinical and molecular genetic findings in COLQ-mutant congenital myasthenic syndromes. *Brain* 131:747-759.2008).
- Mihaylova V, Salih MA, Mukhtar MM, Abuzeid HA, El-Sadig SM, von der Hagen M, Huebner A, Nurnberg G, Abicht A, Muller JS, Lochmuller H, Guergueltcheva V (Refinement of the clinical phenotype in musk-related congenital myasthenic syndromes. *Neurology* 73:1926-1928.2009).
- Miller TM, Dias da Silva MR, Miller HA, Kwiecinski H, Mendell JR, Tawil R, McManis P, Griggs RC, Angelini C, Servidei S, Petajan J, Dalakas MC, Ranum LP, Fu YH, Ptacek LJ (Correlating phenotype and genotype in the periodic paralyses. *Neurology* 63:1647-1655.2004).
- Mine M, Koarada S, Sai T, Miyake K, Kimoto M (Peptide-binding motifs of the mixed haplotype Abetaz/Aalphan major histocompatibility complex class II molecule: a restriction element for auto-reactive T cells in (NZBxNZW)F1 mice. *Immunology* 95:577-584.1998).
- Misgeld T, Burgess RW, Lewis RM, Cunningham JM, Lichtman JW, Sanes JR (Roles of neurotransmitter in synapse formation: development of neuromuscular junctions lacking choline acetyltransferase. *Neuron* 36:635-648.2002).
- Mitchison TJ, Cramer LP (Actin-based cell motility and cell locomotion. *Cell* 84:371-379.1996).
- Monani UR, Pastore MT, Gavrilina TO, Jablonka S, Le TT, Andreassi C, DiCocco JM, Lorson C, Androphy EJ, Sendtner M, Podell M, Burghes AH (A transgene

- carrying an A2G missense mutation in the SMN gene modulates phenotypic severity in mice with severe (type I) spinal muscular atrophy. *J Cell Biol* 160:41-52.2003).
- Monani UR, Sendtner M, Coover DD, Parsons DW, Andreassi C, Le TT, Jablonka S, Schrank B, Rossol W, Prior TW, Morris GE, Burghes AH (The human centromeric survival motor neuron gene (SMN2) rescues embryonic lethality in *Smn(-/-)* mice and results in a mouse with spinal muscular atrophy. *Hum Mol Genet* 9:333-339.2000).
- Montes J, Gordon AM, Pandya S, De Vivo DC, Kaufmann P (Clinical outcome measures in spinal muscular atrophy. *J Child Neurol* 24:968-978.2009).
- Moransard M, Borges LS, Willmann R, Marangi PA, Brenner HR, Ferns MJ, Fuhrer C (Agrin regulates rapsyn interaction with surface acetylcholine receptors, and this underlies cytoskeletal anchoring and clustering. *J Biol Chem* 278:7350-7359.2003).
- Morgan NV, Brueton LA, Cox P, Grealley MT, Tolmie J, Pasha S, Aligianis IA, van Bokhoven H, Marton T, Al-Gazali L, Morton JE, Oley C, Johnson CA, Trembath RC, Brunner HG, Maher ER (Mutations in the embryonal subunit of the acetylcholine receptor (CHRNG) cause lethal and Escobar variants of multiple pterygium syndrome. *Am J Hum Genet* 79:390-395.2006).
- Muller JS, Baumeister SK, Rasic VM, Krause S, Todorovic S, Kugler K, Muller-Felber W, Abicht A, Lochmuller H (Impaired receptor clustering in congenital myasthenic syndrome with novel RAPSN mutations. *Neurology* 67:1159-1164.2006).
- Muller W, Kuhn R, Rajewsky K (Major histocompatibility complex class II hyperexpression on B cells in interleukin 4-transgenic mice does not lead to B cell proliferation and hypergammaglobulinemia. *Eur J Immunol* 21:921-925.1991).
- Mullis KB, White F, Scharf SJ, Saiki RK, Horn GT, Ehrlich HA (Specific enzymatic amplification of DNA in vitro: the polymerase chain reaction. *Cold Spring Harbor Symposium, Quant Biol* 263-273.1986).
- Murray LM, Comley LH, Thomson D, Parkinson N, Talbot K, Gillingwater TH (Selective vulnerability of motor neurons and dissociation of pre- and post-synaptic pathology at the neuromuscular junction in mouse models of spinal muscular atrophy. *Hum Mol Genet* 17:949-962.2008).
- Nakayama AY, Harms MB, Luo L (Small GTPases Rac and Rho in the maintenance of dendritic spines and branches in hippocampal pyramidal neurons. *J Neurosci* 20:5329-5338.2000).
- Namba Y, Ito M, Zu Y, Shigesada K, Maruyama K (Human T cell L-plastin bundles actin filaments in a calcium-dependent manner. *J Biochem* 112:503-507.1992).
- Narver HL, Kong L, Burnett BG, Choe DW, Bosch-Marce M, Taye AA, Eckhaus MA, Sumner CJ (Sustained improvement of spinal muscular atrophy mice treated with trichostatin A plus nutrition. *Ann Neurol* 64:465-470.2008).
- Neumann E, Schaefer-Ridder M, Wang Y, Hofschneider PH (Gene transfer into mouse lymphoma cells by electroporation in high electric fields. *Embo J* 1:841-845.1982).
- Nitkin RM, Smith MA, Magill C, Fallon JR, Yao YM, Wallace BG, McMahan UJ (Identification of agrin, a synaptic organizing protein from Torpedo electric organ. *J Cell Biol* 105:2471-2478.1987).
- Niwa H, Yamamura K, Miyazaki J (Efficient selection for high-expression transfectants with a novel eukaryotic vector. *Gene* 108:193-199.1991).

- Ohno K, Brengman J, Tsujino A, Engel AG (Human endplate acetylcholinesterase deficiency caused by mutations in the collagen-like tail subunit (ColQ) of the asymmetric enzyme. *Proc Natl Acad Sci U S A* 95:9654-9659.1998).
- Ohno K, Engel AG, Shen XM, Selcen D, Brengman J, Harper CM, Tsujino A, Milone M (Rapsyn mutations in humans cause endplate acetylcholine-receptor deficiency and myasthenic syndrome. *Am J Hum Genet* 70:875-885.2002).
- Ohno K, Hutchinson DO, Milone M, Brengman JM, Bouzat C, Sine SM, Engel AG (Congenital myasthenic syndrome caused by prolonged acetylcholine receptor channel openings due to a mutation in the M2 domain of the epsilon subunit. *Proc Natl Acad Sci U S A* 92:758-762.1995).
- Ohno K, Tsujino A, Brengman JM, Harper CM, Bajzer Z, Udd B, Beyring R, Robb S, Kirkham FJ, Engel AG (Choline acetyltransferase mutations cause myasthenic syndrome associated with episodic apnea in humans. *Proc Natl Acad Sci U S A* 98:2017-2022.2001).
- Okamoto K, Narayanan R, Lee SH, Murata K, Hayashi Y (The role of CaMKII as an F-actin-bundling protein crucial for maintenance of dendritic spine structure. *Proc Natl Acad Sci U S A* 104:6418-6423.2007).
- Oprea GE, Krober S, McWhorter ML, Rossoll W, Muller S, Krawczak M, Bassell GJ, Beattie CE, Wirth B (Plastin 3 is a protective modifier of autosomal recessive spinal muscular atrophy. *Science* 320:524-527.2008).
- Pagliardini S, Giavazzi A, Setola V, Lizier C, Di Luca M, DeBiasi S, Battaglia G (Subcellular localization and axonal transport of the survival motor neuron (SMN) protein in the developing rat spinal cord. *Hum Mol Genet* 9:47-56.2000).
- Pak CW, Flynn KC, Bamberg JR (Actin-binding proteins take the reins in growth cones. *Nat Rev Neurosci* 9:136-147.2008).
- Pan L, Zhang YQ, Woodruff E, Broadie K (The *Drosophila* fragile X gene negatively regulates neuronal elaboration and synaptic differentiation. *Curr Biol* 14:1863-1870.2004).
- Pantaloni D, Carlier MF (How profilin promotes actin filament assembly in the presence of thymosin beta 4. *Cell* 75:1007-1014.1993).
- Park GH, Kariya S, Monani UR (Spinal muscular atrophy: new and emerging insights from model mice. *Curr Neurol Neurosci Rep* 10:108-117.2010).
- Passini MA, Bu J, Richards AM, Kinnecom C, Sardi SP, Stanek LM, Hua Y, Rigo F, Matson J, Hung G, Kaye EM, Shihabuddin LS, Krainer AR, Bennett CF, Cheng SH (Antisense oligonucleotides delivered to the mouse CNS ameliorate symptoms of severe spinal muscular atrophy. *Sci Transl Med* 3:72ra18.2011).
- Pato C, Stetzkowski-Marden F, Gaus K, Recouvreur M, Cartaud A, Cartaud J (Role of lipid rafts in agrin-elicited acetylcholine receptor clustering. *Chem Biol Interact* 175:64-67.2008).
- Paushkin S, Charroux B, Abel L, Parkinson RA, Pellizzoni L, Dreyfuss G (The survival motor neuron protein of *Schizosaccharomyces pombe*. Conservation of survival motor neuron interaction domains in divergent organisms. *J Biol Chem* 275:23841-23846.2000).
- Pearn J (Incidence, prevalence, and gene frequency studies of chronic childhood spinal muscular atrophy. *J Med Genet* 15:409-413.1978).
- Peitz M, Pfannkuche K, Rajewsky K, Edenhofer F (Ability of the hydrophobic FGF and basic TAT peptides to promote cellular uptake of recombinant Cre recombinase: a tool for efficient genetic engineering of mammalian genomes. *Proc Natl Acad Sci U S A* 99:4489-4494.2002).

- Pellizzoni L (Chaperoning ribonucleoprotein biogenesis in health and disease. *EMBO Rep* 8:340-345.2007).
- Pellizzoni L, Yong J, Dreyfuss G (Essential Role for the SMN Complex in the Specificity of snRNP Assembly. *Science* 298:1775-1779.2002).
- Piazzon N, Rage F, Schlotter F, Moine H, Branlant C, Massenet S (In vitro and in cellulo evidences for association of the survival of motor neuron complex with the fragile X mental retardation protein. *J Biol Chem* 283:5598-5610.2008).
- Prevost MC, Lesourd M, Arpin M, Vernel F, Mounier J, Hellio R, Sansonetti PJ (Unipolar reorganization of F-actin layer at bacterial division and bundling of actin filaments by plastin correlate with movement of *Shigella flexneri* within HeLa cells. *Infect Immun* 60:4088-4099.1992).
- Prior TW, Krainer AR, Hua Y, Swoboda KJ, Snyder PC, Bridgeman SJ, Burghes AH, Kissel JT (A positive modifier of spinal muscular atrophy in the SMN2 gene. *Am J Hum Genet* 85:408-413.2009).
- Ptacek LJ, George AL, Jr., Griggs RC, Tawil R, Kallen RG, Barchi RL, Robertson M, Leppert MF (Identification of a mutation in the gene causing hyperkalemic periodic paralysis. *Cell* 67:1021-1027.1991).
- Quiram PA, Ohno K, Milone M, Patterson MC, Pruitt NJ, Brengman JM, Sine SM, Engel AG (Mutation causing congenital myasthenia reveals acetylcholine receptor beta/delta subunit interaction essential for assembly. *J Clin Invest* 104:1403-1410.1999).
- Rabionet R, Zelante L, Lopez-Bigas N, D'Agruma L, Melchionda S, Restagno G, Arbones ML, Gasparini P, Estivill X (Molecular basis of childhood deafness resulting from mutations in the GJB2 (connexin 26) gene. *Hum Genet* 106:40-44.2000).
- Rajendra TK, Gonsalvez GB, Walker MP, Shpargel KB, Salz HK, Matera AG (A *Drosophila melanogaster* model of spinal muscular atrophy reveals a function for SMN in striated muscle. *J Cell Biol* 176:831-841.2007).
- Raker VA, Hartmuth K, Kastner B, Luhrmann R (Spliceosomal U snRNP core assembly: Sm proteins assemble onto an Sm site RNA nonanucleotide in a specific and thermodynamically stable manner. *Mol Cell Biol* 19:6554-6565.1999).
- Ralser M, Albrecht M, Nonhoff U, Lengauer T, Lehrach H, Krobitsch S (An integrative approach to gain insights into the cellular function of human ataxin-2. *J Mol Biol* 346:203-214.2005a).
- Ralser M, Nonhoff U, Albrecht M, Lengauer T, Wanker EE, Lehrach H, Krobitsch S (Ataxin-2 and huntingtin interact with endophilin-A complexes to function in plastin-associated pathways. *Hum Mol Genet* 14:2893-2909.2005b).
- Riento K, Ridley AJ (Rocks: multifunctional kinases in cell behaviour. *Nat Rev Mol Cell Biol* 4:446-456.2003).
- Riessland M, Ackermann B, Forster A, Jakubik M, Hauke J, Garbes L, Fritzsche I, Mende Y, Blumcke I, Hahnen E, Wirth B (SAHA ameliorates the SMA phenotype in two mouse models for spinal muscular atrophy. *Hum Mol Genet* 19:2154-2167.2010).
- Riessland M, Brichta L, Hahnen E, Wirth B (The benzamide M344, a novel histone deacetylase inhibitor, significantly increases SMN2 RNA/protein levels in spinal muscular atrophy cells. *Hum Genet* 120:101-110.2006).
- Riley DA (Ultrastructural evidence for axon retraction during the spontaneous elimination of polyneuronal innervation of the rat soleus muscle. *J Neurocytol* 10:425-440.1981).

- Robertson E, Bradley A, Kuehn M, Evans M (Germ-line transmission of genes introduced into cultured pluripotential cells by retroviral vector. *Nature* 323:445-448.1986).
- Rodolico C, Toscano A, Autunno M, Messina S, Nicolosi C, Aguenouz M, Laura M, Girlanda P, Messina C, Vita G (Limb-girdle myasthenia: clinical, electrophysiological and morphological features in familial and autoimmune cases. *Neuromuscul Disord* 12:964-969.2002).
- Rosenthal JL, Taraskevich PS (Reduction of multi-axonal innervation at the neuromuscular junction of the rat during development. *J Physiol* 270:299-310.1977).
- Rossoll W, Bassell GJ (Spinal muscular atrophy and a model for survival of motor neuron protein function in axonal ribonucleoprotein complexes. *Results Probl Cell Differ* 48:289-326.2009).
- Rossoll W, Jablonka S, Andreassi C, Kroning AK, Karle K, Monani UR, Sendtner M (Smn, the spinal muscular atrophy-determining gene product, modulates axon growth and localization of beta-actin mRNA in growth cones of motoneurons. *J Cell Biol* 163:801-812.2003).
- Rossoll W, Kroning AK, Ohndorf UM, Steegborn C, Jablonka S, Sendtner M (Specific interaction of Smn, the spinal muscular atrophy determining gene product, with hnRNP-R and gry-rbp/hnRNP-Q: a role for Smn in RNA processing in motor axons? *Hum Mol Genet* 11:93-105.2002).
- Rudnik-Schoneborn S, Berg C, Zerres K, Betzler C, Grimm T, Eggermann T, Eggermann K, Wirth R, Wirth B, Heller R (Genotype-phenotype studies in infantile spinal muscular atrophy (SMA) type I in Germany: implications for clinical trials and genetic counselling. *Clin Genet* 76:168-178.2009).
- Rudnik-Schoneborn S, Heller R, Berg C, Betzler C, Grimm T, Eggermann T, Eggermann K, Wirth R, Wirth B, Zerres K (Congenital heart disease is a feature of severe infantile spinal muscular atrophy. *J Med Genet* 45:635-638.2008).
- Rudnik-Schöneborn S, Rohrig D, Morgan G, Wirth B, Zerres K (Autosomal recessive proximal spinal muscular atrophy in 101 sibs out of 48 families: clinical picture, influence of gender, and genetic implications. *Am J Med Genet* 51:70-76.1994).
- Ruiz R, Casanas JJ, Torres-Benito L, Cano R, Tabares L (Altered intracellular Ca²⁺-homeostasis in nerve terminals of severe spinal muscular atrophy mice. *J Neurosci* 30:849-857.2010).
- Sakai K, Miyazaki J (A transgenic mouse line that retains Cre recombinase activity in mature oocytes irrespective of the cre transgene transmission. *Biochem Biophys Res Commun* 237:318-324.1997).
- Sanders DB, El-Salem K, Massey JM, McConville J, Vincent A (Clinical aspects of MuSK antibody positive seronegative MG. *Neurology* 60:1978-1980.2003).
- Sanes JR, Lichtman JW (Development of the vertebrate neuromuscular junction. *Annu Rev Neurosci* 22:389-442.1999).
- Sanes JR, Lichtman JW (Induction, assembly, maturation and maintenance of a postsynaptic apparatus. *Nat Rev Neurosci* 2:791-805.2001).
- Sanger F, Coulson AR. (DNA sequencing with chain-terminating inhibitors. *Proc Natl Acad Sci USA* 74:5463-5467.1977).
- Sasaki Y, Itoh F, Kobayashi T, Kikuchi T, Suzuki H, Toyota M, Imai K (Increased expression of T-fimbrin gene after DNA damage in CHO cells and inactivation of T-fimbrin by CpG methylation in human colorectal cancer cells. *Int J Cancer* 97:211-216.2002).

- Scarciolla O, Stuppia L, De Angelis MV, Murru S, Palka C, Giuliani R, Pace M, Di Muzio A, Torrente I, Morella A, Grammatico P, Giacanelli M, Rosatelli MC, Uncini A, Dallapiccola B (Spinal muscular atrophy genotyping by gene dosage using multiple ligation-dependent probe amplification. *Neurogenetics* 7:269-276.2006).
- Schaefer AW, Schoonderwoert VT, Ji L, Mederios N, Danuser G, Forscher P (Coordination of actin filament and microtubule dynamics during neurite outgrowth. *Dev Cell* 15:146-162.2008).
- Schara U, Christen HJ, Durmus H, Hietala M, Krabetz K, Rodolico C, Schreiber G, Topaloglu H, Talim B, Voss W, Pihko H, Abicht A, Muller JS, Lochmuller H (Long-term follow-up in patients with congenital myasthenic syndrome due to CHAT mutations. *Eur J Paediatr Neurol* 14:326-333.2010).
- Schara U, Lochmuller H (Therapeutic strategies in congenital myasthenic syndromes. *Neurotherapeutics* 5:542-547.2008).
- Scheffer H, Cobben JM, Matthijs G, Wirth B (Best practice guidelines for molecular analysis in spinal muscular atrophy. *Eur J Hum Genet* 9:484-491.2001).
- Schlegel A, Stainier DY (Lessons from "lower" organisms: what worms, flies, and zebrafish can teach us about human energy metabolism. *PLoS Genet* 3:e199.2007).
- Schmidt EE, Taylor DS, Prigge JR, Barnett S, Capecchi MR (Illegitimate Cre-dependent chromosome rearrangements in transgenic mouse spermatids. *Proc Natl Acad Sci U S A* 97:13702-13707.2000).
- Schmidt H, Rathjen FG (Signalling mechanisms regulating axonal branching in vivo. *Bioessays* 32:977-985.2010).
- Schrank B, Gotz R, Gunnensen JM, Ure JM, Toyka KV, Smith AG, Sendtner M (Inactivation of the survival motor neuron gene, a candidate gene for human spinal muscular atrophy, leads to massive cell death in early mouse embryos. *Proc Natl Acad Sci U S A* 94:9920-9925.1997).
- Schwenk F, Baron U, Rajewsky K (A cre-transgenic mouse strain for the ubiquitous deletion of loxP-flanked gene segments including deletion in germ cells. *Nucleic Acids Res* 23:5080-5081.1995).
- Selcen D, Milone M, Shen XM, Harper CM, Stans AA, Wieben ED, Engel AG (Dok-7 myasthenia: phenotypic and molecular genetic studies in 16 patients. *Ann Neurol* 64:71-87.2008).
- Selenko P, Sprangers R, Stier G, Buhler D, Fischer U, Sattler M (SMN tudor domain structure and its interaction with the Sm proteins. *Nat Struct Biol* 8:27-31.2001).
- Serio AW, Jeng RL, Haglund CM, Reed SC, Welch MD (Defining a core set of actin cytoskeletal proteins critical for actin-based motility of *Rickettsia*. *Cell Host Microbe* 7:388-398.2010).
- Shababi M, Habibi J, Yang HT, Vale SM, Sewell WA, Lorson CL (Cardiac defects contribute to the pathology of spinal muscular atrophy models. *Hum Mol Genet* 19:4059-4071.2010).
- Shafey D, Cote PD, Kothary R (Hypomorphic Smn knockdown C2C12 myoblasts reveal intrinsic defects in myoblast fusion and myotube morphology. *Exp Cell Res* 311:49-61.2005).
- Shanmugarajan S, Swoboda KJ, Iannaccone ST, Ries WL, Maria BL, Reddy SV (Congenital bone fractures in spinal muscular atrophy: functional role for SMN protein in bone remodeling. *J Child Neurol* 22:967-973.2007).

- Shanmugarajan S, Tsuruga E, Swoboda KJ, Maria BL, Ries WL, Reddy SV (Bone loss in survival motor neuron (Smn(-/-) SMN2) genetic mouse model of spinal muscular atrophy. *J Pathol* 219:52-60.2009).
- Shapira YA, Sadeh ME, Bergtraum MP, Tsujino A, Ohno K, Shen XM, Brengman J, Edwardson S, Matoth I, Engel AG (Three novel COLQ mutations and variation of phenotypic expressivity due to G240X. *Neurology* 58:603-609.2002).
- Sharma A, Lambrechts A, Hao le T, Le TT, Sewry CA, Ampe C, Burghes AH, Morris GE (A role for complexes of survival of motor neurons (SMN) protein with gemins and profilin in neurite-like cytoplasmic extensions of cultured nerve cells. *Exp Cell Res* 309:185-197.2005).
- Shen XM, Ohno K, Fukudome T, Tsujino A, Brengman JM, De Vivo DC, Packer RJ, Engel AG (Congenital myasthenic syndrome caused by low-expressor fast-channel AChR delta subunit mutation. *Neurology* 59:1881-1888.2002).
- Shinomiya H, Nagai K, Hirata H, Kobayashi N, Hasegawa H, Liu F, Sumita K, Asano Y (Preparation and characterization of recombinant murine p65/L-plastin expressed in *Escherichia coli* and high-titer antibodies against the protein. *Biosci Biotechnol Biochem* 67:1368-1375.2003).
- Shupliakov O, Bloom O, Gustafsson JS, Kjaerulff O, Low P, Tomilin N, Pieribone VA, Greengard P, Brodin L (Impaired recycling of synaptic vesicles after acute perturbation of the presynaptic actin cytoskeleton. *Proc Natl Acad Sci U S A* 99:14476-14481.2002).
- Silver DP, Livingston DM (Self-excising retroviral vectors encoding the Cre recombinase overcome Cre-mediated cellular toxicity. *Mol Cell* 8:233-243.2001).
- Silver LM (1995) *Mouse genetics : concepts and applications*. New York: Oxford University Press.
- Silverman GA, Luke CJ, Bhatia SR, Long OS, Vetica AC, Perlmutter DH, Pak SC (Modeling molecular and cellular aspects of human disease using the nematode *Caenorhabditis elegans*. *Pediatr Res* 65:10-18.2009).
- Sleigh JN, Gillingwater TH, Talbot K (The contribution of mouse models to understanding the pathogenesis of spinal muscular atrophy. *Dis Model Mech* 4:457-467.2011).
- Smith AG, Heath JK, Donaldson DD, Wong GG, Moreau J, Stahl M, Rogers D (Inhibition of pluripotential embryonic stem cell differentiation by purified polypeptides. *Nature* 336:688-690.1988).
- Southern EM (Detection of specific sequences among DNA fragments separated by gel electrophoresis. *J Mol Biol* 98:503-517.1975).
- Srour M, Bolduc V, Guergueltcheva V, Lochmuller H, Gendron D, Shevell MI, Poulin C, Mathieu J, Bouchard JP, Brais B (DOK7 mutations presenting as a proximal myopathy in French Canadians. *Neuromuscul Disord* 20:453-457.2010).
- Stetzkowski-Marden F, Gaus K, Recouvreur M, Cartaud A, Cartaud J (Agrin elicits membrane lipid condensation at sites of acetylcholine receptor clusters in C2C12 myotubes. *J Lipid Res* 47:2121-2133.2006).
- Stiess M, Bradke F (Neuronal polarization: The cytoskeleton leads the way. *Dev Neurobiol* 71:430-444.2011).
- Stratigopoulos G, Lanzano P, Deng L, Guo J, Kaufmann P, Darras B, Finkel R, Tawil R, McDermott MP, Martens W, Devivo DC, Chung WK (Association of plastin 3 expression with disease severity in spinal muscular atrophy only in postpubertal females. *Arch Neurol* 67:1252-1256.2010).

- Sugiura Y, Aoki T, Sugiyama Y, Hida C, Ogata M, Yamamoto T (Temperature-sensitive sodium channelopathy with heat-induced myotonia and cold-induced paralysis. *Neurology* 54:2179-2181.2000).
- Sumner CJ, Huynh TN, Markowitz JA, Perhac JS, Hill B, Coovert DD, Schussler K, Chen X, Jarecki J, Burghes AH, Taylor JP, Fischbeck KH (Valproic acid increases SMN levels in spinal muscular atrophy patient cells. *Ann Neurol* 54:647-654.2003).
- Takenawa T, Suetsugu S (The WASP-WAVE protein network: connecting the membrane to the cytoskeleton. *Nat Rev Mol Cell Biol* 8:37-48.2007).
- Talbot K (Spinal muscular atrophy. *J Inherit Metab Dis* 22:545-554.1999).
- Tang H, Sun Z, Goldman D (CaM kinase II-dependent suppression of nicotinic acetylcholine receptor delta-subunit promoter activity. *J Biol Chem* 276:26057-26065.2001).
- Tang N, Gibson H, Germeroth T, Porcu P, Lim HW, Wong HK (T-plastin (PLS3) gene expression differentiates Sezary syndrome from mycosis fungoides and inflammatory skin diseases and can serve as a biomarker to monitor disease progression. *Br J Dermatol* 162:463-466.2010).
- Ticozzi N, Tiloca C, Morelli C, Colombrita C, Poletti B, Doretti A, Maderna L, Messina S, Ratti A, Silani V (Genetics of familial Amyotrophic lateral sclerosis. *Arch Ital Biol* 149:65-82.2011).
- Torres-Benito L, Ruiz R, Tabares L (Synaptic defects in SMA animal models. *Dev Neurobiol*.2011).
- Tsai LK, Tsai MS, Ting CH, Li H (Multiple therapeutic effects of valproic acid in spinal muscular atrophy model mice. *J Mol Med* 86:1243-1254.2008).
- Uchitel O, Engel AG, Walls TJ, Nagel A, Atassi MZ, Brill V (Congenital myasthenic syndromes: II. Syndrome attributed to abnormal interaction of acetylcholine with its receptor. *Muscle Nerve* 16:1293-1301.1993).
- Valenzuela DM, Stitt TN, DiStefano PS, Rojas E, Mattsson K, Compton DL, Nunez L, Park JS, Stark JL, Gies DR, et al. (Receptor tyrosine kinase specific for the skeletal muscle lineage: expression in embryonic muscle, at the neuromuscular junction, and after injury. *Neuron* 15:573-584.1995).
- Valori CF, Ning K, Wyles M, Mead RJ, Grierson AJ, Shaw PJ, Azzouz M (Systemic delivery of scAAV9 expressing SMN prolongs survival in a model of spinal muscular atrophy. *Sci Transl Med* 2:35ra42.2010).
- van Bergeijk J, Rydel-Konecke K, Grothe C, Claus P (The spinal muscular atrophy gene product regulates neurite outgrowth: importance of the C terminus. *Faseb J* 21:1492-1502.2007).
- Vanderhaeghen P, Cheng HJ (Guidance molecules in axon pruning and cell death. *Cold Spring Harb Perspect Biol* 2:a001859.2010).
- Veizain M, Gerard B, Drunat S, Funalot B, Fehrenbach S, N'Guyen-Viet V, Vallat JM, Frebourg T, Tosi M, Martins A, Saugier-veber P (A leaky splicing mutation affecting SMN1 exon 7 inclusion explains an unexpected mild case of spinal muscular atrophy. *Hum Mutat*.2011).
- Veizain M, Saugier-veber P, Goïna E, Touraine R, Manel V, Toutain A, Fehrenbach S, Frebourg T, Pagani F, Tosi M, Martins A (A rare SMN2 variant in a previously unrecognized composite splicing regulatory element induces exon 7 inclusion and reduces the clinical severity of spinal muscular atrophy. *Hum Mutat* 31:E1110-1125.2010).
- Walker MP, Rajendra TK, Saieva L, Fuentes JL, Pellizzoni L, Matera AG (SMN complex localizes to the sarcomeric Z-disc and is a proteolytic target of calpain. *Hum Mol Genet* 17:3399-3410.2008).

- Wang CH, Xu J, Carter TA, Ross BM, Dominski MK, Bellcross CA, Penchaszadeh GK, Munsat TL, Gilliam TC (Characterization of survival motor neuron (SMNT) gene deletions in asymptomatic carriers of spinal muscular atrophy. *Hum Mol Genet* 5:359-365.1996).
- Wang HL, Milone M, Ohno K, Shen XM, Tsujino A, Batocchi AP, Tonali P, Brengman J, Engel AG, Sine SM (Acetylcholine receptor M3 domain: stereochemical and volume contributions to channel gating. *Nat Neurosci* 2:226-233.1999).
- Wang J, Jing Z, Zhang L, Zhou G, Braun J, Yao Y, Wang ZZ (Regulation of acetylcholine receptor clustering by the tumor suppressor APC. *Nat Neurosci* 6:1017-1018.2003).
- Watanabe T, Wang S, Noritake J, Sato K, Fukata M, Takefuji M, Nakagawa M, Izumi N, Akiyama T, Kaibuchi K (Interaction with IQGAP1 links APC to Rac1, Cdc42, and actin filaments during cell polarization and migration. *Dev Cell* 7:871-883.2004).
- Weatherbee SD, Anderson KV, Niswander LA (LDL-receptor-related protein 4 is crucial for formation of the neuromuscular junction. *Development* 133:4993-5000.2006).
- Weimann JM, Zhang YA, Levin ME, Devine WP, Brulet P, McConnell SK (Cortical neurons require Otx1 for the refinement of exuberant axonal projections to subcortical targets. *Neuron* 24:819-831.1999).
- Werdnig G (Zwei frühinfantile hereditäre Fälle von progressiver Muskelatrophie unter dem Bilde der Dystrophie, aber auf neurotischer Grundlage. *Archiv für Psychiatrie und Nervenkrankheiten* 22:437-480.1891).
- Weston C, Gordon C, Teressa G, Hod E, Ren XD, Prives J (Cooperative regulation by Rac and Rho of agrin-induced acetylcholine receptor clustering in muscle cells. *J Biol Chem* 278:6450-6455.2003).
- Weston C, Yee B, Hod E, Prives J (Agrin-induced acetylcholine receptor clustering is mediated by the small guanosine triphosphatases Rac and Cdc42. *J Cell Biol* 150:205-212.2000).
- Wiese S, Herrmann T, Drepper C, Jablonka S, Funk N, Klausmeyer A, Rogers ML, Rush R, Sendtner M (Isolation and enrichment of embryonic mouse motoneurons from the lumbar spinal cord of individual mouse embryos. *Nat Protoc* 5:31-38.2010).
- Williams RL, Hilton DJ, Pease S, Willson TA, Stewart CL, Gearing DP, Wagner EF, Metcalf D, Nicola NA, Gough NM (Myeloid leukaemia inhibitory factor maintains the developmental potential of embryonic stem cells. *Nature* 336:684-687.1988).
- Willmann R, Pun S, Stallmach L, Sadasivam G, Santos AF, Caroni P, Fuhrer C (Cholesterol and lipid microdomains stabilize the postsynapse at the neuromuscular junction. *Embo J* 25:4050-4060.2006).
- Wishart TM, Huang JP, Murray LM, Lamont DJ, Mutsaers CA, Ross J, Geldsetzer P, Ansorge O, Talbot K, Parson SH, Gillingwater TH (SMN deficiency disrupts brain development in a mouse model of severe spinal muscular atrophy. *Hum Mol Genet* 19:4216-4228.2010).
- Wu H, Xiong WC, Mei L (To build a synapse: signaling pathways in neuromuscular junction assembly. *Development* 137:1017-1033.2010).
- Wyatt TJ, Keirstead HS (Stem cell-derived neurotrophic support for the neuromuscular junction in spinal muscular atrophy. *Expert Opin Biol Ther* 10:1587-1594.2010).

- Xu ZL, Mizuguchi H, Ishii-Watabe A, Uchida E, Mayumi T, Hayakawa T (Optimization of transcriptional regulatory elements for constructing plasmid vectors. *Gene* 272:149-156.2001).
- Yang X, Arber S, William C, Li L, Tanabe Y, Jessell TM, Birchmeier C, Burden SJ (Patterning of muscle acetylcholine receptor gene expression in the absence of motor innervation. *Neuron* 30:399-410.2001).
- Yang X, Li W, Prescott ED, Burden SJ, Wang JC (DNA topoisomerase IIbeta and neural development. *Science* 287:131-134.2000).
- Yeung WL, Lam CW, Ng PC (Intra-familial variation in clinical manifestations and response to ephedrine in siblings with congenital myasthenic syndrome caused by novel COLQ mutations. *Dev Med Child Neurol* 52:e243-244.2010).
- Ymlahi-Ouazzani Q, O JB, Paillard E, Ballagny C, Chesneau A, Jadaud A, Mazabraud A, Pollet N (Reduced levels of survival motor neuron protein leads to aberrant motoneuron growth in a *Xenopus* model of muscular atrophy. *Neurogenetics* 11:27-40.2010).
- Young PJ, Le TT, Dunckley M, Nguyen TM, Burghes AH, Morris GE (Nuclear gems and Cajal (coiled) bodies in fetal tissues: nucleolar distribution of the spinal muscular atrophy protein, SMN. *Exp Cell Res* 265:252-261.2001).
- Young PJ, Le TT, thi Man N, Burghes AH, Morris GE (The relationship between SMN, the spinal muscular atrophy protein, and nuclear coiled bodies in differentiated tissues and cultured cells. *Exp Cell Res* 256:365-374.2000).
- Zambrowicz BP, Imamoto A, Fiering S, Herzenberg LA, Kerr WG, Soriano P (Disruption of overlapping transcripts in the ROSA beta geo 26 gene trap strain leads to widespread expression of beta-galactosidase in mouse embryos and hematopoietic cells. *Proc Natl Acad Sci U S A* 94:3789-3794.1997).
- Zapletalova E, Hedvicakova P, Kozak L, Vondracek P, Gaillyova R, Marikova T, Kalina Z, Juttnerova V, Fajkus J, Fajkusova L (Analysis of point mutations in the SMN1 gene in SMA patients bearing a single SMN1 copy. *Neuromuscul Disord* 17:476-481.2007).
- Zerres K, Rudnik-Schoneborn S, Forkert R, Wirth B (Genetic basis of adult-onset spinal muscular atrophy. *Lancet* 346:1162.1995).
- Zerres K, Rudnik-Schoneborn S, Forrest E, Lusakowska A, Borkowska J, Hausmanowa-Petrusewicz I (A collaborative study on the natural history of childhood and juvenile onset proximal spinal muscular atrophy (type II and III SMA): 569 patients. *J Neurol Sci* 146:67-72.1997).
- Zhang B, Luo S, Wang Q, Suzuki T, Xiong WC, Mei L (LRP4 serves as a coreceptor of agrin. *Neuron* 60:285-297.2008a).
- Zhang HL, Pan F, Hong D, Shenoy SM, Singer RH, Bassell GJ (Active transport of the survival motor neuron protein and the role of exon-7 in cytoplasmic localization. *J Neurosci* 23:6627-6637.2003).
- Zhang J, Lefebvre JL, Zhao S, Granato M (Zebrafish unplugged reveals a role for muscle-specific kinase homologs in axonal pathway choice. *Nat Neurosci* 7:1303-1309.2004).
- Zhang Z, Lotti F, Dittmar K, Younis I, Wan L, Kasim M, Dreyfuss G (SMN deficiency causes tissue-specific perturbations in the repertoire of snRNAs and widespread defects in splicing. *Cell* 133:585-600.2008b).
- Zhong N, Zucker RS (Roles of Ca²⁺, hyperpolarization and cyclic nucleotide-activated channel activation, and actin in temporal synaptic tagging. *J Neurosci* 24:4205-4212.2004).

- Zhou D, Mooseker MS, Galan JE (An invasion-associated Salmonella protein modulates the actin-bundling activity of plastin. *Proc Natl Acad Sci U S A* 96:10176-10181.1999a).
- Zhou H, Glass DJ, Yancopoulos GD, Sanes JR (Distinct domains of MuSK mediate its abilities to induce and to associate with postsynaptic specializations. *J Cell Biol* 146:1133-1146.1999b).
- Zhu D, Xiong WC, Mei L (Lipid rafts serve as a signaling platform for nicotinic acetylcholine receptor clustering. *J Neurosci* 26:4841-4851.2006).
- Zhu D, Yang Z, Luo Z, Luo S, Xiong WC, Mei L (Muscle-specific receptor tyrosine kinase endocytosis in acetylcholine receptor clustering in response to agrin. *J Neurosci* 28:1688-1696.2008).
- Zhu T, Mancini JA, Sapieha P, Yang C, Joyal JS, Honore JC, Leduc M, Zaniolo K, Hardy P, Shao Z, Fan L, Hou X, Rivard GE, Chemtob S (Cortactin activation by FVIIa/tissue factor and PAR2 promotes endothelial cell migration. *Am J Physiol Regul Integr Comp Physiol* 300:R577-585.2011).
- Zurita E, Chagoyen M, Cantero M, Alonso R, Gonzalez-Neira A, Lopez-Jimenez A, Lopez-Moreno JA, Landel CP, Benitez J, Pazos F, Montoliu L (Genetic polymorphisms among C57BL/6 mouse inbred strains. *Transgenic Res* 20:481-489.2011).

11 Appendix

Rosa26 targeting vector with *PLS3V5* integrate

SHORT HOMOLOGY ARM ccgcggcaggccctccgagcgtggtggagccgttctgtgagacagccgggtacgagt
 cgtgacgctggaaggggcaagcgggtggtgggcaggaatgcggtccgccctgcagcaaccggagggggagggagaaggg
 agcggaaaagtctccaccggacgcggccatggctcggggggggggggcagcggaggacgcttccggccgacgtctcgtc
 ctgattggctttttctcccgcctgtgtgaaaacacaaatggcgtgtttggtggcgtaaggcgctgtcagttaacggcagccgg
 agtgcgcagccgccggcagcctcgtctgcccactgggtggggcgggaggtagggtgggtgaggcagctgacgtgcgggc
 gcggtcggcctctggcggggcgggggaggggaggggagggcagcgaagtagctcgcgcgagcggccgccaccctcc
 ccttctctgggggagtcgtttaccgcgcggccggcggcctcgtcgtctgattgctcggggccagaaaactggccttgc
 attgctcgtgttcgtgaagttgagtcacccggccagcggggcggcgaggaggcgtcccaggttccggccctcccctc
 ggccccgcgcgcagagtctggccgcgcgccctcgcgaacgtggcaggaagcgcgcgctgggggaggggacgggcagt
 agggctgagcggctgcggggcgggtgcaagcacgttccgacttgagttgctcaagaggggctgctgagccagacctcat
 cgcgcactccggggagtgagggaaggagcaggggctcagttgggctgttttgaggcaggaagcactgtctcccaaagtc
 gctctgagttgtatcagtaaggagctgagtgagtagcggggagaaaggccgacccttctccggaggggggaggggagt
 gttgcaataccttctgggagttctgctcctctggtctgaggaccgctgggctgggagaatccctgcccccttcccct
 cgtgatctgcaactccagctcttCTAGCATCTGTAGGGCGCAGTAGTCCAGGGTTTCTTGATGATG
 TCATACTTATCCTGCTCGCGGTTGAGGACAACTCTTCGCGGTCTTCCAGTGGTTAATT
 AAAGTTATAATCGCTGAGGTAATATTTAAAATCATTTTTCAAATGATTCACAGTTAATTTGC
 GACAATATAATTTTATTTTACATAAACTAGACGCCTTGTCTTCTTCTTCTCGTATTCT
 TCTCTTTTTCATTTTTCTTTCATAAAAATTAACATAGTTATTATCGTATCCATATATGTATC
 TATCGTATAGAGTAAATTTTTGTTGTCATAAATATATATGTCTTTTTTAATGGGGTGTATA
 GTACCGCTGCGCATAGTTTTCTGTAATTTACAACAGTGCTATTTTCTGGTAGTTCTTCG
 GAGTGTGTTGCTTTAATTATTAATTTATATAATCAATGAATTTGGGATCGTCGGTTTTGT
 ACAATATGTTGCCGGCATAGTACGCAGCTTCTTCTAGTTCAATTACACCATTTTTTAGCA
 GCACCGGATTAACATAACTTTCCAAAATGTTGTACGAACCGTTAAACAAAACAGTTCAC
 CTCCCTTTTCTATACTATTGTCTGCGAGCAGTTGTTTGTGTTAAAAATAACAGCCATTGT
 AATGAGACGCACAACTAATATCACAACTGGAAATGTCTATCAATATATAGTTGCTCTA
 GTTATTAATAGTAATCAATTACGGGGTCATTAGTTCATAGCCCATATATGGAGTTCGCG
 TTACATAACTTACGGTAAATGGCCCGCCTGGCTGACCGCCCAACGACCCCGGCCATT
 GACGTCAATAATGACGTATGTTCCCATAGTAACGCCAATAGGGACTTTCCATTGACGTCA
 ATGGGTGGACTATTTACGGTAACTGCCACTTGGCAGTACATCAAGTGTATCATATGC
 CAAGTACGCCCCCTATTGACGTCAATGACGGTAAATGGCCCGCCTGGCATTATGCCCA
 GTACATGACCTTATGGGACTTTTCTACTTGGCAGTACATCTACGTATTAGTCATCGCTAT
 TACCATGCATGGTCGAGGTGAGCCCCACGTTCTGCTTCACTCTCCCCATCTCCCCCCCC
 TCCCCACCCCAATTTTGTATTTATTTATTTTAAATTATTTTGTGCAGCGATGGGGGCGG
 GGGGGGGGGGGGGCGCGCGCCAGGCGGGGCGGGGCGGGGCGAGGGGCGGGGCG
 GGGCGAGGCGGAGAGGTGCGGCGGCAGCCAATCAGAGCGGCGCGCTCCGAAAGTTT
 CCTTTTATGGCGAGGCGGCGGCGGCGGCCCTATAAAAAGCGAAGCGCGCGGCGG
 GCGGGAGTCGCTGCGACGCTGCCTTCGCCCCGTGCCCGCTCCGCCGCCGCTCGCG
 CCGCCCGCCCGGCTCTGACTGACCGGCTTACTCCCACAGGTGAGCGGGCGGGACGG
 CCCTTCTCCTTCGGGCTGTAATTAGCGCTTGGTTAATGACGGCTTGTCTTTTCTGTG
 GCTGCGTGAAAGCCTTGAGGGGCTCCGGGAGGGCCCTTTGTGCGGGGGGAGCGGCTC
 GGGGCTGTCCGCGGGGGGACGGCTGCCTTCGGGGGGGACGGGGCAGGGCGGGGT
 CGGCTTCTGGCGTGTGACCGGCGGCTCTAGAGCTCGCTAGCATCTGTAGGGCGCAGT
 AGTCCAGGGTTTCTTGATGATGTCATACTTATCCTGTCCCTTTTTTTTCCACAGCTCGC
 GGTTGAGGACAACTCTTCGCGGTCTTTCCAGTGGTTAATTAATAACTTCGTATAGCAT
 ACATTATACGAAGTTATGGATCCGAACAACGACCCAACACCCGTGCGTTTTATTCTGTC
 TTTTTATTGCCGATCCCC **NEOMYCIN:** TCAGAAGAACTCGTCAAGAAGGCGATAGAAGG
 CGATGCGCTGCGAATCGGGAGCGGCGATACCGTAAAGCACGAGGAAGCGGTCAGCCC
 ATTCGCCGCCAAGCTCTTCAGCAATATCACGGGTAGCCAACGCTATGTCCTGATAGCGG
 TCCGCCACACCCAGCCGGCCACAGTCGATGAATCCAGAAAAGCGGCCATTTTCCACCA
 TGATATTCGGCAAGCAGGCATCGCCATGGGTACGACGAGATCCTCGCCGTGGGGCAT
 GCGCGCCTTGAGCCTGGCGAACAGTTCGGCTGGCGCGAGCCCTGATGCTCTTCGTC
 CAGATCATCTGATCGACAAGACCGGCTTCCATCCGAGTACGTGCTCGCTCGATGCGAT

GTTTCGCTTGGTGGTTCGAATGGGCAGGTAGCCGGATCAAGCGTATGCAGCCGCCGCAT
TGCATCAGCCATGATGGATACTTTCTCGGCAGGAGCAAGGTGAGATGACAGGAGATCC
TGCCCCGGCACTTCGCCAATAGCAGCCAGTCCCTTCCCGCTTCAGTGACAACGTCGA
GCACAGCTGCGCAAGGAACGCCCGTCGTGGCCAGCCACGATAGCCGCGCTGCCTCGT
CCTGCAGTTCATTACAGGGCACCCGGACAGGTTCGGTCTTGACAAAAAGAACCGGGCGCCC
CTGCGCTGACAGCCGGAACACGGCGGCATCAGAGCAGCCGATTGTCTGTTGTGCCAG
TCATAGCCGAATAGCCTCTCCACCCAAGCGGCCGGAGAACCTGCGTGAATCCATCTT
GTTCAATGGCCGATCCCATATTGGCTGCAGGGTTCGCTCGGTGTTTCGAGGCCACACGCG
TCACCTTAATATGCGAAGTGGACCTGGGACCGCGCCCGCCCGACTGCATCTGCGTGTT
CGAATTCGCCAATGACAAGACGCTGGGCGGGGTTTGCTCGACATTGGGTGGAACATT
CCAGGCCTGGGTGGAGAGGCTTTTTGCTTCTTTCGAAAACCACTGCTCGACATTG
GGTGGAAACATTCCAGGCCTGGGTGGAGAGGCTTTTTGCTTCTTTCGAAAACCACT
TGCTCGACTAGTGATTAAGTTCGACTCGGGGACACCAATATGGCGATCTCGGCCTTTT
CGTTTCTTGGAGCTGGGACATGTTTGCCATCGATCCATCTACCACCAGAACGGCCGTTA
GATCTGCTGCCACCGTTGTTTCCACCGAAGAAACCACCGTTGCCGTAACCACCACGAC
GGTTGTTGCTAAAGAAGCTGCCACCGCCACGGCCACCGTTGTAGCCGCCGTTGTTGTT
ATTGTAGTTGCTCATGTTATTTCTGGCACTTCTTGGTTTTCTTAAAGTGAGGAGGAAC
ATAACCATTCTCGTTGTTGTCGTTGATGCTTAAATTTGCACTTGTTTCGCTCAGTTCAGC
CATAATATGAAATGCTTTTCTTGTGTTCTTACGGAATACCACTTGCCACCTATCACCACA
ACTAACTTTTTCCCGTTCCCTCCATCTCTTTTATATTTTTTTCTCGAGGGATCTTTGTGAA
GGAACCTTACTTCTGTGGTGTGACATAATTGGACAACTACCTACAGAGATTTAAAGCTC
TAAGTAAATATAAAATTTTTAAGTGTATAATGTGTTAACTACTGATTCTAATTGTTTGTG
TATTTAGATTCCAACCTATGGAAGTGAATGGGAGCAGTGGTGGAAATGCCTTTAATG
AGGAAAACCTGTTTTGCTCAGAAGAAATGCCATCTAGTGATGATGAGGCTACTGCTGAC
TCTCAACATTCTACTCCTCCAAAAAAGAGAAAGGTAGAAGACCCCAAGGACTTTCTCT
TCAGAATTGCTAAGTTTTTTGAGTCATGCTGTGTTTAGTAATAGAACTCTTGCTTGCTTTG
CTATTTACACCACAAAGGAAAAAGCTGCACTGCTATACAAGAAAATTATGGAAAAATATT
CTGTAACCTTTATAAGTAGGCATAACAGTTATAATCATAACATACTGTTTTTTCTTACTCC
ACACAGGCATAGAGTGTCTGCTATTAATAACTATGCTCAAAAATTGTGTACCTTTAGCTTT
TTAATTTGTAAGGGGTTAATAAGGAATATTTGATGTATAGTGCCTTGACTAGAGATCATA
ATCAGCCATACCACATTTGTAGAGGTTTACTTGCTTTAAAAAACCTCCCACACCTCCCC
CTGAACCTGAAACATAAAATGAATGCAATTGTTGTTGTTAACTTGTTTATTGCAGCTTATA
ATGGTTACAAATAAAGCAATAGCATCACAATTTCAAAATAAAGCATTTTTTTTCACTGCA
TTCTAGTTGTGGTTTGTCCAAACTCATCAATGTATCTTATCATGTCTGGATCTGACATGGT
AAGTAAGCTTATAACTTCGTATAGCATAACATTATACGAAGTTATGGGCGCGCCACC **PLS3**
: **ATGGATGAGATGGCTACCACTCAGATTTCCAAGATGAGCTTGATGAACTCAAAGAGG**
CCTTTGCAAAGTTGATCTCAACAGCAACGGATTCAATTTGTGACTATGAACTTCATGAGC
TCTTCAAGGAAGCTAATATGCCATTACCAGGATATAAAGTGAGAGAAATTATCAGAAAC
TCATGCTGGATGGTGACAGGAATAAAGATGGGAAAAATAAGTTTTGACGAATTTGTTTATA
TTTTTCAAGAGGTAAAAAGTAGTGATATTGCCAAGACCTTCCGCAAAGCAATCAACAGGA
AAGAAGGATTTGTGCTCTGGGTGGAACCTCAGAGTTGTCCAGCGAAGGAACACAGCAT
TCTTACTCAGAGGAAGAAAAATATGCTTTTGTAACTGGATAAACAAAGCTTTGGAAAAT
GATCCTGATTGTAGACATGTTATACCAATGAACCCTAACACCGATGACCTGTTCAAAGCT
GTTGGTGTGGAATTGTGCTTTGTAAAATGATTAACCTTTCAGTTCCTGATACCATTGAT
GAAAGAGCAATCAACAAGAAGAACTTACACCCTTCATCATTACAGGAAAACCTGAACTTG
GCACTGAACTCTGCTTCTGCCATTGGGTGTCATGTTGTGAACATTGGTGCAGAAGATTT
GAGGGCTGGGAAACCTCATCTGGTTTTGGGACTGCTTTGGCAGATCATTAAAGATCGGTT
TGTTTCGCTGACATTGAATTAAGCAGGAATGAAGCCTTGGCTGCTTTACTCCGAGATGGT
GAGACTTTGGAGGAACTTATGAAATTGTCTCCAGAAGAGCTTCTGCTTAGATGGGCAA
CTTTCATTTGGAAAACCTCGGGCTGGCAAAAAATTAACAACCTTAGTGCTGACATCAAGGA
TTCCAAAGCCTATTTCCATCTTCTCAATCAAATCGCACCAAAAAGGACAAAAGGAAGGTGA
ACCACGGATAGATATTAACATGTCAGGTTTCAATGAAACAGATGATTTGAAGAGAGCTGA
GAGTATGCTTCAACAAGCAGATAAATTAGGTTGCAGACAGTTTGTACCCCTGCTGATGT
TGTCAGTGGAACCCCAAACTCAACTTAGCTTTCGTGGCTAACCTGTTTAAATAAATACCC
AGCACTAACTAAGCCAGAGAACCAGGATATTGACTGGACTCTATTAGAAGGAGAACTC
GTGAAGAAAGAACCTTCCGTAACCTGGATGAACTCTTGGTGTCAATCCTCACGTAAC

CATCTCTATGCTGACCTGCAAGATGCCCTGGTAATCTTACAGTTATATGAACGAATTA
 GTTCCTGTTGACTGGAGTAAGGTTAATAAACCTCCATACCCGAAACTGGGAGCCAACAT
 GAAAAAGCTAGAAAAGTGAACACTATGCTGTTGAATTAGGGAAGCATCCTGCTAAATTCTC
 CCTGGTTGGCATTGGAGGGCAAGACCTGAATGATGGGAACCAAACCCTGACTTTAGCTT
 TAGTCTGGCAGCTGATGAGAAGATATACCCTCAATGTCCTGGAAGATCTTGGAGATGGT
 CAGAAAGCCAATGACGACATCATTGTGAACTGGGTGAACAGAACGTTGAGTGAAGCTG
 GAAAATCAACTTCCATTGAGAGTTTAAAGGACAAGACGATCAGCTCCAGTTTGGCAGTTG
 TGGATTTAATTGATGCCATCCAGCCAGGCTGTATAAACTATGACCTTGTGAAGAGTGGC
 AATCTAACAGAAGATGACAAGCACAATAATGCCAAGTATGCAGTGTCAATGGCTAGAAG
 AATCGGAGCCAGAGTGTATGCTCTCCCTGAAGACCTTGTGGAAGTAAAGCCCAAGATG
 GTCATGACTGTGTTTGCATGTTTGTGATGGGCAGGGGAATGAAGAGAGTG **V5-TAG: AAGG**
GCAATTCTGCAGATATCCAGCACAGTGGCGGCCGCTCGAGTCTAGAGGGCCCGCGTT
CGAAGGTAAGCCTATCCCTAACCTCTCCTCGGTCTCGATTCTACGCGTACCGGTCATC
ATCACCATCACCAT **TGA**GGCGCGCCGCGGCCGCGATCAATTCCGGTACCGAAGTTCCCTA
 TTCCGAAGTTCCCTATTCTCTAGAAAGTATAGGAACTTCCCTCGAGGGTACCCCAATTCCGC
 CCCCCCCCCCCCCCTAACGTTACTGGCCGAAGCCGCTTGAATAAGGCCGGTGTGCGT
 TTGTCTATATGTTATTTCCACCATATTGCCGTCTTTTGGCAATGTGAGGGCCCGGAAAC
 CTGGCCCTGTCTTCTTGACGAGCATTCTAGGGGTCTTTCCCTCTCGCCAAGGAATG
 CAAGGTCTGTTGAATGTCGTGAAGGAAGCAGTTCCTCTGGAAGCTTCTTGAAGACAAAC
 AACGTCTGTAGCGACCCTTTCAGGCAGCGGAACCCCCACCTGGCGACAGGTGCCTC
 TGCGGCCAAAAGCCACGTGTATAAGATACACCTGCAAAGCGGCACAACCCCAAGTGCC
 ACGTTGTGAGTTGGATAGTTGTGGAAGAGTCAAATGGCTCTCCTCAAGCGTATTCAAC
 AAGGGGCTGAAGGATGCCCAGAAGGTACCCATTGTATGGGATCTGATCTGGGGCCTC
 GGTGCACATGCTTTACATGTGTTTGTGAGGTTAAAAACGTCTAGGCCCCCCGAACC
 ACGGGGACGTGGTTTTCTTTGAAAAACACGATGATAATATGGCCACAACC **GFP: ATGG**
TGAGCAAGGGCGAGGAGCTGTTACCGGGGTGGTGCCCATCCTGGTTCGAGCTGGACG
GCGACGTAACGGCCACAAGTTCAGCGTGTCCGGCGAGGGCGAGGGCGATGCCACCT
ACGGCAAGCTGACCCTGAAGTTCATCTGCACCACCGGCAAGCTGCCCGTGCCCTGGCC
CACCCTCGTGACCACCCTGACCTACGGCGTGCAGTGCTTCAGCCGCTACCCCGACCAC
ATGAAGCAGCACGACTTCTTCAAGTCCGCCATGCCCGAAGGCTACGTCCAGGAGCGCA
CCATCTTCTTCAAGGACGACGGCAACTACAAGACCCGCGCCGAGGTGAAGTTCGAGGG
CGACACCCTGGTGAACCGCATCGAGCTGAAGGGCATCGACTTCAAGGAGGACGGCAAC
ATCCTGGGGCACAAGCTGGAGTACAACACAAGCCACAACGTCTATATCATGGCCGA
CAAGCAGAAGAACGGCATCAAGGTGAACTTCAAGATCCGCCACAACATCGAGGACGGC
AGCGTGCAGCTCGCCGACCACTACCAGCAGAACACCCCATCGGCGACGGCCCCGTG
CTGCTGCCCGACAACCACTACCTGAGCACCCAGTCCGCCCTGAGCAAAGACCCCAACG
AGAAGCGCGATCACATGGTCTGCTGGAGTTCGTGACCGCCGCGGGATCACTCTCGG
CATGGACGAGCTGTACAAG **TAA**TCCGGGATCCGGAGAGCTCCCAACGAAGTTCCCTATTC
 CGAAGTTCCCTATTCTCTAGAAAGTATAGGAACTTCCCTCGAGGTTGGATGCAGCCCGGGG
 GATCCACTAGTTCTAGAGCGGCCGATCAGCCTCGACTGTGCCTTCTAGTTGCCAGCCAT
 CTGTTGTTTGGCCCTCCCCCGTGCCTTCTTGACCCTGGAAGGTGCCACTCCCACTGTC
 CTTTCTAATAAAATGAGGAAATTGCATCGCATTGTCTGAGTAGGTGTCAATTCTATTCTG
 GGGGGTGGGGTGGGGCAGGACAGCAAGGGGGAGGATTGGGAAGACAATAGCAGGCA
 TGCTGGGGATGCGGTGGGCTCTATGGCTTCTGAGGCGGAAAGAACCAGCTGGGGCTC
 GAGATCCACTAGTTCTAGCCTCGAGGCTAGAGCGGCCGCGCGGATATCGAATTCTG **LO**
NG HOMOLOGY ARM: ctagaagatgggagggtctctgggaggctaaaggctaacctgggtgtggcggtgtc
 ctgcaggggaattgaacaggtgtaaaattggagggaacaagactcccacagatttcggtttgtcggaagtttttaataggggc
 aataggaaaatggaggatagggtcatctggggttatgcagcaaaactacaggtatattgctgtatccgcctcggagattccat
 gaggagataaagacatgtcaccgagttatactctcctgcttagatcctactacagtatgaaatacagtggtcgaggttagactatg
 taagcagatttaacatttaagagcccagttactatccatttctcccgtccttctgcagcctatcaaaaaggatttagaacact
 catttagccccatttattactggttatccaacccttagacagagcattggcattttcccttctgatcttagaagctgatga
 ctcatgaaaccagacagattgattacatacaccacaaatcgaggctgtagctggggcctcaacactgcagttctttataactcctt
 agtacacttttgtgatccttgccttgatccttaattttcagtgctatcacctctcccgtcaggtggtgtccacatttgggctattctcag
 tccagggagtttaacaacaatagatgtattgagaatccaacctaaagcttaacttccactccatgaatgcctctctcttttctcatt
 ataactgagctataccattaatggttccaggtgagtgctctctcccataatactgatgtatctacatattgccaggctgatatttaa
 gacataaaggatatttatttagccacatggtattgactgctactaaaatttgcattgtacacatctgaaaagggtgttctt

gctgtttcctgtgtgaaattgttatccgctcacaattccacacaacatacgagccggaagcataaagtgtaaagcctgggggccta
atgagtgagtaactcacattaattgctgctcactgccgcttccagtcgggaaacctgctgctgagctgcattaatgaatc
ggccaacgcgcggggagaggcggttgctattggcgctcttccgcttctcgtcactgactgctgctgctggctgctggctg
cgcgagcgggtatcagctcactcaaaaggcggtataacggttatccacagaatcaggggataacgcaggaaagaacatgtgag
caaaaggccagcaaaaggccaggaaccgtaaaaaggccgctgtgctggcgttttccataggctccgccccctgacgagcat
cacaanaatcgacgctcaagtacagaggtggcgaaccgacagactataaagataaccaggcgtttccccctggaagctcct
cgtgctctcctgttccgaccctgccgcttaccggatacctgtccgcttctccctcgggaagcgtggcgcttctcatagctcag
ctgtaggatctcagttcggttaggtcgtcctcaagctggctgtgtgcacgaacccccctcagcccagccgctgctgctta
tccggtaactatcgtctgagtccaaccggtaagacagacttatcgccactggcagcagccactggtaacaggattagcagag
cgaggtatgtaggggtgtacagagttctgaagtgggtgcctaactacggctacactagaaggacagatatttggtatctgctc
tgctgaagccagttacctcggaaaaagagttgtagcttgcctggcgaacaaaccaccgctggtagcgggtgtttttgtttg
aagcagcagattacgcgcagaaaaaaggatctcaagaagatcctttgacttttctacggggtctgacgctcagtggaacgaa
aactcacgtaagggtttgtgatgagattatcaaaaaggatctcacctagatccttttaataaaaaatgaagtttaaatcaat
taaagtatatatgagtaactggctgacagttaccaatgcttaatacagttagggcacctatctcagcgatctgtctatttctcatcca
tagttgctgactccccgctgtgtagataactacgatacgggaggggtaccatctggccccagtgctgcaatgataccgcgagac
ccacgctcaccggctccagattatcagcaataaaccagccagccggaaggccgagcgcagaagtggtcctgcaactttatc
cgctccatccagcttattaattgttgcgggaagctagagtaagtagttcgccagtaatagtttgcaacgttgttgcattgctac
aggcatcgtgtgtcacgctcgttggatggcttcaactcagctccggtcccaacgatcaaggcgagttacatgatccccatgt
tgtcaaaaaagcggtagctcctcggctcctccgatcgtgtcagaagtaagttggccgagtggtatcaatcatggtatggcagc
actgcataattcttactgtcatgcatccgtaagatgctttctgtgactggtagtactcaaccaagtcattctgagaatagtgtatg
cggcgaccgagttgctctgcccggcgtcaatacgggataataccgcgccacatagcagaactttaaagtgctcatattggaa
aacgttctcggggcgaaaactctcaaggatcttaccgctgttgagatccagttcgtatgaaccactcgtgcacccaactgatctc
agcatctttactttcaccagcgttctgggtgagcaaaaacaggaaggcaaaatgccgcaaaaaagggaataaggcgacac
ggaaatgtgaatactatactctccttttcaatatttgaagcatttatcagggttattgtctcatgagcggatacatattgaaatgat
ttgaaaaataaacaataggggtccgctcacatttccccgaaaagtgccacctaaattgtaagcgttaataattttgtaaaattcg
cgtaaaattttgttaaatcagctcatttttaaccaataggccgaaatcgccaaaatcccttataaatcaaaagaatagaccgagat
agggtgagtggttccagtttgaacaagagtcactattaagaacgtggactccaacgtcaaaggcgaaaaaccgtctat
cagggcgatggccactacgtgaacctaccctaatcaagttttggggtcaggtgccgtaagcactaaatcggaacccta
aaggagccccgatttagagctgacgggaaagccggcgaacgtggcgagaaaggaagggaagaaagcgaagggag
cggcgctagggcgctggcaagtgtagcggctcagctgcgtaaccaccaccccggcgcttaatgcgcccgtacaggg
cgctcccattcgccattcaggtcgcgaactgttgggaaggcgatcgggtcgggcttctcgtattacgccagctggcga
gggggatgtgctgcaaggcgattaagttgggtaaccgaggggtttccagtcacgacggtgtaaacgacggccagtgagcgc
gcgtaatacgcactcactatagggcgaattggagct

12 Acknowledgements

Ich möchte mich bei meiner Betreuerin Frau Prof. Dr. Brunhilde Wirth für das Überlassen dieses spannenden Projekts, Ihr stetiges Bemühen, die zahlreichen fachlichen Gespräche sowie die nützlichen Anregungen bedanken. Weiterhin möchte ich Ihr für die zahlreichen Gelegenheiten danken, regelmäßig an internationalen Fachkonferenzen und Fortbildungen teilnehmen zu können. Frau Prof. Dr. Sigrun Korsching möchte ich für die Übernahme des Koreferats und Herrn Prof. Dr. Ansgar Büschges für die Übernahme des Vorsitzes der Prüfungskommission danken.

Zweimal durfte ich am größten US-amerikanischen Fachtreffen, der „Families of SMA Conference“, teilnehmen. Neben den vielen hervorragenden Wissenschaftsbeiträgen waren es jedoch immer die zahlreich anwesenden (und oft noch so jungen) Patienten und deren Familien, die mich mit Ihrer trotz aller schwierigen Umstände positiven Denkweise, dem unermesslichen Engagement und Ihrem festen Glauben an eine zukünftige Therapieform zu tiefst beeindruckt und bewegt haben. Gerade die zwischenmenschlichen Eindrücke und Gespräche über die SMA mit Betroffenen habe ich als sehr sinngeladend für meine Arbeit empfunden. Allen „Families“ und insbesondere Herrn und Frau Schwersenz von der „Initiative SMA Deutschland“ daher ein herzliches Dankeschön!

Weiterhin möchte ich mich bei meiner Arbeitsgruppe bedanken: Insbesondere bei Sandra Kröber für Ihren hervorragenden „Technical Support“ und die vielen fachlichen Hilfen, die weit darüber hinaus gingen, sowie Deine Freundschaft! Auch möchte ich Sandra in folgende Dankesreihe eingliedern: Markus Riessland, Lutz Garbes, Irmgard Hölker und Julia Schreml einen herzlichen Dank für Ihre fachliche Unterstützung und die vielen lustigen Momente im Labor. In der Hoffnung, keinen vergessen zu haben, natürlich auch ein ganz großes „Danke“ an den Rest der Gruppe: Anja Förster, Anna Kaczmarek, Antonella Di Domenico, Immanuel Weber, Kristina Roßbach, Lilian Martinez, Ludwig Heesen, Markus Storbeck, Miriam Jakubik, Mohsen Hosseini, Sebastian Seufert und Ylva Mende.

Natürlich auch mit eingeschlossen sind alle weiteren Kollegen aus der Frauenklinik und dem ZMMK, der AG Brüning (Vielen Dank an Dr. Thomas Wunderlich für das Überlassen des ROSA-CAGS Vektors) und Cloppenburg. Moreover, I would like to thank Dr. Tom Gillingwater (Edinburgh, Scotland) for all his good suggestions on my project as well as kindly providing me with the PowerPoint slides of his talk at the FSMA conference in 2011.

Zuletzt möchte ich mich ganz herzlich bei meiner gesamten Familie bedanken, ganz besonders jedoch bei Michaela, für Deine fortwährende Unterstützung, für Dein großes Verständnis an arbeitsreichen Wochenenden und die vielen aufmunternden Worte!

13 Erklärung

Ich versichere, dass ich die von mir vorgelegte Dissertation selbständig angefertigt, die benutzten Quellen und Hilfsmittel vollständig angeben und die Stellen der Arbeit - einschließlich Tabellen, Karten und Abbildungen -, die anderen Werken im Wortlaut oder dem Sinn nach entnommen sind, in jedem Einzelfall als Entlehnung kenntlich gemacht habe; dass diese Dissertation noch keiner anderen Fakultät oder Universität zur Prüfung vorgelegen hat; dass sie noch nicht veröffentlicht worden ist sowie, dass ich eine solche Veröffentlichung vor Abschluss des Promotionsverfahrens nicht vornehmen werde. Die Bestimmungen der Promotionsordnung sind mir bekannt. Die von mir vorgelegte Dissertation ist von Prof. Dr. rer. nat. Brunhilde Wirth und Prof. Dr. rer. nat. Sigrun Korsching betreut und in der Arbeitsgruppe von Prof. Dr. rer. nat. Brunhilde Wirth durchgeführt worden.

Köln, den

(Bastian Ackermann, Dipl.-Biologe)

14 Curriculum Vitae

Name	Bastian Ackermann
Geburtsort	Geldern
Geburtsdatum	25.09.1980
Familienstand	Ledig
Staatsangehörigkeit	Deutsch

Berufserfahrung:

Juli 2007 – Oktober 2011

Promotionsarbeit in der Arbeitsgruppe von Frau Prof. Dr. Brunhilde Wirth, Institut für Humangenetik, Universität zu Köln

Titel: Analysis of the modifying influence of Plastin 3 (PLS3) on Spinal Muscular Atrophy (SMA) by generation of transgenic mouse models

Akademische Ausbildung

September 2006 - Juli 2007

Beginn einer Promotionsarbeit in der Arbeitsgruppe von Dr. Klaus Rohr, Institut für Entwicklungsbiologie, Universität zu Köln (Aufgrund beruflicher Umorientierung von Herrn Dr. Rohr konnte diese Arbeit nicht zuende geführt werden)

Titel: *Untersuchungen zum Ablösemechanismus des Schilddrüsenprimordiums vom Pharynxepithel während der Frühentwicklung im Zebrafisch (Danio rerio)*

Februar - August 2006

Projektdurchführung in der Arbeitsgruppe von Prof. Joan K. Heath, Colon and Cell Biology Laboratory, Ludwig Institute for Cancer Research, Melbourne (Australien)

Titel: *Cloning and characterization of zebrafish mutants with abnormalities in intestinal development*

März 2005 - Dezember 2005

Diplomarbeit in der Arbeitsgruppe von Prof. Dr. Diethard Tautz, Institut für Genetik, Universität zu Köln

Titel: *Untersuchungen zur Funktion der Gene Ol-her1/11 und Ol-her13/2 während der Somitogenese in Medaka (Oryzias latipes) (Gesamtnote: 1,0)*

Oktober 2000 - März 2005

Studium der Biologie an der Universität zu Köln

Schwerpunktfächer: Genetik, Biochemie, Entwicklungsbiologie

Schulische Ausbildung**Juni 2000**

Erwerb der allgemeinen Hochschulreife am Lise-Meitner-Gymnasium, Geldern

Nebenberufliches Engagement:**August 2009 – Juli 2011**

Studentischer Vertreter des Zentrum für Molekulare Medizin Köln (ZMMK)

Juni 2008 – Januar 2011

Mitglied der International Graduate School for Biological Sciences,
Universität zu Köln

Oktober 2007 – Januar 2011

Finanzvorstand der Biotechnologischen Studenteninitiative Köln (Bts, Bio meets Industry).
Organisation von Vorträgen von Vertretern der Industrie für Studenten und Interessierte
anderer Fakultäten.

Köln, den

(Bastian Ackermann, Dipl.-Biologe)